A MULTIDISCIPLINARY ENGINEERING GEOLOGICAL INVESTIGATION OF CLIFF COLLAPSE AT REDCLIFFS IN THE 22 FEBRUARY AND 13 JUNE 2011 EARTHQUAKES

A thesis

submitted in partial fulfilment

of the requirements for the Degree

of

Master of Science in Engineering Geology

in the University of Canterbury

by **Reuben Lo Bing Quan**

Department of Geological Sciences

University of Canterbury

2013

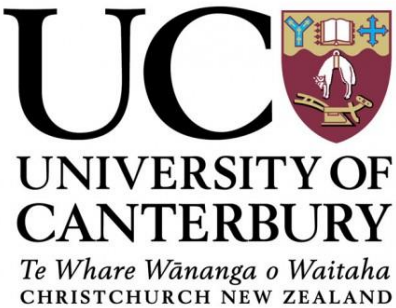

I dedicate this master's thesis to my family and friends, and to the 185 people who lost their lives in the 22 February 2011 Christchurch Earthquake.

Abstract

The collapse of Redcliffs' cliff in the 22 February 2011 and 13 June 2011 earthquakes were the first times ever a major failure incident occurred at Redcliffs in approximately 6000 years. This master's thesis is a multidisciplinary engineering geological investigation sought to study these particular failure incidents, focusing on collecting the data necessary to explain the cause and effect of the cliff collapsing in the event of two major earthquakes.

This study provides quantitative and qualitative data about the geotechnical attributes and engineering geological nature of the sea-cut cliff located at Redcliffs. Results from surveying the geology of Redcliffs show that the exposed lithology of the cliff face is a variably jointed rock body of welded and (relatively intact) unwelded ignimbrite, a predominantly massive unit of brecciated tuff, and a covering of wind-blown loess and soil deposit (commonly found throughout Canterbury) on top of the cliff. Moreover, detailing the external component of the slope profile shows that Redcliffs' cliff is a 40 – 80 m cliff with two intersecting (NE and SE facing) slope aspects. The (remotely) measured geometry of the cliff face comprises of multiple outstanding gradients, averaging a slope angle of ~67 ° (post-13 June 2011), where the steepest components are ~80 °, whereas the gentle sloping sections are ~44 °.

The physical structure of Redcliffs' cliff drastically changed after each collapse, whereby seismically induced alterations to the slope geometry resulted in material deposited on the talus at the base of the cliff. Prior to the first collapse, the variance of the gradient down the slope was minimal, with the SE Face being the most variable with up to three major gradients on one cross section. However, after each major collapse, the variability increased with more parts of the cliff face having more than one major gradient that is steeper or gentler than the remainder of the slope. The estimated volume of material lost as a result of the gradient changes was 28,267 m^3 in February and 11,360 m^3 in June 2011. In addition, surveys of the cliff top after the failure incidents revealed the development of fissures along the cliff edge. Monitoring 10 fissures over three months indicated that fissured by the cliff edge respond to intense seismicity (generally $\geq M_w$ 4) by widening.

Redcliffs' cliff collapsed on two separate occasions as a result of an accumulated amount of damage of the rock masses in the cliff (caused by weathering and erosion over time), and two M_w 6.2 trigger earthquakes which shook the Redcliffs and the surrounding area at a Peak Ground Acceleration (PGA) estimated to be around 2 g. The results of the theoretical study suggests that PGA levels felt on-site during both instances of failure are the result of three major factors: source of the quake and the site affected; topographic amplification of the ground movement; the short distance between the source and the cliff for both fault ruptures; the focus of seismic energy in the direction of thrust faulting along a path that intercepts Redcliffs (and the Port Hills).

Ultimately, failure on the NE and SE Faces of Redcliffs' cliff was concluded to be global as every part of the exposed cliff face deposited a significant volume of material on the talus at the base of the cliff, with the exception of one section on the NE Face. The cliff collapses was a concurrent process that is a single (non-monotonic) event that operated as a complex series of (primarily) toppling rock falls, some sliding of blocks, and slumping of the soil mantle on top of the cliff. The first collapse had a mixture of equivalent continua slope movement of the heavily weathered / damaged surface of the cliff face, and discontinuous slope movement of the jointed inner slope (behind the heavily weathered surface); whereas the second collapse resulted in only discontinuous slope movement on account of the freshly exposed cliff face that had damage to the rock masses, in the form of old and (relatively) new discontinuous fractures, induced by earthquakes and aftershocks leading up to the point of failure.

Contents

List of Figures

List of Tables

Chapter One: Introduction

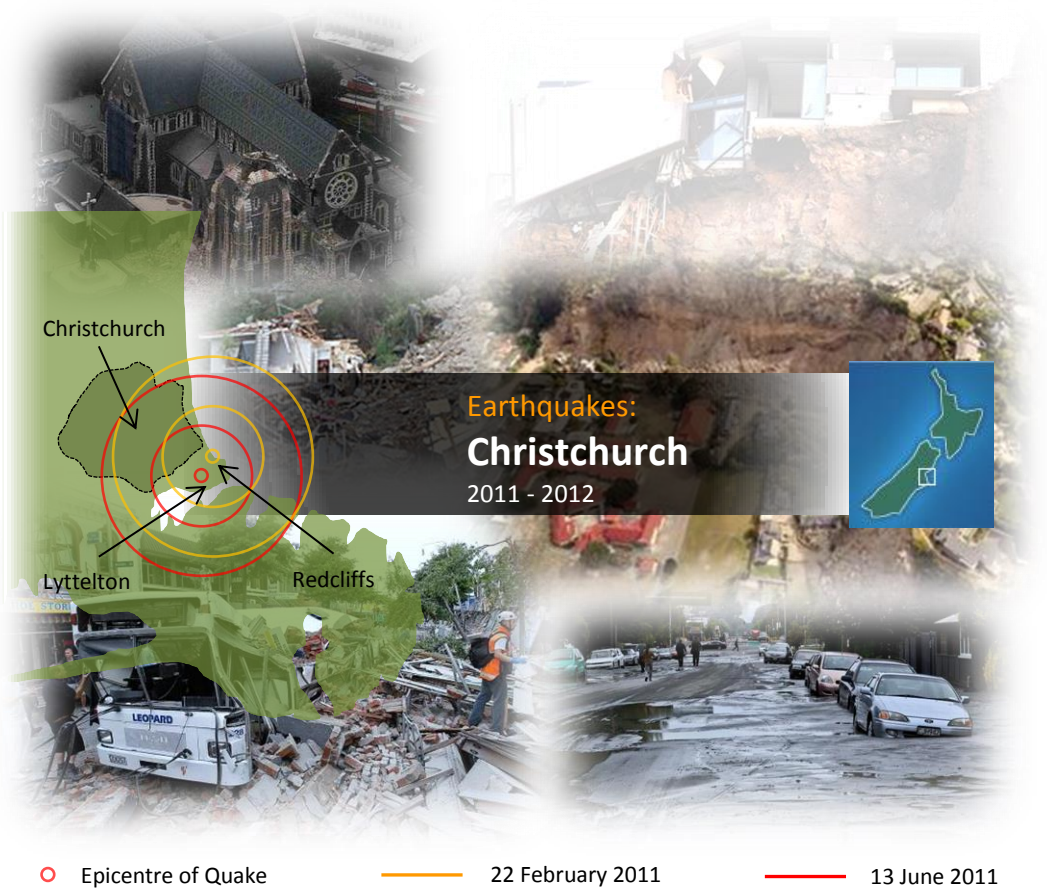

Figure 1 – Collage of photographs illustrating the severity of the Christchurch earthquakes that struck on 22 February 2011 and 13 June 2011

1.1 Introduction

The Canterbury Earthquakes sequence of 2010-2012 caused widespread damage across Christchurch, especially in the central city, eastern and coastal suburbs (Figure 1). However, unlike the rest of Christchurch, the coastal suburbs of Sumner and Redcliffs sustained not only damage on buildings and infrastructure, but also widespread rockfall events, including the collapse of four major sea-cut cliffs along the east coast of the Port Hills (Figures 2). Subsequent failure of the cliffs at Redcliffs, Peacock's Gallop, Whitewash Head, and in Sumner (Figure 3) resulted in large volumes of rock detaching from the cliff face, retreat of cliff faces, and the ensuing runout of the debris onto the rockfall talus (scree) at the base of the respective cliffs and the flat land at their toe. Out of the four cliffs that collapsed as a result of the (trigger) earthquakes, Redcliff's cliff was selected by the author of this master's thesis to investigate the failure incidents (i.e. cliff collapse) from an engineering geological perspective.

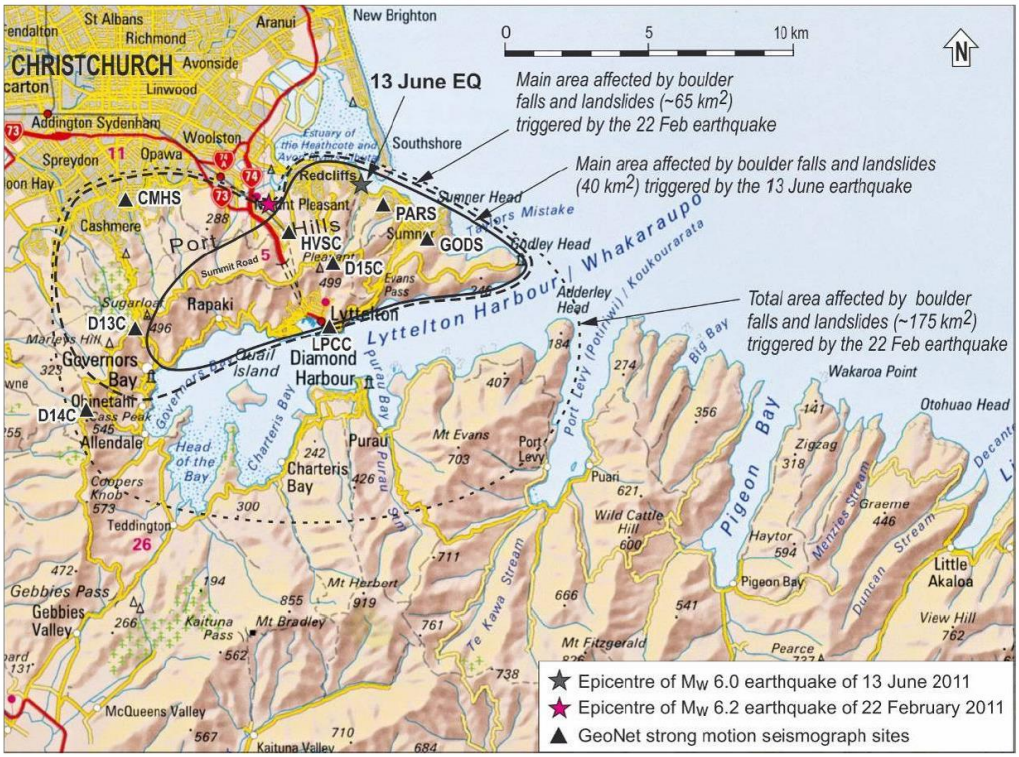

Figure 2 - Location map highlighting the areas affected by rockfalls, triggered as a result of the February and June 2011 Canterbury Earthquakes (modified after (Hancox et al., 2002).

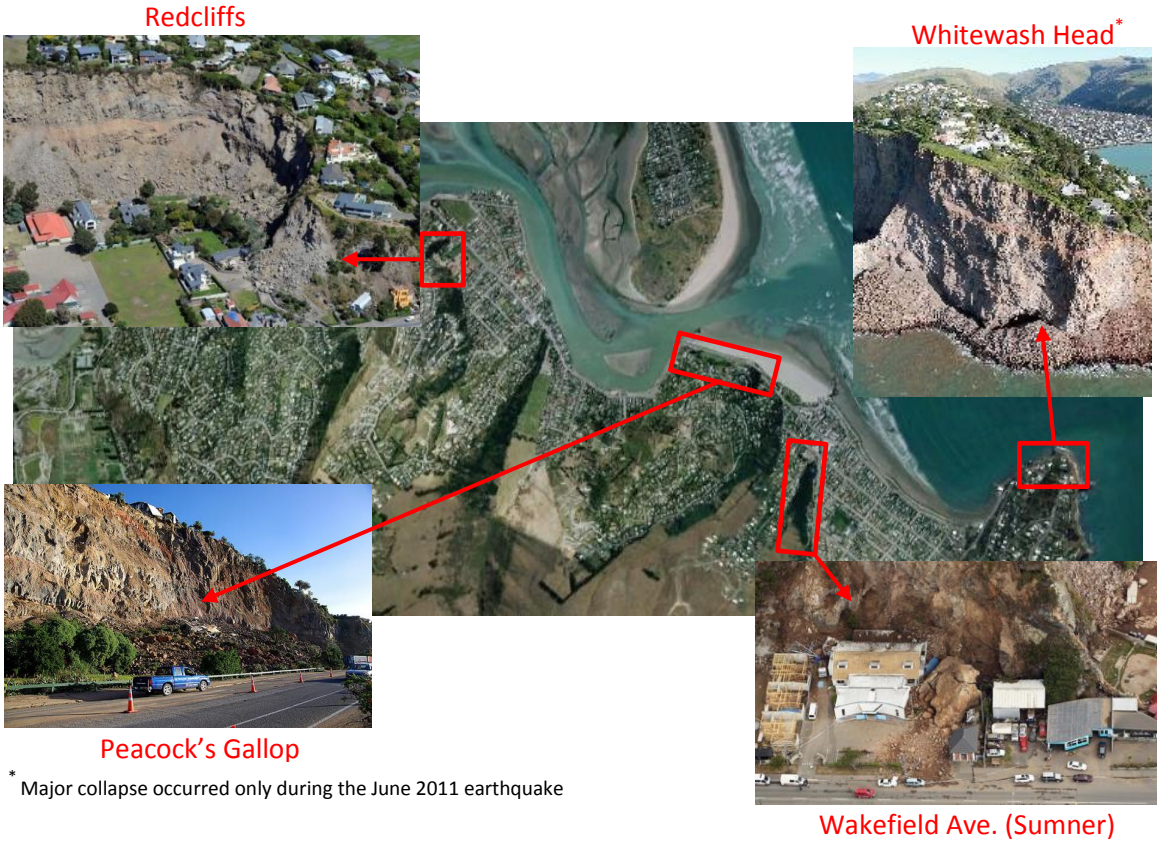

* Major collapse occurred only during the June 2011 earthquake

Figure 3 - Series of images showing the locations of four major sea-cut cliffs (Sumner, Redcliffs, Peacocks Gallop, and Whitewash Head) which collapsed along the eastern edge of the Port Hills as a result of the February and June 2011 earthquakes.

1.2 Christchurch Earthquake Sequences, 2010 – 2012

The nature of all major seismic activity in 2011 are considered "triggered events", i.e. earthquakes that are triggered by changes in the regional stresses (Stramondo et al., 2011). Initial changes to the regional stress in the Canterbury Region began with the rupture of the Greendale Fault on 4 September 2010 near Darfield, which is located approximately 48 km west of Christchurch City (GNS, 2011). Labelled as the Darfield Earthquake, the magnitude M_w 7.1 earthquake struck 40 km west of Christchurch City at 4.35 am (NZST), at a depth of 10 km (GNS, 2011). The impact of the Darfield Earthquake on Christchurch was minimal due to the timing of the event, depth of the rupture and the relative distance between the focus and Christchurch. As of October 2012, there have been 4092 recorded seismic events ranging between M_w 3.0 and 7.1, with the order of magnitude being less than the Darfield Earthquake continuing into 2011 and 2012 (Figures 4 and 5; Table 1). It was in February and June 2011 which two M_w 6.2 earthquakes triggered widespread rockfall in the Port Hills, including the collapse of Redcliffs' cliff. The following is a review of these key triggered events.

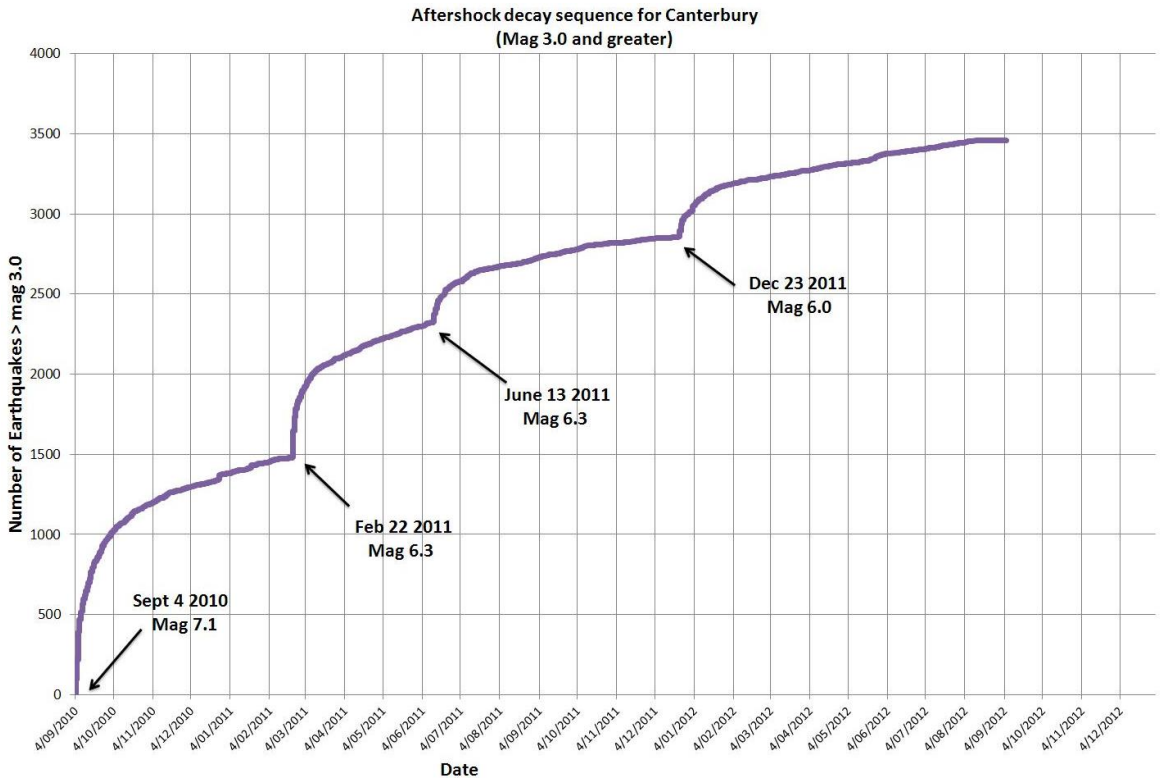

Figure 4 - A graph plot of all earthquakes and aftershocks as of 4 September 2010, up till 4 October 2012 illustrating pattern of seismic activity after each major earthquake in 2011 (GeoNet, 2012).

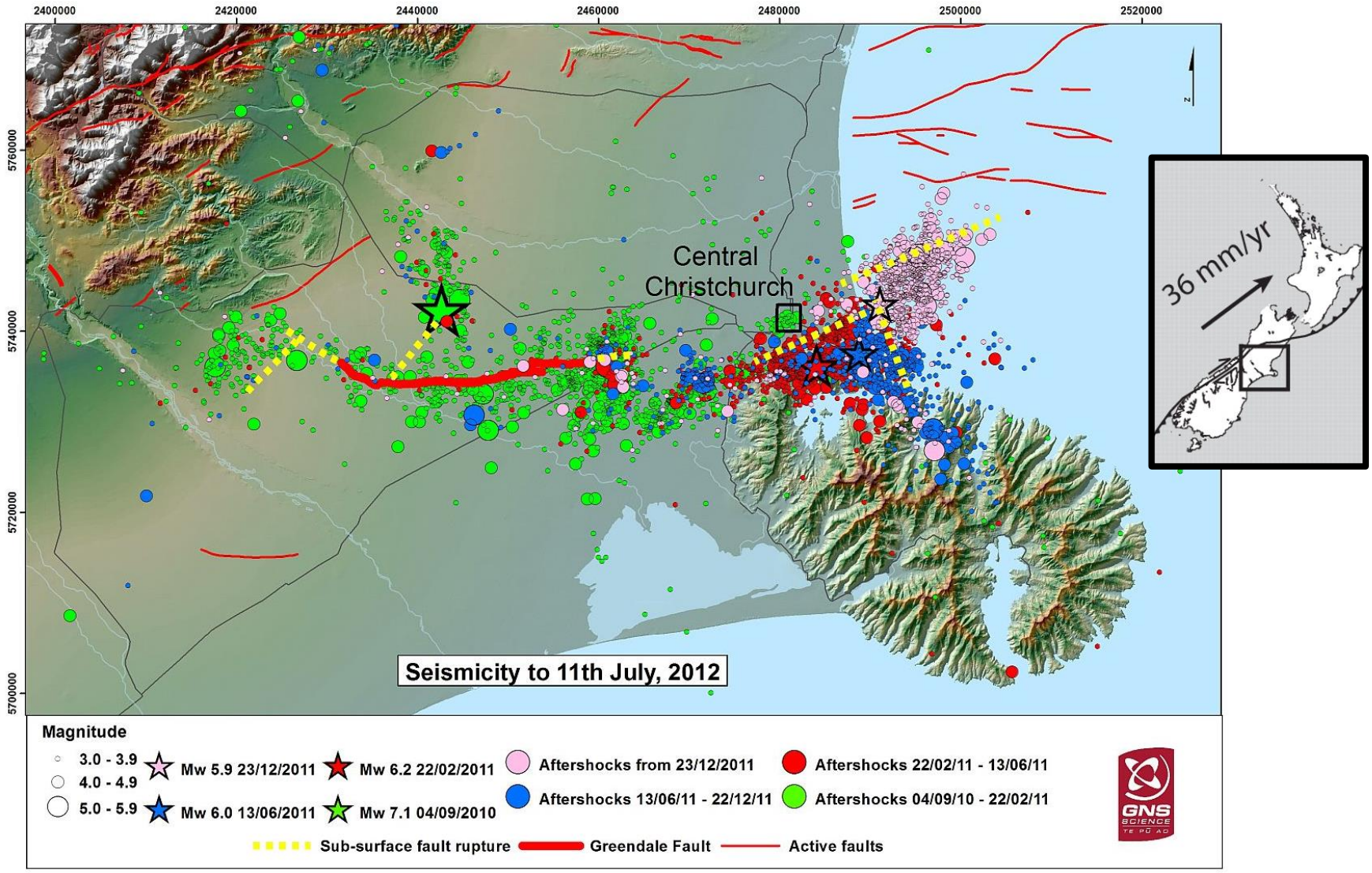

Figure 5 - Map illustrating of the number of seismic events the Canterbury region has encountered since September 2010 until August 2011 (Massey et al., 2012).

Table 1 – The number of earthquakes in the Canterbury Region between September 4 2010 and October 2012 grouped based on the magnitude (M_L) range (modified after (GeoNet, 2012).

Numbers of Canterbury region earthquakes from 4 September 2010 to October 2012	
Magnitude range (M_w)	Number
7.0 and above	1
6.0 - 6.9	3
5.0 - 5.9	54
4.0 - 4.9	487
3.0 - 3.9	3547

1.2.1 22 February 2011 (12:51 pm)

Cliff collapse at Redcliffs (and three other hilly parts of the Sumner area) happened on 22 February 2011 at 12:51 pm (NZST), with the rupture of a previous unknown fault, approximately 10 km southwest of Christchurch City, producing a M_w 6.2 earthquake (GNS Science, 2011).

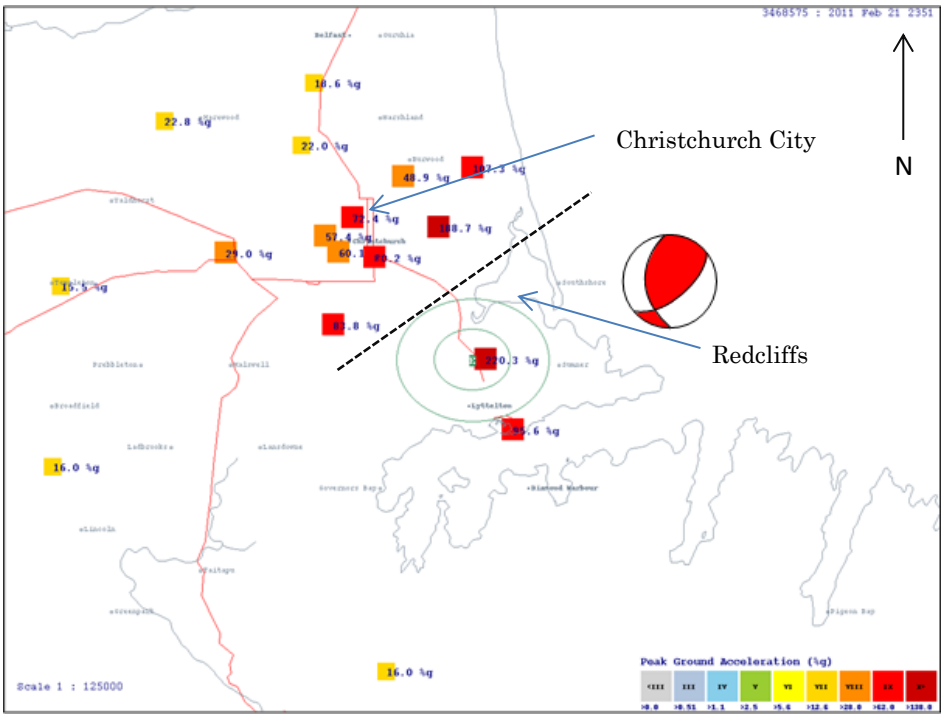

Figure 6 – An outline map of Christchurch modified to illustrate PGA values measured across Christchurch during the event of the 22 February 2011 earthquake, as well as present the location of the fault zone that ruptured (modified after GeoNet, 2012). The green letter E represents the epicentre of the quake, the dashed black line represents the orientation of the fault zone and the 'beach ball' represents type of fault responsible.

The fault responsible, since termed the Port Hills fault, is a reverse-thrust fault approximately 14 km in length, extending from Cashmere to the Avon-Heatcote estuary in a NE – SW orientaiton (GNS Science, 2011). The fault rupture occurred 5 km beneath the surface with a measured Peak Ground Acceleration (PGA) of 2.2 g (220.3 %) near the epicentre (Figure 5), > 1.4 g within the vicinity (including Redcliffs), and a maximum intensity of MM 9 (GeoNet, 2012).

In spite of being an earthquake smaller in magnitude compared to the Darfield Earthquake, the timing of the event, the relatively shorter distance, fault mechanism and shallow rupture beneath Christchurch caused widespread destruction. Collapsed buildings and liquefaction were apparent throughout all Christchurch, with isolated rockfall (and rockslide) events occurring along the east coast of the Port Hills and Lyttelton area (Figure 6) (Dellow et al., 2011).

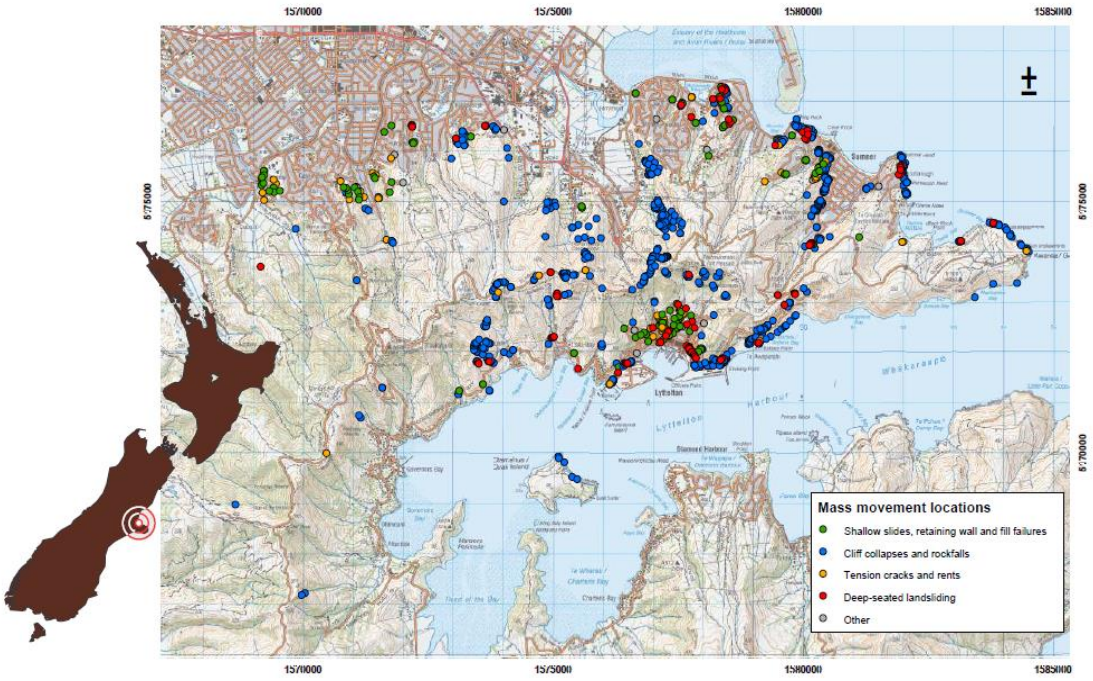

Figure 7 – Map showing the distribution of various types of mass movement that occurred due to the 22 February 2011 aftershock (Dellow et al., 2011).

1.2.2 13 June 2011 (02:20 pm)

Four months later on 13 June 2011 at 02:20 pm (NZST), an hour and 20 minutes after a preliminary M_w 5.6 quake in the same, a second M_w 6.2 trigger earthquake occurred just south of Redcliffs. The resulting fault rupture struck 7 km beneath the epicentre, roughly a few with a maximum PGA 2.13 g (212.7 %) measured within the vicinity (GeoNet, 2012). The June 13 events occurred on a NNW-SSE trending strike-slip fault,

extending from Brighton Spit towards Port Levy, revealing another new fault that intersects a part of the February rupture zone (Figures 7 and 8).

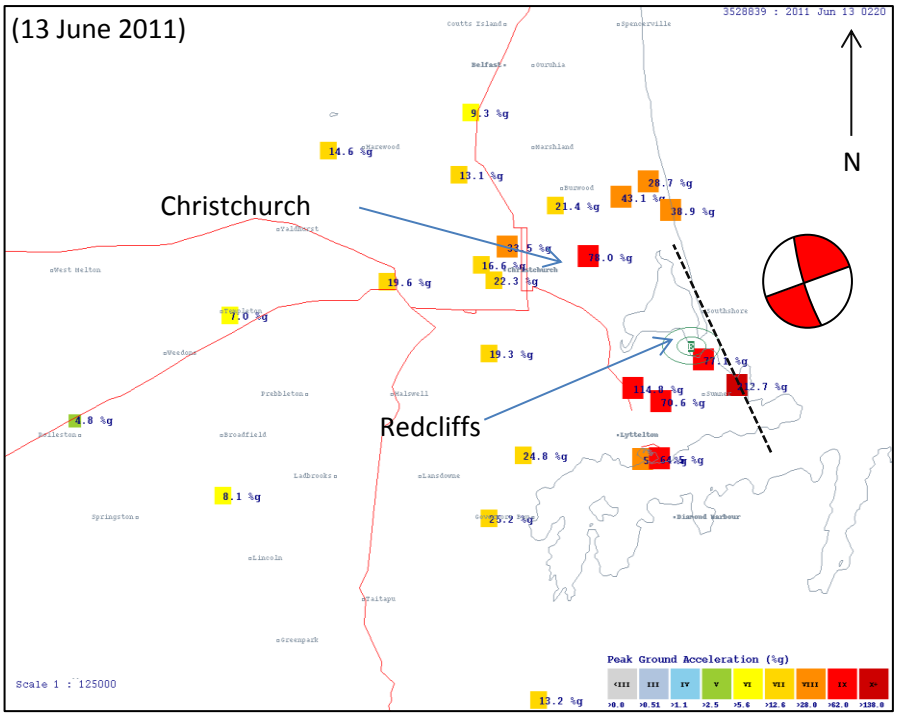

Figure 8 – A second outline map of Christchurch modified illustrate PGA values measured across Christchurch during the 13 June 2011 earthquake, as well as present the location of the fault zone that ruptured (Page, 2011). The green letter E represents the epicentre of the quake, the dashed black line represents the orientation of the fault zone and the 'beach ball' represents type of fault responsible.

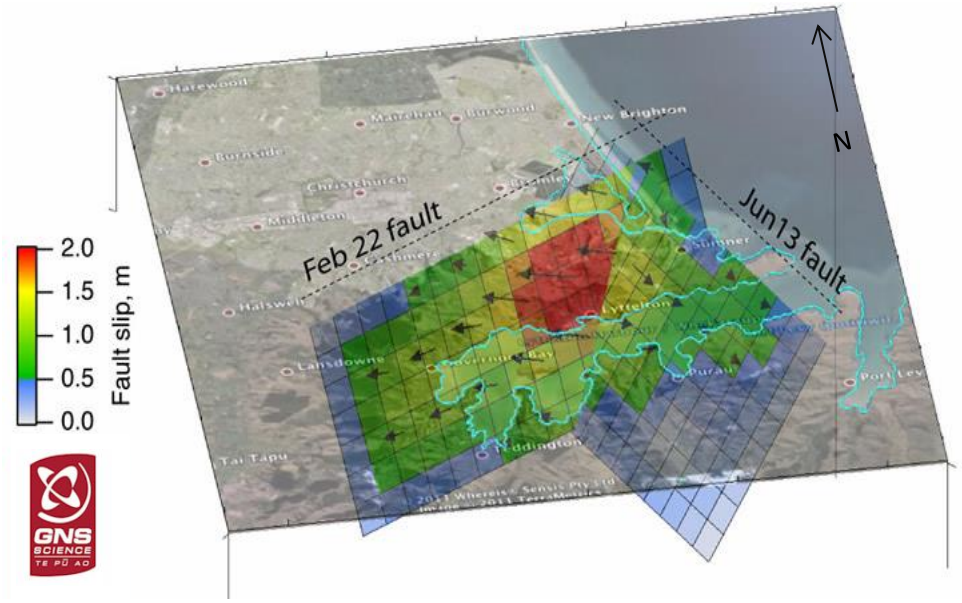

Figure 9 - A map illustrating the ground displacement caused by both the February and June 2011 aftershocks, where slip occurs down to about 7-8 km depth and up to about 1 km from the surface. The squares of the fault surfaces measure 1 km x 1 km. The arrows represent the direction of slip with the length of the arrow proportional to the size of the slip. The colours display the amount the two sides of the fault slipped past each other during the earthquakes. Red signifies of slip greater than 1.8 m; yellow is more than 1.2 m; green is more than 0.6 m (GNS Science, 2011).

Similar to the February incident, this earthquake caused liquefaction, damage to infrastructure within the vicinity of the quake and further rock fall incidents in the Port hills, including a second major cliff collapse in Redcliffs. Such resemblances in terms of the severity of the quake, and the subsequent damage caused, were expected, as the properties of the earthquake were similar to that of the first trigger earthquake four months earlier – i.e. relatively shallow rupture, high peak ground accelerations and short distance to the suburbs and city of Christchurch.

1.3 Study Area: Redcliffs

1.3.1 Location

Redcliffs' cliff is an east-facing near-vertical rock slope located directly behind Redcliffs School, in the coastal suburb of Redcliffs, north of the Port Hills, Christchurch, New Zealand. The cliff is approximately 0.029 km^2 in area, and varies in height between ~30 – 40 m high at the northern end (Balmoral Lane), and locally increases up to ~70 m high at the southern end (Glendevere Terrace) (Figure 10). The boundaries of the investigation site run from 24 Glendevere Terrace on the top of the cliff, towards 8D Balmoral Lane (Figure 10).

1.3.2 Redcliffs' Geology

Redcliffs' cliff is one of four main sea-cut cliffs situated in the Port hills, located on the north-eastern side of Banks Peninsula (Figure #), the largest accumulation of Miocene volcanic rocks on the east coast of the South Island, New Zealand (Forsyth, Barrell, & Jongens, 2008). Port Hills is comprised of a sequential body of volcanic lavas, ash horizons, and intrusions, mantled by soils of varying thicknesses, typically ~1 m thick and locally more than 5 m thick, derived from wind-blown sand and silt (i.e. loess). The volcanic rocks are a sequence of hard, jointed basaltic and trachytic lava flows cut by an assortment of intrusive dykes, and interbedded with breccia (scoria), agglomerate (coarse angular gravel), compact sandy tuff beds, and ancient buried soils (Altaye, 1989; McDowell, 1989). It is the mechanics of this general body of volcanic rocks that are attributed to the collapse of Redcliffs' cliff, making the volcanic rock mass(es) one of the main focal point of this study.

The volcanic rock formations of Redcliffs can be classified differently depending on which theory is being referenced concerning the origins of the volcanic deposits (Sewell et al., 1992 vs. Hampton, 2010). This is primarily due to Redcliffs' cliff being in a recognized (complex) zone of overlapping volcanics that has been interpreted differently

by many scientists since research began investigating the geological origins of Banks Peninsula (Altaye, 1989; Sewell, 1988; Sewell et al., 1992; Hampton, 2010).

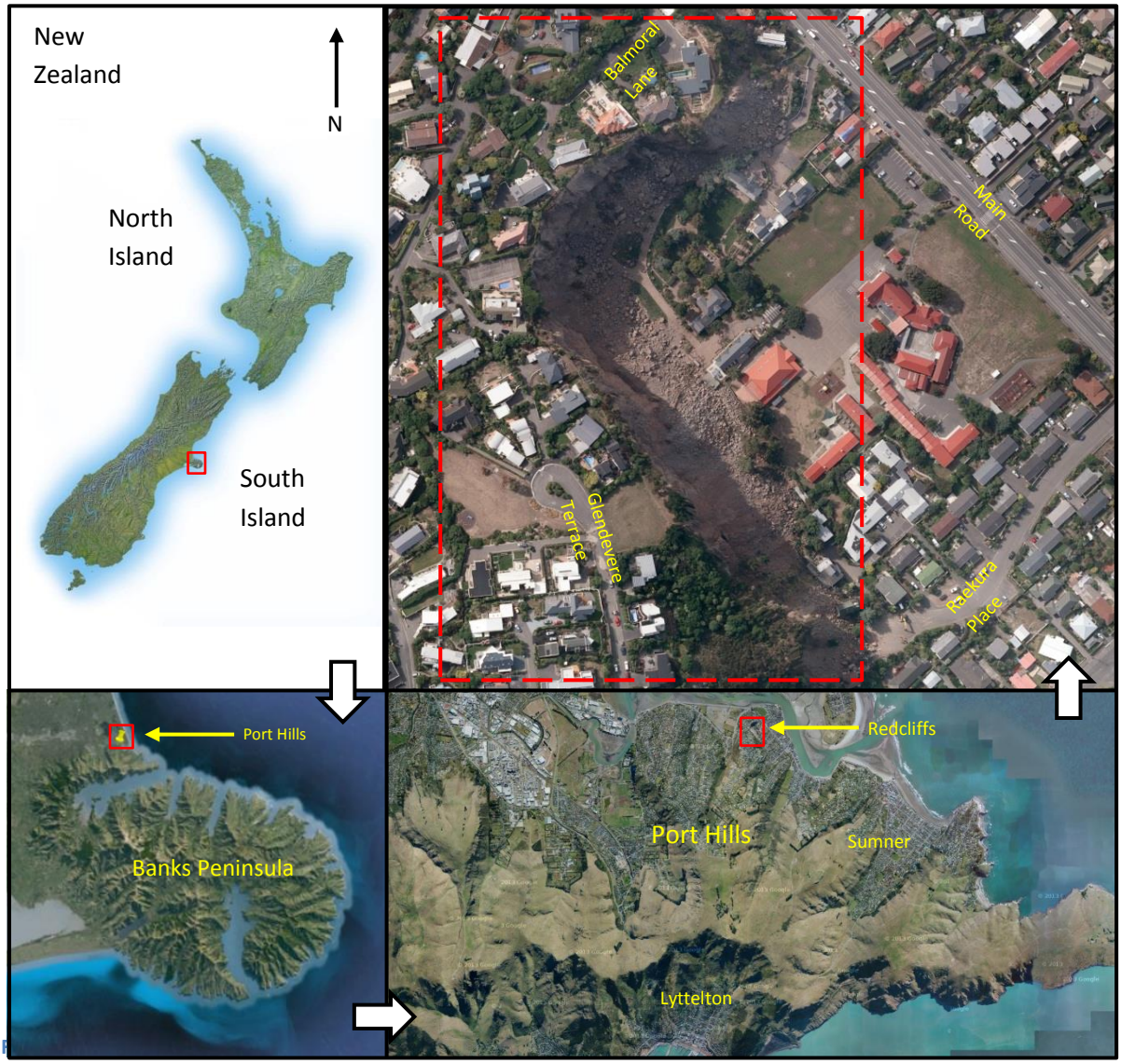

New Zealand, and the position of the boundaries on-site to conduct the site investigation(s).

For instance, Sewell et al (1992) considered the area of Redcliffs to be near the intersection of Lyttelton 2 and Mount Pleasant formations of Lyttelton Volcano that formed 11 – 9.7 Ma (Figure 11) (Altaye, 1989; Sewell, 1988; and Sewell et al., 1992). However, the most recent study on the geology of the Lyttelton Volcano by Hampton (2010) proposed a new theory about the growth, structure, and evolution of the Lyttleton Volcanic Complex; thus redefining the rock formations of the Sumner – Redcliffs area as part of the Whakaraupo Cone eruptions, derived from eruptive IX, X and XI during the Late Miocene (Figure 12).

Diamond Harbour Volcanic Group (8.1 - 5.8 Ma)
Stoddart Basalt (ds)
Kaioruru Hawaiite (dk)

Church Basalt (cb)
Chateau Intrusives (ci)
Darra Basanitoid (cd)

Akaroa Volcanic Group (9.0 - 8.0 Ma)
Te Oka Formation (ae) Mt Sinclair Formation (am) Onawe Syenite (ao)
Duvachelle Gabbro (ad) Lushington Breccia (al) French Hill Formation (af)
Tikao Trachyte (at)

Mt Herbert Volcanic Group (9.7 - 8.0 Ma)
Herbert Peak Hawaiite (hh) Port Levy Formation (hp)
Orton Bradley Formation (ho)
Mt Bradley Volcaniclastic Member (hob)

Lyttelton Volcanic Group (11 - 9.7 Ma)
Mt Pleasant Formation (lp)
Lyttelton Volcanic Group (l)

Mt. Pleasant formation – the Upper Miocene period when Redcliffs and the rest of the Port Hills were formed

Governors Bay Andesite (gb) (~13 - 11 Ma)

Allandale Rhyolite (ra) (~13 - 11 Ma)

PROBABLE UNCONFORMITY

Burnt Hill Group (Early Miocene)
Bradley sandstone (bb)

UNCONFORMITY

Eyre Group(Paleocene - Eocene)
Marine Drive Formation (em)

View Hill Volcanics (ev)

Charteris Bay Sandstone (ec)

Broken River Formation (eb)

PROBABLE UNCONFORMITY

Mount Somers Volcanic Group (80.9 Ma)
Gebbies Rhyolite (me) McQueens Andesite (mm)
Gebbies Pass Plant Beds (mer)

REGIONAL UNCONFORMITY

Torlesse Supergroup (t) (Triassic)

Figure 11 - Stratigraphic Sequence of Banks Peninsula proposed by (Sewell et. al, 1992), classifying the rocks of the Redcliffs' area as part of the Mt. Pleasant formation.

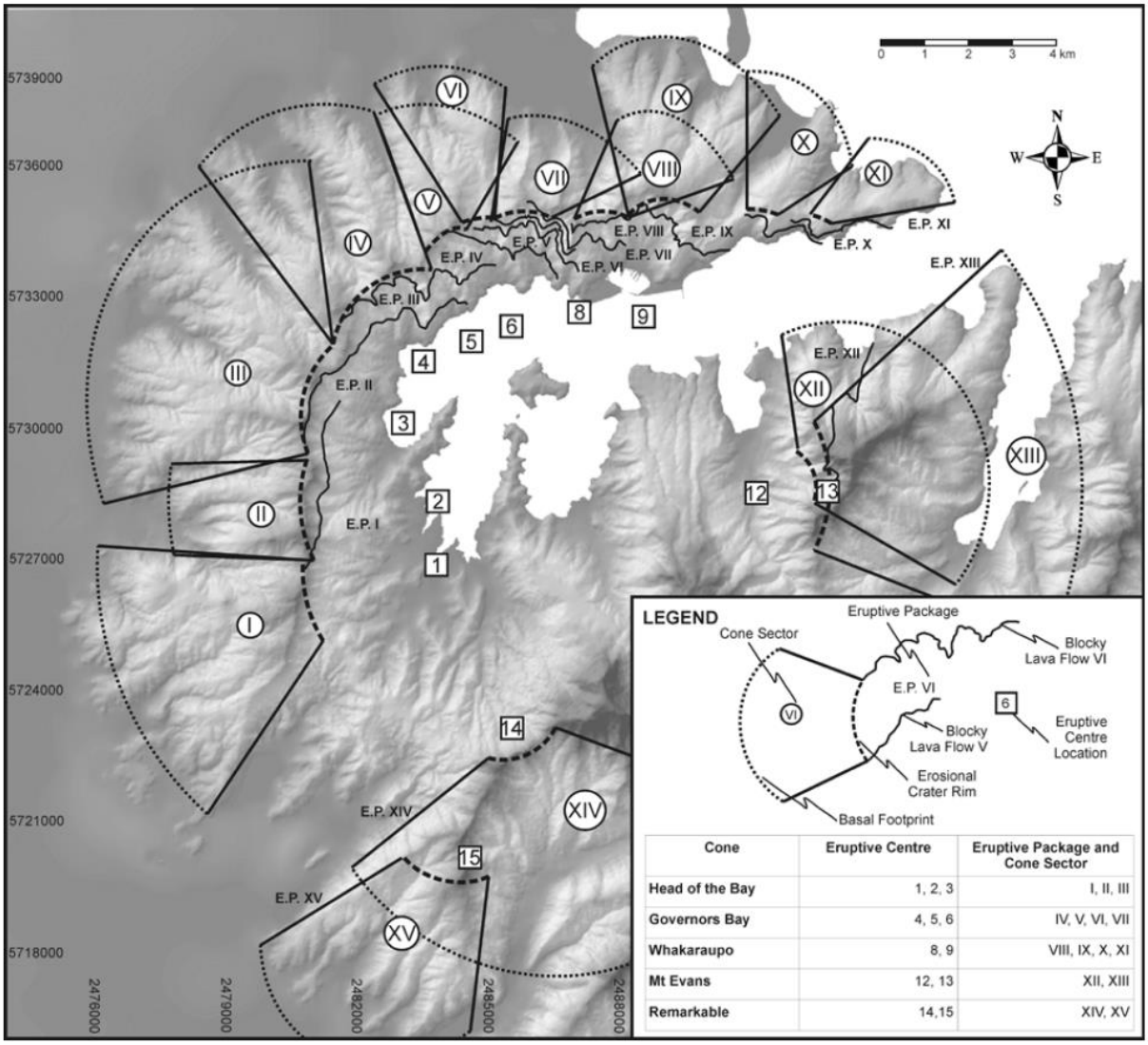

Cone	Eruptive Centre	Eruptive Package and Cone Sector
Head of the Bay	1, 2, 3	I, II, III
Governors Bay	4, 5, 6	IV, V, VI, VII
Whakaraupo	8, 9	VIII, IX, X, XI
Mt Evans	12, 13	XII, XIII
Remarkable	14,15	XIV, XV

Figure 12 – Map from Hampton (2010) showing the location Redcliffs' cliff with respect to the designated eruptive package of the area. The entire image (including summary table) presents the relationship of cones and eruptive packages on Lyttelton Volcano. Eruptive packages are defined as boundaries on the map, each linking to an eruptive centre, cone sector and blocky lava flow. Note, eruptive centres 10 and 11 are incorporated to be sourced from eruptive centre 9 (Hampton, 2010).

1.4 Purpose of Study

The following master's project is an engineering geological investigation-based study of the collapse of Redcliffs' cliff. For the purpose of this thesis, the only earthquakes that will be addressed in detail within the Canterbury Earthquake sequence (timeline) are ones which contributed to the collapse of Redcliffs' cliff, particularly the M_w 6.2 earthquakes which triggered the major collapse on 22 February and 13 June 2011.

From an observational stand point, it is evident that the damage caused by the major earthquakes on 22 February and 13 June 2011 exposed the unstable nature of Redcliffs' cliff (and other cliffs around the Port Hills) when faced with severe

earthquakes that have a PGA > 2 g. However, what is observed is merely the outcome of the seismically induced failure, which only proves that the critical seismic shaking caused by the major earthquakes in 2011 resulted in substantial mass movement from the cliff face at Redcliffs in the form of rockfall and rockslide off the cliff face, particularly during the February event. This study plans to further elaborate the account of this event by collecting and compiling relevant data aimed at providing a possible theoretical (but also testable) explanation about the behaviour of the cliff as it failed due the event of a major earthquake.

Since the first recorded incident of Redcliffs' cliff collapsing on 22 February 2011, it has revealed the gap in knowledge / understanding of rock mechanics for the cliffs of the Port Hills – in this instance from two separate instances of earthquake loading. It is the intention of this thesis to conduct an engineering geological investigation (structured as a post-failure characterisation study) to:

i. Create a database of information describing the: engineering geological properties of the cliff, the post-failure (physical) changes to the surface area of the cliff that resulted from the failure-inducing earthquakes; and regarding the trigger mechanisms (that caused the collapse).
ii. Formulate a scientific hypothesis as to 'how', and 'why' did the seismically-induced cliff collapses take place at Redcliffs (22 February and 13 June 2011) using the database of information collected, and in doing so, assess the extent of changes to the cliff as a result of each collapse.

1.5 Thesis Structure

The organisation for the thesis is as follows:

Chapter 2 – Research Approach and Method

Keywords: acquisition, approach, severity, failure, study

Chapter 3 – Engineering Geological Characterisation of Redcliffs

Keywords: geological, geotechnical, modelling, post-failure

Chapter 4 – Assessing the cliff collapse(s)

Keywords: mechanism, mechanics, failure, earthquakes

Chapter 5 – Summary and Conclusion

Keywords: overall, model, cause, behaviour

Chapter Two: Research Approaches

2.1 Introduction

The following chapter is an overview of the literature reviewed to develop the combined research approaches that were carried out to accomplish the aims set out in Section 1.4 to study the collapse of Redcliffs' cliff in the 22 February 2011 and 13 June 2011 earthquakes. In essence, the two research approaches used in this study were:

- Data-acquisition – collecting data and information to develop and engineering geological model of Redcliffs' cliff; and
- Literature research – using information gathered from credible sources (i.e. scientific journals, textbooks, websites) to assess the deformation mechanisms and failure mechanism involved in causing the collapses of Redcliffs' cliff.

The overall approach to this study is unique because the underlying theme of this study essentially encompasses two separate studies, i.e. characterising the engineering geological properties of a site, and assessing different aspects of a seismically induced cliff collapse – not a common combination found in scientific literature. Because there isn't literature that covers both aspects of this study together, two separate reviews will be done to evaluate the work done in the past collecting data from a rock slope, and studies done on: the intensity of earthquakes, and failure behaviour.

2.2 Data-acquisition Approach

The data-acquisition approach was the first approach reviewed concerning the typical methods used to conduct a site investigation, intended to develop an engineering geological model of a rock slope.

2.2.1 Pseudostatic Slope Analysis

In essence, the selection of data and information (objectives) needed for this study is fundamentally the same as the variables needed to conduct a Pseudostatic Slope Analysis (Hoek & Bray, 1981; Matasovic, 1991; Wyli & Mah, 2004; Hoek, 2007), but with a few added details about the cliff and earthquakes.

Publications such as Ling & Cheng (1997); Hack et al. (2007); and Mavrouli et al., (2009) are examples of attempts at applying the Pseudostatic Slope Analysis on rock

slopes, where all three investigations focused on gathering the necessary data to derive variables needed (from the jointed rock masses) to input into the limit equilibrium equation (EQ 1) to derive the Factor of Safety (FS). Essentially, when FS < 1 the slope is expected to fail; however, if FS = 1 the slope will generally resist seismic loading; and if FS > 1 the slope will remain stable.

$$Safety\ Factor\ (SF) = \frac{Resisting\ Force\ (F_r)}{Driving\ Force\ (F_i)} \qquad \text{(EQ 1)}$$

EQ 1 is a summarized version of the overall equation to determine SF with individual equations used to calculate F_r and F_i (Wyli & Mah, 2004). The typical data gathered [1 – 8] to determine F_r and F_i for the equilibrium analysis includes (Hoek, 2007):

i. The slope angle and slope height;
ii. Depth of tension crack (if any)[1];
iii. Rock mass characteristics of the slope material, such as cohesive strength, friction angle, unit weight of rock[2];
iv. Amount of water present in the failure surface / tension crack;
v. Weight and base area of rock wedge resting on failure surface[3];
vi. Estimated angle of failure plane, typically from some form of discontinuity; and
vii. The intensity of the earthquake, i.e. Peak Ground Acceleration (PGA) measured on-site[4].

Evidently, when comparing between the information needed for this study and the assortment of variables needed for a Pseudostatic Slope Analysis, only three (i, iii, iv) out of these (eight) assorted variables are exactly the kind of data needed for this study, that is to say, (i) relates to the geometric measurements of the cliff face; (iii) relates to the description of the rock (and soil) units; and (iv) relates to the qualitative details about the failure-inducing earthquakes.

As for the five remaining variables, they are indirectly related to the assortment of information needed for this study, i.e. they are based loosely on the underlying themes of deformation characteristics (ii); condition of slope (ix); characteristics of failure (v, vi) are all considered as part of the qualitative description of the cliff's surface area.

2.2.2 General Field Surveys

The standard practice of conducting a field survey is the typical approach used to collect engineering geology data and information describing the geological makeup of the site of interest. It, the practice, typically involves the classification of soil and rock in samples or in the mass, followed by testing the basic properties of chosen materials.

The approach generally comprises two key assessments: the first assessment is a background study, i.e. a desk study of collected site data, in the form of literature, and aerial photographs. This is followed by a preliminary reconnaissance, i.e. a general walk over the site, to verify the expected geology on-site – determined initially by the desk study (Bell, 2007). The second assessment is the site exploration, where the classification and testing of materials are carried out on-site (or later in a lab) in order to understand the nature of the engineering geological conditions on-site and those of its surroundings (Clayton et al., 1996).

Classification involves the identification and description of soil and rock samples using a standardized phraseology such as Muschamps (2005) – an accepted field description of soil and rock (guideline) used in New Zealand. The classification process takes place on-site, unlike the measurements and testing of the material properties. Those, on the other hand, can either done in a lab or in the field depending on the parameters of interest, and the instruments needed to carry out the testing. The standard parameters measured are generally related to basic (geotechnical) properties of the material such as strength, density, and deformability (Price & De Freitas, 2009).

Lourenço et al. (2010) and Apuani et al. (2005) are examples of the type of approach expected of the engineering geological and geotechnical characterisation of a rock slope, that is, describing the geological conditions and evaluating the geotechnical parameters based on data gathered using expertise judgement, field surveying techniques and laboratory tests – an approach that is expected of this study.

2.2.3 Remote Surveys

A remote approach to measuring the orientation of discontinuities and assessing slope deformation has been gaining popularity as a standard approach to survey the structural / geometric properties of a large slope. Techniques such as laser scanning and terrestrial photogrammetry are amongst the most frequent choice when needing

to survey a slope but hindered by the sheer size of the slope, and the difficulties one would encounter (regarding safety and accessibility to the slope) if measurements were to be taken directly from a large near-vertical rock slope.

Terrestrial Laser Scanning

Terrestrial laser scanning (TLS) is a widely used technique to survey the deformation of a large slope. The aim of these types of surveys typically involves surveying and monitoring a slope by creating three-dimensional models of the slope over a set period of time. Buckley et al. (2008) dicusses this approach at length, focusing on reviewing the workflow of acquiring and using LiDAR data, i.e. from selecting an appropriate field area and planning the survey, to acquiring and processing data to create high resolution models of large (potentially hazardous) slopesc, and (lastly) extracting useful geological data pertaining to the site of interest.

In essence, choosing a site and planning the survey comes down to two main factors: the feasibility of being able maximize coverage, while having a clear line of sight from the instrument to the target surface; and also being able to repeat the measurements with ease over an extended period of time to monitor slope deformation (Buckley et al., 2008). Once there is sufficient TLS (point cloud) data, it is processed and converted into three-dimensional models, which is typically followed by generating multiples of two-dimensional cross sections (slope profiles). Quantitative and qualitative data is then extracted from these models calculating the severity and / or rate of deformation on the slope (surface) in response to weathering and erosional processes over time.

Examples of this workflow being applied include Chandler & Moore (1989); Lim et al. (2005); Rosser et al. (2005); Chen et al. (2006); and Nguyen et al. (2011), all of which use the standard approach mentioned above. However, out of these four case examples, only three of which used TLS to monitor and model slope deformation over time. Lim et al. (2005) on the other hand uses airborne LiDAR to survey the slope since the investigation was regarding a major landslide. However, other than the data-acquisition technique used, the steps taken to process and model the slope was the same as how the other cases approached the investigation.

Terrestrial Photogrammetry

Terrestrial photogrammetry is another remote surveying technique commonly used to survey inaccessible outcrops. It is a useful characterisation tool for discontinuity characterization on rock cuts from rock slopes with limited accessibility, particularly dip and dip direction computations of discontinuous rock masses (Roncella et al., 2005). Unlike the point cloud models generated using the TLS technique, the three-dimensional surface models generated using terrestrial photogrammetry has the ability to include discontinuities that appear as linear traces in the model (Haneberg, 2008).

As shown in Reid & Harrison (2000) and Sturzenegger & Stead (2009), the process of this technique consists of taking multiple digital photographs of an outcrop at different angles, which are then processed in commercially available software such as Sirovision to produce three dimensional surface models of the outcrop. It is in these models where the discontinuities are mapped and the computer software subsequently measures the corresponding dip and dip directions. These measurements are then transferred onto discontinuity analysis software such as Dips, where the data is processed and analysed accordingly.

Overall, this remote surveying technique is considered a quick, simple, and effective method that provides virtual mapping capabilities to identify, map, and calculate the orientation of modelled discontinuities using the same experienced-based logical processes used in a traditional on-site approach (Haneberg, 2008).

2.3 Literature Research Approach

The second review done for this study is on the content used for literature-based approach, focusing on providing explanations regarding seismically-induced slope failures such as the cliff collapses at Redcliffs in the 22 February and 13 June 2011 earthquake. This topic of review includes, the nature of earthquakes (i.e. the influences behind ground shaking), and slope failure behaviour that will be used in order to:

- Explain the factors influenced the ground shaking intensity in the 22 February 2011 and 13 June 2011 earthquakes that made these two seismic events effective trigger mechanisms;

- Characterising the failure behaviour (i.e. the types of failure) involved in the collapse of Redcliffs' cliff in the 22 February 2011 and 13 June 2011 earthquakes.

2.3.1 Ground Shaking Intensity

There have been many studies done on the intensity of resultant ground motion from earthquakes, specifically pertaining to certain aspects of the geological environment surrounding the propagating waves, i.e. Site Effects; Path Effects; and Source Effects. Examples of literature discussing these effects on ground motion and seismic wave propagation include:

- Ben-Menahem & Singh (2000), Wood (2007) discuss the characteristics of attenuating ground motion the further seismic waves have to travel (Path Effect). Zhao et al. (1997) on the other hand, is an example of collecting peak ground acceleration (PGA) measurements around the world of multiple earthquakes to show the different rates of decrease in peak ground acceleration over distance for different fault types.
- Bradley (2012) discusses about forward directivity (Source Effect), which is the alignment of the rupture front, direction of slip, and source-to-site direction that increases the intensity of ground movement, and how it is relevant to the shaking felt in Christchurch during the Darfield (2010) Earthquake and the Christchurch (2011) Earthquakes.
- Spudich et al, (1999) demonstrates that reverse and thrust-faulting earthquakes (Source Effect) have relatively higher ground motions than compared to normal-faulting / strike-slip events in an extensional regime by comparing the severity of various earthquakes around the world caused by different fault types.
- Geli, et al. (1988) discuss about topographic amplification (Site Effect) by comparing the ground motion felt at the at the base of elevated topography and the ground acceleration measurements at the top of the hill in order to determine the distribution of amplification and deamplification on elevated terrain.

While these approaches to studying seismic shaking are appropriate to proving the Site Effects, Path Effects, and Source Effects influencing earthquake-induced ground motion, it is not the intention of this study to do so. Instead, this study intends to collate the fundamental principles shown in these studies and apply them to the

environment of Redcliffs' cliff and of the faults that ruptured on 22 February 2011 and 13 June 2011, in order to show how these two earthquakes subsequently caused the sever level of shaking felt on-site that triggered the collapses of Redcliffs' cliff.

2.3.2 Characterising Failure Behaviour

There are a number approaches identified that are typically used to characterise the failure behaviour a slope based on the controls that determine the resultant failure mode in response to destabilisation of the slope. These approaches either use observable characteristics or quantitative data to determine the likeliest mode(s) of failure to occur on a slope at the point of failure.

For instance, Day (2002) uses the block sizes found at the base of the slope (typically an accumulation that forms a talus) to determine whether rock fall and / or rock slides occurred in past failures, which suggests the likeliest potential failure mode in the event of the next failure incident. Goodman & Kieffer (2000) also proposes a similar method, using empirical observations to recognise modes of failure on a slope. However, instead of using blocks of rock found at the base of the slope, to determine whether rock fall or rock slide occurred, a correlation is made between failure modes and the types of materials (i.e. rock masses and soils known to have undergone such failure modes) to the types of rock masses and / or soil material identified on the slope of interest.

Kinematic analysis is an approach which uses the quantitative characteristics (dip and dip direction orientation) of discontinuities to analyse the potential for the various modes of rock slope failures (plane, wedge, toppling failures). It is a quantitative analysis based on the Markland's test, which suggests that "plane failure is likely to occur when a major discontinuity dips in the same direction (within 20°) as the slope face, at an angle gentler than the slope angle but greater than the friction angle along the failure plane" (Hoek & Bray, 1981).

Another discontinuity based method that is commonly used is based on the recognized density of discontinuities within the rock mass(es) of the slope. However, instead of determining whether a slope is likely to topple or slide, this approach determines whether the failure is structurally-controlled (Discontinuous) or under residual conditions (Equivalent Continuum). Typically used in rock tunnelling projects (Wu & Kulatilake, 2012; Barla & Barla, 2000), it can also be applied to discontinuous rock slopes as well (Wylie & Mah, 2004). An example of this approach

being used is Agliardi et al. (2013), who used a combination of kinematic analysis and the Equivalent Continuum vs. Discontinuum approach to determine the likely failure mode and control of the rock slope of interest.

2.4 Summary

Overall, this study requires two very different approaches towards investigating, or rather, studying the various aspects of Redcliffs' cliff collapsing in the 22 February 2011 and 13 June 2011 earthquakes. The types of literature that were reviewed to formulate the overall approach of this study include:

- Data-acquisition methods typically used when investigating a rock slope, typically done remotely if the site proves to be too dangerous to approach; and
- The topics that a literature-research approach covers when assessing the:
    - Severity of seismic shaking, focusing on specific environmental factors regarding site effects, source effects, path effects, and
    - The sorts of failure modes a rock slope that can occur at the point of failure that can be interpreted differently depending on which aspect of a rock slope is focused on.

Chapter Three: Data Collection Methods

3.1 Introduction

The following chapter is a brief outline of the method selection process carried out whilst choosing the appropriate methods based on site limitations and the resources available to conduct the field investigation. This chapter will present the: overall method selection process; and discuss about the site limitations faced when planning the field investigation, including how this subsequently influenced the approach towards surveying Redcliffs' cliff.

3.2 Selecting Methods for Data Collection

Development of the field methodology used in this project was done using a process of evaluation and testing of methods, using the methods reviewed in the literature review as a basis (Sections 2.2.2 and 2.2.3), to methodically evaluate the specific type of information / results needed for the adopted approach to study the seismically-induced collapse of Redcliffs' cliff, while also taking into consideration the restrictions imposed on-site. The general outline of this process is as follows:

Step 1: Evaluate Content and Methods

a) Identify the specific goals of the survey, i.e. what components of the slope needed to be outlined and classified.
b) Determine the corresponding types of field methods typically used to acquire the relevant data needed to describe parts of the slope identified in a)

Step 2: Feasibility Test (Field Reconnaissance)

c) Select from the refined list of methods, choosing remote methods first, and conduct preliminary tests with the chosen method(s) on-site. If successful in acquiring the necessary data, proceed with using the selected method. If not, repeat the start of d) and select another method.
d) For methods with no remote alternative, i.e. requires interaction with an outcrop, conduct a site reconnaissance to find an alternate representative / proxy site.

The outcome of following through with the two-step process was a survey methodology comprised of 12 methods (Table 2, Figure 13). Each method is described in further detail in Appendix I, including the specific type of equipment used.

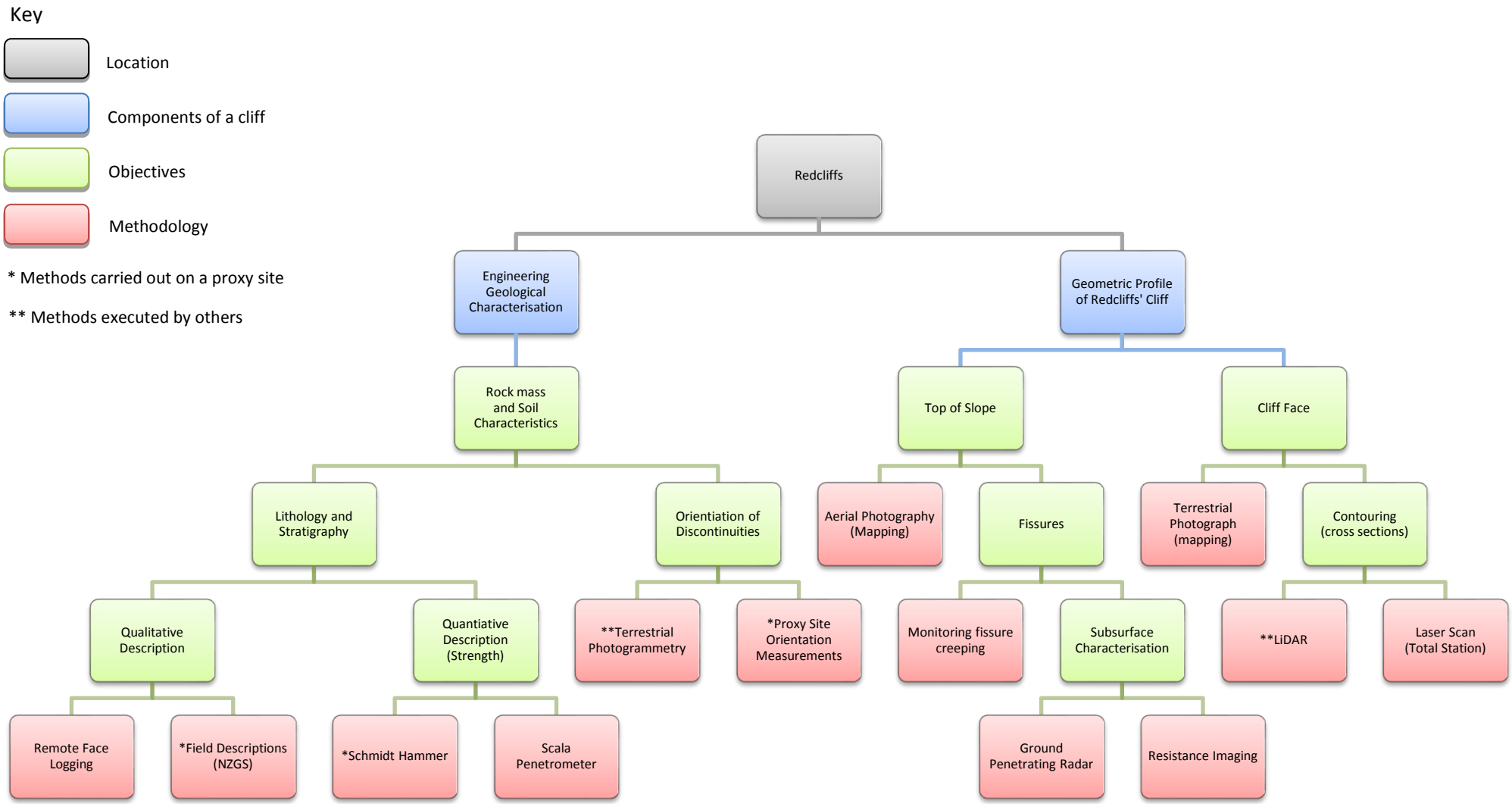

Figure 13 - Hierarchy chart summarizing the project data-acquisition methodology, highlighting the investigation objectives and relative methods chosen

Table 2 - Summary table of the methods selected to conduct the field investigation aspect of the study.

Selection of Methods			
Field Survey	Remote Face Logging (Part I, II)	Scala Penetrometer Test	Monitoring cliff top fissures
	Engineering Geological Description	Examining Aerial Photography	Ground Penetrating Radar
Resistance Tomography		Laser Scanning	Schmidt Hammer Test
		Aerial LiDAR Analysis	Terrestrial Photogrammetry

3.3 Addressing Site Limitations

While there were a number of factors to consider when dealing with the logistics of planning a field investigation, the main contributing factor which influenced the subsequent (predominantly indirect) approach towards surveying the cliff was the limitations surrounding the (in-) accessibility on-site; specifically, the proximity one could approach the cliff (face) without compromising the safety of being on-site. This was done as a safety precaution so as to address the risk of uncertainty behind the cliffs' (in-) stability after a major collapse.

At the time, the risk of approaching Redcliffs' cliff (post-failure) was deemed to be relatively high considering the M_w 6.2 earthquakes not only triggered a major collapse, but also could have weakened the rock mass(es) that had not detached from the slope. This meant that there is an even greater potential for further rock fall to occur either naturally (i.e. due to gravity), or re-activation due to aftershocks. Hence techniques that required outcrops to closely inspect / test on such as Engineering Geological Descriptions, and Schmidt Hammer Tests had to be done on another site which had matching characteristics as those observed on Redcliffs' cliff.

Initially, the only part of the cliff that was not accessible was the cliff face and the base of the cliff / head of the talus slope (Figure 14). However, these restrictions were later revised shortly after M_w 6.2 earthquake on 13 June 2011 to extend the boundary further outwards to the toe of the talus slope, and away from the cliff edge on top of the cliff.

Figure 2 - Illustrating the original site restrictions and the revised site restrictions after the June aftershock

3.3.1 Proxy Site Selection

As mentioned earlier, determining the engineering geological and geotechnical properties of the rock and soil units that make up the cliff was the only aspect of the investigation which required up close inspection of intact rock and soil samples (which requires outcrops). To address this need of an outcrop(s), a site reconnaissance was conducted to find another site which had the same lithology as that of the cliff. In the end, a proxy site was chosen on the other side of the hill, directly behind the cliff face, which consisted of outcrops in the form of roadside cuttings running up the hill (Figure 15).

Proxy Sites chosen to analyse rock and ash

Figure 15 - Aerial photograph highlighting the sections (road side cuttings) on the western hill, directly behind the cliff face used as a proxy site(s) to carry out surveying techniques which required access to an outcrop.

3.4 Summary

While this chapter is particularly short compared to the other chapters in this thesis, it is the most straightforward way to present the thought processes that went into selecting the methods to conduct the field investigation whilst considering the limitations of working on-site. The inaccessibility of the cliff face meant that additional steps were taken to work around this limitation, for the techniques which required outcrops to test on, in search for a supplementary proxy site on the other side of the hill to provide outcrops that resemble the lithology of the cliff.

Chapter Four: Characterisation of Redcliffs

4.1 Introduction

Characterising the properties of rock masses is an integral part of any geological investigation regarding a rock slope. Particularly in the field of engineering geology, characterisation of a slope is done by collecting empirical data that will contribute to both the quantitative and qualitative understanding of rock mass stability concerning the slope of interest; which in this case is Redcliffs' cliff.

For this project, the ultimate aim was to cross-examine the data collected in order to deduce the behaviour of Redcliffs' cliff in the event of a major earthquake, i.e. identify the mechanisms / controls that led to the collapse of the Redcliff's' cliff and isolate the changes that happened to the cliff face on 22 February and 13 June 2011. To accomplish such an aim, the engineering geological criteria for evaluating slope (in-) stability must first be established. This was done by conducting empirical field investigations, including field mapping and geotechnical surveys, aimed at developing a detailed engineering geological model of the cliff face.

The following chapter presents a (post-failure) characterisation of Redcliffs' cliff and cliff face using the survey data collected between the months of April and November 2011. Each result will focus on integral parts of the cliff that are applicable towards assessing the cliff collapsing, such as the geomechanics and external geometry of the near-vertical slope. Furthermore, the results will also reflect upon the effectiveness of the methodology used whilst surveying the cliff based on the quality of information that was ascertained from each qualitative and quantitative result.

4.2 Description of terminology

The list of terminology that will be used in this chapter is explained below.

- Surface Fractures – cracks that form on the cliff face as a result of a major earthquake / aftershock;
- Fissures – cracks that form on the ground (on top of the cliff) as a result of a major earthquake / aftershock;
- Fragmented slope – the term used to describe a cross section slope profile consisting of multiple major slope gradients;
- Uniform gradient – a cross section slope profile that has only one major gradient.

4.3 General Framework of Results

Considering the assortment of surveys conducted during the field investigation portion of this project, the results modelling the hillside are grouped accordingly into three main categories based on the three particular aspects of characterisation:

I. **Geological** – aimed at distinguishing between the main units of rock and soil, and grouping them based on their mechanical properties;
II. **Geotechnical** – focuses on assessing the mechanical behaviour through geomechanical characterisation of the intact rock samples, combined with the use of geotechnical classification systems;
III. **Geomorphological (localised)** – aims to address the physical changes to Redcliffs' cliff by determining particular geometrical changes to the cliff top and cliff face as a result of the cliff collapsing twice.

4.4 Geological Characterisation

Much like any other volcanic environments, due to its origins, the geology within the area of Redcliffs (cliff) and the rest of the Port Hills is heterogeneous, mainly comprised of volcanic rocks with various mechanical / chemical properties and random distribution patterns.

To address such a complex variation and distribution of the rocks and soils at the site, a simplistic approach was implemented at first to divide the units exposed on the cliff face into generalised rock and soil categories (Figure 16). This was followed by further grouping the units by classifying the characteristics observed of each unit identified and estimating the proportions of each unit residing within the cliff. The result of this approach isolated five geological units within the cliff face (Figures 17 and 18); however, only four of these were successfully classified. In summary,

- There are five identified units that make up the entire cliff face, four of which are exposed on the cliff face and one unit hidden behind the talus.
- The stratum of the cliff face contains one unit of soil overlaying a main body of rock containing three types of volcanic deposits.

The overlying soil is an organic top soil mixed with wind-blown loess, a common surface deposit found throughout the Canterbury Region. In the case of Redcliff's cliff, it covers the top 5-8 % of the top of the cliff.

Figure 16 – Annotated photograph of Redcliffs' cliff (courtesy of Rob Hunter from Tonkin & Taylor) highlighting the boundaries of each individual units mapped on the freshly exposed cliff face and the allocated NE and SE Face labels for the two sections of the cliff facing perpendicular to each other.

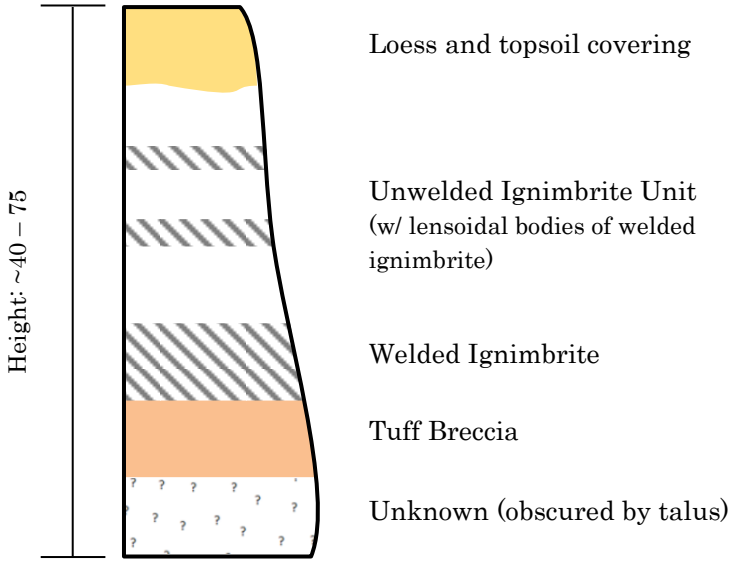

Figure 17 – Generalised stratigraphic column illustrating the wide-ranging stratigraphy of the geological units present within the Redcliffs' cliff face. The thicknesses of each unit are not presented on this figure due to the variability of each unit across the cliff (see Figure 3).

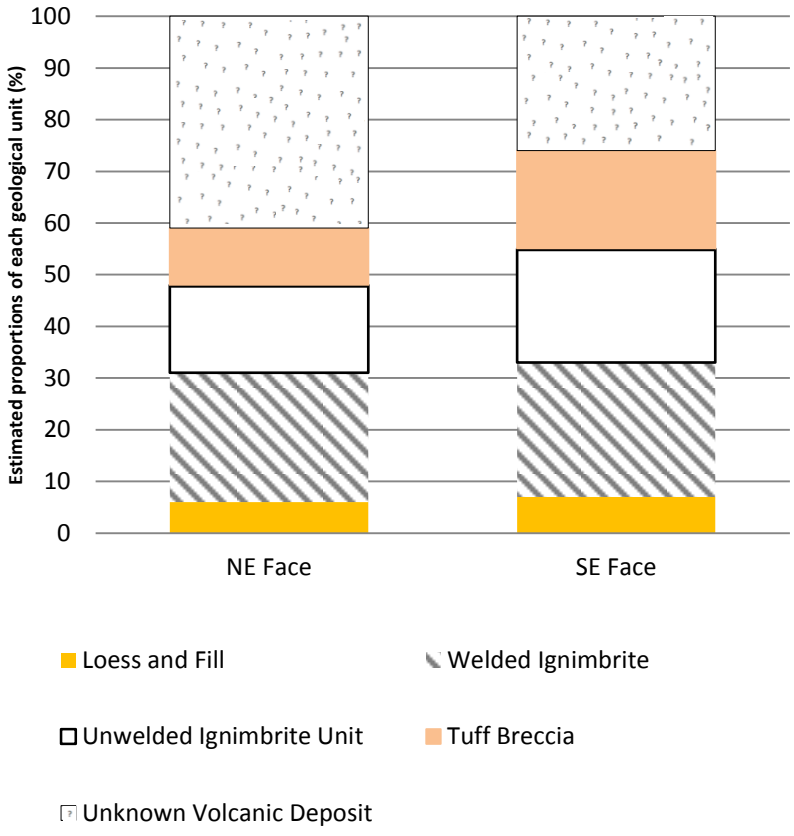

Figure 18 – A graph illustrating the percentage based approximations made by breaking down the cliff into its geological composition. To further elaborate on the axes: the NE and SE faces represent the two slopes segments which make up the cliff; while 100% represents the entirety of each segment of the cliff.

The main body of rock is comprised of welded and unwelded ignimbrite, and a layer of tuff breccia, making up between 50 – 60 % of the cliff face. These volcanic deposits are commonly found on the hilly north-west side of Banks Peninsula, which amassed as a result of multiple eruptions of the Lyttelton Volcano during the late Miocene to form the Mt. Pleasant Formation (Altaye, 1989; Hampton, 2011).

Furthermore, there is a fifth (unknown) geological unit present beneath the three layers of basalt rock and tuff. While it makes up the lower 30 – 40% part of the cliff face (Figure 18), it is labelled as an "unknown" because of the inability neither to examine it at a distance away from the cliff face (as it is obstructed by the talus), nor to access an outcrop nearby to identify up close what it is. Drilling information was not available at this site.

4.5 Geotechnical Characterisation

After completing a brief geological characterisation, the next step was to elaborate on the rock and soil components identified. This was done by determining the geotechnical properties of each respective geological unit, using five different qualitative and quantitative classification techniques:

I. NZGS Field description of soil and rock (Muschamps, 2005);
II. Geological Strength Index;
III. Hoek-Brown and Barton-Bandis Criterion;
IV. Photogrammetry;
V. Scala Penetrometer;

Out of these five methods, only four of which are field-surveying techniques, which were used to collect data on-site; while the last technique (i.e. Hoek-Brown and Barton-Bandis Criterion) uses a predetermined database of quantitative data to calculate certain strength properties within a rockmass, given certain field- or lab-derived parameters.

The first technique used was the NZGS field description guide, developed by Muschamps (2005), to conduct a geotechnical field survey. It was chosen as a starting point because, as a fundamental technique most commonly used by engineering geologists in New Zealand, the guide covers all the necessary properties within soil and rock that need to be characterised. However, not only was the NZGS-framed field survey a starting point, it was also the main focal point behind the

follow-up approaches used to characterise the geotechnical properties of Redcliffs' cliff (Figure 19), whereby the four remaining techniques used were merely supplementary techniques that either:

a) Verified certain attributes proposed from surveying the proxy-site (i.e. photogrammetry); and / or
b) Further supported the characterisation of certain rock / soil characteristics (i.e. GSI, Scala Penetrometer, Hoek-Brown and Barton Bandis Criterion).

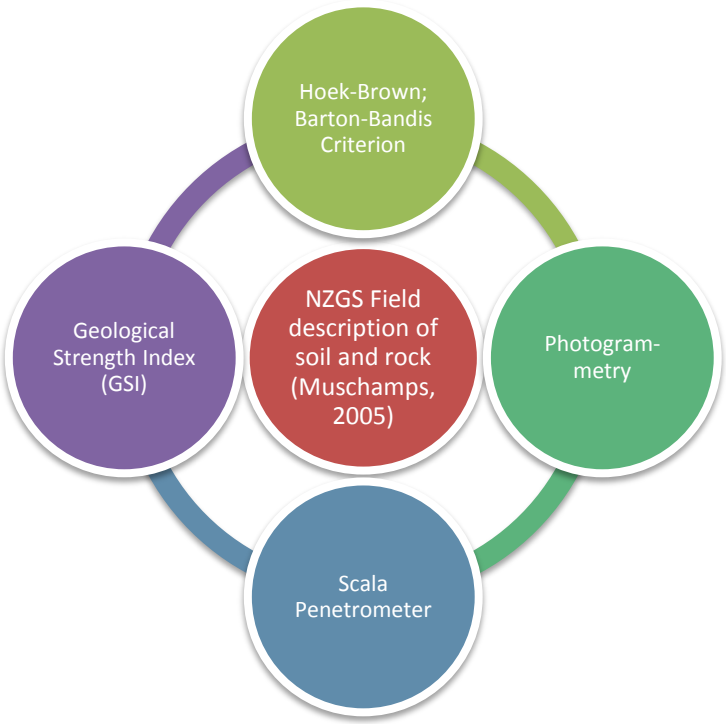

Figure 19 - A diagram illustrating the relevance of the techniques used to characterise the geotechnical characteristics of Redcliffs' cliff.

To present the results of this (predominantly field-based) investigation, the results are group into their respective rock and soil categories. Within each category, the descriptions using the general classification method (i.e. NZGS field description guide) are first presented, followed by the results of the subsidary techniques.

4.5.1 Volcanic Rockmasses

The first four (out of the five) techniques listed previously were used to assess the geotechnical characteristics of the rock masses that make up Redcliffs' cliff. Out of these four, only the Geological Strength Index (GSI) and orientation of the rock mass joints could be done remotely; whereas the remaining two (including the NZGS field descriptions) required contact with an outcrop(s), as they are physical / mechanical characterisation tests that determine geotechnical properties such as the strength of the rock masses, and of the joints surfaces.

As stated in Section 3.3.1, a proxy-site was used instead to conduct the characterisation tests when the need for intact rock samples arose (Figure 20).

Figure 20 - Satellite image of Redcliffs highlighting the soil survey sites and the proxy-sites used to conduct the rock characterisation tests (Google, 2010). The red lines running along the road are the roadside cuttings / outcrops used as a proxy site.

NZGS Field Descriptions

There are three volcanically-sourced rock components that comprise over two-thirds of the (recently) exposed cliff face (Tables 3 – 5). These include:

- Slightly-to-moderately weathered, dark greenish grey WELDED IGNIMBRITE; (overall) Very strong but slightly weaker in non-welded segments, joints vary from closely spaced to wide (>10 m) [MT. PLEASANT formation]
- Slightly-to-moderately weathered, yellowish grey UNWELDED IGNIMBRITE; Strong, exfoliation jointing [MT. PLEASANT formation]
- Slightly-to-moderately weathered, oxidised reddish brown TUFF BRECCIA; moderately strong, entire unit comprised of thinly bedded divisions [MT. PLEASANT formation]

Table 3- Summary table characterising the welded ignimbrite component of Redcliffs' cliff using the NZGS field description guide (Muschamps, 2005)

Features		Comments
Weathering	Slightly – moderately weathered	Aside from the thick (main) flows, individual thin (minor) flows in the form of lensoidal bodies are also found present in the cliff face, estimated to be up to ~5 m thick.
Colour	Dark greenish grey	
Fabric		
Rock Name	Welded Ignimbrite	
Qualifying Features		
Strength	Strong– very strong*	There are welded and non-welded components within the ignimbrite, which means it has two different mechanical characteristics within the same volcanic rockmass – the latter being the weaker of the two. It is also the only unit with a complex system of (well-developed) joints observed on the cliff face. Contact is gradational between the blocks and the lava breccia.
Discontinuities	Comprises of joints that form perpendicular to the surface. Spacing of the joints ranges between 1.5 – 25 m; with the narrow(er) spacing exhibiting predominantly prismatic (columnar) / tabular (subangular) shaped blocks of varying sizes. Persistence also varies depending on size of the flow(s), from a few meters up 10 – 20 m, and tends to terminate at another joint. Joint surface(s) are generally rough; varying between planar / stepped / undulating; tight – moderately narrow aperture; considered to have a manganese oxide or calcite coating; and not likely to contain clay or silt fill.	
Geological Information	Eruptive Phase IX (Mt. Pleasant Formation)	

*Strength characterised based on surveys done on the proxy site

Table 4 - Summary table characterising the unwelded ignimbrite (breccia) component of Redcliffs' cliff using the NZGS field description guide (Muschamps, 2005)

Features		Comments
Weathering	Slightly – Moderately Weathered	Variably fine to coarse matrix, poorly graded, contains angular – subangular broken lava fragments. Fragments suggest vesicular and scoriaceous attributes, thus suggesting being susceptible to weathering due to porosity.
Colour	Yellowish Grey	
Fabric		
Rock Name	Unwelded Ignimbrite	
Qualifying Features		
Strength	Moderately Strong – Strong*	In the far eastern end of the cliff face, there are blocks of rock that appear to be somewhat hollowed-out with rounded edges are likely to be the result of weathering of the exposed unwelded material.
Discontinuities	Predominantly massive, poorly jointed with cases of exfoliation joints/cracks observed on cliff face that run along the strike of the cliff face.	
Geological Information	Eruptive Phase IX (Mt. Pleasant Formation)	

*Strength characterised based on surveys done on the proxy site

Table 5 - Summary table characterising the cemented tuff component of Redcliffs' cliff using the NZGS field description guide (Muschamps, 2005)

Features		Comments
Weathering	Moderately weathered	The proxy site suggests that a bake zone is present between top of the tuff layer and the overlying welded ignimbrite (being part-breccia); where the contact zone is also gradational into the brecciated basaltic unit.
Colour	Oxidised reddish brown	
Fabric		
Rock Name	Tuff	
Qualifying Features		
Strength	Weak – Moderately Strong*	Bedding appears to be continuous and varies along the cliff face with the exposed areas estimated to be between 1 - 3 m thick in total with individual layers present within the tuff unit. Strength of tuff varies depending on the level of weathering as the exposed tuff is typically weak to moderately strong, unless it is highly weathered then it is very weak and friable; thus the exposed surfaces are very prone to cracking and easily eroded.
Discontinuities	A series of small bedding planes, and fractures found within the exposed unit of tuff. Otherwise can be considered a massive unit considering no jointing present within the rock mass.	
Geological Information	Eruptive Phase IX (Mt. Pleasant Formation)	

*Strength characterised based on surveys done on the proxy site

Weathering

Based on empirical observation of the cliff face, from aerial photographs taken and on-site accounts, grades of weathering were given to classify the weathering conditions of the rock masses shown on cliff face before and after the 22 February and 13 June 2011 collapse. The grading was done based on the classification guidelines of Muschamp (2005). The results are as follows (Table 6).

Table 6 - Weathering grades of cliff face before and after the collapse in the 22 February 2011 and 13 June 2011 earthquakes. Grading is only presented for the overall cliff face since inspection of the site remotely suggests no significant difference between individual rock masses when survey across the NE and SE slope aspects.

		Grade	Abbreviation
22 February 2011	Before	III	MW
	After	I	UW
13 June 2011	Before	I – II	UW – SW
	After	I	UW

The grade of weathering before the first collapse in February was considered moderately weathered (MW). While it was not possible to gather on-site accounts of the slope condition prior to 22 February 2011, the satellite imagery taken of Redcliffs' cliff before the February collapse shows a cliff face covered in vegetation (i.e. trees and bushes) (Figure 21). This suggests the majority slope surface has the capability to sustain vegetation growth, which is only possible (in part) if part of the rock masses on the cliff face breaks down into soil.

Naturally, there is no weathering of the surface of the cliff face immediately after a collapse; therefore, the cliff face is considered unweathered (fresh). However, prior to the collapse in June 2011, some discolouration of the rock masses was noted on the cliff face which suggests slight weathering of the rock masses after being exposed for roughly four months (post-February 2011 collapse).

Geological Strength Index (GSI)

In addition to the NZGS field descriptions, a second observation-based technique using the geological strength index (GSI; Hoek et al., 2002) was also used concurrently to further characterise the nature of the volcanic rock sequence.

After thoroughly surveying the cliff face, and inspecting airborne photographs taken of the cliff before and after the 22 February and 13 June 2011 (M_w 6.2) earthquake,

Pre-22 February 2011

Post-22 February 2011

Post-13 June 2011

Figure 21 – Satellite images taken before and after the February 2011 collapse and post-June 2011 collapse of Redcliffs' cliff (Google, 2010). It is clear based on the satellite images that before the collapse in the 22 February 2011 earthquake that the cliff face had remain stable for a significant amount of time considering the flourish of vegetation seen across the cliff face and the weathered discolouration of the rock masses.

it was concluded that there is variability across the cliff face at three different sample scales (before each collapsing incident): the overall slope; between the NE and SE Face; and within each rock mass (within the respective slope aspect).

To address this variable nature of the intact cliff material at different moments in time, all chosen GSI estimations for each unit of rock was given as a range instead of a definitive GSI unit (Figure 22).

GIS: NE Face vs. SE Face

Based on the degree of variability, looking at the post-February and post-June 2011 conditions of the cliff face, the unwelded ignimbrite has by far the greatest difference in terms of structure and condition of the slope between the NE and SE Faces.

For the most part, starting from the western end of the cliff, the unwelded ignimbrite has a (predominantly) massive – (slightly) blocky structure. However, while the condition of a majority of the slope is consistent, the condition of the unit at the far eastern tip of the cliff appears to have altered into a unit comprising of irregular exfoliation joints, with a rougher joint surface, and large angular blocks (Figure 23). There is no known explanation as to why the surface properties of this particular part of the cliff had changed. Although the notion of figuring out why is beyond the scope of this study, it was hypothesised that the changes may be related to the positioning of that particular slope aspect, which may have influenced on the rate of erosion at that section of the cliff face.

Structural changes are also evident for the welded ignimbrite, but not as severe as the unwelded ignimbrite. Comparing the NE and SE Faces, not including the small lensoidal bodies, the persistence of the joints on the NE Face are shorter than those on the SE Face, thus making smaller blocks. In contrast, the joints on the NE Face are less rounded and not as sharp, thus making the blocks appear to have "straighter" edge(s), if joints are prominent enough, and are thus more columnar-shaped (Figure 24). The only unit that did not exhibit an inconsistent structure and/or condition of the rock mass is the unit of tuff breccia as it appears to maintain a predominantly intact – blocky structure with a poor to good surface condition. However, it should be noted that there is a difference between what was observed on the cliff face and on the proxy-site; whereby the proxy-site outcrop appears to be more brecciated with more prominent evidence of large subangular blocks of broken lava embedded within the tuff matrix (Figure 24).

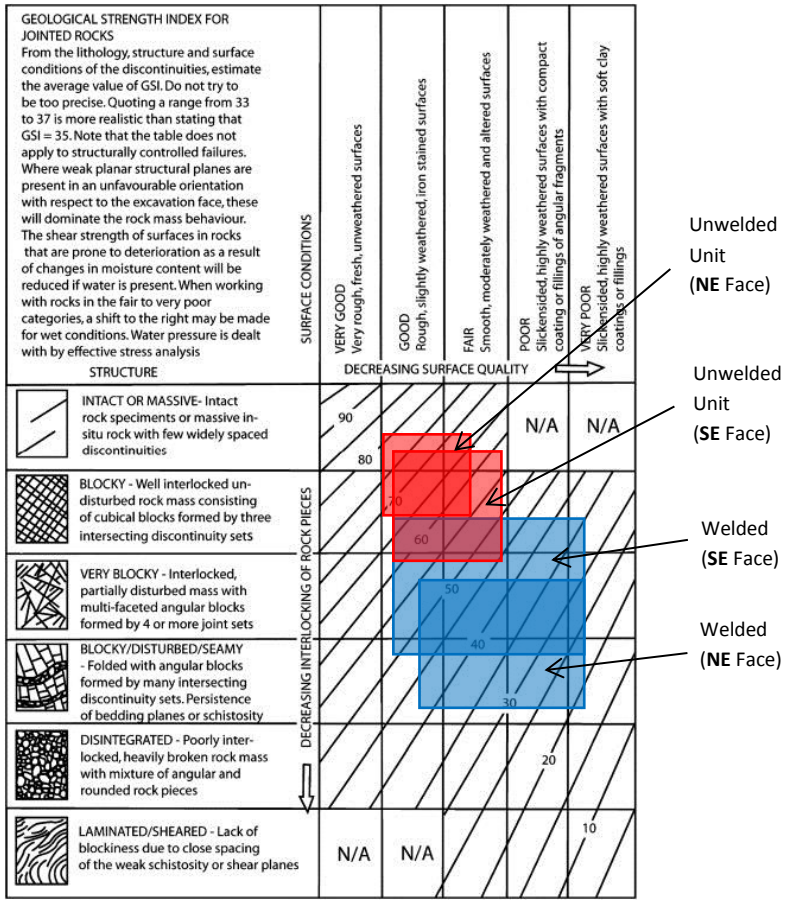

(Post- 22 February 2011)	Unwelded Ignimbrite	Welded Ignimbrite
NE Face:	~ 55 – 82	~ 18 – 45
SE Face:	~ 45 – 77	~ 23 – 67

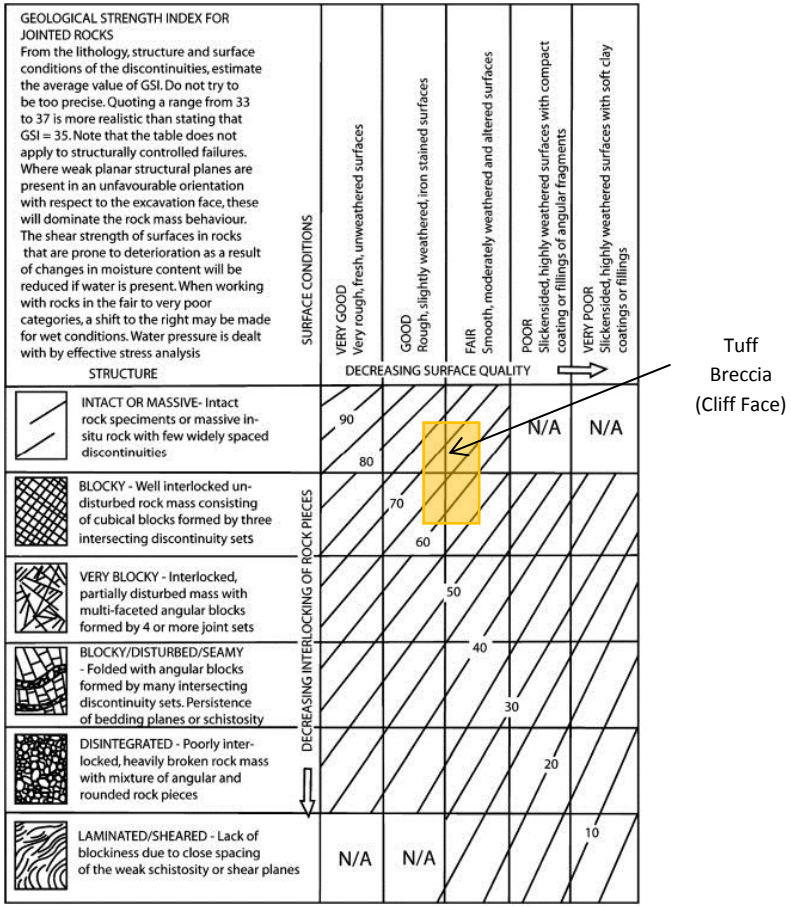

(Post- 22 February 2011)	Cliff Face and Proxy-Site
Tuff:	~ 54 – 77

Figure 22 – Estimated range of GSI values for the unwelded, welded ignimbrite, and tuff units taking into consideration of on the (weathered) pre- and post-collapse conditions of cliff face (modified after Hoek et al., 2002)

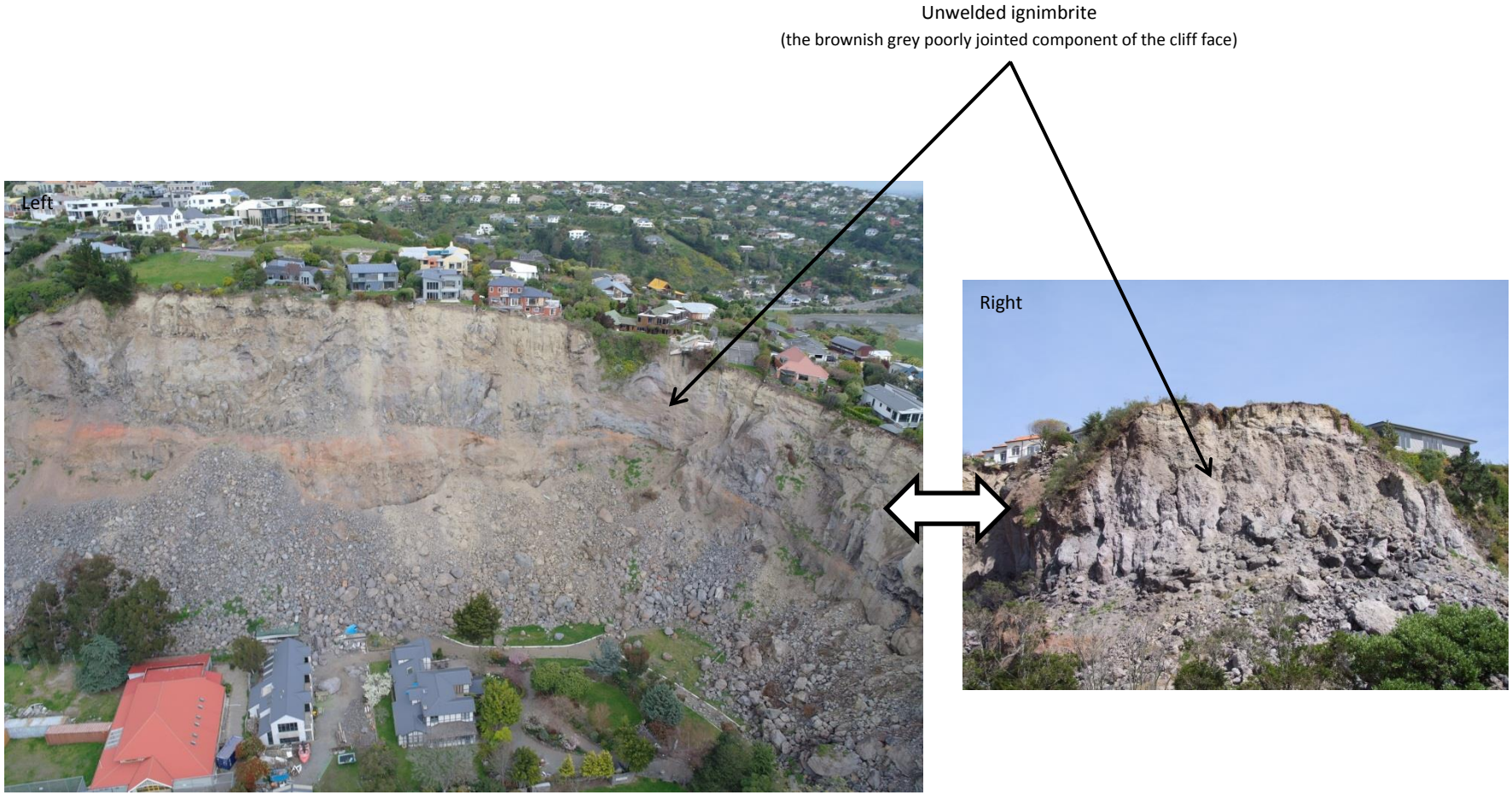

Figure 23 - A comparison between a majority of the cliff face and the far eastern tip in terms of the structure and condition of the unwelded ignimbrite. For the majority of the cliff face (left), the unwelded ignimbrite appears to be lacking in jointing, whereas the eastern tip (right) appears to have a large number of what seems to be exfoliation joints defining tabular-like blocks within the slope.

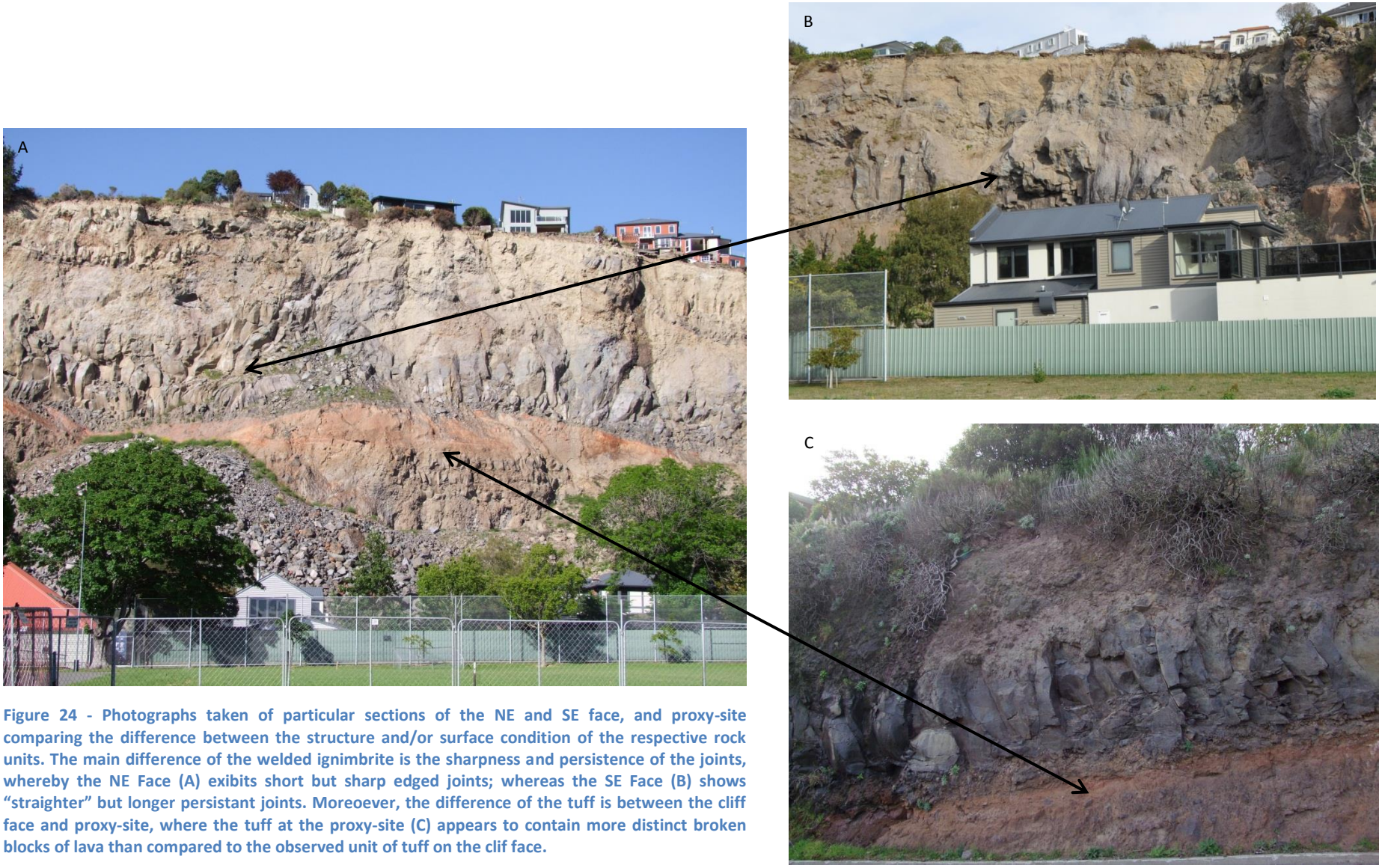

Figure 24 - Photographs taken of particular sections of the NE and SE face, and proxy-site comparing the difference between the structure and/or surface condition of the respective rock units. The main difference of the welded ignimbrite is the sharpness and persistence of the joints, whereby the NE Face (A) exibits short but sharp edged joints; whereas the SE Face (B) shows "straighter" but longer persistant joints. Moreoever, the difference of the tuff is between the cliff face and proxy-site, where the tuff at the proxy-site (C) appears to contain more distinct broken blocks of lava than compared to the observed unit of tuff on the clif face.

However, without being able to inspect the unit of tuff on the cliff face up close, it was not possible to conclusively decide whether there is an actual significant difference in terms of the structure and concentration of lava fragments between the tuff exposed on the cliff and at the proxy-site.

Schmidt Hammer Test

The strength test conducted in the field required the use of an L-Schmidt Hammer. It was a simple index test used to determine the surface strength of rock samples. The test was carried out at the proxy site, collecting rebound (index) values that are converted to compressive strength values.

However, the method could only be applied to the jointed blocks of welded ignimbrite as the unwelded ignimbrite and tuff outcrops along the roadside cuttings lacked the necessary levelled joint surface to take measurements from. Particular attention was also made when selecting samples to test on since it was a test done on a representative outcrop. This meant it had to match the graded conditions according to the GSI values representing the ignimbrite blocks on the cliff face (Figure 25).

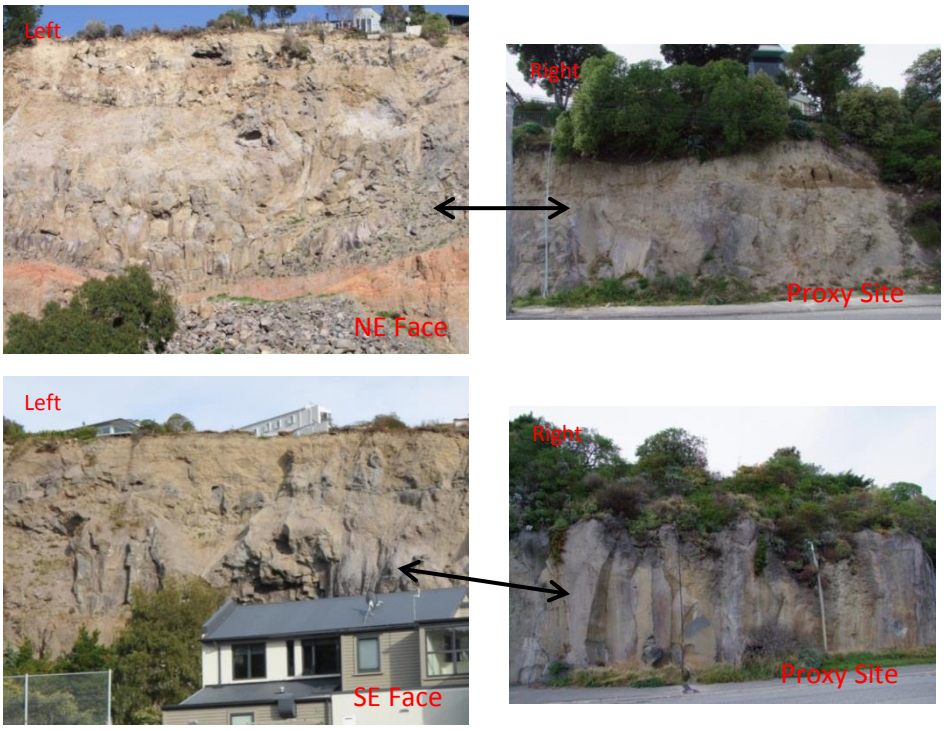

Figure 25 - Photographs comparing between the jointed blocks of welded ignimbrite on the cliff face (left) and the proxy-site outcrops (right) of the same unit chosen to represent the cliff to conduct a Schmidt Hammer test.

A total of 150 rebound measurements (R) were taken on a number of welded ignimbrite joint surfaces, at multiple orientations. The tabulated results show the

majority of the R values are ≥ 30, with the highest concentration (72 out of 150) found within the index rebound range of 40 – 50 (Figure 26).

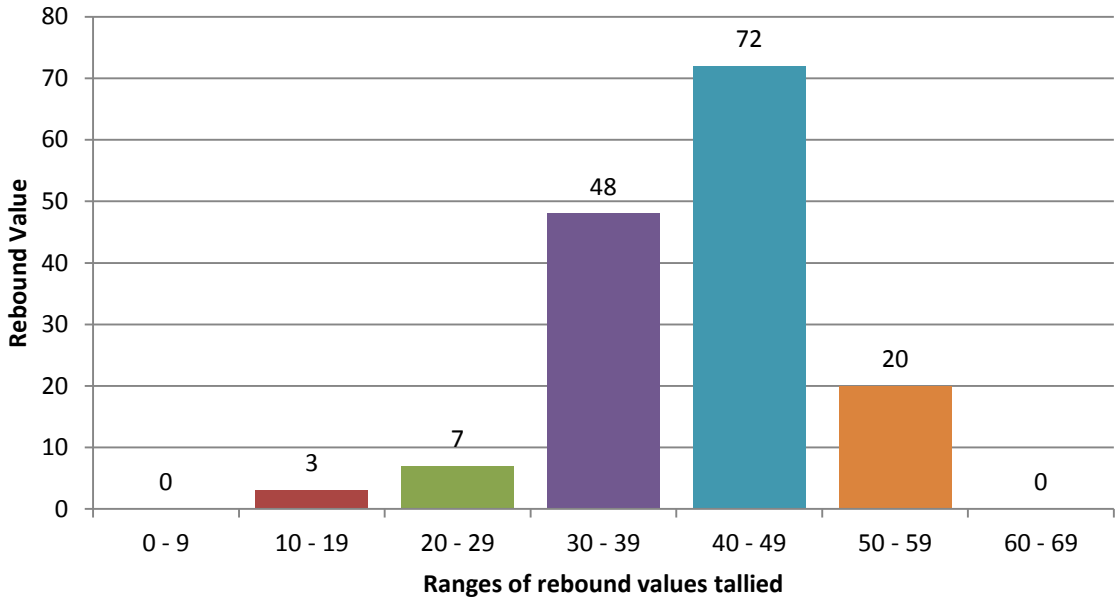

Figure 26 – Tally of R values illustrating the spread of 150 R-values measured at the proxy site on welded ignimbrite.

Table 7 summarizes the results of a statistical analysis conducted on the spread of R values collected, showing the results of the two most common orientations measured and the overall measurements (combining all orientations). Based on the results, it is clear that the average rebound value is ~41, which is lower than the combined mode, and far lower than what was expected based on field strength estimates of the rock mass.

Table 7 - L-Schmidt Rebound values for oriented (R value) Schmidt Hammer measurements. Note, only two orientations are presented individually since nearly all the surfaces measured on were dipping in a near-vertical orientation.

		L-Schmidt Hammer Rebound Value (R)		
		←	↙	Combined (including the negligible orientations)
Average		41	42	41
Median		40	43	42
Mode		48	38	48
Range	Min	20	30	30
	Max	54	53	55
Standard Deviation		7.32	5.39	7.57

From a mathematical standpoint, the low average can be explained by the high standard deviation, suggesting the values are spread out over a large range. This large range is likely attributed to the variable condition of the joint surfaces of different blocks, with the lower R values taken from blocks of rock with much weaker joint surfaces. While the cause of weakening the joint surfaces is not fully known, it is most likely caused by a combination of external factors such as weathering of the exposed blocks, with different blocks weathered / weakened at different rates.

UCS and JCS Conversion

The average R values were used to estimate the strength of the welded ignimbrite, specifically the uniaxial compressive strength (UCS) of intact rock and joint wall compressive strength (JCS). This was done because of the difference in strength and degree of weathering between the intact rock and joint surface of the same rock sample (Johansson, 2003).

If the joint wall is unaffected by weathering, its strength equals the strength of the intact rock (i.e. UCS = JCS). On the other hand, assuming there was extensive weathering and saturation of the rock sample, the joint wall strength would decrease, which means a contrast in compressive strength values between the intact rock and joint surface, necessitating another strength variable expressed as JCS (Barton, 1973). To convert the respective R values into JCS and UCS values, the values acquired to do the conversion are as follows:

- Since it was not possible to determine the density of the welded ignimbrite rock mass, the value had to be sourced from other reliable means. Hence, the assumed density of basaltic welded ignimbrite is estimated to be 29 kN/m^3 based on measurements taken by Freundt & Schmincke (1995) as the characteristics of basaltic welded ignimbrite described in the paper is similar to that found at Redcliffs.
- Both values from the two hammer orientations are used instead of only one in order to propose a potential strength range rather than a definitive strength value of the welded ignimbrite.
- Based on the measurements taken, it is believed that the average R values represents a weaker joint surface that does not correspond to the condition of the intact rock mass; therefore, the overall averages were only used to calculate JCS.

- On the other hand, the upper (50 – 59) range of R values represents a group of samples that are not as weak and therefore would provide a closer representation of the strong - very strong intact rock (as described earlier based on the NZGS field descriptions of the welded ignimbrite), hence the average of the 50 – 59 range of R values (which is 51 for both hammer orientations) was used to determine the estimated UCS range.

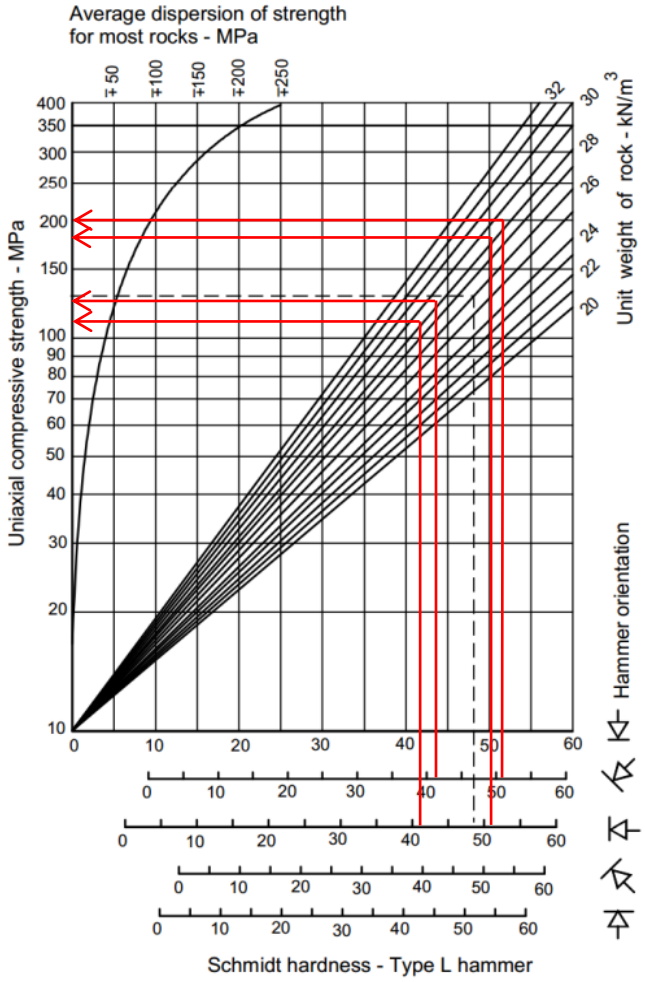

Table 8 - Summary table showing the estimated JCS values.

Joint wall compressive strength (JCS)		
Orientation	R Values	JCS (MPa)
	41	110
	42	130

Table 9 - Summary table showing the estimated UCS values.

Uniaxial compressive strength (UCS)		
Orientation	R Values	UCS (MPa)
	51	185
	51	200

Figure 27 - Conversion graph for an L-Schmidt Hammer (modified from Hoek, 2007) used to determine the UCS and JCS of welded ignimbrite. Summary tables of the estimated values are shown on Table 8 and 9.

The results shown above in Figure 27, and summarized in Tables 8 and 9, indicate that the welded ignimbrite has a high compressive strength range with an estimated JCS: 110 – 130 MPa, and UCS: 185 – 200 MPa. These high JCS and UCS ranges were expected as initial field descriptions (using the NZGS field guidelines) suggested the UCS of a strong – very strong rock to be around 50 – 250 MPa, of which both conversion results fall within this range.

Hoek-Brown and Barton-Bandis Criterion

The aim for the geotechnical section of this field investigation is to determine the rock mass and joint strength parameters using the empirical rock mass data collected at Redcliffs, specifically for the:

- Barton-Bandis Criterion (EQ 2; ϕ_b, JRC, JCS)

$$T' = \delta'_n tan\left[\emptyset_b + JRC log_{10}\left(\frac{JCS}{\delta'_n}\right)\right] \quad \text{(EQ 2)}$$

Where ϕ_b is the base friction angle for rocks; JRC is the joint roughness coefficient; JCS is the joint compressive strength (Hoek et al., 2002). The results are as follows (Table 10):

Table 10 - The Barton-Bandis Criterion Parameters

	Barton-Bandis Criterion		
	ϕ_b (°)	JRC	JCS (MPa)
Welded Ignimbrite	36.5[1]	13	120

[1]this parameter was derived using the rock mass a database in *RocData*, matching the rock type with the corresponding basic friction angle.

- Generalised Hoek-Brown Criterion (EQ3; m_b, s, a)

$$\delta'_1 = \delta'_3\left(m_b\frac{\delta'_3}{\delta_c} + s\right)^a \quad \text{(EQ 3)}$$

where σ_{ci} is the unconfined compressive strength (UCS) of the intact rock; σ'_1 and σ'_3 are, respectively, the major and minor effective principal stresses; m_b, s, and a are rock mass constants, which can be calculated using the following equations (EQ 4 – 6) (Hoek et al., 2002):

$$m_b = exp\left(\frac{GSI-100}{28-14D}\right)m_i \quad \text{(EQ 4)}$$

$$s = exp\left(\frac{GSI-100}{9-3D}\right)m_i \quad \text{(EQ 5)}$$

$$a = 0.5 + \frac{1}{6}[exp(-GSI/15) - exp(-20/3)] \quad \text{(EQ 6)}$$

GSI is the geological strength index; mi is the intact rock parameter; and D is the disturbance factor. The results of the calculations are as follows (Table 11):

Table 11 - The input parameters and resulting (calculated) Generalised Hoek-Brown Criterion parameters

		Parameters			Generalised Hoek-Brown Criterion		
		UCS (MPa)	GSI	m_i	m_b	s	a
Welded Ignimbrite	NE Face	193	38	25	2.731	0.001	0.513
	SE Face		45		3.506	0.0022	0.508
Unwelded Ignimbrite	NE Face	75[2]	69	20	6.61	0.0319	0.501
	SE Face		60		4.793	0.0117	0.503
Tuff		25[2]	65	13	3.725	0.0205	0.502

[2] theses input parameters used in the calculation were derived from a database in *RocData*, which matches field based estimation of strength with a predetermined UCS value.

The summary tables presented above (Tables 10 and 11) are a compilation of the expected parameter values for: the General Hoek-Brown Criterion of the unwelded, welded ignimbrite, and tuff; and the Barton-Bandis Criterion based on the data collected either on-site, or through other means to derive the parameters needed when quantitative field data was not attainable. As briefly mentioned in the captions at the bottom of the result tables, part of the variables were derived using *RocData*, computer software that not only determines soil and rock mass strength parameters but also contains a database of qualitative parameters for various sorts of rock masses that are correlated with field-based descriptions.

Terrestrial Photogrammetry

Terrestrial photogrammetry was aimed at further characterising the jointed ignimbrite. The process begins with five digital photogrammetric pairs of data, provided by Marc-Andre Brideau (who surveyed the cliff face shortly after the June earthquake), converted into a number of three-dimensional models (Brideau, 2011). These models were then used to measure the orientation of joints presented in the form of planes and traces, whereby:

- Planes represent discontinuities that were defined from the model surface; and
- Traces represent the partial of a discontinuity identified from the 3D model.

A total of 433 measurements made across the entire cliff face and plotted onto six stereonets, labelled as Photogrammetry Face 1-5, based on the sections of the cliff scanned (Figure 28). Processing of the data takes place using a computer program called *Dips*, which produced one summary stereronet, combining all the measurements taken (Figure 29), and six individual stereonets, (Appendix II).In addition, nine dip / dip direction measurements were also made at the proxy-site welded ignimbrite to complement the remote survey measurements to compare the similarities of the joint orientation between the two sites (Figure 30).

Figure 28 – Annotated satellite image of the cliff face showing sections (1 – 5) of the cliff scanned using photogrammetry

Figure 31 summarizes all the joint sets isolated while analysing the various stereonets, revealing distribution patterns. The most obvious pattern of which is that majority of the dip of the joints are> 60° and a small minority are < 30°. This array of steeply / near-horizontal dipping joints supports the observation that the welded ignimbrite has steeply dipping (columnar) joints, as well as cross-joints, i.e. irregular intersecting joints that are roughly perpendicular to the prism axis (Spry, 1962), which influences the persistence of the near-vertical joints, and thus the overall size of the intact block.

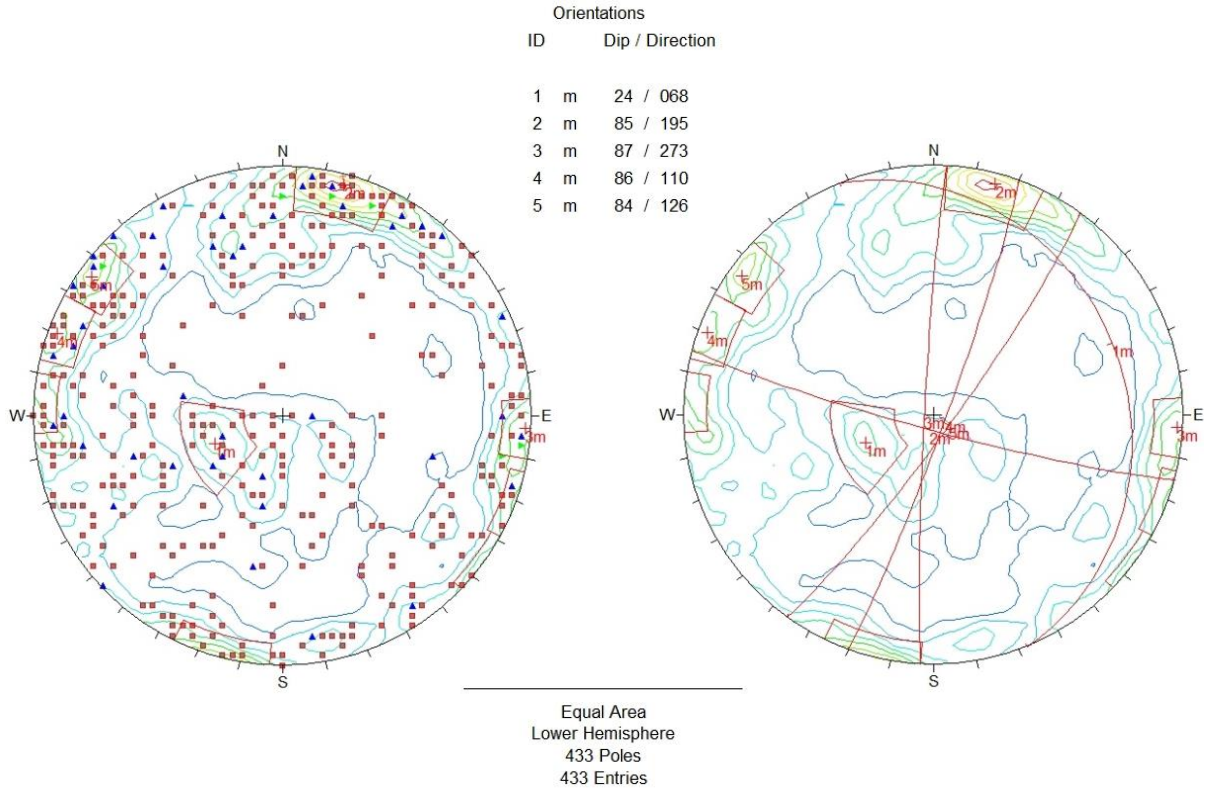

Figure 29 – Stereonets representing all 433 poles derived from plane and trace measurements taken from all the 3D photogrammetry models. The left stereonet shows the individual plots and the sets selected based on the concentrations of plots. The right stereonet shows the resulting planes drawn based on the sets selected.

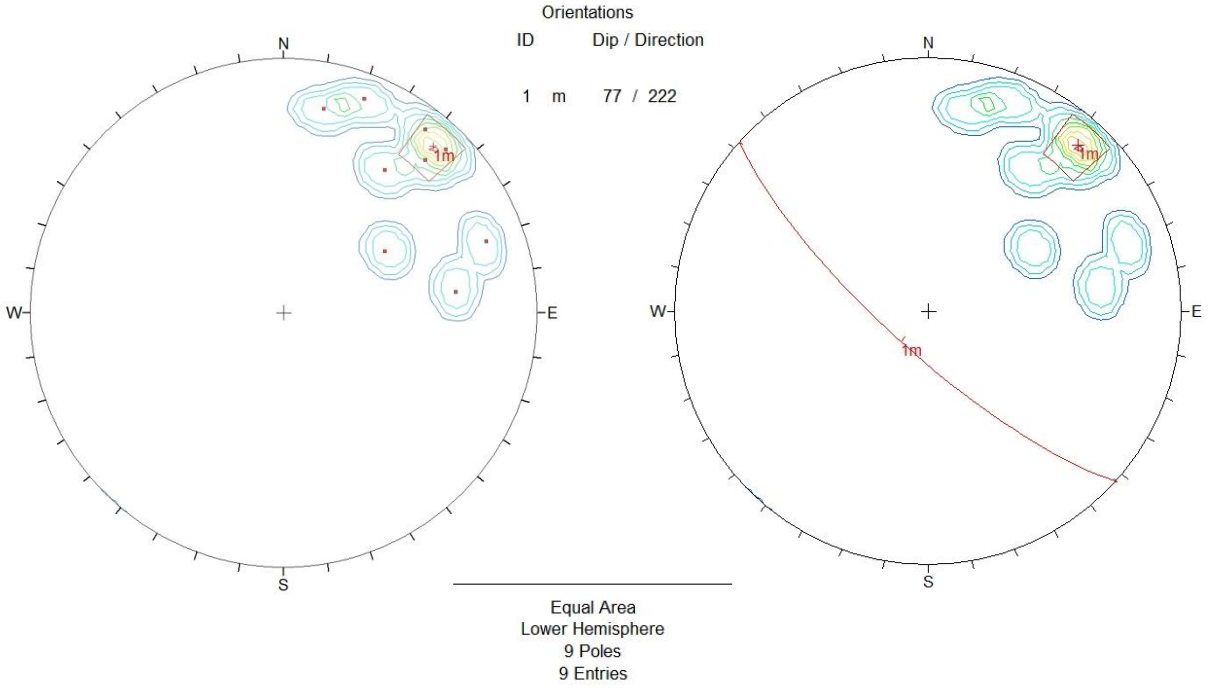

Figure 30 - Stereonets representing welded ignimbrite dip / dip direction measurements made at the proxy site. The left stereonet shows the individual plots and the sets selected based on the concentrations of plots, and the right stereonet shows the resulting planes drawn based on the sets selected.

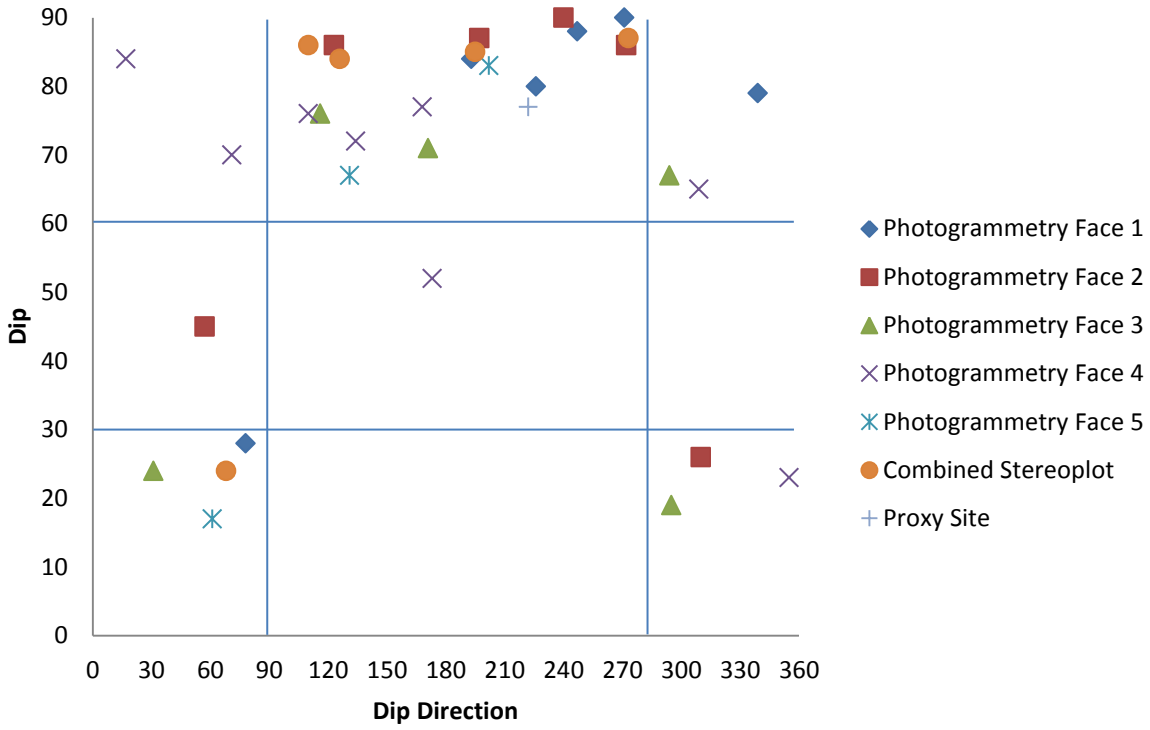

Figure 30 - Graph summarizing the distribution of discontinuity sets identified while analysing dip/dip direction data using *Dips*.

The dip directions of the discontinuities reveal a secondary pattern concerning the main discontinuity sets. For the steeply dipping joints, a majority of them have an orientation within the range of 90° – 280°, which suggests the joints generally dip to the south. In terms of an E-W dipping orientation (with respect to the south), while Face 2 have joint sets facing in either direction, it seems that Faces 3 and 4 of the cliff face favours a more SE direction, whereas Faces 1 and 5 favour a SW direction.

Moreover, as for the near-horizontal discontinuity sets, there is a contrast in orientation compared to the steeply dipping joints, whereby the cross-joints dip in the general north direction, with Photogrammetry Faces 1 and 5 favouring the NE, Faces 2 and 4 favouring the NW, and Face 3 favouring both directions. It was initially thought that these near-horizontal discontinuities were merely cross-joints, however after mapping the strike and dip orientation of these near-vertical discontinuities (Figure 31), it is within reason to assume, based on the overall direction of the dips, that the dip range 16° – 28° and corresponding dip direction of 30°– 75°; 300° – 355° represents the bedding orientation (Hampton, S., 2013, pers comm. 13 June).

Figure 31 - The strike and dip orientation of the main near-horizontal discontinuities mapped on the cliff face, showing general direction of the dip is in a SE direction

4.5.2Soil Mantle

Although the soil does not influence the stability of the cliff, characterisation of the soil does fall within the scope of this project since the soil unit did react (significantly) to the trigger earthquakes, and part of it near the cliff edge was entrained in the collapse. The soil unit was characterised to determine its strength using a scala penetrometer.

NZGS Field Descriptions

The mantle soil is characterised as being (Table 12): Sandy SILT, Peat / Organic Top Soil; light yellowish brown. Packed, slightly moist, moderate plasticity, moderate sensitivity, CANTERBURY WIND-BLOWN SAND AND SILT

Table 12 - Summary table characterising the welded ignimbrite component of Redcliffs' cliff using the NZGS field description guide (Muschamps, 2005)

Features	
Subordinate Fraction	Sandy
Major Fraction	Silt
Minor Fraction	Peat / Organic top soil
Colour	Light yellowish brown
Structure	Fissured near the cliff edges (post-cliff collapse)
Qualifying Features	
Strength	Packed
Moisture Condition	Predominantly dry, but slightly moist top soil
Grading	
Bedding	Sub horizontal, thickness varies up to ~5 m (including 1-2 m topsoil)
Plasticity	Moderate
Sensitivity	Moderate
Majority Fraction	
Weathering of clasts	
Subordinate Fraction	
Minor Fraction	
Additional structures	
Additional Information	Wind-blown loess commonly found within the Canterbury Region

Scala Penetrometer

To gauge the strength of the soil mass, a strength test was conducted (post-June 2011 collapse) on two different plots of land on top of the cliff (Figure 20) using a scala penetrometer. The tests were also conducted on dry and saturated patches of soil within each site to compare the strength of the soil under different levels of saturation. The results of this test are summarized in Figures 32 – 35.

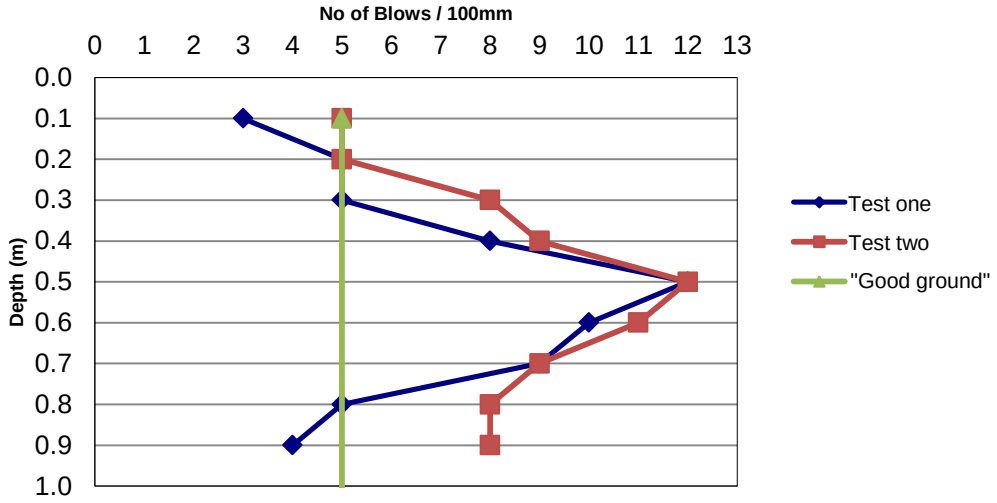

Figure 22 - Dry soil (with ~1 cm overlying top soil) at site 1

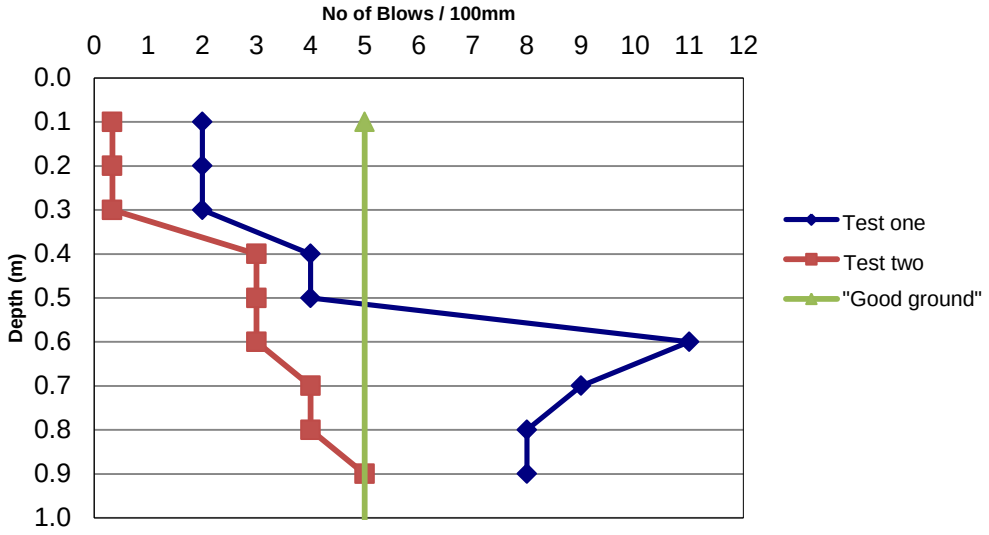

Figure 33 - Saturated soil (with ~1 cm overlying top soil) at site 1

The reason why two separate sites were chosen is because characteristics between the two sites had varying thickness of top soil, which can vary from 10s mm up to 100s mm. This provides a better representation of the overall soil mantle conditions, accounting for the variable thickness within the soil mantle (i.e. thickness between the (upper) top soil and the (lower) loess).

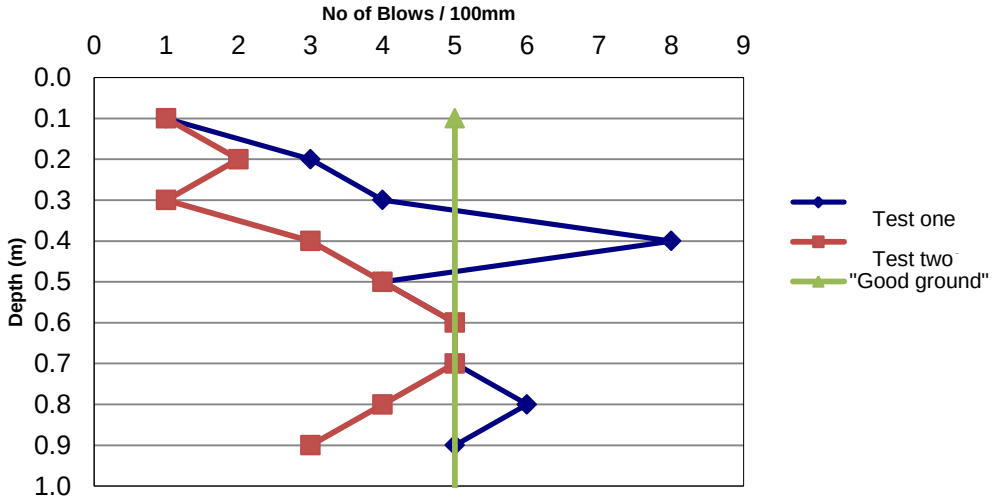

Figure 34 - Dry soil at site 2

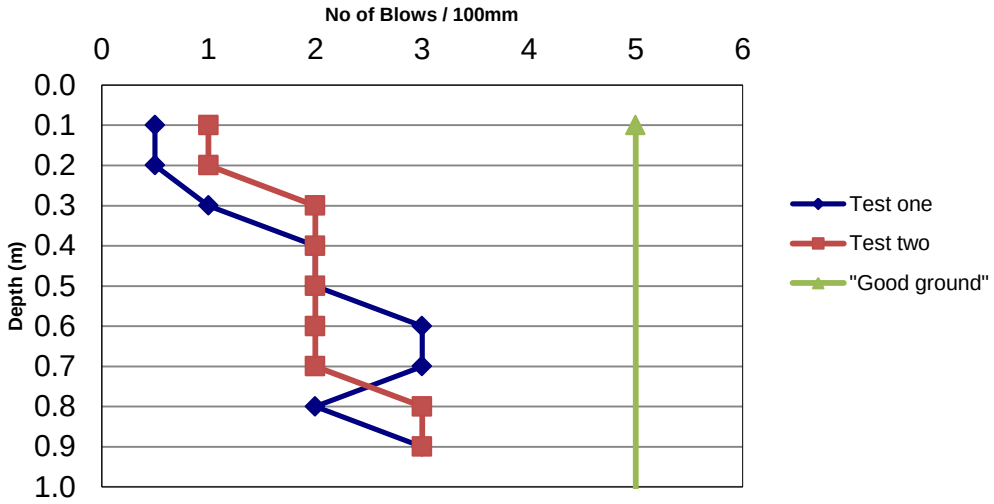

Figure 35 – Saturated soil at site 2

The tests revealed that the unit of soil has an upper (top soil) component that is generally weak regardless of saturation levels, where it takes 1 – 4 blows before reaching the "good" soil – which takes ≥ 5 blows to penetrate 100 mm into the soil mass. Furthermore, The only general patter seen is that: i) an increase in depth increases the number of blows required to penetrate another 100 mm, with the exception of a blow count reversal ~0.7 – 0.8 m; ii) based on the minimum amount of blows at site 2, there is much weaker soil located closer the to the cliff edge; iii) saturated loess (Figure 33 and 35) appears to be just as weak (or even weaker) than the top soil. It isn't clear why the blow count decreases at 0.8 m, though it proves a change in consolidation within the "good" part of the soil body (possibly an intra-unconsolidated boundary). However, due to the shortage of time and resources at the time of conducting this investigation, this inquiry was not further pursued.

4.6 Geomorphological Characterisation

Other than establishing the geological components that make up the hillside, a second major field investigation was carried out concurrently to document the seismically-induced physical changes of Redcliffs' cliff. Particular emphasis was placed on mapping the surface area of the cliff, modelling the slope, as well as attempting to further study the fissures created on the cliff top.

At the time, undertaking such a survey on the top of the cliff / near the cliff edge was considered not only a major task but also a major risk considering the uncertain level of safety of being on-site shortly after each major earthquake. Some of the major risks included:

- Houses which had collapsed and / or was deemed structurally unsafe located near the cliff edge (where majority of the fissures were present);
- The possibility of an aftershock triggering more rockfall from the cliff face.

Arguably, this meant that access was strictly limited to areas that did not compromise the safety of being on-site; thus, limiting the potential to record all the physical changes to the cliff. Nevertheless, compromises were made to also use remote surveying techniques in addition to field surveying to collect as much data as possible documenting post-failure characteristics whilst falling on the side of caution and safety.

4.6.1 Surface mapping and modelling of the cliff

One of the top priorities whilst surveying the hillside was to log all physical changes done to the surface of the cliff as a result of the two major earthquakes. This included surficial changes (i.e. formation of cracks / fractures / fissure) and changes to the geometry of the slope. The task was split into two components focusing on mapping and modelling the cliff top and cliff face between 8B Balmoral Lane and the section of the cliff top directly above Raekura Place (Figure 16) using a combination of: remote sensing data disclosed in the form of aerial photographs; LiDAR digital elevation models; and Total Station laser scans taken of the cliff face before and after each major earthquake.

Cliff Top

To present the physical changes done to the cliff top, an aerial map (Map 1) was drawn on a scale of 1:50 to illustrate the following features identified whilst surveying between 8B Balmoral Lane and the cliff top directly above Raekura Place:

- Outlines of the cliff edge before and after each major cliff collapse;
- The sizes of rockfall material deposited at the base of the cliff as a result of the two earthquakes;
- Spread pattern of the talus;
- The location of ground displacements identified in the form of building foundation / retaining wall cracks and fissures.

This map provides a summation of all the important changes that occurred on-site as a result of the earthquakes in a simple yet effective way to observe / interpret the seismically-induced changes to the cliff top. By projecting the outlines of particular features at set moments in time (i.e. before and after the earthquake) and overlapping the outlines on a single map, this provides information to draw conclusions from regarding the primary and secondary cliff collapse in 2011.

Further Investigation of cliff top

In addition to mapping the cliff top, further investigations were conducted to determine if any of the cliff top fissures were creeping, i.e. increasing in size over time, and whether the fissures penetrated into the (volcanic) bedrock. However, the investigations were unsuccessful / cut short due complications regarding the equipment used as well as accessing the site after the 13 June 2011 earthquake. Nevertheless, the results of the unsuccessful / incomplete investigations are presented below to capture the lessons learned from this investigation.

Monitoring Fissures

As early as March 2011, a select number of fissures along the cliff edge were monitored; an investigation started by Mark Yetton from Geotech Ltd shortly after the February 2011 collapse. The aim of monitoring cracks near the cliff edge was to determine their behaviour over time due to the external forces such as gravity, weathering and seismicity. A total of 10 fissures were selected and monitored (Figures 36 and 37), starting from 23 March 2011 to the 17 June 2011 (Table 13).

According to the survey results, there was a contrast in behaviour throughout all 10 of the fissures monitored over the three or so months (Figure 38). Most of the fissures did widen over the monitored period of time (sites 1 – 3, 5 – 9), except for site 4 and 10 – which only widened after the 13 June earthquake. Additionally, old fractures that developed in the 22 February 2011 earthquake were destroyed and new ones created as a result of the 13 June 2011 earthquake at sites 7 – 10.

Figure 36 - Aerial photograph displaying the locations of the 11 fractures identified, but only 10 were monitored between April and early June 2011.

In addition, as part of the monitoring process, the results from the short-term monitoring of fissures were overlapped with data regarding the seismicity and rainfall within the same timeline to see if there was any correlation between the external factors and widening of the fissures. The findings from the results shows that the general trend of fissures widening appears to correlate with seismicity within the timeline whereby, prior to a fissure(s) widening, an earthquake / aftershock ≥ M_w 4 does rupture within the vicinity of Redcliffs.

While this is not conclusive evidence, it does suggest strong correlation between strong seismicity (i.e. ≥ M_w 4) and the subsequent widening of fissures, particularly after the 13 June 2011 earthquake – with the exception of the aftershock in 25 May 2011 as none of the fissures widened as a result of the M_w 4.1 quake. It is uncertain why the cliff face was not affected by this particular quake since it struck only ~3 km away from Redcliffs, and at a depth of 6 km. However, one theory as to the ineffectiveness of causing the fissures to widen would be directivity of the M_w 4.1 quake (i.e. the direction of fault slope / thrust) since the relatively short distance away and a shallow depth rules out the proximity factor.

The idea of fissures widening independently of seismicity was also considered whilst monitoring the fissures on-site (i.e. influenced by gravity and / or rainfall). However, since a relatively major seismic incident always precedes the widening of fissures, it impossible to determine whether external factors (other than seismicity) had any major influence in widening the fissures using this dataset.

Figure 37 - A collage of photographs taken at showing examples of some of the fissures formed as a result of the February earthquake and the variation of responses to the 13 June 2011 earthquake. The rest of photographs documenting the changes to the cliff edge fissures can be found in Appendix II.

Table 13 - the measurements of the gap taken of selected fissures at the start of monitoring

	Starting Width Measurements taken on the 23 March 2011									
Width Measurements (mm)	Site 1	Site 2	Site 3	Site 4	Site 5	Site 6	Site 7	Site 8	Site 9	Site 10
	580	695	7440	647	194	1530	545	3875	491	621

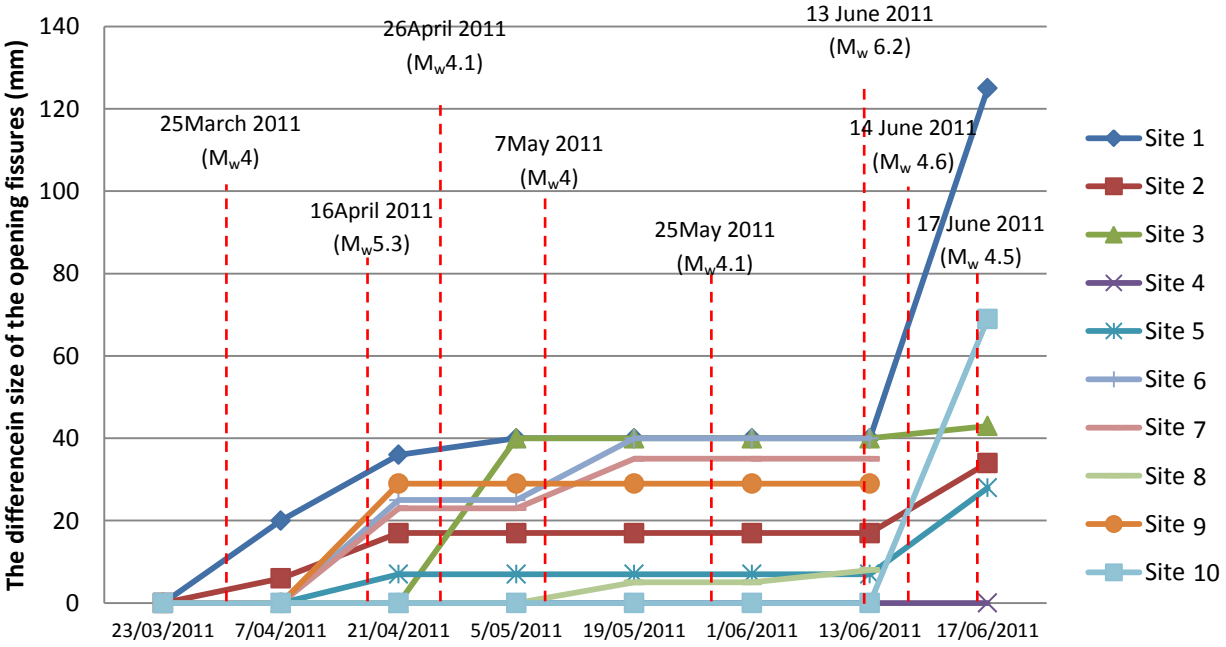

Figure 38 – Results of incremental widening for fissures monitored fortnightly between March and June 2011, starting at 23 March 2011. Each point represents the difference (i.e. increase) in the size of the fissures with respect to the previous measurement, and the red dashed lines represent key seismic incidents within the timeline.

Overall, despite the limited amount of data collected, it was enough to suggest that seismicity is the leading cause behind widening of the fissures. However, even though there is no distinctive pattern in the correlated data to suggest rainfall as major influence, from a strength perspective, as demonstrated with the scala results in saturated soil, it is likely that saturation of the soil would have contributed to some extent towards helping widen the fissures in the event of a large enough quake.

Subsurface Investigation

In an attempt to further analyse the fissures found on top of the cliff, near the cliff edge, a geophysical subsurface investigation was undertaken at the cliff top to measure the depth at which fissures penetrated into the cliff. Preliminary test runs of the equipment were conducted on an open plot of land (Figure 39) to test the response of the Ground Penetrating Radar and Resistivity Tomography to the subsurface geology of the cliff.

Figure 39 - Aerial photograph showing the location of the test site (red arrow) and the specific bearing across the land which was surveyed (yellow dashed line). The orange dashed line represents a pipe buried within the soil that was used as a reference point.

The conclusions drawn from the results obtained from the GPR and Resistivity Imaging established that neither method was successful in imaging the subsurface geology of the cliff. Both methods were successful in identifying the underground pipe close to the edge of the cliff (Figures 40 and 41). However, both surveys only managed to survey down to ~4 m into the cliff. This meant that even though it was possible to detect subsurface features (such as the pipe near the cliff edge), the lack in depth of penetration from both geophysical methods meant that it was not feasible to proceed with the methods on the selected surface fractures of interest since neither methods could penetrate into bedrock.

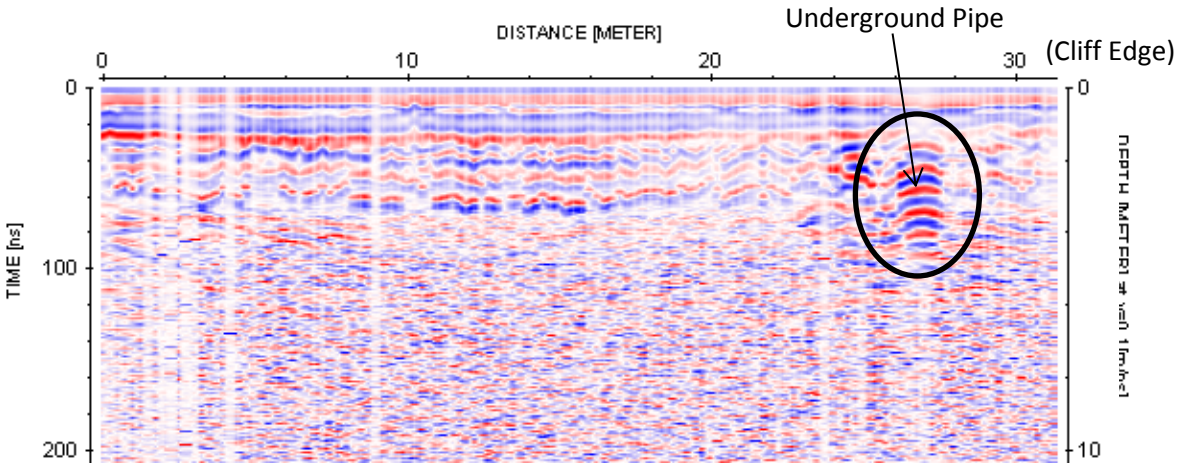

Figure 40 - Result from the GPR survey of the test site successfully imaging only down to ~4 m of the cliff top

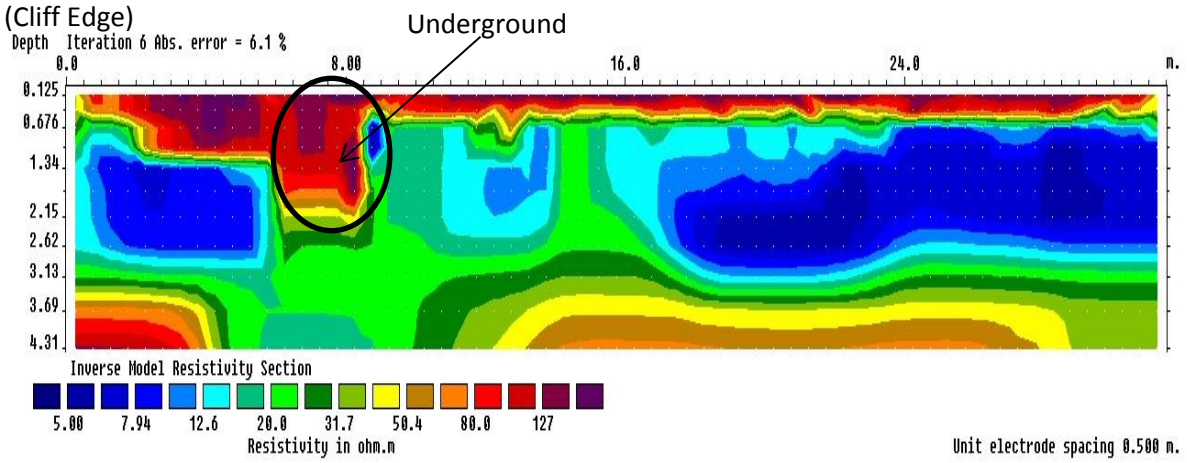

Figure 41 - A graphical representation of the resistivity tomography survey conducted imaging down to just over 4 m into the cliff

Cliff Face

The task of surveying the cliff face was done in two phases. The first phase involved mapping a planar view of the cliff face, similar to what was done with the cliff top. This included mapping the positioning of the sequence of lava flows, as well as where the main / most apparent discontinuities (i.e. bedding plane, joints and fractures) observed on the cliff face. The results of this mapping can be found in Map 2.

The second phase focused on measuring the slope geometry of the cliff face in an attempt to quantitatively capture the geometric changes to the slope surface after the February and June 2011 major (M_w 6.2) seismic events. To accomplish such a task, a series of cross sections were compiled using the resources and data available at the time to model the slope geometry before and after each major rock-slope failure incident.

The main techniques of acquiring slope geometry data included the use of:

- Airborne LiDAR digital elevation models produced in 2003 and March 2011, used to measure the slope surface before and after the 22 February 2011 collapse (courtesy of GNS Science),in addition to using
- Terrestrial laser scans from Total Station surveys conducted between the months of October and November 2011 in order to represent the cliff post- 13 June 2011 (Table 14).

Table 14 - Summary table detailing the dates and sources of data the cross sections were generated from. The airborne LiDAR data was provided by John Thyne (GIS Manager) from the Geography Department

Set Number	1	2	3
Dates of Cross Sections	6-7-2003 (pre-22February 2011)	8-3-2011 (Post-22 February 2011)	Sequence of scans between August November 2011 (Post-13 June 2011)
Methodology	Airborne LIDAR		Total Station
Panel:	CCC172	BX241830; BX241831; BX241930; BX241931	

The end result is a compilation of data plots, which were made into 3 overlapping sets of 24 cross sections representing the cliff face before and after the 22 February and 13 June 2011 major earthquakes (Table 15).

Table 15 - Number of cross sections created representing each face taken at one period of time

	Face 1	Face 2	Face 3	Face 4	Face 5	Face 6	Face 7	Total
Number of cross sections	3	2	4	3	4	6	2	24

The height and major slope gradients were measured from the resultant cross sections made (Figures 42). The slope angles were then translated onto a planar map of the cliff face to produce gradient models representing the cliff face before and after each major collapse (Figures 43 – 45). These individually annotated cross sections can be found in Appendix III. As a result of measuring the gradients of the cross section models, the data revealed a cliff with: a slope height between 40 – 80 m; multiple slope gradients of varying degrees ranging between 20° and 115° from the horizontal (or 25° into the slope); and an average talus slope angle of roughly 25°.

Cross Section Face 6.3

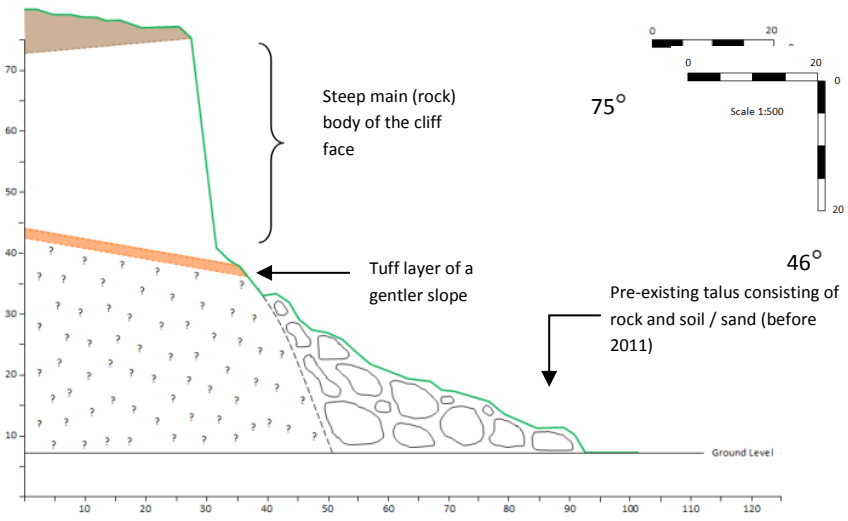

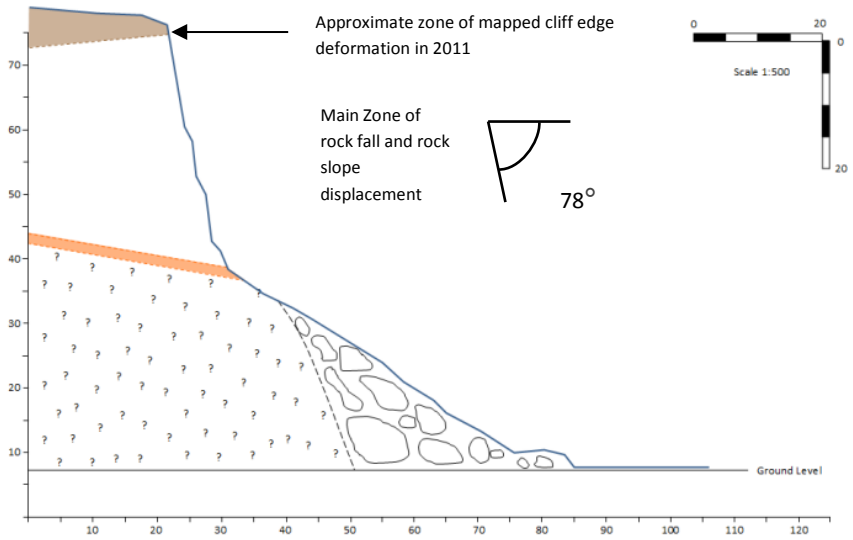

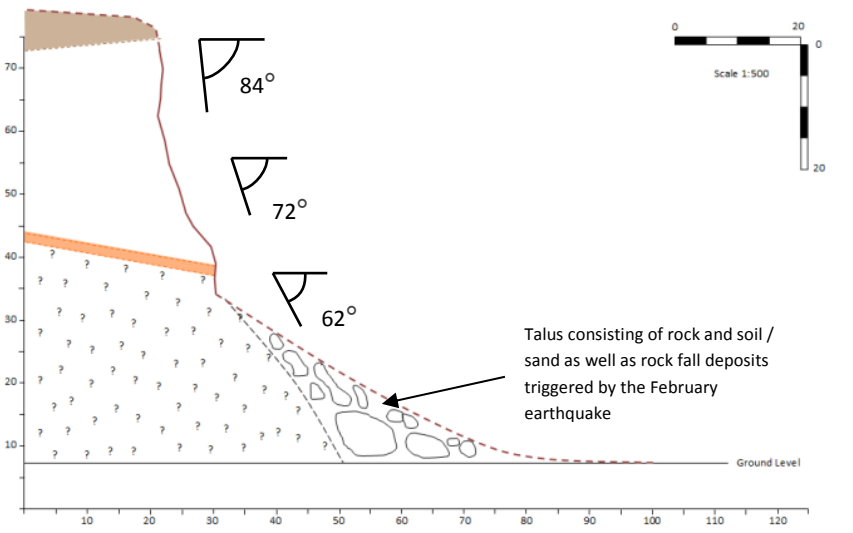

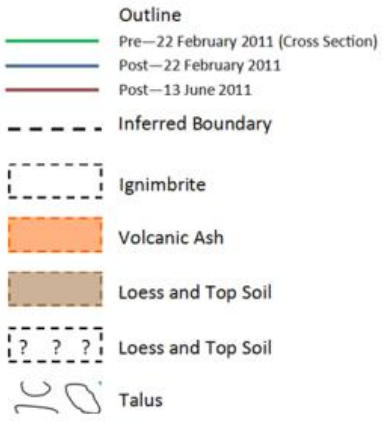

Figure 42 - an example of a section of the cliff face evolving over the course of the two major earthquakes

(A) Pre February 2011

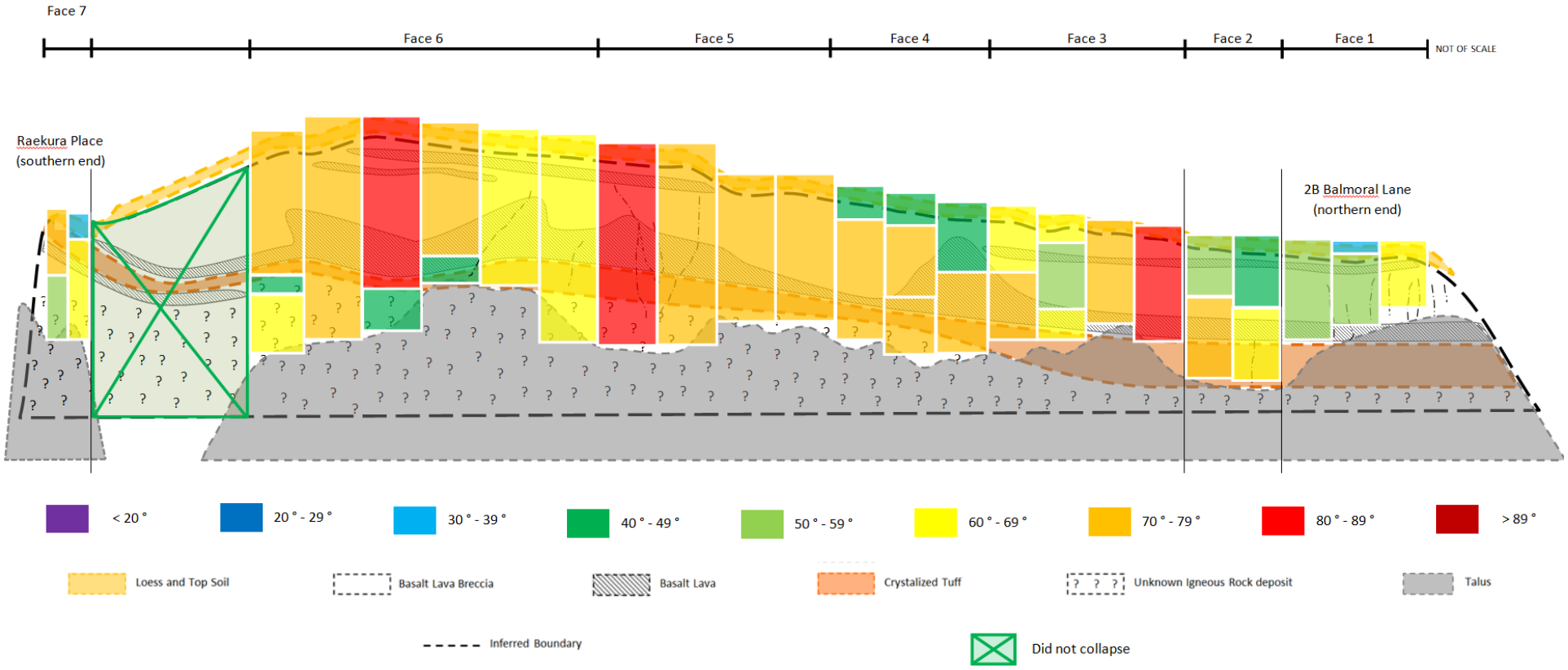

2003	Face 7		Face 6						Face 5				Face 4			Face 3				Face 2		Face 1		
Upper	71	38	73		82	75							42	47	49	60	68			50	49		39	
Middle	-	66	43	72			66	68	81	78	70	73	75	71	-	-	53	77	80	71	-	56	56	65
Lower	53		67		46	46								74	74	70	66				67			

Figure 43 – Models of Redcliffs' cliff illustrating the major cliff-face gradients surveyed before and after each major collapse. (A) pre-Februaruy 2011, (B) post-February 2011; (C) post-June 2011

(B) Post February 2011

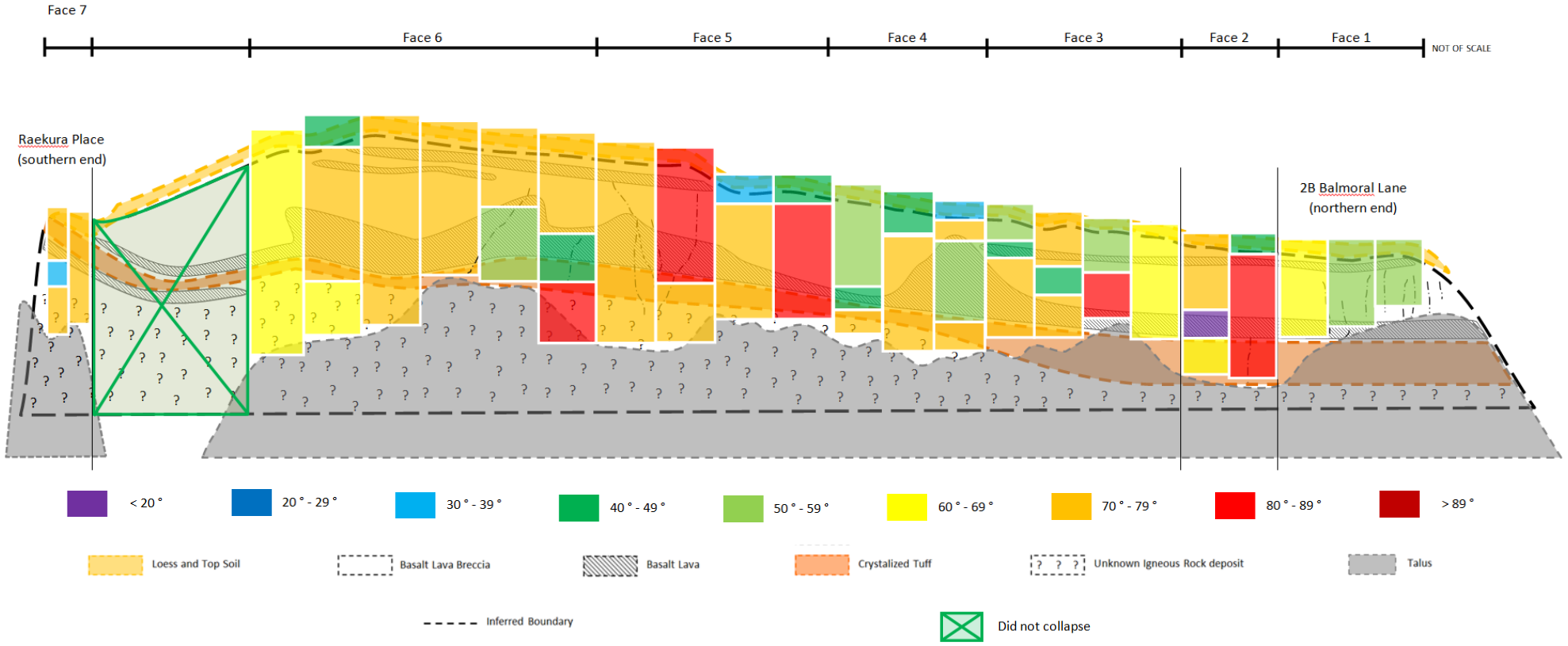

Post-Feb 2011	Face 7		Face 6						Face 5				Face 4			Face 3				Face 2		Face 1		
Upper	79			44			73	70		81	33	49	73	44	36	58	74	55		76	23			
Middle	35	79	69	76	78	78	-	48	76		71	83	37	73	79 54	46	46	83	68	19	76	65	56	58
Lower	76			64			56	81		70			72		78	78	73			61				

Figure 44 – Slope geometry after the 22 February 2011 earthquake. See Figure 43 for annotation.

(C) Post June 2011

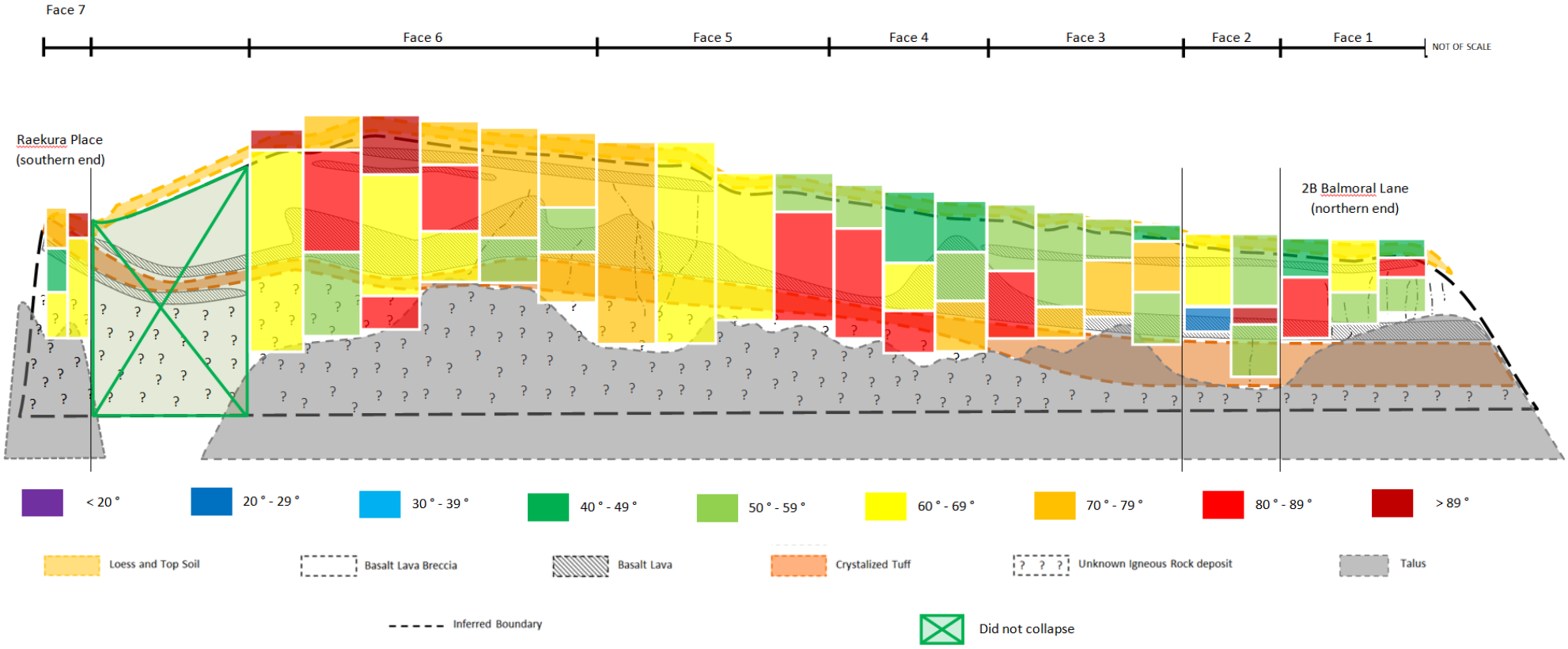

Post-June 2011	Face 7		Face 6						Face 5				Face 4			Face 3				Face 2		Face 1		
Upper	79	98	101	72	92	72	78	76	73	66	69	51	51	45	42	52	52	52	44	68	54	42	60	42
Middle	45	67	62	86	68	84		56				83	80	68	56	-		-	76	24	115	81	52	83
Lower	68			53	84	62	56	77						86	78	80	76	89	59		52			51

Figure 45 - Slope geometry after the 13 June 2011 earthquake See Figure 43 for annotation

Synopsis of Redcliffs' slope geometry

After examining all the cross-sections, three common slope-outlines were identified which represented the general slope profile across the cliff (Figure 46). Each of these three cross-sectional slope profile shows that the cliff face is made up of different slope angles and varying numbers of major slope gradients of different sizes. This is attributed to the heterogeneous nature of the rock masses that combine to make up the main rock body of the cliff.

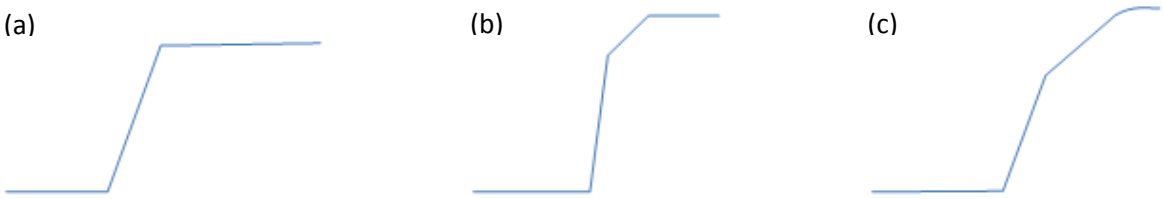

Figure 46 - Outlines of the three major cliff profiles present across the Redcliffs cliff face. (a) A cliff profile representing a slope either strong rock formations that of the same rock mass strength or a relatively strong top. (b) A slope with a weak top and a strong base / main body. (c) An overall weak slope with an even weaker top.

The slope profile of Redcliffs is a relatively steep cliff where, the overall slope height ranges between 40 – 80 m, with a slope angle > 30°. However, when comparing between the slope aspects of the NE and SE Face, in general, the SE Face (Face 1 – 4) has an average slope angle of < 63°, whereas the NE Face (Face 5 – 7) is much steeper with an average slope angle ≥ 65°. This pattern of steepness of remains consistent even after each earthquake-induced failure event. For instance, after the June 2011 collapse, the NE face still remains the steepest part of the cliff, with a maximum average dip angle of 72° ± 13, while the gentlest dipping part of the cliff face is still the SE face with the lowest dip angle of 59° ± 18. The remainder of the results from this comparative analysis is summarized in Table 16.

Table 16 - The averaged dip orientations calculated using the dip angle values measured from the cross sections (which were generated using Total Station laser scans and LiDAR digital elevation models)

	Average Slope Angles (°)		
	SE Face (Face 1-4)	NE Face (Face 5-6)	Overall Cliff Face
Pre-February 2011 (2003)	62 ± 12 (1 S.D.)	65 ± 13 (1 S.D.)	63 ±13 (1 S.D.)
Post-February 2011	60 ± 18 (1 S.D.)	67 ± 14 (1 S.D.)	63 ±17 (1 S.D.)
Post-June 2011	62 ± 19 (1 S.D.)	72 ± 13 (1 S.D.)	67 ±18 (1 S.D.)

*S.D. – standard deviation

Post-failure geometric changes

Figures 43 – 45 are three planar models of Redcliffs' cliff illustrating the major gradients of the cliff face. These models were created by measuring the major gradients from each of the cross sections of Redcliffs' cliff before the February 2011 collapse, and after the February and June 2011 collapses. These planar models reflect the geometrical changes to the slope surface after each collapse. Essentially, the major outcome after each collapse, aside from the volume of material that detaches from the cliff face, is the increase in fragmentation of the slope surface gradient.

Initially (pre-22 February 2011 collapse), the cliff face was fairly uniform only a few sections of the cliff face that had three major slope gradients, mainly found on the SE Face (Faces 1 – 4) and some in the NE Face as well (Face 6 and 7). However, after the initial collapse, the number of major gradients increased, particularly in the NE Face (Face 5). After the second collapse on 13 June 2011, nearly all parts of the cliff face that did collapse had at least two major slope gradients, except for part of Face 5. The only part of the slope that remained unaltered after two major collapses was between Face 6 and 7 as that section of the cliff face did not respond to the failure-inducing earthquakes like the rest of the cliff face. It remains unclear as to why the part of the slope between Face 6 and 7 did not fail even though that particular part of the cliff is presumed to have similar attributes to the rest of the cliff face.

In essence, these differences in overall slope angles between the NE and SE Face (pre- and post-collapses) comes down to the different rock mass characteristics of the exposed rock masses that make up the respective slope aspects, that is to say the varying strength and structural properties between the unwelded / unwelded ignimbrite and tuff. While it is not clear whether there is a principle influence, it is apparent that both the strength and structural characteristics within the rock masses take part in the development process of creating the steep (slope) gradient(s).

Strength of the rock masses

The strength of the rock masses is important in developing a near-vertical slope as it resists against weathering and erosion, as well as any in-situ stress that can trigger deformation mechanisms within the rock masses. In the case of Redcliffs' cliff, it is assumed that the overall strength of the cliff face (according to the results above) is influenced to a certain extent by the proportion of welded ignimbrite – the hardest

rock mass that exists within the cliff. The reasoning behind this assumption is that, in a near-vertical rock slope comprised of multiple rock masses seen on Redcliffs' cliff, the rock mass which covers a greater part within the slope body would have more control over the overall stability / behaviour of the slope than the smaller sized rock masses (thinner units; unwelded ignimbrite and tuff); especially when the dominant (welded ignimbrite) rock mass also contains the main near-vertical discontinuity sets identified on the slope.

Looking at the distribution of between the three rock masses within lithology of the exposed cliff face (Map 2), a greater portion of the (steeper) NE Face is covered by the welded ignimbrite, i.e. larger (main) rock mass and (minor) lensoidal bodies of unwelded ignimbrite, than the (gentler) SE Face. Evidently, this statement contradicts the quantitative estimations made in Figure 18 which suggests that the proportion of welded ignimbrite between the NE and SE Face is roughly the same. However, those estimations were made in relation to the size of the respective slope aspects; and since the NE Face is larger than that of the SE Face, it implies that the resultant estimated proportions of welded ignimbrite in the NE Face is more than in the SE Face.

Overall, while this is not considered definitive proof, from the data present, it can be assumed that there is some correlation between the steepness of Redcliffs' cliff and the percentage of welded ignimbrite within the cliff.

Structural controls of the rock masses

The structural properties within the rock masses is also considered an important factor in developing a steep slope gradient, specifically regarding the dip orientation of the discontinuities – since Redcliffs' cliff is considered discontinuous rock slope. This is in relation to the (potential) failure surface within a rock mass as the strength of a mechanical discontinuity is typically less than the strength of the intact rock that surrounds the discontinuity.

Considering a cliff face is essentially a merger of resultant failure surfaces exposed on a hillside, the overall gradient(s) of a rock slope would be controlled by the orientation of the failure surface(s). Moreover, since failures occur along the path of least resistance, it will most likely occur along discontinuity planes that daylight the slope. For Redcliffs' cliff, the dominant discontinuity set(s) are near-vertically oriented. Hence, assuming failure predominantly occurs along these discontinuities,

when failure does occur, it exposes near-vertical failure surfaces; thus forming a near-vertical slope.

4.7 SWOT Analysis

To conclude this chapter, a SWOT analysis (strengths, weaknesses, opportunities and threats) is conducted to evaluate the approaches used and subsequent results attained characterising Redcliffs' cliff. At the same time, the main points of this chapter will also be incorporated into the discussion as part of the self-assessment.

4.7.1 Strengths

- While it was a challenge to survey a cliff face that had limit access, this major field investigation overcame the physical limitations of not being able to have any physical interaction with the site of interest (i.e. Redcliffs' cliff).
- By developing a remote-based methodology, this investigation was successful in obtaining engineering geological data in a very challenging environment; enough to provide a detailed enough (post-failure) engineering geological description of the Redcliffs' cliff. Overall, the result of this chapter sets the foundation of geological and geotechnical information regarding Redcliffs' cliff.
- Some of the main geological characteristics identified whilst surveying the cliff face include the following:
    - The cliff is one of four sea-cut cliffs in the Port Hills comprised of a sequence of volcanic deposits, covered by a deposit of loess and soil.
    - The sequence of units exposed on the cliff face (from top to bottom) begins with a unit of loess and soil covering a main rock body of volcanic deposits containing, unwelded and welded ignimbrite overlaying a layer of cemented tuff.
- Collect the rock mass characteristics using the remote approach (i.e. the proxy site) was successful in collecting some geotechnical data, showing that:
    - The breccia and basalt lava are very strong units of jointed rock with the latter of the two containing closely spaced, near-vertically dipping (columnar) joints.
    - Tuff was identified as being the weakest rock in the cliff as it is mainly comprised of consolidated volcanic ash. It is also the only massive rock unit presumed to have discontinuities present only in the form of

internal fractures form as a result of in-situ stresses and earthquake loading.

- Compiling cross-sectional laser scans of the cliff face before and after each major collapse provided an insight as to the geometric evolution of the rockslope, increasing the mean slope gradient from 63° to 67° (post-13 June 2011).

4.7.2 Weaknesses

- The restricted access on-site and limited resources while conducting this investigation meant that a more "remote" approach had to be used over the conventional approach when surveying the cliff face.
- The main body of geotechnical results were only acquired through field surveys conducted on exposed outcrops at proxy sites, and remote (field) surveys of the cliff face. Unfortunately it was not possible determine the all of the Hoek-Brown and Barton-Bandis Criterion using the field measurements alone and some of the variables had to be sourced from RocData that had predetermine variables with corresponding field descriptions.
    - Ideally, this approach would have been suitable (more accurate) provided that it accompanies some form of lab work and/or more surveys conducted on the cliff face to help moderate the certainty of attributes proposed concerning the cliff face (using remote / proxy site data collected).

4.7.3 Opportunities

- It is still not fully known why a section at the western end of the cliff face (between Face 6 and 7) did not collapse. This provides an opportunity to study what factors caused that section of the cliff face to remain stable while the rest of Redcliffs' cliff collapsed after to major earthquakes.
- Undoubtedly, safety is the utmost concern when surveying a slope of this scale. however, with the adequate safety protocols, there is the potential to further test some of the investigations conducted in this project, such as:
    - Acquire intact samples from the cliff face (when possible) and process the samples in the lab to test and verify the classifications made on-site/proxy site of the cliff's intact rock and rockmass strength;

- More concise mapping of the lava flows, and joint pattern of the ignimbrite could be done to refine the maps presented in this chapter provided access is granted to approach the cliff face;
- Modelling of the cliff face could also be refined by using more powerful laser scanning equipment such has terrestrial LiDAR (as it would generate more point clouds that would capture more points on the surface of the cliff face; thus creating a more accurate three-dimensional model(s) representing slope geometry of the cliff face.
- Use other (penetrative) methods to analyse the depth of penetration of cliff top fissures.

4.7.4 Threats

- Ultimately, while the rockslope is essentially characterised, refinement of the data and information presented in this chapter is needed for progress to be made characterising Redcliffs' cliff. However this solely depends on the accessibility on-site, as in having physical contact with the cliff face, something that was not possible to attain over the course of this investigation.

Chapter Five: Assessing the cliff collapses

5.1 Introduction

Staying on point with the aim of characterisation, the analytical component of this study aims to break down the key mechanisms involved in causing Redcliffs' cliff to collapse, and evaluate the behaviour of the cliff when failure ensues using the data collected, combined with the knowledge of engineering geology and of slopes interacting with failure-inducing earthquakes.

The overall outcome of this chapter will focus on assessing specific components regarding the process of failure, i.e. the mechanics and mechanisms involved in pre-failure; amidst-failure; and post-failure, which includes:

i) Identifying and reviewing the failure mechanisms involved in the collapse of the cliff based on the:
   - Deformation mechanisms which caused the cliff to collapse;
   - The likely behaviour of the rock masses within the rock slope that would have ensued as Redcliffs' cliff began to collapse; followed by

ii) Evaluating the severity of both failure incidents using the quantitative data collected whilst surveying the cliff and demonstrating how the failure incidents have affected the geometry and overall stability of the cliff face.

5.2 Pre-Failure: Deformation Mechanisms

For the purpose of this discussion, deformation mechanisms are considered as determinants, i.e. external factors that either trigger failure incidents or facilitate in the process of inducing slope instability (Braathen et al., 2004). In other words, these determinants either act as:

- Triggers – the driving forces that overwhelm the resistance forces, thus causing failure to occur; and/or
- Enabling Factors – these are extrinsic factors that condition the slope for failure, which does not include the pre-existing conditions such as jointing in basalt lava (as a result of the lava cooling).

Examples of deformation mechanisms include: excessive rainfall, ground motion induced by earthquake, at time (no apparent trigger or enabling factors). In most cases, varied combinations of topographical, geological, climatological factors, and time, determine whether failures occur or not (Dorren, 2003).

To determine the deformation mechanisms that were involved in the collapse of Redcliffs' cliff on 22 February and 13 June 2011, an analytical three-stage approach was be used to diagnose the mechanisms involved in triggering the cliff collapsing incidents, similar to the approach recommended by (Owen et al., 2011). Figure 1 outlines this process, beginning with the collection of evidence representing deformation on-site, and identifying triggers / enabling factors that occur in the area. This is followed by matching the most likely factors (mechanisms) needed in order for certain aspects of deformation to occur; as well as assessing the criteria that makes the (chosen) mechanisms effective failure-inducing mechanisms.

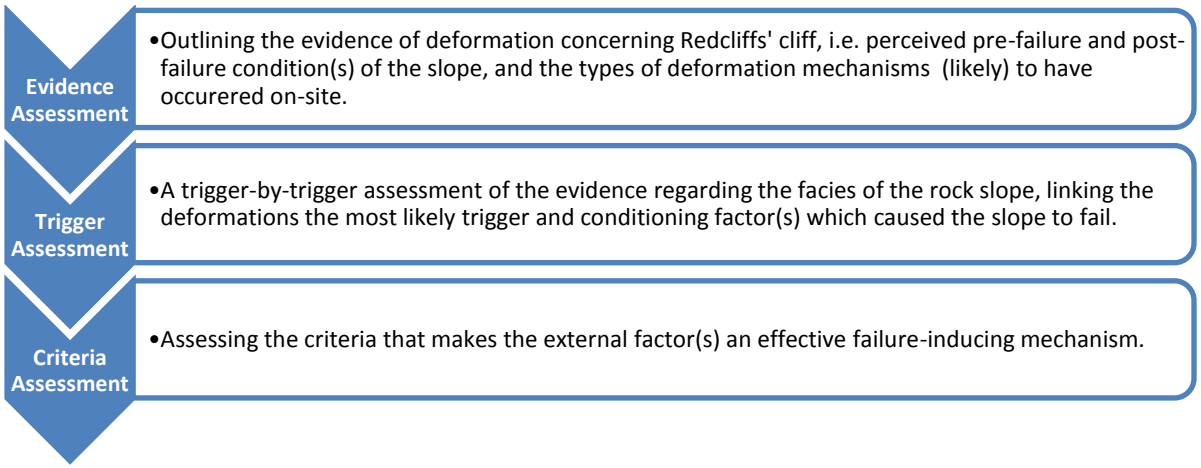

Figure 47 - The three-step process of evaluating the deformation mechanisms involved in helping to cause the collapse of Redcliffs' cliff.

3.1.1 Trigger (Mechanism)

The task of recognizing the transient (short-lived) deformation mechanism that triggered Redcliffs' cliff to collapse on 22 February and 13 June 2011 was straightforward, seeing as after the M_w 6.2 earthquakes that happened on the same day, it was well documented in Figures 43 - 45 that:

i) The landscape of the cliff (i.e. cliff top and cliff face) had inadvertently changed;
ii) There was an increase in volume of the talus slope; and
iii) Rock fall debris was found beyond the toe of the talus after each respective major earthquake.

Based on these post-earthquake accounts of the cliff, it became apparent that the Redcliffs' cliff responded to intense ground movement caused by two different faults rupturing nearby on 22 February and 13 June 2011. This implies that earthquake-loading from the M_w 6.2 earthquakes acted as triggering mechanisms which stressed the cliff till the point of failure.

Effectiveness as a trigger mechanism

The main reason why the February and June 2011 (M_w 6.2) earthquakes were effective triggering mechanisms was due to the intensity level of the shaking felt at Redcliffs, and the rest of the Port Hills. As seismic waves propagated through the area, this provided enough of a driving force to overcome resistant (frictional) forces that kept Redcliffs' cliff intact and stable for an extended period of time.

The criteria required for earthquakes to be an effective trigger mechanism stems from a complex relationship between the fault rupture and the subsequent ground movement. In the context of seismic events that occurred within the timeline of Redcliffs' cliff collapsing twice, i.e. from 4 September 2010 to June 2011, there were only four major earthquakes (M_w 7.1, 6.2, 6.2, and 5.3) that struck Redcliffs and the rest of the Port Hills area. Out of the four, only the M_w 6.2 earthquakes were intense enough to have made a significant impact, causing many widespread rockfalls and cliff collapses, including the collapse of Redcliffs cliff (Massey, et. al, 2012). This suggests that the magnitude of an earthquake does not directly influence the intensity needed to be an effective trigger mechanism, considering the strongest (M_w 7.1) earthquake did not trigger Redcliffs' cliff to collapse.

Alternatively, the intensity from either M_w 6.2 earthquake was only effective mainly due to the forceful level of shaking felt on-site (i.e. the measured PGA at Redcliffs). Massey, et. al, (2012) proves this relationship in the comparison between the PGA measured at the Port Hills after each major seismic incident took place and the respective severity of cliff collapses. The result was a table of results forecasting the nature / severity of cliff collapses expected within a set range of PGA values, and their likelihood of occurring within the next year and over the next 50 years (Table 17). This yielded four different thresholds in the form of PGA bands where, the greater PGA bands, the more severe the cliff collapses are in terms of frequency and volume of material removed from the cliff(s).

The M_w 5.6 earthquake (which happened roughly an hour before the main M_w 6.2 on 13 June 2011) was not cited as part of this discussion as the outcome of the quake was overshadowed by the follow-up M_w 6.2 incident. Considering the short span of time between earthquakes, there wasn't time to catalogue the impact; which meant that the damage done / slope failures caused by either earthquakes was indistinguishable. Even though the first earthquake was considered intense enough have made an impact; however for simplicity sake, all damage done that particular day is attributed to the more intense M_w 6.2 earthquake.

Table 17 - The peak ground acceleration bands and the range damage each PGA band is capable of doing within the (estimated) annual frequency of occurrence within the next 1-year period and over the next 50 years (Massey et al., 2012)

PGA band	Frequency – events per year		Description
	Current – within the next 1-year period	Over the next 50 years*	
0.1 – 0.4	0.6	0.12	Cliff collapses tend to be minimal at this range of acceleration
0.4 – 1.0	0.17	0.03	Cliff collapses occur at this range but their numbers tend to be limited and localised
1.0 – 2.0	0.016	0.003	This is the acceleration range of the 22 February and 13 June 2011 earthquakes
2.0 – 5.0	0.0008	0.0002	Could trigger more (in number) and larger (in volume) cliff collapses than the 22 February and 13 June 2011 earthquakes

To further demonstrate that the intensity of either M_w 6.2 trigger-earthquake is not only dependant on the magnitude of the quake, a summary table was compiled describing the four major earthquakes. This table displays the relationships between the properties of each fault rupture; the subsequent intensity of each quake felt on the Port Hills and Redcliffs; and the severity of the resulting slope failures (Table 18).

Earthquake-intensity measurements, when compared side by side, indicate that the M_w 6.2 earthquakes in February and June 2011 were by no means earthquakes with the strongest magnitude in terms of magnitude, and yet made the most impact in the Port Hills by acting as (cliff-collapsing) trigger mechanisms. However, the same earthquakes had peak ground accelerations (PGA) measured at ~2 g within the Port Hills area, which was roughly twice as much as the PGA values measured for the M_w 7.1 and M_w 5.3 earthquakes that struck the same area in September 2010 and April 2011. This shows that it is the vertical and horizontal PGA endured on-site that determines whether the source earthquake was intense enough to act as a trigger mechanism; whereby, the greater the PGA, the more severe the slope failures – increasing in scale.

In other words, the shaking intensity, established as being the sole criteria for an earthquake acting as a trigger mechanism, correlates to the PGA values measures on-site. Moreover, Table 18 also shows that the overall PGA values measured in the Port

Table 18 – Modified summary of the main 2010/2011 Canterbury earthquakes and their measured peak ground acceleration (PGA) records taken from accelerometers located in the Port Hills taken from (Massey et al., 2012) – not including the Mw 5.6 earthquake that struck roughly an hour prior to the Mw 6.2 earthquake on 13/06/2011. The listed stations are GeoNet Strong-motion recording sites: CMHS - Cashmere High School; GODS – Godley Drive; HVSC – Heathcote Valley Primary School; LPCC – Lyttelton Port Company; PARS – Panorama Road. Additional information added to the table are gathered from the archives of the GeoNet Website (GNS Science, 2012).

Date (NZ Time)	Moment Magnitude (M_w)	Source Fault			Focus Depth (km)	Mercalli Intensity Scale (MM)	PGA Horizontal [1] (g)	PGA Vertical (g)	Strong Motion Station	Distance from epicentre		Direction of Wave Propagation [2]	Consequences in Port Hills
		Orientation	Rupture Type	General Direction of Slip						To Motion Station (km)	To Redcliffs (km)		
4/09/2010	7.1	E-W surface rupture	Complex	E-W	10	X	0.3	0.3	CMHS	37.3	45	E	A few localised rockfalls and cliff collapses
							0.6	0.0	HVSC	44.3			
22/02/2011	6.2	NE-SW	Oblique-reverse thrust	NW	5.0	IX	0.5	0.9	CMHS	4.7	5.0	NE	Many widespread rockfalls, cliff collapses and landslides occurred over *all of the Port Hills*
							2.1	**2.2**	HVSC	2.5			
							1.3	0.5	LPCC	3.0			
16/04/2011	5.3	N/A	N/A	N/A	10.6	VI	0.2	0.1	CMHS	11.5	4.8	NW	Some localised rockfalls and cliff collapses
							0.8	0.4	PARS	0.9			
							0.2	0.1	LPCC	3.3			
13/06/2011	6.2	NNW-SSE [3]	Strike-slip	NNW-SSE	7.0	IX	**2.2**	**1.1**	GODS	5.22	1.4	NNW	Many widespread rockfalls, cliff collapses and landslides occurred *in the epicentral region*
							1.0	0.7	PARS	4.45			
							0.4 [4]	0.1	LPCC	4.1			

N/A – Information was not available at the time of compiling this database

[1] Calculated using the maximum vector of both horizontal components

[2] Relative to Redcliffs' site

[3] Has an E-W trending component at the northern end of the fault

[4] Recorded by adjacent station Lyttelton Port, Cashin Quay (LPQC)

[5] Except the northern component slipped in the NE direction)

Hills varies depending on a variety of factors regarding fault rupture(s) translating into ground movement felt on the surface. In engineering seismology terms, these factors include source-to-location-specific, site-specific, and (travel) path-specific influences which control the level of ground motion experienced on the surface of the earth when a fault ruptures.

Review of fault characteristics

The following is a review of the main factors that influenced the intensity of the trigger earthquakes, and briefly discusses how each effect (in theory) is an effective trigger mechanism. The main factors reviewed (in respect to the trigger earthquakes) include:

- The distance seismic waves travelled from source-to-site;
- The type of fault(s) that ruptured;
- Direction of the wave propagation; and
- Amplification of incoming seismic waves in the site of interest.

Path Effect: Source-to-Site Distance

One of the principal controls understood to have made the M_w 6.2 earthquakes effective trigger mechanisms, compared to the other major earthquakes that occurred in the past, is due to a path-specific factor concerning the lack of attenuation of the seismic waves. This lack of attenuation is caused by the short (travel) distance between source of the earthquake and location – in this case being Redcliffs' cliff.

The standard behaviour of propagating (seismic) waves regarding distanced travelled is the dispersion of the waves as it begins to travel away from the fault rupture (Ben-Menahem & Singh, 2000). As seismic waves travel through the medium of earth, they refract and reflect through different densities and stiffness, and begin to dissipate at a certain rate, which decreases the resulting ground movement as seismic waves propagate further away from the earthquake source (Cagniard, 1962). This is due to the loss the energy from the seismic waves as it strikes differing subsurface material properties. Upon striking a boundary between differing material properties, the wave energy is transmitted, reflected and converted into other wave-types / other forms of energy such as heat and sound. Zhao et al., 1997 demonstrates this principle of wave theory for different fault types and rupturing at different depths, based on data collected around the world (including

New Zealand), showing the decreasing trend of ground movement in the form of PGA values over the distances travelled away from the source of the quake (Figure 47).

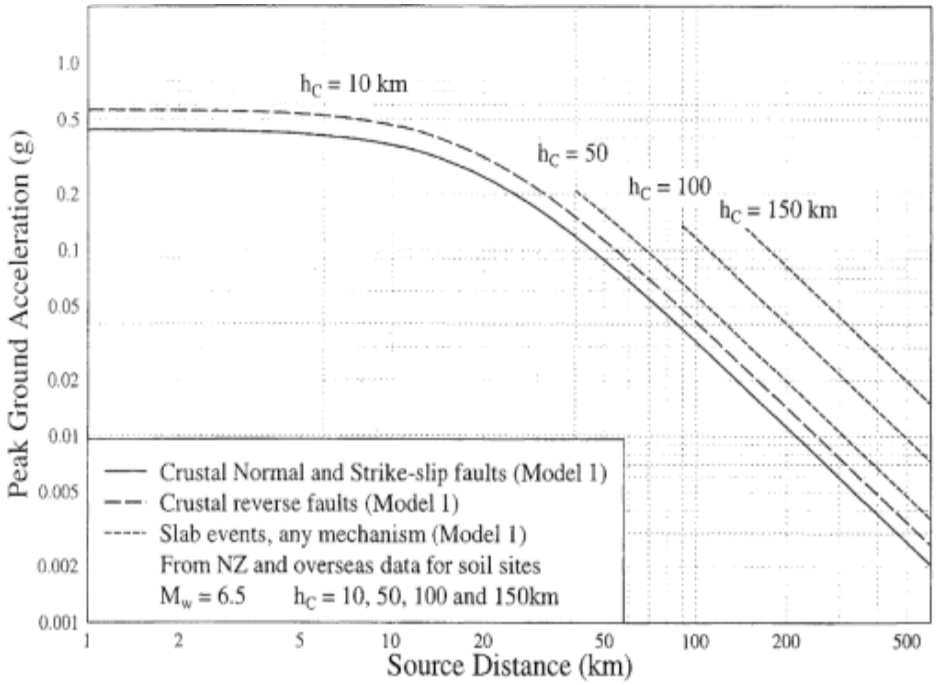

Figure 47 - A graph illustrating the effect of depth (h_c) and mechanism (of different types of faults) and the PGA plotted against source distance. PGA is a quantified measurement for the amount of (vertical) shaking an area experiences. The graph displays a decreasing trend of measured PGA values over the distance travelled away from the source (Zhao et al., 1997).

Furthermore, recent studies such as Wood (2007) also show that the shorter distance travelled also "groups" the seismic waves of different velocities together causing prolonged, amplified ground shakings of greater (collective) intensity. This occurs as waves did not have the opportunity to travel far enough to "spread out" the impact timings of the wavefronts from different seismic waves, which further proves that the PGA on a site closer to the source of a quake would be far greater than that of site further away from the source.

Comparing between the four major earthquakes listed in Table 18, the M_w 6.2 Christchurch earthquakes which triggered the cliff to collapse in February and June 2011 only travelled a respective 5.0 and 1.4 km from the epicentre to Redcliffs' cliff, whereas to the Darfield earthquake on 4 September 2011 which occurred at a much greater distance of 45 km away from Redcliffs. This meant that,

i. The distance of the M_w 6.2 Christchurch earthquakes (relative to Redcliffs' cliff) would have been too short to affect (weaken) the PGA felt at Redcliffs (Figure 48). In essence, there would have been more than enough potential

energy in the seismic waves from either of the earthquakes to generate a great enough PGA to shake / stress the cliff till the point of triggering a major cliff collapse.

ii. In retrospective, for the Darfield (4 September 2011) earthquake to act as a triggering mechanism of Redcliffs' cliff, the source of the earthquake would have to be much closer to the site.

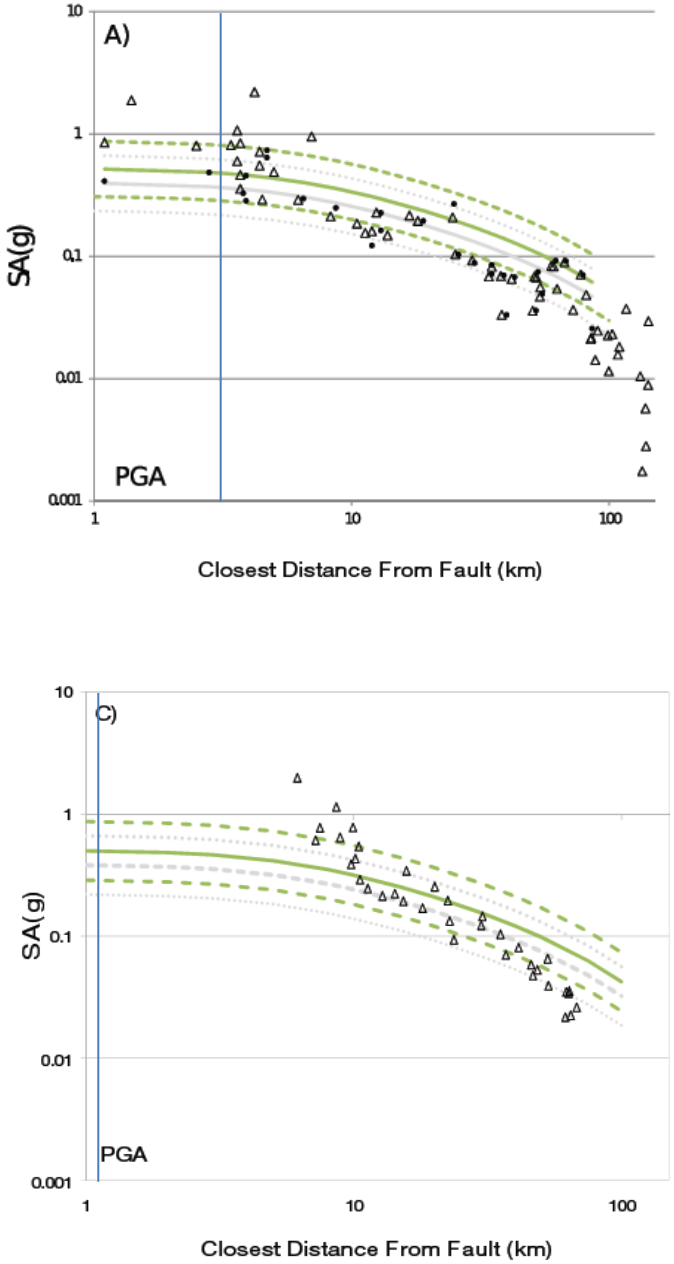

Figure 48 - A chart of the ground motion intensity over a distance 100 km of the February (A) and June (B) 2011 Mw 6.2 earthquakes (Fry & Gerstenberger, 2011). Triangles represent the PGA values, the curved lines represent a predicted ground motion from (McVerry et al., 2006), and the vertical straight blue line represents where Redcliffs would lie in terms of distance away from the earthquake source.

Source Effect: Fault Type and Directivity

Source effects are characteristics of an earthquake source, commonly referred to as earthquake source parameters. Based on the information collected about the four major seismic events that struck Redcliffs, and the rest of Christchurch (Table 18), the trigger-earthquakes that caused Redcliffs' cliff to collapse shows that earthquakes have to be of size (magnitude) and occur at a shallow enough depth as a prerequisite for becoming an effective trigger mechanism. Furthermore, the faulting mechanism (type of faulting) of either earthquake might have also helped increase the intensity of the trigger earthquakes, particularly the February 2011 event.

Empirical studies such as (Campbell, 1997) and (Spudich et al, 1999) demonstrated that reverse and thrust-faulting earthquakes have relatively higher ground motions than compared to normal-faulting / strike-slip events in an extensional regime, which might have lower ground motions than other types of shallow crustal events. Hence, from a theoretical standpoint, being an oblique-reverse-thrust fault (referring to the M_w 6.2 February earthquake) might have helped increase the intensity of the trigger earthquakes, more-so than the strike-slip June 2011 incident. While there may be other factors in play, this underlying principle of thrust faults inducing harsher ground motions than strike-slip faults could explain the significant difference in the vertical component of PGA between the February and June 2011 (M_w 6.2) trigger earthquakes since the June earthquake only measured PGA (vert.) 1.1 g, whereas the February earthquake had a measured PGA (vert.) of 2.2 g.

Another source effect recognised to have a direct effect on influencing the intense (trigger-based) ground motions felt at Redcliffs, and the rest of the eastern suburbs of Christchurch, is related to the direction at which the seismic waves travel with respect to the destination. This phenomenon is a well-known seismological principle called (rupture) directivity, which occurs in the near-source region, only when there is an alignment of the rupture front, direction of slip, and source-to-site direction (Campbell, 2003; Bradley, 2012).

Directivity can occur in either a forward or backward direction, with both directions affecting the intensity / severity of ground shaking in a contrasting manner. Forward directivity conveys the most interest to an engineering geologist due to its particularly large damage potential than compared to backward directivity. From an engineering geological perspective, the significance of this effect increases when the

earthquake magnitude increases as it results in larger rupture duration (Bradley, 2012).

In essence, forward directivity increases the amplitude of seismic waves (and shortens the duration) that propagates in the forward direction of rupture propagation (Campbell, 2003). This in turn focuses a large portion of radiated seismic energy from a single pulse, which (subsequently) generates stronger ground motions; thus increasing the intensity of the quake felt along the direction of rupture similar to that or a much larger quake (Bradley, 2012; GNS Science, No date). On the other hand, for rupture propagations directed "away" from the site of interest, i.e. backward directivity, the decrease in amplitude would inadvertently result in ground motion with a longer duration; thus decreasing the intensity of the earthquake (Somerville, 2003).

The effect of forward directivity only occurs near the source region in earthquakes for all magnitudes, but not in all directions from a fault in the near-source region (Boatwright, 2007). Considering the type of faults that ruptured on 22 February and 13 June 2011, it's positioning, and location with respect to Redcliffs (cliff), it is believed that Redcliffs is situated within this path of forward directivity from both M_w 6.2 earthquakes seeing as the direction of slip and (resultant) rupture propagation of both faults are oriented in that general direction (i.e. towards Redcliffs) (Figures 49 and 50).

Site-specific Effects: Topographic Amplification

Site-specific influences deals with the amplification and / or attenuation of incoming seismic waves as it strikes the site of interest. The main factors that can influence such a change are related to the combined geology of the site and its topography – both of which are relevant to the case of the trigger earthquakes and Redcliffs' cliff. Topographical amplification (or attenuation) not only involves the physical aspect of an undulating surface, as in the slope orientation, shape and dimensions of topography such as hills and cliffs, but is also influenced by lithology, such as irregularities like the impedance contrast within the layers of a subsurface / surficial material deposits (Faccioli et al, 2002; Geli et al, 1988; Ashford et al., 1997; Sepulveda et al., 2005).

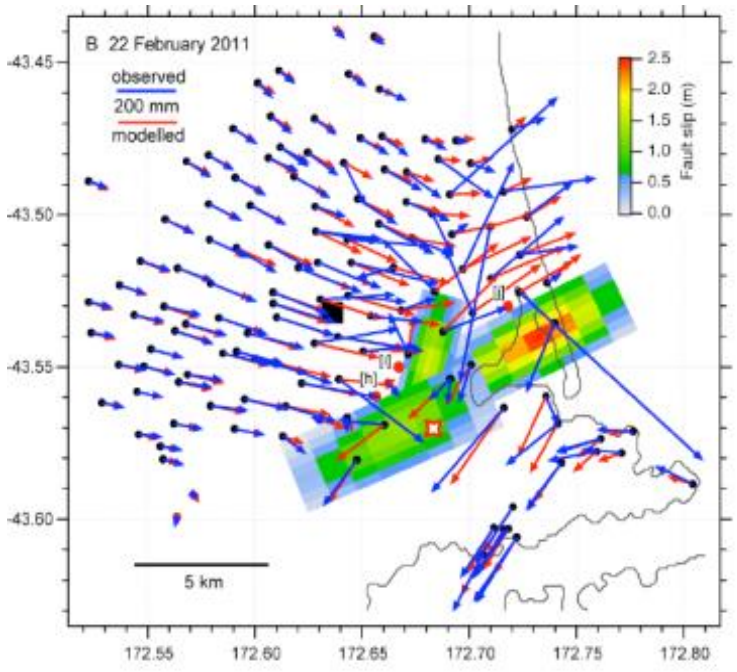

Figure 49 - Illustration of displacements and slip of the February earthquake, derived from GPS and DInSAR data. Most of the fault-slip trends WSW-ESE with some aspects focused in the NNE-SSE orientation - towards Redcliffs. The red colour zone represents the maximum skip of 2.5 m with white representing no slip. Red dots with nearby letters in square brackets (e.g. [a]) are located where the centres of the fault segments would outcrop if extended to the surface (Beavan et al., 2012).

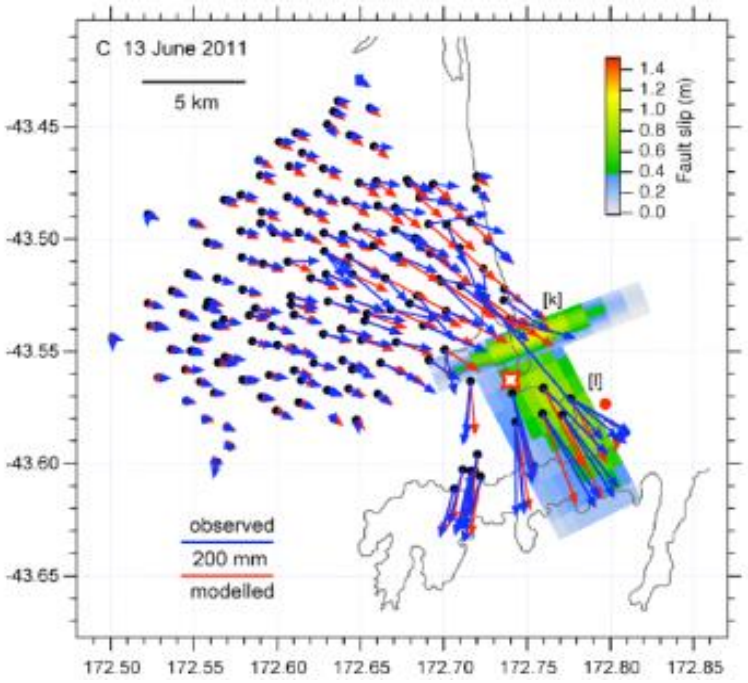

Figure 50 - Illustration of displacements and slip for the June earthquake, derived from GPS and DInSAR data. General fault-slip trends in a NNW-SSE direction (towards Redcliffs and the rest of the Port Hills) with some aspects trending perpendicularly in direction in a ENE-WSW orientation. The red colour zone represents the maximum skip of 2.5 m with white representing no slip. Red dots with nearby letters in square brackets (e.g. [k]) are positions where the centres of the fault segments would outcrop if extended to the surface (Beavan et al., 2012).

Influence by the hilly topography (Redcliffs' cliff) is visually the most apparent factor, since post-earthquake damages to houses on top of the cliff (by the cliff edge) are evidently greater than those located at the base of the cliff (i.e. on flat land), and the fact that slope orientation and slope height provide easily observable indices with influence on topographic effects. Sepulveda, et al. (2005) summarized analytical and empirical studies done by (Geli et al., 1988; Ashford et al., 1997; Ashford & Sitar, 1997; Poppelliers & Pavlis, 2002; Assimaki & Gazetas, 2004) relating the conduct of seismic amplification on slopes into six main principles, showing that:

I. Peak amplification occurs close to the slope of the slope, with complex differential response along the slope, while de-amplification takes places at the base;
II. Amplifications are higher for the more destructive S-waves than compared to the P-waves;
III. Ground motion at the crest of the slope is amplified for inclined waves travelling into the slope and attenuated for waves travelling away from the slope;
IV. The undulating topography scatters a significant amount of body-wave energy into high frequency waves, which may play a key role in the disturbance along the slope;
V. For slopes, peaks of amplification are associated to certain ratios of slope height to seismic wavelength (i.e. natural frequency); and that
VI. Layering of slope materials may produce resonance effects and interference with the topographic effect, generating higher amplifications.

While it remains to be seen if topographic amplification was a significant factor in increasing the intensity of the ground motion felt at Redcliffs, assuming that it did occur, it is within reason to assume that all six principles apply to the amplification of the Mw 6.2 earthquakes (in some extent) which caused Redcliffs' cliff to collapse twice over the course of four months. Theoretically speaking, it is estimated that the pure topographic amplification felt in the cliff would be a factor of 2 at most (Kawase, 2003).

In essence, the integration of seismic ground motion and a hilly surface configuration causes steep slopes (and ridges) to undergo a complex amplification – de-amplification response patterns to seismic ground motion, and also differential motions, especially in the upper parts of the hill (Geli et al., 1988). This can

subsequently increase the ground accelerations felt on-site, which may trigger slope failures that would be stable under regional shaking conditions (Sepulveda et al., 2005). Considering that Redcliffs' cliff is a particularly steep slope (i.e. > 60° on average), this influence becomes more apparent as the topographic effect tends to decrease with slope angle (Ashford et al., 1997).

However, the significance of topography cannot be fully accredited to just the surface topography as many studies such as Steidl, et al (1996) and Spiduch et al (1996) suggest that even on a rock site (like Redcliffs) has strong site effects due to the subsurface structure below. While surface and subsurface topography both have their merits in amplifying ground motion on-site, it makes it difficult to differentiate between the two to be able to distinguish which is the main influence / cause of amplification, unless we know the subsurface velocity structure of the site in detail.

Overview of Trigger Earthquakes

The first trigger earthquake struck SW of Redcliffs on an oblique reverse-thrust fault that trends WSW-ENE (Figure 6). The fault rupture began with a minor slip on the southern end of the fault, between the two sides of the fault roughly 6 km below the epicentre (GNS Science, 2011). Evidently, the southern end of the fault shifts up and north-westward, causing forward directivity in a NW direction (i.e. towards the city of Christchurch). However, the northern end of the fault also moved, but in the opposite (SE) direction, causing a slip greater than 2.5 m at 4 km depth, centred at the Avon-Heathcote Estuary. It is because of this misalignment between the direction of slip on the fault and inferred direction of rupture on the fault that caused the forward directivity to prevail in the smaller area of eastern suburbs of Christchurch (i.e. where Redcliffs is located) since it was located SE of the northern end of the fault (Aagaard et al., 2004; Bradley & Cubrinovski, 2011); Holden, 2011).

The second trigger earthquake happened roughly four months after the first rupture on a NNW-SSE trending strike-slip fault located NW of Redcliffs, between Brighton Spit and near the mouth of Lyttleton Harbour (Figure 8). Rupturing of this fault resulted in the a predominantly unilateral slip on western side of the fault moving in a SE direction, while the east side moved in the opposite direction, producing a maximum slip producing a maximum slip of 1.5 km at 4.5 km depth beneath the Brighton Spit and Sumner (GNS, 2011). GPS displacements recorded in the eastern Port Hills also suggested the rupture included a left-lateral slip on the NNW-trending fault plane, which is consistent with a NW trend of aftershocks leading

from the earthquake location across the Bank Peninsula (Figure 50). However, it is the result of a SW slip of the western side of the fault that was understood to have caused forward directivity in the eastern suburbs of Christchurch / Sumner – Redcliffs area.

Overall, the general consensus is that directivity from both earthquakes (including 22nd February 2011) resulted parts of the Port Hills to move south, or southwest, and up; with parts of the hills rising by more than 40 cm (GNS, 2011).

5.2.1 Enabling Factors

In addition to the seismic trigger mechanisms encountered by Redcliffs' cliff, other external factors were also considered to have made an impact in helping to destabilize Redcliffs' cliff. Unlike triggers which caused the collapse, these factors / mechanisms that contributed to either failure incidents differ as they function as enablers which help facilitate the potential for failure to occur.

First collapse - 22 February 2011

Time was identified as being the main enabling factor which contributed to the collapse of Redcliffs' cliff on 22 February 2011, that is to say no apparent trigger was recognized as being the sole conditioning / enabling factor considering how long the same cliff face has been exposed to the elements (i.e. factors that weaken the slope).

While it is unknown when the last major alteration of the cliff occur, it is believed that excessive changes to the geometry of the slope had not happen in a long period of time, possibly going as far back as ~9000 years ago when the cliffs were modified by wave action (Massey et al, 2012). This meant that for an extensive period of time, the same material properties on the cliff face were exposed to erosion, weathering, and (potentially historical) seismic activity, which significantly weakened the exposed heterogeneous and anisotropic rockmass. Some of the more specific examples of causes that alter the structure of the slope include:

- Erosion from sources such as water from rainfall, wind, and gravity removing material from the cliff face;
- Physical (mechanical) weathering such as: freeze-thaw weathering, hydraulic action, salt-crystal growth;
- Deep chemical weathering of the rocks solutions from rainfall or sea altering the chemistry of the rocks and forming clay minerals;

- Biological weathering in the form of vegetation such as bushes and trees growing on the slopes embedding its roots into the slope face fracturing the slope in the process, as well as releasing bio-chemicals into break down the rockmass;

Eventhough such factors involved with time (and gravity) weakened the cliff / conditioned the cliff to fail, it did not possess the capabilities to trigger a collapse. This is attributed to the strength of the discontinuities and intact rock mass that made up the cliff (even as the exposed surface was thoroughly weakened) and the physical geometry of the slope at the time that made the cliff structurally very stable, considering the in-situ stresses the Redcliffs cliff endures as a large/tall near-vertical rock slope .

Other enabling factors were also considered whilst evaluating the cause of collapse(s), particularly saturation of the rockmass and soil through excessive rainfall. However, considering the summer weather, which consists mainly of sunshine and particularly low levels of precipitation in the area of Christchurch at the time leading up to the first collapse (Corbett, 2011; WeatherSpark, No Date), it was highly unlikely that there was enough moisture in the rock and soil (or even any) to have helped cause material to detach from the cliff as it collapsed for the first time.

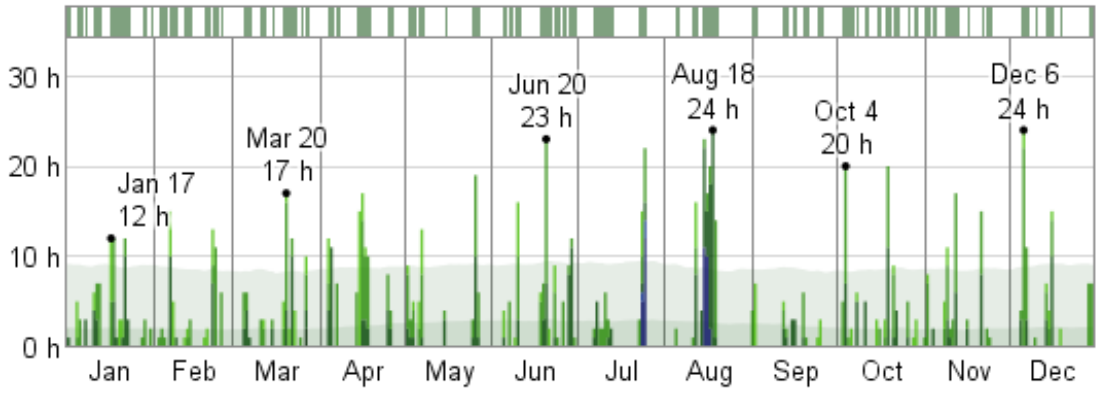

Figure 51 - A graph summarising the daily number of hourly observed precipitation reports during 2011, colour coded according to precipitation type, and stacked in order of severity (WeatherSpark, No Date). Heavy, moderate, and light rain (dark to light green), drizzle (lightest green). The faint shaded areas indicate climate normal. The bar at the top of the graph is green if any precipitation was observed that day and white otherwise.

Second collapse – 13 June 2011

Similarly to the initial collapse of Redcliffs' cliff, the weather (rainfall), seismic activity, and overall time were considered when deducing the trigger mechanisms

that caused the second collapse. However, based on the information gathered regarding these three factors considered, the only trigger mechanism identified to have contributed significantly to the slope failure was the seismic activity that happened up till the point of the M_w 6.2 trigger earthquake that initiated failure on the cliff face.

Kanari (2008) understood that in order for failure to occur under s seismic influence, a sequence of earthquakes is required to trigger a slope failure rather than an isolated earthquake. This emphasises the fact that rockmasses require the right condition for failure, where in a seismically-induced incident, a certain level of 'maturity' is needed of deformation within the rockmass to weaken the slope enough for an earthquake to trigger failure. This was the case for the second collapse. Not only did earthquakes play a role in this rock slope failure as a trigger, but also initiating factor which conditioned / weakened the slope by putting additional strain and stress on discontinuities present within the rockmass.

The nature of time and weather were considered as secondary trigger mechanisms to the earthquake. However, time was disregarded as a trigger mechanism in this instance, seeing as the second major collapse of Redcliffs' cliff happened on the 13 June 2011, just short of four months after the initial collapse of the same cliff face. This was simply not enough time for the (freshly) exposed cliff face to have weakened to the same level as it was just prior to the first collapse.

As for the effect of rainfall, even though there was an increase amount of rainfall in the area, given that it was the winter season, there is no evidence to suggest that there was sufficient amount water in the cliff to have assisted in the collapse of Redcliffs' cliff. While rainfall did occur prior to the failure incident (Corbett, 2011; WeatherSpark, No Date), it was not intense (nor continuous) enough of a rainfall event to have significantly raised saturation levels in the cliff. In addition, assuming that not all the water that infiltrated the porous parts of the body of rock and soil had already escaped the slope, the resulting water pressure generated by the rainfall would have not been significant enough to have any affect the effective stress and shear strength along the discontinuities present in the slope.

3.1.2 Summary

Henceforth, with the knowledge and information gathered about the cliff and earthquake, it is within reason to propose that:

1. The first cliff collapse, the act of time as an "enabling" triggering mechanism could only condition the slope to collapse, whereas the actual trigger to initiate the collapse was the ML 6.2 earthquake on 22 February 2011.
2. Seismicity acted as both the trigger (mechanism) and enabling factor in the 13 June 2011 cliff collapse, whereby the combined series of major seismic activity leading up to the major M_L 6.3 earthquake, including 22 February 2011 earthquake, provided the necessary impact to weaken / condition the slope for a seismically induced failure.
3. Even though time proved to be ineffective in trigger a collapse, it was a crucial factor in initiating a greater volume of material falling / sliding down the cliff. As a trigger mechanism to condition the slope however, a series of earthquakes are not as effective as exposure to 'the elements' over time.

Ultimately, the measurements and deductions made regarding the earthquake triggers revealed a fundamental trait regarding the intensity of earthquakes. It proved that the intensity of an earthquake (i.e. the intense ground movement) is dictated by certain physical factors that are: source-to-location-specific, site- specific, and (travel) path-specific factors which control the severity of the ground motion. In the case of Redcliffs' cliff and the rest of Port Hills, the minimal distance travelled and attenuation of the seismic waves from two M_w 6.2 earthquakes in the vicinity of the Port Hills area provided the right conditions for the two respective earthquakes (with PGA ~ 2 g) to act as triggering mechanisms.

While the stress of major earthquakes, such as ones that occurred in February and June 2011, can weaken the internal structure and cause sea-cut cliffs such as Redcliffs' cliff to collapse, it is highly likely that the process of weakening can only occur within the deformation components (i.e. discontinuities) considering the significant strength of the intact rockmass of the sea-cut cliff. However, earthquakes and aftershocks are not the only trigger mechanisms that alter the structural stability of the cliff. The factor of time played a major role in weakening the slope prior to the first collapse of Redcliffs' cliff. It encompasses all weakening (trigger) mechanisms with the ability to not only weaken the discontinuities, but also the intact rockmass through extensive chemical and physical weathering. Consequently, this would have weakened the cliff face even further, potentially causing a greater volume of material to detach from the cliff face in the event of the major earthquake trigger in February 2011.

5.3 Amidst Failure: Slope-Failure Mechanics

On 22 February and 13 June 2011, the resultant shaking from two Mw 6.2 earthquakes caused Redcliffs' cliff to shake at a PGA ~2 g. The shaking-intensity from the two major earthquakes was severe enough to have stressed the cliff, exceeding the (stability) threshold that is needed to produce earthquake-induced slope movement. As a result, failure occurred across the entire cliff face, with the exception of one section on the NE Face of the cliff. While it is not clearly understood why that particular section did not collapse like the rest of the cliff face, for all intents and purposes, any notion / referral to failure across the (entire) cliff face excludes the un-collapsed section of the cliff face for the remainder of this discussion.

The following subsection will present the results from a literature research and kinematic analysis done to classify the failure modes involved in the February and June 2011 collapse of Redcliffs' cliff. The results consist of analysing the collapse of Redcliffs' cliff from two different perspectives: from a global perspective – i.e. the overall failure of the entire cliff face; and a localised perspective – i.e. looking at failure of the individual slope aspects (NE and SE Face), and the individual soil and rock masses, in an attempt to understand how the slope-failure mechanics of Redcliffs' cliff operated at the point of failure.

5.3.1 Global Perspective

Based on the surveys conducted to determine the physical changes done to the cliff after both failure incidents, the data suggest that material was loss from all parts of the cliff face above the talus, which meant that each individual unit within the exposed strata failed (to some extent). Looking at the Redcliffs' cliff in its entirety, this meant that, from a global perspective, the failure incidents can be considered as a global failure, where both the February and June 2011 failure incidents were single (non-monotonically occurring) events; that is to say, failure mechanisms within each rock unit act alone as a result of earthquake loading, but released from the slope in conjunction with other blocks and produced an overall disjointed failure surface on the slope made from multiple failure planes, encompassing failure of all four geological units that make up the exposed cliff face.

Continuum vs. Discontinuum

Classifying the failure of Redcliffs' cliff from a global perspective was done based on the frequency of the discontinuities present (i.e. based on the block sizes) that control

the overall rock mass behaviour of the slope. Depending on the frequency, there are four possible types:

i. Intact Rock (no discontinuities) – Continuum;
ii. Individual, discrete discontinuities – Continuum + Interfaces (structurally controlled);
iii. Few sets of spaced discontinuities – Discontinuum (structurally controlled);
iv. Many sets of closely-spaced discontinuities – Equivalent Continuum.

First Collapse: 22 February 2011

For the first collapse in February 2011, the slope movement was classified as a structurally-controlled Discontinuum, however, there is reason to suggest that (partial) Equivalent Continuum could have occurred as well. The idea was brought on by considering the overall structural condition of the inner and outer (near-surface) part of the slope (i.e. the distribution and frequency of discontinuities; the variable block sizes throughout the body of rock) that inevitably detaches from the cliff (failure body; Figure 52) in the 22 February 2011 earthquake.

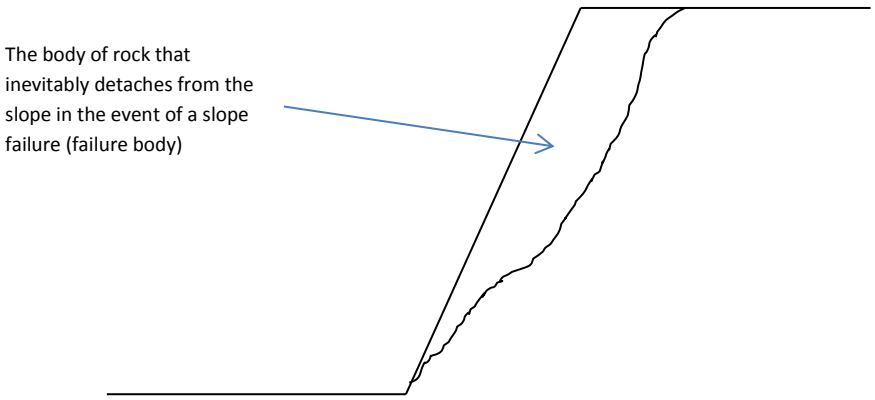

Table 52 – Illustration of a 'failure body", which the represents the section of the cliff face that inevitably fails; describing all the blocks of rock that detach from the cliff face as a whole.

Since the occurrence of major discontinuities such as (columnar) joint sets are consistent throughout a rock mass, the only type of discontinuity that can vary (and potentially alter the structural controls for failure) are the fractures, or rather, defects brought on by factors such as: intense ground motion (earthquakes); in-situ stresses; or mechanical weathering. It is the different types of mechanical weathering (over time) which has led to the consideration of two different conditions, and, thus, different failure behaviours within the blocks that detaches from the cliff face (failure body).

Inner part of failure body

Based on the empirical evidence presented in Section 4.6.1 describing the structural characteristics and slope condition of Redcliffs' cliff, it is presumed that discontinuous failure occurred within the inner part of the failure body. This is because:

- The overall strength of the slope is considered to be very high, which limits the formation of other defects; and
- Unlike the outer component of the failure body, it does not have contact with the atmosphere which limits the type of factors to that can create additional defects, i.e. mainly seismic-based defect forming conditions.

Furthermore, based on post-failure description of the cliff face (Map 2), there were only a few fractures identified on the NE Face and SE Face that developed as a result of the intense seismic shaking. This reinforces the overall high level of strength of the cliff since the previously concealed part of the cliff had the capability to resist / limit the formation of additional defects within the rock mass body after a seismically-induced collapse. Hence, it is unlikely that the inner part of the failure body contained a high enough number (density) of defects in the rock masses to alter the structurally-controlled failure.

Outer part of failure body

While defects typically develop in random parts of the cliff (along a path of least resistance), some defects caused by mechanical weathering tend to occur only on or near the surface of the slope (with assistance from direct contact with the atmosphere), which suggests a particular concentration of defects (and thus further weakening of) near the slope surface than compared to within the slope. Even though the overall rock mass body of Redcliffs' cliff is considered very strong, given: the cliff is roughly 3,600 (± 100) years old (McFadgen & Goff, 2005), and the last documented collapse of Redcliffs' cliff was ~19 years ago in 1992 (Bell, 1992), it is well within reason to assume that mechanical weathering of the cliff face would have modified the strength and overall structure of the rock masses, particularly the near-surface of the cliff face.

An example of mechanical weathering that can only happen on the slope surface (seen happen on Redcliffs' cliff) is the growth of vegetation. Well-grown vegetation (i.e. trees and bushes) on the cliff face suggests that there are plant roots already

exists in the slope, which would have exerted physical pressure on the surrounding rock mass when the plant(s) were growing. The process of plant growth would have either caused defects to further widen, and / or develop new defects on the slope surface. Furthermore, not only would plant growth on the cliff face increase the size and number of defects on in the slope surface, but also allow for more water to seep into the rock mass through the cracks. This increases the potential of frost wedging (expansion of water as it freezes in the cracks) occurring on the surface of the slope, causing defects to widen even more; thus weakening the rock mass even further.

Another example likely to have occurred is the exfoliation of the rock mass(es) where blocks have the potential to expand into free space, creating exfoliation joints. This is based on the observations made after the first collapse in February 2011, which shows indications of exfoliation joints on the far eastern side of the SE Face (Figure 23). While it isn't clear if those exfoliation joints formed before or after the failure incident, it further proves that the near-surface of the cliff face is capable of undergoing the process of exfoliation within the near-surface of the cliff face.

Based on these observations, it can be argued that mechanical weathering up till the collapse of Redcliffs' cliff in the 22 February 2011 earthquake would increase the density of defects in the near-surface of the cliff face This in turn would decrease the block sizes in the rock mass, possibly to the point where the dominant structural patterns disappear (Martin & Chandler, 1994), and subsequently shift the rock masses into a continuum-like behaviour (otherwise known as equivalent continuum) with no recognisable structural control.

Second Collapse: 13 June 2011

Unlike the conditions of the cliff just prior to the first collapse, the condition of the cliff before the second collapse was only slightly worsened by damage from intense seismic shaking (including the earthquake that triggered the first collapse) leading up to the collapse in June 2011. Mechanical weathering would have not been a factor since the weathering process only began after the new surface of the cliff face, which is not enough time (considering the overall rock mass strength of the cliff) to form new defects on the slope surface. This meant that the second collapse was occurred under mainly post-seismic residual conditions (i.e. defects mainly created by intense seismic shaking leading up to the failure incident), rather than weathering- and seismic-based conditions of the first collapse.

While the fractures created by further rock mass disruption during seismic activity would not have led to an Equivalent Continuum, it would have meant an increase in the number of discontinuities which would mean an increase in discontinuous movement as the second collapse ensued. This would explain the more fragmented look of the slope geometry after the second collapse.

Overall Conclusion

Considering the overall slope behaviour on a global scale, even though there suggestive evidence that rock mass damage from mechanical weathering for an extended period of time has resulted in the shift of part of the slope movement to Equivalent Continuum in the February 2011 collapse, the principle slope movement for both the February and June 2011 collapse is believed to have been Discontinuum.

5.3.2 Localised Perspective

Looking past the Equivalent Continuum slope movement of the severely damaged (weathered) outer-surface of the cliff face, the Discontinuum slope movement is a multifaceted amalgamation of failure modes. The assortment of failure modes are arise from the complex lithology comprised of three different rock masses with different rock mass properties that is:

- Relatively massive, weak (low shear strength) unit of tuff;
- Very strong, well jointed unit of welded ignimbrite; and a
- Relatively strong, poorly jointed unit of unwelded ignimbrite.

With such a contrast in properties, it cannot be said definitively that one particular mode of failure was the sole component behind the entire collapse of Redcliffs' cliff.

To try and narrow down the potential failure modes likely to have occurred within the relatively unweathered (discontinuous) body of rock, three individual techniques are used to determine whether toppling or planar; wedge are the most likely failure modes to have occurred during the collapses in February and June 2011.

Kinematic Analysis

A semi-quantitative approach was first attempted using the photogrammetry (discontinuity) data presented in Section 4.5.1 to conduct a kinematic back-analysis to determine whether it is kinematically possible for the cliff face to have toppled and / or slid during either failure incident. The following generalisations were used during the course of this analysis to determine the variables in Table 19:

- The friction angles of the joints within the columnar jointed rock mass were calculated using the Barton-Bandis Failure Criterion (Table 10), assuming the density of welded ignimbrite is 29 kN/m^3 (Freundt & Schmincke, 1995);
- The slope angles were averaged for both the NE and SE-facing slopes;
- Despite the fact that slope angles of the cliff face has changed after each seismic event, the average dip of the SE facing slope before and after both earthquakes only had a difference of < 1 deg. This wasn't a significant enough change to warrant a need to use different slope angles after each seismic period. However, as for the NE-facing slope, the difference of an average slope angle between post- June and pre / post-February was 5°; which was a large enough change to warrant the use of both slope angles.

- **Table 19 - Summary table of the averaged values used for the kinematic analysis**

Features		Northeast-facing Slope (Face 5-6)	Southeast-facing Slope (Face 1-4)
Cliff face orientation	Dip	67°, 72° [1]	62°
	Dip Direction	51°	150°
Slope Height[2]		40 m	27 m
Friction Angle (Barton-Bandis Failure Criterion)		44°	45°
Discontinuity Pole Plots (Stereonet Face number)		1 and 2	3, 4 and 5

[1] two dip angles were used to reflect the overall slope angle for post-February and post-June on the NE Face
[2] the slope height was averaged for the NE and SE Faces, and assumes the entire slope is comprised of only welded ignimbrite for the purpose of this analysis

Discussion

Two separate kinematic analyses were conducted on the north eastern cliff face to account for the change in average dip of the cliff face after the February collapse. However, regardless of the change in the dip, the results were the same:

- There is no evidence of wedge sliding;
- Both sets of stereonets (Figures 54 and 55) indicated ~16 % of the poles from the four main sets are kinematically able to topple;
- Roughly 11 % of the poles indicated the potential for planar sliding, which isn't that significant of a difference to be able to distinguish which was the dominant failure mode of the NE Face.

Kinematic Analysis Results of SE – facing cliff face

Slope orientation: 62 / 150 (dip/dip direction); Friction Angle: 45°

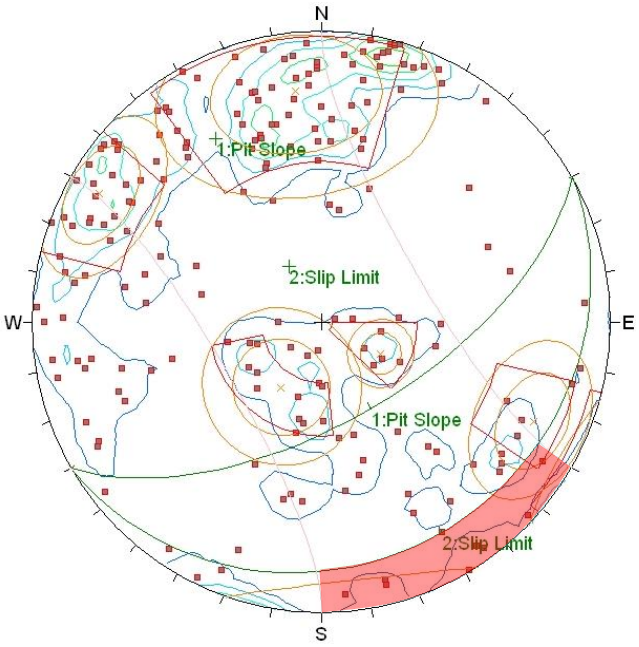

Toppling

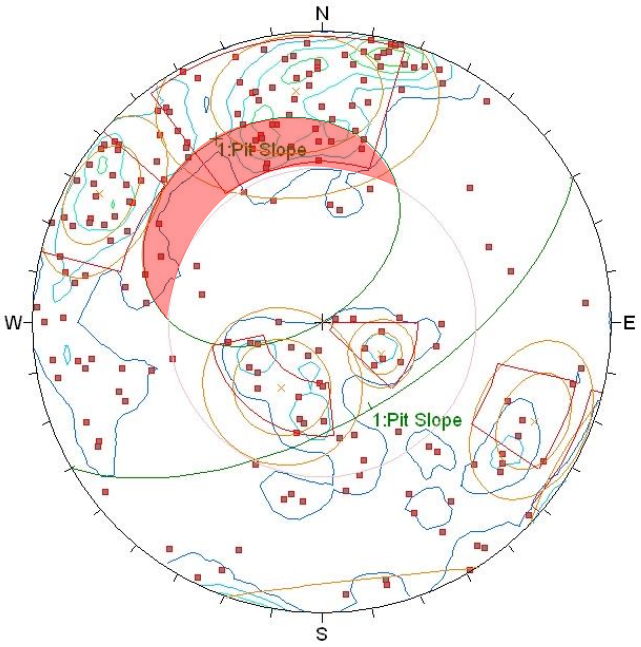

Planar Sliding

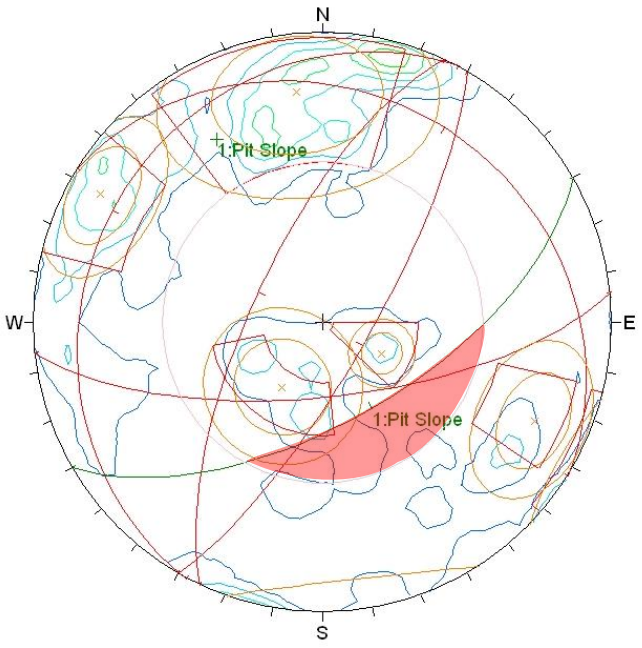

Orientations

ID		Dip / Direction
1		62 / 150
1	w	69 / 174
2	w	77 / 120
3	w	19 / 298
4	w	22 / 032
5	w	70 / 295

Equal Area
Lower Hemisphere
195 Poles
195 Entries

Wedge Failure

Figure 53 - Results of the kinematic analysis in determining the potential for toppling, planar sliding and wedge failure for the SE-facing cliff face. The area highlighted in red represents the zone of failure for the respective types of failure. This result is applicable to the SE face before and after each earthquake since the overall slope angle remained nearly the same throughout.

Kinematic Analysis Results of NE – facing cliff face (post-February 2011)

Slope orientation: 67 / 51 (dip/dip direction); Friction Angle: 44°

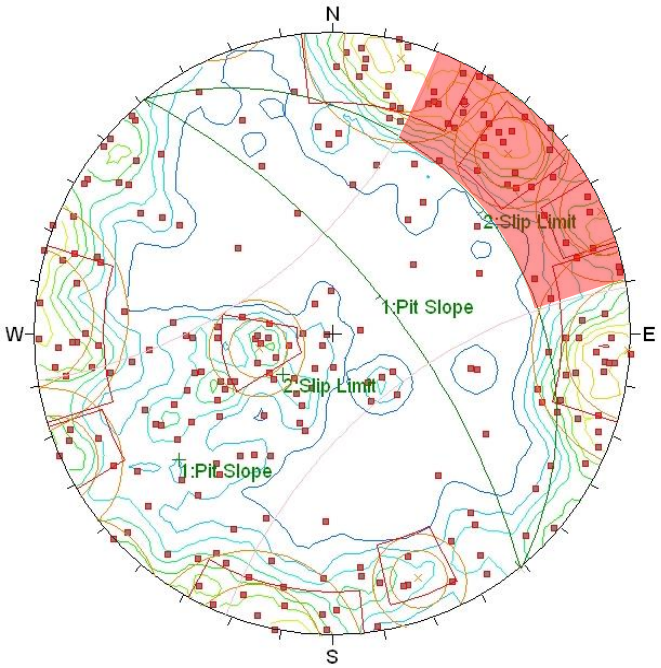

Toppling

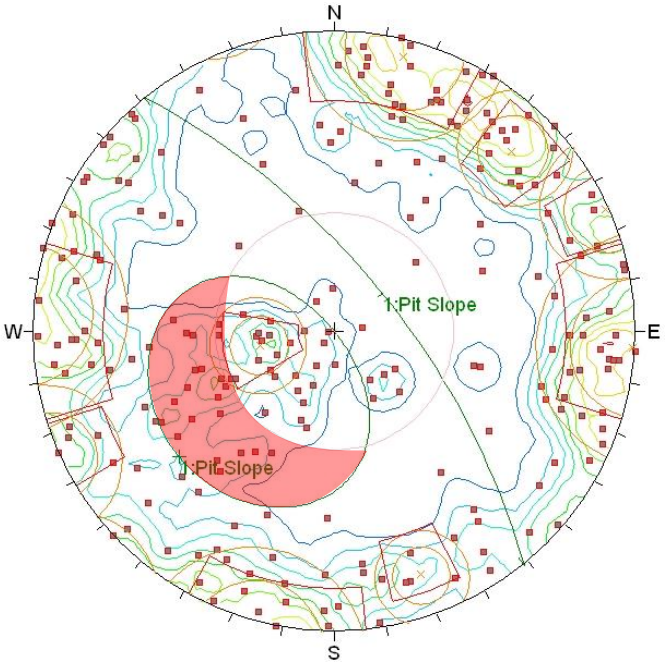

Planar Sliding

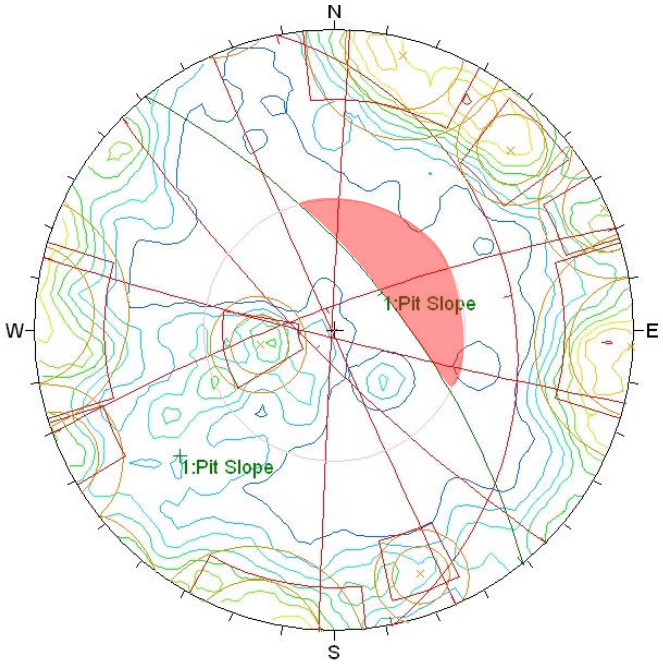

Orientations

ID		Dip / Direction
1		67 / 051
1	w	87 / 194
2	w	80 / 225
3	w	89 / 246
4	w	89 / 273
5	w	81 / 340
6	w	28 / 079

Equal Angle
Lower Hemisphere
238 Poles
238 Entries

Wedge Failure

Figure 54 – Results of the kinematic analysis for the NE Face post-February 2011. The area highlighted in red represents the zone of failure for the respective types of failure.

Kinematic Analysis Results of NE – facing cliff face (post-June 2011)

Slope orientation: 72 / 51 (dip/dip direction); Friction Angle: 43°

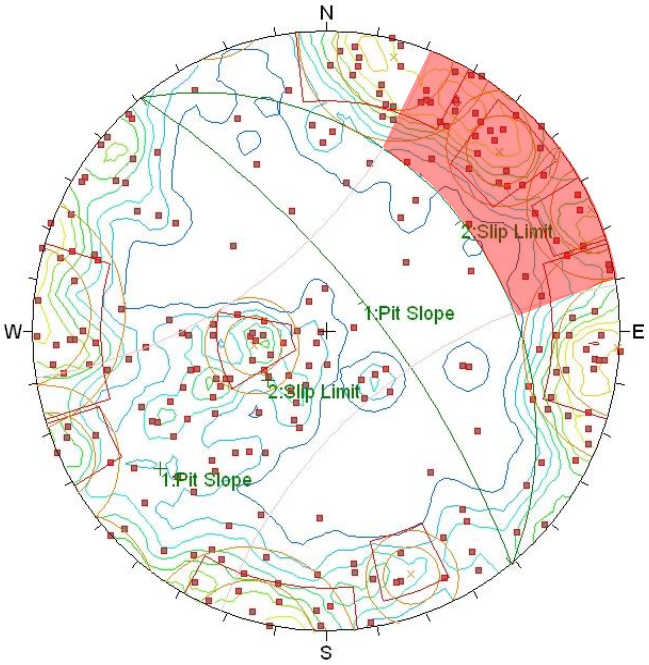

Toppling

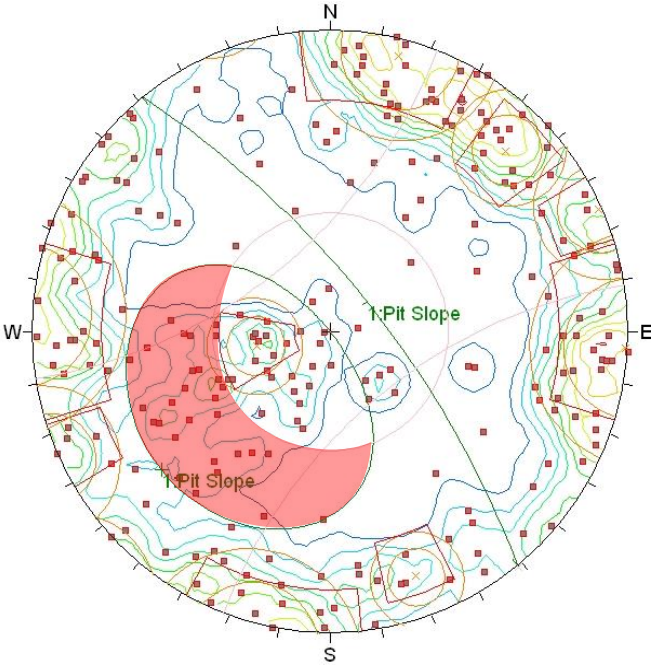

Planar Sliding

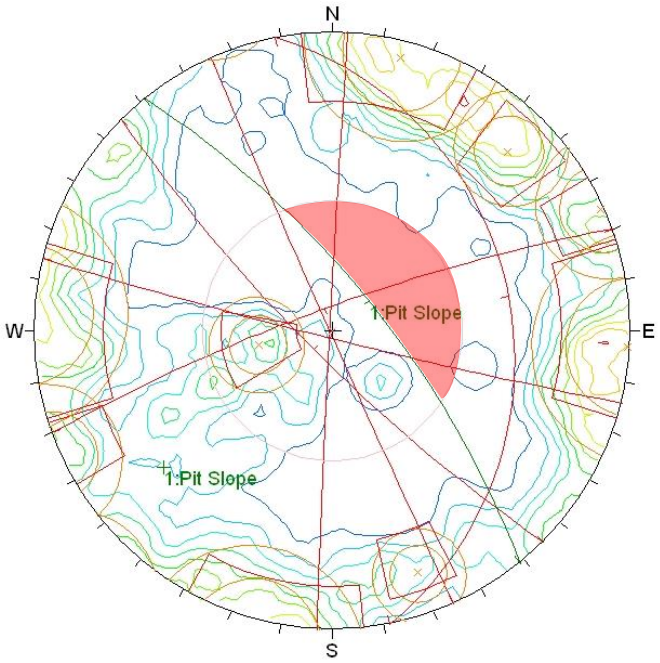

Orientations

ID		Dip / Direction
1		72 / 051
1	w	87 / 194
2	w	80 / 225
3	w	89 / 246
4	w	89 / 273
5	w	81 / 340
6	w	28 / 079

Equal Angle
Lower Hemisphere
238 Poles
238 Entries

Wedge Failure

Figure 55 - Results of the kinematic analysis for the NE Face post-February 2011. The area highlighted in red represents the zone of failure for the respective types of failure.

As for the SE Face (Figure 53), the result of the kinematic analysis shows:

- There is no evidence of wedge sliding failure;
- Approximately 8 % of poles had the potential for planar sliding failure and <5 % of poles had the potential for toppling.
- In addition the ~8 % of poles that fell within the daylight envelope zone of planar failure had an averaged dip of roughly 55˚, similar to the NE face.

Conclusion

From the evidence presented above regarding the kinematic analysis, it is likely that both planar sliding and toppling failure did occur on the discontinuous rock body in the event of the 22 February 2011 and 13 June 2011 earthquakes, which resulted in the deposition of material on the talus at the base of the cliff.

Goodman & Kieffer (2000)

The second attempt was a qualitative approach looking to provide a more descriptive account of the toppling and planar sliding failure identified by the kinematic analysis, as well as include an account of the (potential) failure mode for the soil mantle, by linking empirical evidence collected from surveying the cliff face and cliff top with the types of failure modes proposed by Goodman & Kieffer (2000). Such a comparison is done on the presumption that "wherever one can see a rock face exposed along the surface of a fault, bedding plane, joint, or other discontinuity, it follows that what once covered this surface has been removed" (Goodman & Kieffer, 2000).

The reason behind using a more constructive description is because if one is to account for a mixture of rock mass types and structures within a slope such as Redcliffs' cliff, it cannot be expected that a single mode of failure will cover all the bases in terms of classifying the mode(s) of failure that operated as the cliff collapsed on February and June 2011. On the contrary, it is within reason to find more than one of the simple failure modes at work within a single sliding mass, Simply put, one part may be toppling, another sliding, another experiencing erosion, and yet another suffering from new fractures and the destruction of previously continuous rock volumes (Goodman & Kieffer, 2000).

The result of the cross-comparison between empirical data regarding the "evidence" left behind by the detachment of material from the cliff face, and the (robust) list of failure modes are five potential failure modes that are likely to have occurred when Redcliffs' cliff collapsed on 22 February and 13 June 2011. Out of the five, three are related to the

welded and unwelded ignimbrite; one for the tuff; and another one to describe the failure of the soil mantle (Table 20).

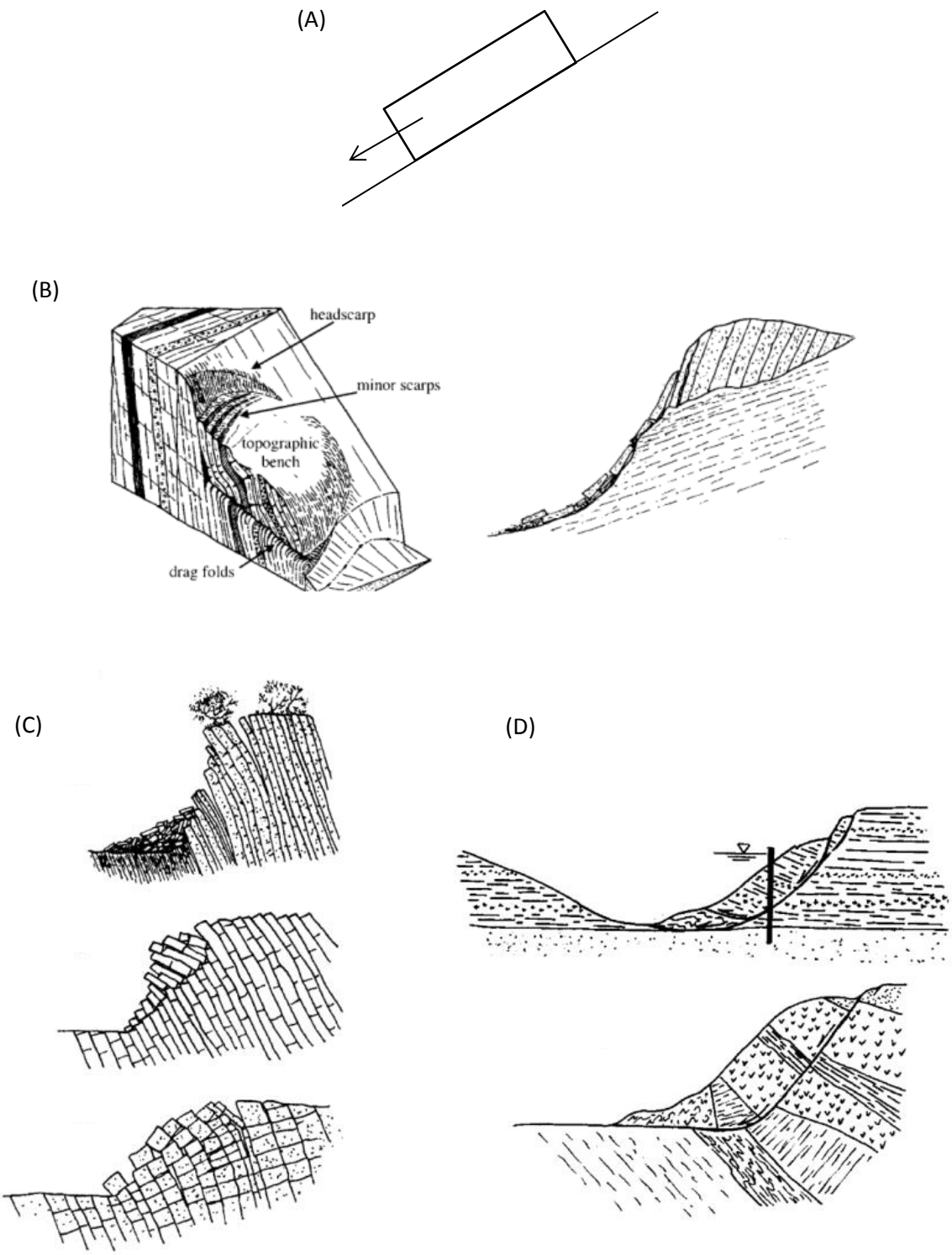

Figure 56 – Illustrations of the failure mode descriptions selected that match the descriptions of the soil and rock masses that make up Redcliffs' cliff. A) Block sliding on a single plane; B) Rock slumping; C) Toppling; D) Rock Bridge cracking; D) Soil type slumping (images for B – D are provided by Goodman and Kieffer, 2000).

Table 20 - Summary table of the failure modes that match the empirical evidence describing the post-failure characteristics of Redcliffs' cliff. Illustrations for each of the failure modes are presented in Figure 56.

Failure Mode	Definition	Typical Materials	Comment
Ravelling	The process of gradual erosion, particle-by-particle or block-by-block	Poorly cemented conglomerates and breccias; very highly fractured hard rocks; layered rock masses being loosened by active weathering, e.g. thinly bedded sandstone/shale	This is the likeliest general failure mode to occur to all rocks exposed when in-situ stresses are the only stresses in play.
Block sliding on a single plane	The act of sliding without rotation along a face; single or multiple blocks	Hard or soft rocks with well-defined discontinuities and jointing, e.g. layered sedimentary rocks, volcanic flow rocks, block-jointed granite, foliated metamorphic rocks	Likely to have occurred for the basalt lava flow and/or breccia rocks on top of the cemented tuff as they are hard rocks with observable well define discontinuities and jointing
Rock slumping	Backward rotation of single or multiple blocks, moving into edge/face contact to form one or more detached beams	Hard rocks with regular, parallel joints dipping toward but not daylighting into free space and one flat-lying joints that does daylight into free space. Multiple block modes typically develop in foliated metamorphic rocks and steeply dipping sedimentary rocks; single block modes develop in block-jointed granites, sandstones and volcanic flow rocks.	Alternative (but more likely) failure mode to have occurred for the basalt lava as it does contain "relatively" parallel joints (i.e. columnar jointing) dipping towards but not daylighting into free space and "relatively" parallel one flat-lying joint (bedding plane) that does daylight into free space.
Toppling	Forward rotation about an edge – single or multiple blocks	Hard rocks with regular, parallel joints dipping away from the free space, with or without crossing joints; foliated metamorphic rocks and steeply	Recognized as the likeliest failure mode for the basalt lava component due to the parallel (columnar) joints and cross-joints found on exposed basalt rock. Additionally, further proof also provided the form of a kinematic analysis conducted on the exposed basalt lava outcrops on the cliff face.
Rock bridge cracking	Failure of intact rock that restrains block motion, through compressive, tensile or flexural cracking	Weak rock forming rock bridges; hard or soft rocks with impersistent discontinuities (as in some layered sedimentary rocks, volcanic flow rocks, block-jointed granite, foliated, or jointed metamorphic rocks)	Another potential mode of failure likely to have occurred during the collapse of Redcliffs' cliff due to the recognised impersistent discontinuities within the rock slope.
Soil type slumping	Shearing with backward rotation, as in clay soils	Weathered or softened clay shales; thick fault gouge; altered zones; soft tuffs. High pore pressure zones	Like mode of failure for the soil mantle on top of the cliff considering the elevated topography of the hillside.

Rockfall vs. Rockslide

The final approach used classifies the incident(s) as either a rockfall or rockslide based on a classification process, which uses the block sizes of rocks deposited at the base of a slope (Day, 2002). It is a simple classification method that can be done based on the observations made of the rock fall debris deposited at the base of the cliff. While it is not a conclusive way to determine the failure mode(s), it was a simple approach used while surveying the cliff that provided an insight as to how the blocks of rock travelled down the slope.

Table 21 – Summary table relating the definition of rock falls and rock slides to the evidence of the respective behave based on the classification methodology by Day (2002).

Behavioural Terms	Definition	Evidence of respective behaviour (Day, 2002)
Rock falls	The free falling nature of rock(s), where triggers such as seismicity causes rock to detach from the cliff (Stokes & Varnes, 1995).	The block sizes of rockfall debris tend to be smaller as they generally break apart upon hitting the ground after being propelled into the air for a brief moment.
Rock slides	The failure of rock from a cliff resulting from shear displacement along a particular failure surface resulting in the inundation of rock at the toe of the cliff.	The block sizes for rock sliding incidents are much larger because the blocks of rock tend to only slide down the failure surface which provides less of an impact as the rock hits the ground

The overall conclusion drawn from using this approach (whilst mapping the talus; Map 1) suggests that both cliff collapses were rockfall incidents since majority of debris are average sized boulders with a few large boulders spread across the talus from one end of the cliff face to the other. The only concentration of large boulders were identified near the SE Face, specifically beneath 8E and 8F Balmoral Lane. However, considering the relatively short height of the slope at that part of the cliff face; the properties of the discontinuities within the source rockmass (most likely breccia); and (ultimately) the fact that the source of the boulder originated at a height above a second geological unit (i.e. cemented tuff acting as a step), it is possible that the boulder did slide initially as part of the failure mode but into free space only to remain airborne for a brief moment before impacting the talus catchment.

5.3.3Summary

Four methods have been used to characterise the failure behaviour of Redcliffs' cliff in the 22 February 2011 and 13 June 2011 earthquakes from multiple perspectives in order to provide a descriptive account to the failure incidents. Comparing between all four methods, both the Continuum vs. Discontinuum, Rockfall vs. Rockslide approach focused on the block sizes as a factor to characterise failure, whether it is based on the density of defects within a rock mass or through post-failure observations of recently deposited debris at the base of a rock slope.

In contrast the other two approaches focuses on characterising the failure based on the kinematic aspect of failure, whereby determining if a slope has the capability to either topple or (planar / wedge) slide. The kinematic analysis is the only quantitative approach used in this part of the study, using discontinuity orientations, slope height and rock mass properties to numerically determine the mode of failure; whereas Goodman & Keiffer (2000) correlates modes failure to certain rock types or soil that are known to undergo such failures.

Overall, using these four methods, it is understood that the collapse of Redcliffs' cliff in the February and June 2011 earthquakes were:

- Discontinuous for both the February and June 2011 incidents;
- The discontinuous rock masses within the cliff have the capability of toppling and planar sliding, which implies that both failure modes would have occurred in both failure events.
- Furthermore, in addition to toppling and planar sliding, it is possible that slumping of the rock masses and soil on top of the cliff and rock bridge cracking of the tuff.

5.4 Post Failure: Comparative Analysis

The following comparative analysis uses the information gathered by overlapping of the cliff top and cliff face models (Chapter Three) in order to gauge the severity of each collapse based on the gradient changes of the slope surface and the (estimated) volume of material detached from the cliff face after each collapsing incident.

5.4.1Loss or Gain

The first set of comparisons made was to determine which parts of the cliff face underwent positive or negative changes to the slope in terms of slope material loss or

gained as a result of the earthquakes. This was done by overlapping the corresponding sets of cross sections and noting whether the cross section had receded as a result of the cliff collapse or instead appeared to have increased in size after the seismically-induced cliff collapse (Figure 57). The rest of the overlapping (annotated) cross sections can be found in Appendix IV.

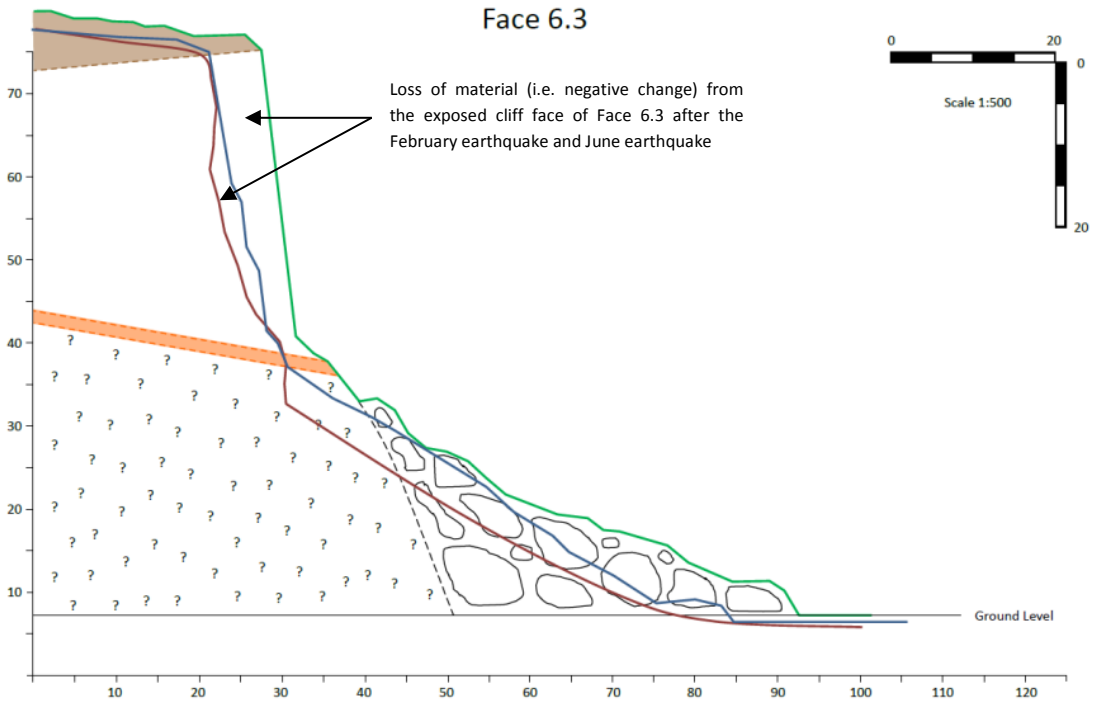

Figure 57 - An annotated example of overlapping cross section Face 6.3.

Results of this comparison (Figure 58) shows that the post-February and (most of) the post-June 2011 cross sections exhibited loss of material in the form of a receded cross sections outlines from the overlapping of cross section. However, a few sections of the NE Face did reveal an alleged "positive change", i.e. gain in material on the slope after the June earthquake.

It is very likely these positive overlaps are false readings, as the range of error is rather high as survey (laser scan) models with contrasting resolutions were combined to produce an overlapping sequence. However, there is a possibility that the overlaps may hold some truth considering that Massey et al (2012) also noted a positive gain on the surface of the NE Face after the June earthquake as well (Figure 58).

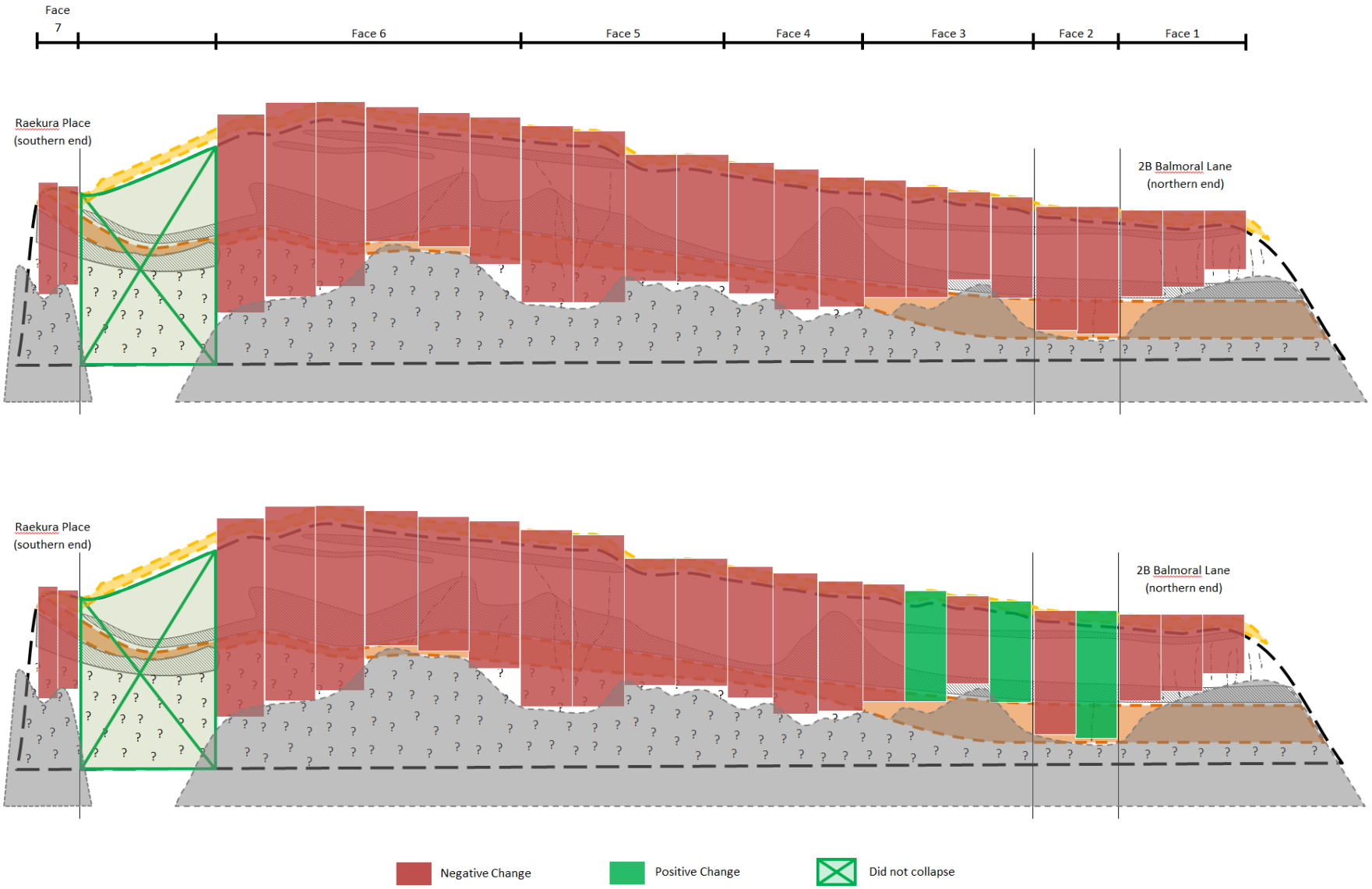

Figure 58 – The resulting positive and negative change models for the collapse of Redcliffs' cliff in A) 22 February 2011; B) 13 June 2011 earthquakes

In theory, this positive gain of material on the slope could either suggest:

i) Not all material that detached from the cliff face travelled down the full length of the slope and some remained on the slope face; or, under extreme circumstances,
ii) Assuming that some of the fissures on top of the cliff may not be directly resulted from the seismic shaking but instead from a part of the cliff sliding away from the cliff, this positive change could be an indication of slope deformation (of some level) in the eastern end of the cliff.

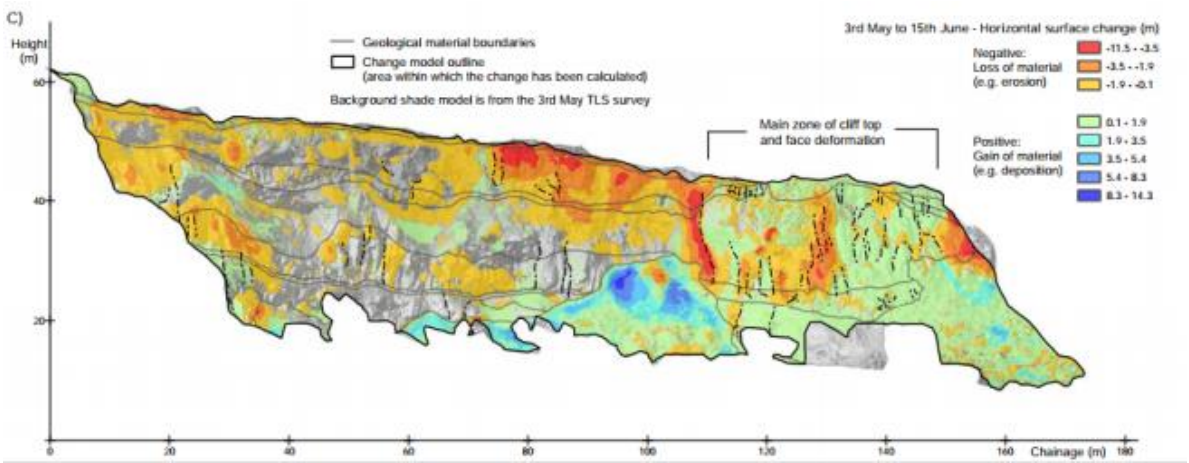

Figure 59 - Surface change model of Redcliffs' cliff face created to represent the cliff face after the June 2011 earthquake (Massey etal,, 2012).

5.4.2 Gradient Changes

The second set of comparative results focused on measuring the specific gradient changes to the main parts of each cross section, to determine whether sections of the slope steepened or levelled as a result of the cliff face receding (Figures 60 and 61). This was done by overlapping the planar models (Figures 43 - 45) of the slope gradients and calculating the angular changes for each corresponding slope section on the cliff face. Overall, the result of overlapping the planar models is null as it shows no particular pattern in the distribution of steepening or levelling of the slope gradients after each collapse.

5.4.3 Quantifying the Change

Using the geometric information gathered from the change models, an attempt was made to quantify the changes done to the cliff face after each collapse. This included determine the changes in surface area of the cliff top and the volume of material that detached from the cliff face after each major collapse.

Post February 2011

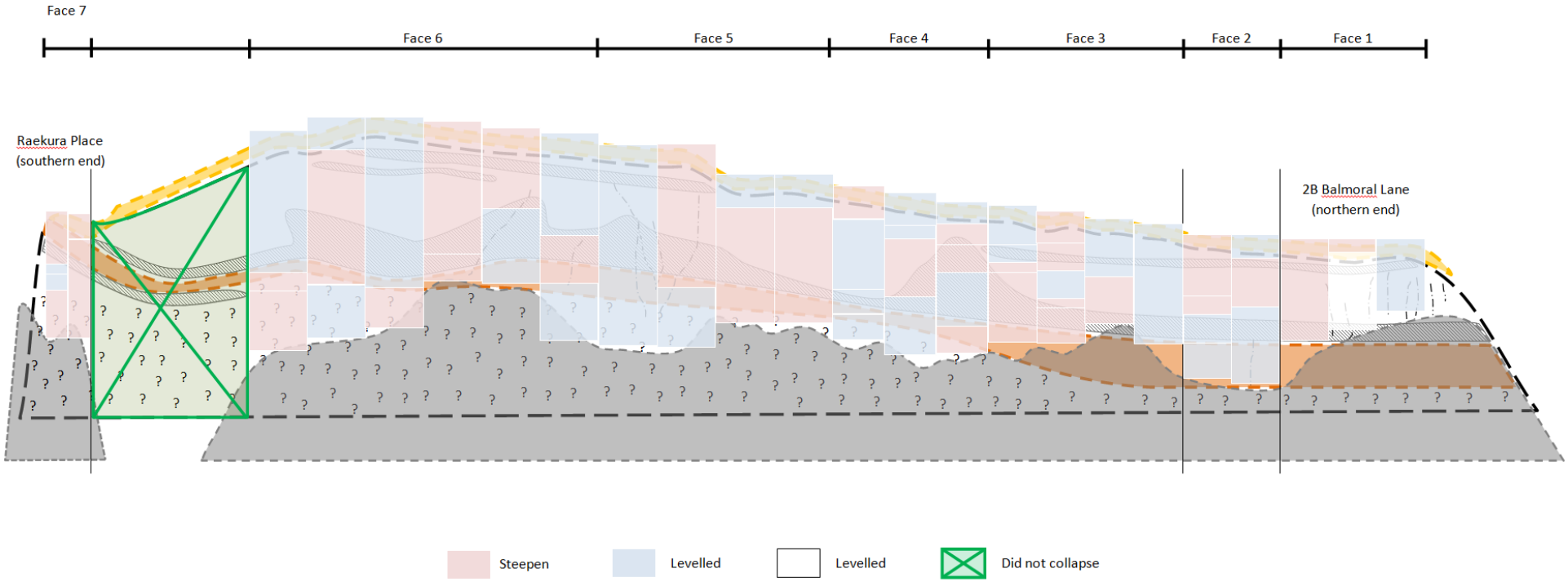

Post-Feb 2011	Face 7		Face 6						Face 5				Face 4			Face 3				Face 2		Face 1		
Upper	8	41	4	28	4	3	7	2		3	37	24	31	3	13	2	6	22		26	26		17	
Middle	36		26	4	-	-	-	20		-			2	27	30	14	21	-		5	27			
	18	13	-	-	-	-	-	-	5	-	1	10	38	2	5	18	7	-	12	52	-	9	0	7
	-		-	-	-	-	-	-		-					20	-	20	-		-	-			
Lower	23		2	8	32	32	10	13		8			3	1	4	8	7	6		10	9			

Figure 60 - The resulting different in slope gradients after the first collapse in February 2011, based on overlapping the slope gradient measurements Figure 43 and 44.

Post June 2011

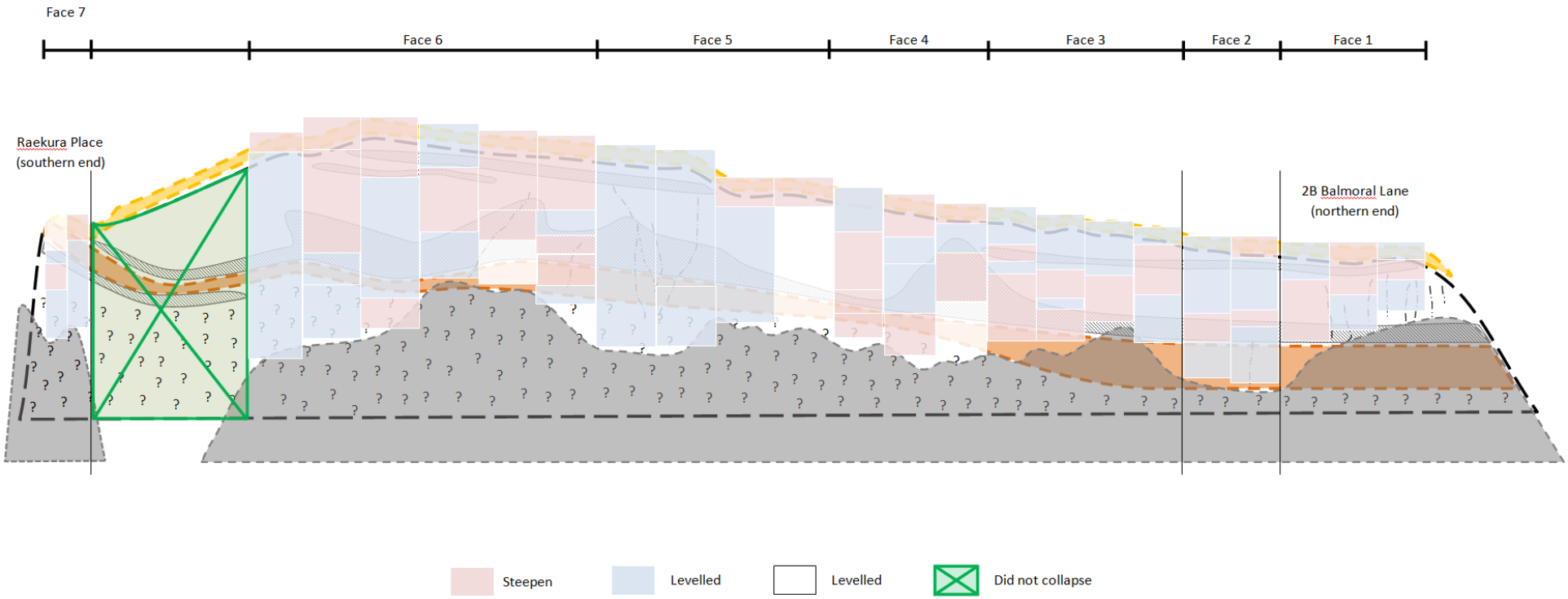

Post-June 2011	Face 7		Face 6						Face 5				Face 4			Face 3				Face 2		Face 1		
Upper	0	19	32	28	14	6	5	6		15	36	2	22	1	6	6	22	3	24	8	31	23	4	16
Middle	34			10	10	6	30	20		-	-	-	7	28	37	6	6	-	8	8	22	-	-	25
	10	12	7	23	-	-	-	8	3	-	-	-	43	5	2	26	21	-	-	-	39	-	-	-
	-			-	-	-	-	29		-	-	-	-	-	0	-	-	-	-	-	-	-	-	-
Lower	8			11	6	16	0	4		4	2	0	7	13	0	2	3	6	9	9	24	16	4	7

Figure 61 - The resulting different in slope gradients after the first collapse in February 2011, based on overlapping the slope gradient measurements Figure 44 and 45.

Cliff Edge Lengths

The first set of measurements taken was of the length of the cliff top by placing a piece of string on top of the (drawn) aerial map of the cliff top (Map 1). String was chosen as the best measurement tool at the time to accommodate for the waviness of the cliff edge line. The overall length of the cliff edge and the sectioned length of Face 1 - 4 and 5 – 7 (including the area between Face 6 and 7) are summarized in Figure 62.

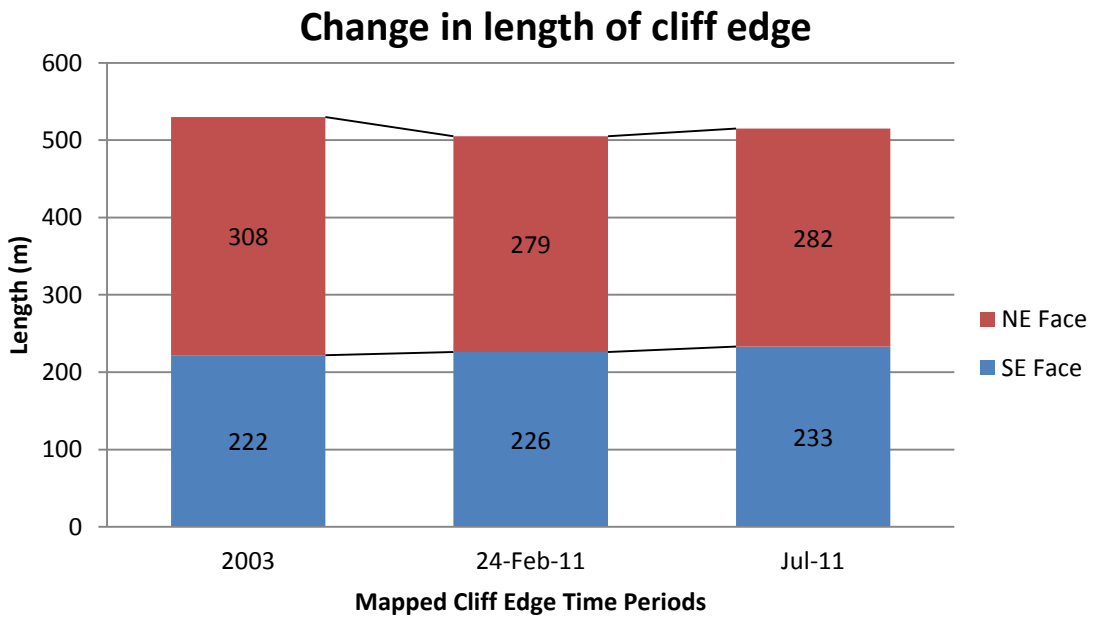

Figure 62 - Length of the cliff edge before and after the February 22 and June 13 2011 earthquakes.

The results show an overall shortening of the cliff edge after the first collapse, with some lengthening occurring after the second cliff collapsing incident. This suggests that the first collapse decreased the waviness of the cliff edge which may be the result of a more uniform collapse of the cliff overall; whereas the second collapse was more concentrated in certain sections along the cliff edge, which increased the waviness of the cliff edge once again. While the NE Face follows the same pattern, the SE face has steadily increase in length which suggest an increase in waviness of the cliff edge on account of more localised collapsed of the cliff (including the cliff top) after each earthquake.

Cliff Top Area

The cliff top area lost after each earthquake was quantified by counting the number of 0.076 cm^2 grid squares between successive cliff edges (Figure 63). The number of squares are then tallied up and converted to the true scale of 1:1000 to calculate the total surface area lost along the cliff edge.

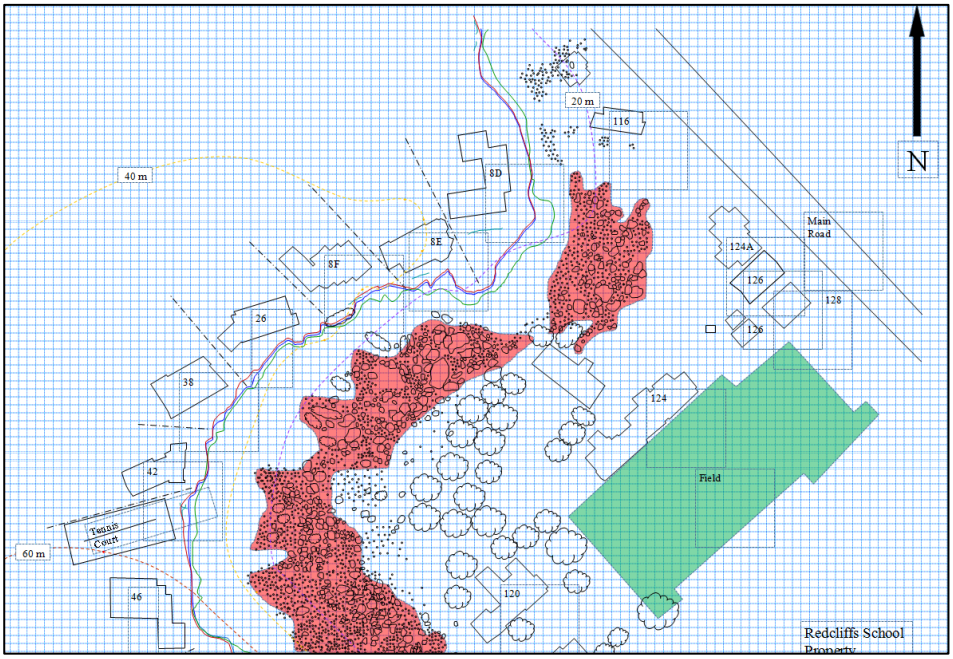

Figure 63 - Illustration of the 0.076 cm2 grids used to measure the loss of area on the cliff top of the successive cliff edges.

$$Area\ (m^2) = (\text{number of squares} * 0.076\ cm^2 * \frac{10^6}{10^4})$$

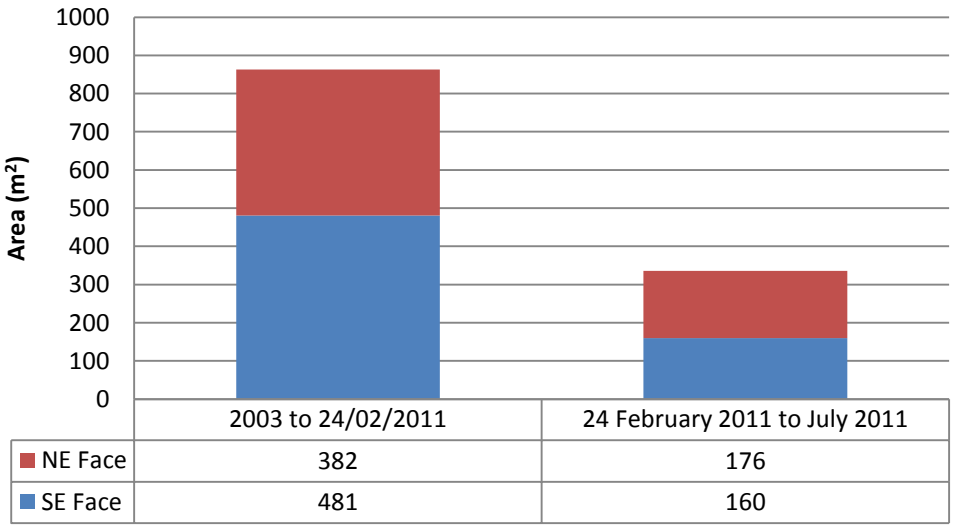

Figure 64 - Estimates are the cliff top (NE and SE Face) lost after each failure incident.

Figure 64 represents the area of the cliff top that has fallen away between the selected time periods when the mapping survey was conducted. Minor loss may have occurred from other triggers during the time intervals, particularly during the 8 years between the pre-quake position of the cliff edge and the post-February 2011 earthquake, however it is certain that the main loss of area from the cliff top is due to the earthquakes that occurred after February 22 2011.

The data suggests a large difference in the area lost after the February and June 2011 earthquakes, whereby more of the cliff top fell after the February earthquake overall in comparison to the June earthquake. However, when comparing between the NE and SE face, the SE face loss more area from the cliff top than the NE after the February earthquake, whereas the NE face loss more area from the cliff top after the July earthquake compared to the SE face.

Cliff Edge Retreat

The overall distance the cliff edge retreated since Redcliffs collapsed using the area and length measurement results. This was done by assuming the cliff top (when observed in plain view) is shaped like a trapezoid, where the bases of the trapezoid (L_1 and L_2) represent the successive cliff edges (i.e. the lengths of the pre (L_1) and post- collapse (L_2) cliff edges before and after the February and June earthquakes), and the corresponding cliff top area lost (calculated previously) represents the area of a trapezoid (A).

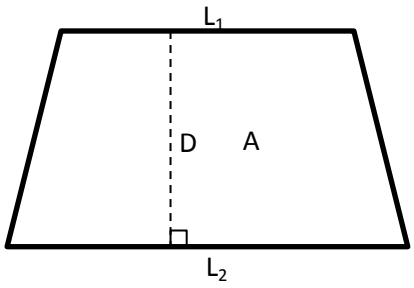

Figure 65 - Trapezium shape representing the plan view of a (generalized and straightened) cliff edge. L_1 represents the pre-collapsed cliff edge and L_2 represents the new (post collapse) cliff edge. While in the diagram, L_1 is drawn shorter than L_2, it does not indicate that $L_1 > L_2$, as the length of the cliff edge post-February (L_2) is shorter than pre-February (L_2)

$$A = \frac{(L_1 + L_2)D}{2} \quad \text{(EQ 7)}$$

By rearranging the main equation to calculate the area of a trapezoid, the height (D) between L_1 and L_2 can be calculated, which represents the overall distance the cliff edge retreated.

$$2A = (L_1 + L_2)D \quad \text{(EQ 8)}$$

$$\frac{2A}{(L_1 + L_2)} = D \quad \text{(EQ 9)}$$

Table 22 - Overall distance the cliff edge retreat calculated using the equation for a trapezoid

	Overall distance the cliff edge retreated (D)	
	24-February 2012	30 July 2012
SE Face (Face 1-4)	1.3 m	0.63 m
NE Face (Face 5-7)	2.2 m	0.70 m

The results indicates that the cliff edge retreated a greater distance overall after the February 22 earthquake compared to after the June 13 2011 earthquake (Table 22). Furthermore, when comparing between slope aspects, the SE face receded less in comparison to the NE face after both earthquake incidents as well which suggests the cliff edge on the NE Face has a tendency to retreat further back in comparison to the SE Face in the event of a major cliff collapse.

Volume of Material Lost

The equation to determine the volume of a quadrilateral prism was used to estimate the volume of material that fell from Redcliffs after February and June 2011, where the volume (V) is determined by the height of the prism (h) and the area of the base (B) of the prism (Figure 62). The main assumption for this calculation assumes the body of the total material which fell from the cliff is in the shape of a prism whereby, the two end face (i.e. top and bottom) are of the same shape and the sides are parallelograms.

Separate calculations were made to the SE and NE face with the available data to provide a comparison as to how much slope material fell on either face. The specific values measured for the base area and height used for the calculations are summarized in Table 23.

Separate calculations were made to the SE and NE face with the available data to provide a comparison as to how much slope material fell on either face. The specific values measured for the base area and height used for the calculations are summarized in Table 23.

$$V = Bh \qquad \text{(EQ 10)}$$

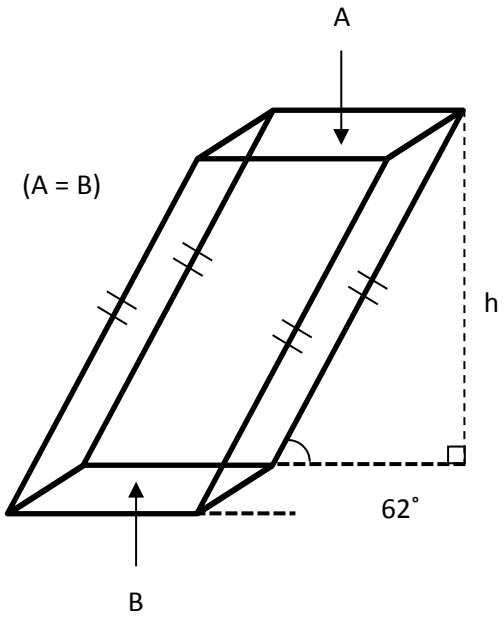

Figure 62 - A parallelogram prism presenting the volume of material the cliff face lost as a result of the earthquakes. The angular sides represent the overall slope angle pre and post collapse. They are assumed to be the same angle due to the nature of the calculation being an estimate / rough calculation and also because to the slope angles being nearly the same after each collapse

The assumption is made that the area on the top and bottom of the prism not only represents the area lost on the cliff top at Redcliffs but also the area loss at the base. The reason for this second assumption is due to the overall slope angles of the respective NE and SE face after each major cliff collapse remaining relatively the same. By assuming the initial slope angle and the resulting slope angle averages after a seismically-induced cliff collapse are the same, this meant that the overall shape of the material that fell after both earthquakes can be treated as a parallelogram prism.

Table 23 - the measurements used to calculate the volume of material which collapsed of the Redcliffs cliff face

		Variables	
		NE Face	SE Face
Base Area	24-February 2012	382 m^2	481 m^2
	30 July 2012	176 m^2	160 m^2
Exposed Cliff Face Height		40 m	27 m

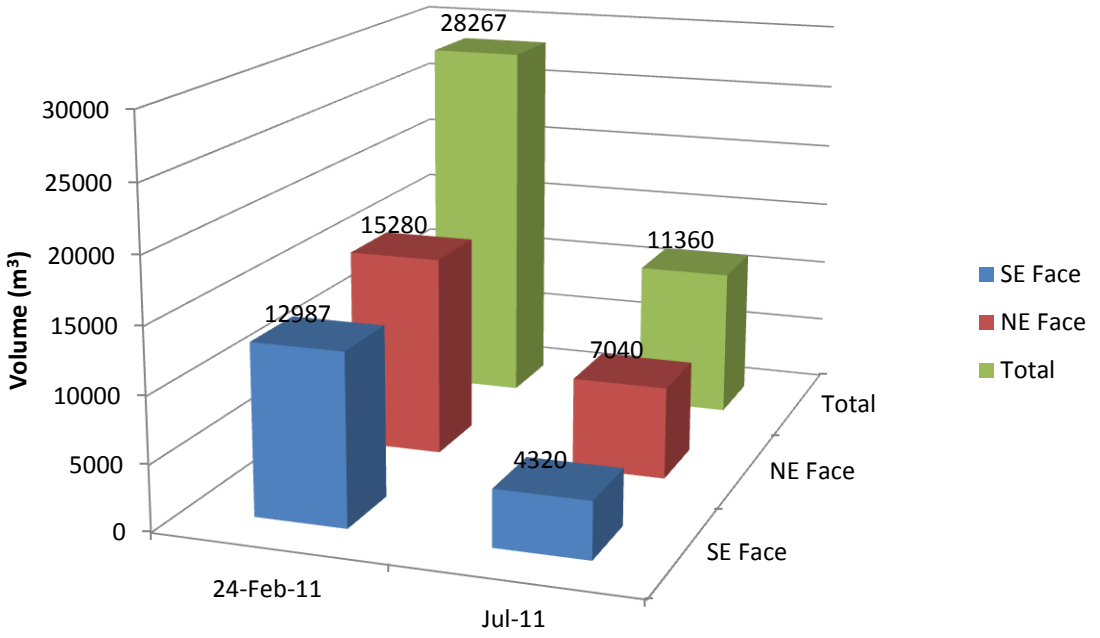

Figure 63 - Estimation of the volume of material which came down from the Redcliffs cliff as a result of the February and June 2011 earthquake. The dates used correspond to when the measurements were taken needed to make the calculation possible, thus representing the volume of material the cliff loss up till that specific point in time.

The results presented in Figure 63 reflect the variables for the base area used, whereby a greater volume of material from the cliff face had fallen as a result of the earthquake on February 22 2011 in comparison to the June 13 2011 earthquake. This subsequent decrease in volume of rock and soil material falling from the cliff face after the June 2011 is due to the removal of most of the already weakened / eroded rock and soil from the cliff face (including the seismically weakened material) as a result of the February earthquake. On the other hand, the rock and soil which came down from Redcliffs because of the June 13 2011 quake are likely to be only seismically weakened material triggered by the February and June earthquakes.

When comparing between the two main slope aspects, the results show that more material was removed from the NE face after the February and June earthquake in 2011 in comparison to the SE face. This is due to the fact that the NE face is taller and has a greater length in comparison to the SE face, thus a greater surface area of the cliff face, which means that there is a greater potential for material to fall from the NE face than the SE facing part of Redcliffs.

The height is further emphasised as a factor in the volume of material loss when comparing a volume per length ratio between the slope aspects, where: the NE and SE Face was calculated to have a similar ratio of material loss per meter of 1:~7000

m^3 as a result of the February earthquake. This is not as apparent for the June earthquake, as the NE Face was calculated to have a ratio of ~10,000 m^3 per meter and the SE Face has a ratio of ~7000 m^3 per meter which suggests the height is not a deterministic factor for the difference in volume from the two slope aspects after the June collapse.

5.4.4 Summary

Overall, this comparative analysis is a mathematical attempt in trying to quantify the resultant changes to Redcliffs' cliff after two major failure incidents. Even though a number of assumptions have been made, ultimately, this basic numerical approach is successful in calculating: the surface area lost on top of the cliff as a result of the cliff collapse, and the volume of material lost from the cliff face after both failure incidents.

Chapter Six: Summary and Conclusion

6.1 Introduction

This investigative study into the collapse of a sea-cut cliff at Redcliffs during the 22 February 2011 and 13 June 2011 (M_w 6.2) earthquakes consisted of two main aims:

i. Describing the engineering geological characteristics of the rock mass and soil properties that form Redcliffs' cliff;
ii. Evaluate the deformation mechanisms and failure mechanics that were involved in the failure process of Redcliffs' cliff collapsing twice over the course of roughly four months.

The overall approach used to carry out this study involved two different research approaches. The first approach uses of field surveying techniques to acquire quantitative and qualitative data, and the second approach utilises studies done on the influences of earthquake-induced ground movement and rock slope failure behaviour in order to implement a literature-research approach explaining how and why did Redcliffs' cliff collapse. The main findings of this study are as follows.

6.2 Engineering Geological Model of Redcliffs' cliff

The results of the first part of the study present an assortment of information about Redcliffs' cliff, specifically concerning the engineering geological and geotechnical characteristics of the rock mass and soil lithology, and the deformation of the slope after two major collapses.

6.2.1 Rock mass and Soil Properties

Preliminary background research of the Redcliffs' area has found that the undulating terrain was the result of volcanic activity during the late Miocene (9.7 – 11 Ma) as part of the Mt. Pleasant Formation (Altaye, 1989; Sewell, 1988; and Sewell et al., 1992), or more recently, classified as part of Eruptive Phase XI (Hampton, 2010). The basaltic volcano responsible for the volcanic deposition is called Lyttelton Volcano.

Localised (remote) surveying of the site revealed three distinct volcanic rock deposits that make up the main rock body (exposed on the cliff face), and a soil mantle that covers the top of Redcliffs' cliff. The lowest lying unit found on the cliff face was identified as a layer of cemented Tuff. It lies above an unknown fifth unit – hidden from view by the talus slopes, and takes up an estimated 11 – 19 % of the cliff face.

The unit of tuff is classified as a brecciated unit of rock with a gradational contact zone, that has low shear strength, and a relatively intact (poorly jointed) rock mass.

Above the unit of tuff is a large body of welded and unwelded ignimbrite, which takes up a combined 43 – 48 % of the exposed portion of the cliff face. The main portion of the welded component resides between the tuff and unwelded ignimbrite. It is a strong-to-very strong rock with structural characteristics of a jointed (blocky) rock mass comprised of near-vertical (columnar) joints, which have variable spacing (1.5 – 2.5 m) and persistence. Furthermore, there are also cross-joints found within the welded rock mass that are perpendicular to the main near-vertical joint sets. Joint surface measurements, from a proxy site, indicated the welded ignimbrite has a Joint Wall Strength (JCS) of 100 – 120 MPa, which roughly correlates (based on the fresh surface measurements) to a Uniaxial Compressive Strength (UCS) of 165 – 177 MPa.

The unwelded component of the (large) ignimbrite body, on the other hand, is described as having dissimilar characteristics than that of the welded ignimbrite. That is to say, it is weaker (moderately strong-to-strong) and poorly jointed, with cases of exfoliation (near-vertical) joints / cracks observed on the cliff face that run along the strike of the slope.

The only unit of soil present on-site resides on the upper 6 – 7 % of the cliff face. It is a combination of wind-blown loess, and (organic) soil commonly found throughout the Canterbury Region. While it is unknown how thick the upper layer of organic soil is, i.e. where the boundary between the organic soil and underlying loess is within the soil mantle, the scala penetrometer test results points out that good / firm soil can be found 0.5 m in the soil body.

6.2.2 Structural Properties

Processing of terrestrial photogrammetry data (courtesy of Marc-Andre Brideau) revealed two distinct sets of discontinuities from the exposed cliff face. The first of which are near-vertical discontinuity sets oriented at a dip range of 66 – 90 °, and a dip direction of 120 - 270 °. These are presumed to be the near-vertical join sets observed on the cliff face. As regard to the second major set, they are near-horizontal discontinuities oriented at a dip range of 16 – 28 ° and a dip direction of 30 - 75 °; 300 - 355 °, which, in this study, are assumed to be the bedding orientation.

While the presumption is made that the major discontinuity sets identified are the orientations of the near-vertical joint sets and bedding planes, unfortunately it cannot be said with absolute certainty which characteristics these discontinuity measurements truly represent, on account of the lack of additional (geological) information regarding which surfaces the measurements were taken from.

6.3 External Properties

In terms of the deformation (changes) to the slope, the results of mapping the cliff top and cliff face (Maps 1 and 2) are as follows:

- The mapping has identified a series of resultant fissures on top of the cliff, particularly along the cliff edge.
- Most of the fissures were responsive to major aftershocks and earthquakes and were not influenced by the in-situ stresses of gravity and rainfall.
- Mapping of the cliff top also illustrated that the cliff edge receded, losing an estimated 863 m^2 on top of the cliff after the first collapse in February and 330 m^2 as a result of the second collapse in June 2011 (Figure 64).

The cross sections and planar maps shows that the cliff face comprises of a number of major gradients, with an overall slope angle of ~67˚ (post-13 June 2011), where the steepest components are ~80˚ and the gentle sloping gradients are ~ 44˚. Over the course of two major collapses, the cliff face geometry has evolved; dividing what once was semi-uniform slopes sections of a cliff (an incline with one and / or two slope gradients) into a cliff face with at least two or three major gradients on a number of slope sections. The (taller) NE Face steepened the most, starting off at an average of 65˚ before the first collapse and increasing to 72˚ after the June incident; whereas the SE Face decreased in steepness before after the February earthquake, only to steepen to 62˚ after the June incident – the same average slope angle before the February collapse.

In addition, the resulting cross section models have also provided terrestrial measurements of the slope height, estimated to be ~40 – 80 m, where on average the NE Face is taller (~40 m) than the SE Face (~27 m).

6.4 Cause of collapse

Investigating the deformation mechanisms that were involved in the process of causing Redcliffs' cliff to collapse on 22 February and 13 June 2011 revealed: the

unique circumstances surrounding the two failure-inducing earthquakes, which made the earthquakes effective trigger mechanisms; and different weakening processes involved in the process of inducing failure on Redcliffs' cliff.

Firstly, the investigation shows that the failure-inducing earthquakes were only effective triggering mechanisms due to the intensity of the shaking felt on-site (Redcliffs). This level of intensity encountered is dependent on certain characteristics concerning the source of the quake (fault zone) and the setting of the site affected by the quake, i.e. in relation to source effects; path effects; and site effects.

Source Effects

- The direction of thrust / slip of the fault as it ruptures played a significant role in providing the intense ground movement needed to trigger the collapse of Redcliffs' cliff. This phenomenon is known as directivity, where wave energy focuses in the direction of rupture. In the case of Redcliffs cliff, the location of the site coincided with the path of rupture for both (Mw 6.2) trigger earthquakes
- The type of fault which caused the earthquake is believed to have also influenced the level of ground motion felt, or rather PGA, at Redcliffs, as studies have shown that the thrust faults produce ground movement of greater intensity than strike-slip faults. In the case of the first trigger earthquake ($PGA_{vert.} = 1.1$), it occurred on a thrust fault; whereas the second trigger earthquake ($PGA_{vert.} = 2.0$) happened on a strike-slip fault.

Path Effects

- The short distance between the source of the fault rupture and Redcliffs cliff was recognised as a key factor in contributing to the intense ground movement felt on-site.
- Comparing between the magnitude of the three largest earthquakes that struck Redcliffs cliff (Mw 7.1; 6.2; 6.2), the smaller two Mw 6.2 earthquakes were the only seismic events which caused Redcliffs' cliff to collapse. This is because the Mw 7.1 earthquake occurred ~45 km away from Redcliffs; whereas the Mw 6.2 earthquakes which occurred on 22 February 2011 and 13 June 2011 happened 5 km and 1.4 km respectively.

Site Effects

- The topography at the Redcliffs is the main site effect was identified as having an influence in amplifying the seismic waves and the resultant (failure-inducing) shaking felt on-site.
- While it isn't certain how much amplification occurred to the seismic waves as it propagated through Redcliffs cliff, the general consensus of topographic amplification suggests that any site related amplification would increase the seismicity (at most) by a factor of two.

Second, the investigation has also revealed that the circumstances behind the failure-inducing processes for both collapses were slightly different when comparing between the two events. While both cliff collapses were triggered by two separate earthquakes of roughly the same magnitude (M_w 6.2) and peak ground acceleration (PGA = ~2 g), the conditioning factors (i.e. the process of weakening the rock mass) that helped to induce failure for the first collapse in February 2011 is different to the factors which contributed to the second collapse in June 2011. Essentially, this difference is attributed to the assortment of weakening processes Redcliffs' cliff endured, and the length of time the cliff was left exposed to these weakening factors prior to the first and second collapse.

For instance, the processes involved in the first collapse on 22 February 2011 were a combination of a (trigger) earthquake and time – where "time" used in the context of this discussion is defined as an accumulation of weathering and erosion process that can happen to an exposed sea-cut cliff, and (possible) unaccounted earthquakes that have occurred in the past. Prior to the first collapse, it is understood that the cliff had been intact and stable for a lengthy period of time, on account of the spread of well-grown vegetation seen on the cliff face prior to collapse (Figure 21). This meant that the same cliff face has been exposed to a number of weakening processes, and, considering the length of time the same cliff face was exposed, all of which are accountable for weakening the slope.

As for the second collapse in the 13 June 2011 earthquake, it occurred four months after the first major collapse, which was considered too short of a time period for the new slope surface to be affected severely enough by weathering and erosion. Hence, seismicity was the only weakening factor that was considered effective in weakening the slope. This notion was considered when fractures were observed on the post-

failure surface of the cliff face after the February 2011 incident. This meant that a strong enough quake could induce the formation of fractures in the cliff, thus weakening the overall rock mass. Since there were a number of major aftershocks occurring leading up to the second major failure, it is not beyond reason to assume that additional fractures formed within the cliff face as a result of aftershock seismicity, thus weakening the overall rock mass the cliff prior to the second collapse in June 2011.

6.5 Failure Behaviour

Studying the way in which Redcliffs' cliff collapse was done using four separate approaches, two of which focused on block sizes (Continuum vs. Discontinuum; and Rockfall vs. Rockslide). The other two methods used a kinematic approach, focusing on rock mass characteristics (Kinematic Analysis; Goodman and Kieffer (2000)) to determine the potential of failures modes such as toppling or sliding occurring on the rock slope of interest. The findings from this study of failure behaviour of Redcliffs' are as follows:

- The first failure in February 2011 is described as equivalent continua slope movement of the outer (highly weathered / damaged / weakened) surface and discontinuous slope movement of the inner portion of the cliff face that failed.
- As for the second major collapse in June 2011, the failure is perceived only as discontinuous slope movement on account of the well-spaced arrangement of fractures / joints that break at the point of failure.
- Kinematic analysis was conducted on the discontinuity sets of data, which revealed that that both the NE and SE Face had the potential for toppling and planar sliding to occur during failure. This meant that both toppling and planar sliding would have occurred during both failure incidents.
- The approach proposed by Goodman & Kieffer (2000) suggest the following failure modes which can (and thus have) occurred on Redcliffs cliff: ravelling, block sliding on a single plane, rock slumping, toppling of the welded and unwelded ignimbrite; rock bridge cracking of the tuff; soil type slumping of the wind-blown loess and soil mantle.

The closing comparative analysis done on assessing the collapse of Redcliffs' cliff calculated that the NE Face 22,320 m^3 and the SE Face loss 13707 m^3 after both failure incidents, resulting in a significant deposition of material on the talus.

6.6 Main points of this study

- This successful study comprises of two major components: creating an engineering geological post-failure model of Redcliffs' cliff; and studying about the trigger earthquakes and failure behaviour of the cliff, both of which use different approaches to conduct the respective investigations.
- The lithology of the exposed component of Redcliffs' cliff consists of: a unit of a moderately strong tuff sitting below a relatively dense, strong-to-very strong body of welded and unwelded ignimbrite, and a soil mantle covering the top of the cliff.
- There two slope aspects to the cliff face (NE and SE Face), both of which have distinctive rock mass characteristics when compared between one another.
- Modelling the geometry of the slope shows the slope gradient getting increasingly fragmented (i.e. increasing in the number of slope gradients after each collapse
- The M_w 6.2 earthquakes which caused the collapse of Redcliffs' cliff was the result of intense ground shaking (PGA = ~2 g). This level of intensity is attributed to a number of factors regarding the source of the quake, the site of Redcliffs and the path seismic waves travel from the source to the site.
- The way in which Redcliffs' cliff collapse cannot be narrowed down to a single mode of failure as the study conducted suggests that it has the capability to topple and slide (not wedge), even though it was also characterised as being predominantly discontinuous that resulted in rock fall.
- The estimated loss of material after the February collapse was 28,267 m^3 and 11,360 m^3 after the June 2011 failure incident.

6.7 Future Research Recommendations

Subsequent to this project, it is anticipated that the following suggestion could be worthwhile areas for future research that would benefit to the understanding of the geological properties that make up the cliffs in the Port Hills (including Redcliffs' cliff); their susceptibility to seismically-induced failure and respective modes of failure.

- Correlate the findings of this study with other cliff / near-vertical rock slopes studies being done in the Port Hills;
- Use the qualitative and quantitative results in this study to further develop an engineering geological rock mass profile of the Port Hills.

Acknowledgements

Given the hardships and struggles faced in the process of completing this master's thesis, this has been one of the most challenging moments of my life and I owe each an every person that has helped me throughout the progression of this thesis, particularly in times when I was at my lowest.

I would like to express my thanks for David Bell who brought this topic of interest to my attention, my supervisors Dr. Marlene Villeneuve (Head), Dr. David Nobes (Co.), David Bell, and Samuel Hampton for their patient guidance, enthusiastic encouragement and countless useful critiques of my research work. This thesis would not have possible without you.

I would also like to thank the Matthew Cockcroft, Sacha Baldwin-Cunningham, Cathy Higgins, and the rest of the technical staff of the Geology Department for their help in offering me the resources and sharing their technical knowledge that I needed to conduct the (on-site) field investigations.

Finally, I wish to thank my parents, Albert Lo and Angela Lo, and my friends, Pamela Wong, Joanne Sirichai, Joseph Kwak, Jasveet Sandhu, Samreet Singh, Andrew Choi, Michael Sohn, and Harrison Lim for their relentless support and encouragement throughout my study.

Bibliography

Aagaard, B., Hall, J., & Heaton, T. (2004). Effects of Fault Dip and Slip Rake Angles on Near-Source Ground Motions: Why Rupture Directivity Was Minimal in the 1999 Chi-Chi, Taiwan, Earthquake. *Bulletin of the Seismological Society of America, 94*(1), 155-170.

Agliardi, F., Crosta, G. M., Valle, C., & Rivolta, C. (2013). Structurally-controlled instability, damage and slope failure in a porphyry rock mass. *Tectonophysics*.

Altaye, E. (1989). *The Geology and Geochemistry of the North-Eastern sector of Lyttleton Volcano, Banks Peninsula, New Zealand.* Christchurch: University of Canterbury.

Ashford, S., & Sitar, N. (1997). Analysis of topographic amplification of inclined shear waves in a steep coastal bluff. *Bulletin of the seismological society of America, 87*(3), 692-700.

Ashford, S., Sitar, N., Lysmer, J., & Deng, N. (1997). Topographic effects on the seismic response of steep slopes. *Bulletin of the Seismological Society of America, 87*(3), 701-709.

Assimaki, D., & Gazetas, G. (2004). Soil and topographic amplification on canyon banks and the 1999 Athens earthquake. *Journal of Earthquake Engineering, 8*(1), 1-43.

Barla, G., & Barla, M. (2000). Continuum and Discontinuum Modelling in tunnel engineering. *Rudarsko-Geološko-Naftni Zbornik, 12*, 45-57.

Barton, N. (1973). Review of a new shear-strength criterion for rock fractures. *Engineering Geology, 7*, 287-332.

Beavan, J., J., L., Levick, S., & Jones, K. (2012). *Ground displacements and dilatational strains caused by the 2010-2011 Canterbury Earthquakes.* GNS Science Consultancy Report 2012/67.

Beavan, J., Lee, J., Levick, S., & Jones, K. (2012). *Ground displacements and dilatational strains caused by the 2010-2011 Canterbury earthquakes.* GNS Science Consultancy Report.

Bell, D. (1992). *Rockfall protection measures for 44 Raekura Place.* Christchurch: University of Canterbury, Canterprise Report.

Bell, F. (2007). *Engineering Geology, Second Edition.* Elsevier Ltd.

Ben-Menahem, A., & Singh, S. (2000). *Seismic waves and sources.* Toronto: Courier Dover Publications.

Boatwright, J. (2007). The Persistence of Directivity in Small Earthquakes. *Bulletin of the Seismological Society of America*, 1850-1861.

Braathen, A., Blikra, L., Berg, S., & Karlsen, F. (2004). Rock-slope failure in Norway; type, geometry, deformation mechanisms and stability. *Norwegian Journal of Geology, 84*, 67-88.

Bradley, B. (2012). Observed Ground Motions in the 4 September 2010 Darfield Earthquake and 22 February 2011 Christchurch Earthquakes. . *New Zealand Society for Earthquake Engineering*

Conference (p. Paper Number 037). Christchurch: University of Canterbury. Civil and Natural Resources Engineering.

Bradley, B., & Cubrinovski, M. (2011). Near-source strong ground motions observed in the 22 February 2011 Christchurch earthquake. *Bulletin of the New Zealand Society for Earthquake Engineering, 44*(4), 181-194.

Bradley, B., & Cubrinovski, M. (2011). Near-source Strong Ground Motions Observed in the 22 February 2011 Christchurch Earthquake. *Seismological Research Letters, 82*(6), 853-865.

Cagniard, L. F. (1962). *Reflection and refraction of progressive seismic waves.* New York: McGraw-Hill.

Campbell, K. (1997). Empirical near-source attenuation relationsihps for horizontal and vertical components of peak ground acceleration, peak ground velocity, and pseudo-absolute acceleration response spectra. *Seismological Research Letters, 68*(1), 154-179.

Campbell, K. (2003). Strong-motion attenuation relations. In H. edited by Lee, H. Kanamori, P. Jennings, & C. Kisslinger, *International Handbook of Earthquake & Engineering Seismology, Part 2* (pp. 1003-1012). Oregon.

Corbett, D. (2011). *2011 - The Weather in Review*. Retrieved May 17, 2013, from MetService Blog: http://blog.metservice.com/2011/

Day, R. D. (2002). *Geotechnical Earthquake Engineering Handbook.* United States of America: McGraw-Hill.

Dellow, G. D., Massey, C. I., Davies, T. R., Read, S. A., Bruce, Z. R., VanDissen, R., et al. (2011). *Port Hills Poster.* Retrieved March 10, 2012, from Geonet: http://www.geonet.org.nz/content/download/8885/58050/file/CM11002PC_Port_Hills_poster.pdf

Dorren, L. (2003). A review of rockfall mechanics and modelling approaches. *Progress in Physical Geography, 27*(1), 69-87.

Faccioli, E., Vainini, M., & Frassine, L. (2002). "Complex" site effects in earthquake ground motion, including topography. *In Proc. of 12th European Conference on Earthquake Engineering.*

Forsyth, P. J., Barrell, D. J., & Jongens, R. (2008). *Geology of the Christchurch Area, 1:250000 Geological Map 16.* Lower Hutt: Institute of Geological & Nuclear Sciences.

Freundt, A., & Schmincke, H. (1995). Eruption and emplacement of a basaltic welded ignimbrite during caldera formation on Gran Canaria. *Bulletin of Volcanology, 56*(8), 640-659.

Fry, B., & Gerstenberger, M. (2011). Large apparent stresses from the Canterbury earthquakes of 2010 and 2011. *Seismological Research Letters, 82*(6), 833-838.

Geli, L., Bard, P., & Jullien, B. (1988). The Effect of Topography on Earthquake Ground Motion: A Review and New Results. *Bulletin of the Seismological Society of America, 78*(1), 42-63.

GeoNet. (2012). *Aftershocks*. Retrieved October 2012, from GeoNet: http://info.geonet.org.nz/display/home/Aftershocks

GeoNet. (2012). *M 6.3, Christchurch, 22 February 2011*. Retrieved July 16, 2012, from GeoNet: http://info.geonet.org.nz/display/quake/M+6.3%2C+Christchurch%2C+22+February+2011

GeoNet. (2012). *New Zealand Earthquake Report*. Retrieved July 16, 2012, from GeoNet: http://geonet.org.nz/quakes/region/newzealand/3528839

GNS. (2011, September 6). *Graphic shows two main Christchurch fault ruptures - 06/09/2011*. Retrieved July 23, 2012, from GNS Science: http://www.gns.cri.nz/Home/News-and-Events/Media-Releases/Two-main-faults

GNS. (2011). *M 7.1, Darfield (Canterbury), September 4 2010*. Retrieved March 10, 2012, from GeoNet: http://www.geonet.org.nz/earthquake/historic-earthquakes/top-nz/quake-13.html

GNS Science. (2011, September 6). *Graphic shows two main Christchurch fault ruptures - 06/09/2011*. Retrieved July 23, 2012, from GNS Science: http://www.gns.cri.nz/Home/News-and-Events/Media-Releases/Two-main-faults

GNS Science. (2011). *M 6.3, Christchurch, February 22 2011*. Retrieved March 10, 2012, from GeoNet: http://www.geonet.org.nz/earthquake/historic-earthquakes/top-nz/quake-14.html

GNS Science. (2011). *The hidden fault that caused the February 2011 Christchurch earthquake*. Retrieved April 1, 2012, from GNS Science: http://www.gns.cri.nz/Home/Our-Science/Natural-Hazards/Recent-Events/Canterbury-quake/Hidden-fault

GNS Science. (2011). *The hidden fault that caused the February 2011 Christchurch earthquake*. Retrieved July 23, 2012, from GNS Science: http://www.gns.cri.nz/Home/News-and-Events/Media-Releases/Most-damaging-quake-since-1931/Canterbury-quake/Hidden-fault

GNS Science. (2012). *Canterbury Quakes*. Retrieved June 30, 2012, from GeoNet: http://info.geonet.org.nz/display/home/Canterbury+Quakes

GNS Science. (No date). *Does the direction of rupture influence the size of the impact in different places?* Retrieved May 19, 2013, from GNS Science: http://www.gns.cri.nz/Home/Learning/Science-Topics/Earthquakes/Monitoring-Earthquakes/Other-earthquake-questions/Does-the-direction-of-rupture-influence-the-size-of-the-impact-in-different-places

Goodman, R. E., & Kieffer, D. S. (2000, August). Behaviour of Rock in slopes. *Journal of Geotechnical and Geoenvironmental Engineering*, 675-684.

Google. (2010). Google Earth (Version 6) [Computer Program].

Hampton, S. (2010). *Growth, Structure and Evolution of the Lyttleton Volcanic Complex, Banks Peninsula, New Zealand.* University of Canterbury. 7-11.

Hancox, G., Perrin, N., & Dellow, G. (2002). Recent studies of historical earthquake-induced landsliding, ground damage, and MM intensity in New Zealand. *Bulletin of the New Zealand Society for Earthquake Engineering, 35*(2), 59-95.

Haneberg, W. (2008). Using close range terrestrial digital photogrammetry for 3-D rock slope modelling and discontinuity mapping in the United States. *Bulletin of Engineering Geology and the Environment, 67*(4), 457469.

Hoek, E. (2007). Shear strength of discontinuities. In *Practical Rock Engineering.*

Hoek, E., & Bray, J. (1981). *Rock slope engineering.* Taylor & Francis.

Hoek, E., Carlos, C., & Brent, C. (2002). Hoek-Brown failure criterion – 2002 Edition. *Proceedings of NARMS-TAC*, (pp. 267-273).

Holden, C. (2011). Kinematic Source Model of the 22 February 2011 Mw 6.2 Christchurch Earthquake Using Strong Motion Data. *Seismological Research Letters, 82*(6), 783-788.

Johansson, F. (2003). *Stability Analysis of Large Structures Founded on Rock - An introductory study, Doctoral Thesis.* Stockholm: Royal Institute of Technology.

Kanari, M. (2008). *Evaluation of rockfall hazard to Qiryat Shemona - possible correlation to earthquakes. M.Sc. Thesis.* Tel Aviv: Department of Geophysics and Planetary Sciences, Tel Aviv University.

Kawase, H. (2003). Site Effects on Strong Ground Motions. In *International Handbook of Earthquake & Engineering Seismology, Part 2* (pp. 1013-1030).

Kvalstad, T., Andersen, L., Forsberg, C., Berg, K., Bryn, P., & Wangen, M. (2005). The Storegga slide: evaluation of triggering sources and slide mechanics. *Marine and Petroleum Geology, 22*(1-2), 245-256.

Li, Y., Wang, J., Jung, W., & Ahmad, G. (2012). Mechanical properties of intact rock and fractures in welded tuff from Newberry Volcano. *Stanford Geothermal Workshop.* Stanford.

Massey, C., Yetton, M., Lukovic, B., McSaveney, H., Heron, D., & Bruce, Z. (2012). *Canterbury Earthquakes 2010/11 Port Hills Slope Stability: Pilot study for assessing life-safety risk from cliff collapse.* Wellington: GNS Science.

Massey, C., Yetton, M., Lukovic, B., McSaveney, M., Heron, D., & Bruce, Z. (2012). *Canterbury Earthquakes 2010/11 Port Hills Slope Stability: Pilot study for assessing life-safety risk from cliff collapse.* Wellington: GNS Science.

Massey, C., Yetton, M., Lukovic, B., McSaveney, M., Heron, D., & Bruce, Z. (2012). *Canterbury Earthquakes 2010/11 Port Hills Slope Stability: Pilot study for assessing life-safety risk from cliff collapse, GNS Science Consultancy Report 2012/57.* GNS Science.

McDowell, B. (1989). *Site Investigations for Residential Development on the Port Hills, Christchurch.* Christchurch: Geology Department, University of Canterbury.

McFadgen, B., & Goff, J. (2005). An earth systems approach to understanding the tectonic and cultural landscapes of linked marine embayments: Avon-Heathcote Estuary (Ihutai) and Lake Ellesmere (Waihora), New Zealand. *Journal of Quaternary Science, 20*(3), 220-237.

McVerry, G., Zhao, J., Abrahamson, N., & Somerville, P. (2006). Response spectral attenuation relations for crustal and subduction zone earthquakes. *Bulletin for the New Zealand Society of Earthquake Engineering, 39*, 1-58.

Muschamps, K. (2005). *Field Description of Soil and Rock - Guideline for the field classification and description of soil and rock for engineering purposes.* Wellington: NZ Geotechnical Society Inc.

Owen, G., Moretti, M., & Alfaro, P. (2011). Recognising triggers for soft-sediment deformation: Current understanding and future directions. *Sedimentary Geology, 235*(3-4), 133-140.

Page, S. (2011). *Jun 13 2011 - Large earthquakes strike south-east of Christchurch*. Retrieved July 16, 2012, from GeoNet: http://www.geonet.org.nz/news/archives/2011/jun-2011-large-earthquakes-strike-south-east-of-christchurch.html

pers. comm. Hampton, S. (n.d.).

Poppelliers, C., & Pavlis, G. (2002). The seismic response of a steep slope: High resolution observations with a dense, three-component seismic array. *Bulletin of the Seismological Society of America, 92*(8), 3102-3115.

Price, D., & De Freitas, M. (2009). *Engineering geology: principles and practice.* Springer.

Reid, T., & Harrison, J. (2000). A semi-automated methodology for discontinuity trace detection in digital images of rock mass exposures. *International Journal of Rock Mechanics and Mining Sciences, 37*(7), 1073-1089.

Roncella, R., Forlani, G., & Remondino, F. (2005). Photogrammetry for geological applications: automatic retrieval fo discontinuity orientation in rock slopes. *Internation Society for Optics and Photonics*, 17-27.

Sepulveda, S., Murphy, M., & Petley, D. (2005). Topographic controls on coseismic rock slides during the 1999 Chi-Chi earthquake, Taiwan. *Quaterly journal of engineering geology and hydrogeology, 38*(2), 189-196.

Sewell, R. (1988). Late Miocene volcanic stratigraphy of central Banks Peninsula, Cantebrury, New Zealand. *New Zealand Journal of Geology and Geophysics*, 41-64.

Sewell, R., Weaver, S., & Reay, M. (1992). *Geology of Banks Peninsula. (Institute of Geological and Nuclear Sciences Map 3, scale 1:100,000).* Lower Hutt: Institue of Geological and Nuclear Sciences Ltd.

Somerville, P. (2003). Magnitude scaling of the near fault rupture directivity pulse. *Physics of The Earth and Planetary Interiors, 137*, 201-212.

Spry, A. (1962). The origin of columnar jointing, particularly in basalt flows. *Geological Society of Australia, 8*(2), 191-216.

Stramondo, S., Kyriakopoulos, C., Bignami, C., Chini, M., Melini, D., Moro, M., et al. (2011, September 22). Did the September 2010 (Darfield) earthquake trigger the February 2011 (Christchurch) event? *Scientific Repots*, 1-7.

Sturzenegger, M., & Stead, M. (2009). Close-range terrestrial digital photogrammetry and terrestrial laser scanning for discontinuity characterization on rock cuts. *Engineering Geology, 106*(3-4), 163-182.

WeatherSpark. (No Date). *Historical Weather For 2011 in Christchurch, New Zealand*. Retrieved May 17, 2013, from WeatherSpark: http://weatherspark.com/history/32739/2011/Christchurch-Canterbury-New-Zealand

Wood, M. M. (2007). *UPSeis - an educational site for budding seismologists*. Retrieved July 22, 2012, from MichiganTech: http://www.geo.mtu.edu/UPSeis/waves.html

Wright, S., & Rathje, E. (2003). Triggering Mechanisms of Slope Instability and their Relationship to Earthquakes and Tsunamis. *Pure and applied geophysics, 160*(10-11), 1865-1877.

Wu, Q., & Kulatilake, P. (2012). Application of equivalent continuum and discontinuum stress analyses in three-dimensions to investigate stability of a rock tunnel in a dam site in China. *Computer and Geotechnics, 46*, 48-68.

Wylie, D., & Mah, C. (2004). *Rock slope engineering.* Taylor and Francis.

Zhao, X. J., Dowrick, D. J., & McVerry, G. H. (1997). Attenuation of Peak Ground Accelerations in New Zealand Earthquakes. *Bulletin of the New Zealand National Society for Earthquake Engineering, 30*(2), 133-158.

Appendix I

Assortment of methods used to survey Redcliffs' cliff

General Characterisation

Methodology	Purpose	Equipment	Processing Software	Procedure	Additional Literature	Comments
Remote Face Logging (Part I) (Field Survey)	Create a geological face log identifying the boundaries of individual geological units exposed on the cliff face	Pencil and Paper Digital Camera (DSLR)	Microsoft Publisher	Lithology was initially logged on-site using (printed) photographs taken of the cliff face. The logs were then refined with digitally enhanced photographs of the cliff face.		Being one of the few methods used to survey the cliff directly, the level of detail is limited by what is observed from Redcliffs school as well as photographs.
Engineering Geological Description (Field Survey)	Describe qualitatively in engineering geological terms the lithology identified from the face log	Pencil and Paper		Field descriptions were made of each unit of rock and soil following the New Zealand Geotechnical Society guidelines	Muschamps et al, 2005	Detailed descriptions of the geological units were done by surveying selected outcrops located at a proxy site (which included the orientation of measureable discontinuities)

Rock mass Characterisation

Methodology	Purpose	Equipment	Processing Software	Procedure	Additional Literature	Comments
Schmidt Hammer Test	Measure the compressive strength of the welded ignimbrite	L-Schmidt Hammer	Microsoft Excel	150 rebound measurements were taken on selected outcrops that matched the jointed characteristics observed from the cliff face. The data collected was tabulated and sorted based on orientation of the Schmidt Hammer before a parametric statistical analysis was conducted to evaluate the spread of data. The results of the analysis were then used (converted) using a conversion graph (Hoek, 2007) to determine the JCS and UCS of the welded ignimbrite.	(Katz, Reches, & Roegiers, 2000); (Day & Goudie, 1997)	The rebound measurements were taken on rock faces (outcrops) at the proxy site, located along McCormacks Bay Road and Glenstrae Road.
Terrestrial Photogrammetry	Determine the orientation of joints	Nikkon 300s Digital Camera 50 mm and 105 mm focal length lenses RTK GPS	Siro 3D Siro joint (CSIRO, 2010) DIPS	Cliff face is divided into five segments (Figure 4). Photographs are taken by two digital cameras positioned at opposite angles facing the targeted rock face. The photographs are uploaded onto *Siro3D* to generate a three-dimensional model of the outcrop Dip and dip direction measurements are then taken from the models, which are then uploaded to *DIPS* where they are plotted on a stereonet to determine the major joint sets.	(Struzenegger and Stead 2009 a, b); (Brideau et al, 2011)	The technique was executed by Marc-Andre Brideau from the University of Auckland (Brideau et al, 2011), who shared the data with the author of this study.

Soil Characterisation

Methodology	Purpose	Equipment	Processing Software	Procedure	Additional Literature	Comments
Scala Penetrometer Test	To measure the strength of the (mantle) loess soils	Pencil and Paper Scala Penetrometer	Microsoft Excel	Penetrometer rod was hammered into the ground with a predetermined weight. The number of blows it took for the rod to penetrate 10 cm of soil is recorded until the full length of the rod (or 90 cm) is in the ground. The recorded data is tabulated and graphed to determine the (compact) strength of the soil.		Measurements were taken from two separate locations found at the cull de sac end of Glendevere Terrace to provide a spread of data representing the overall soil strength across the top of the cliff.

Mapping the surface area of the cliff

Methodology	Purpose	Equipment	Processing Software	Procedure	Additional Literature	Comments
Examining Aerial Photography	To visually evaluate the extent of the cliff edge retreating as a result of the February and June 2011 aftershocks. To provide a basis of information to build on, or rather a graphical representation of the fundamental changes that occurred, adding additional information to the map, such as surface fractures, that was sighted during the field survey that followed on.		Microsoft Publisher	Photographs taken in 2003 and the 24 February 2011 were analysed to record any changes to the land above the cliff after the February aftershock. The main changes were identified by a visual comparison between the two images. Both images were then mapped out on a scale of 1:500, tracing the outlines of certain features such as buildings, the cliff edge and talus to isolate critical components surrounding the cliff that were affected by the February aftershock. The outlines of the cliff edge at then overlapped to determine how far the cliff edge has retreated as a result of the February 22 and June13 2011 aftershock.		The aerial photographs available at the time of conducting this investigation were from Google Earth (2003) and a website called coordinates.com (post-February 2011) Unfortunately no aerial post-June 2011 photographs were available at the time of this investigation, meaning that all changed mapped as a result of the June aftershock are inferred based on field observations
Remote Face Logging (Part II) (field survey)	To map post-failure surface deformation of the cliff top and cliff face.	Pencil and Paper Aerial photograph (cliff top) Planar photograph (cliff face)	Microsoft Publisher	All surface alterations, including lateral spreading, fissures and cracks in retaining walls / foundations were mapped on the aerial photograph whilst on top of the cliff. These mapped alterations are then transferred onto the aerial photograph outline (template) to create a detailed (post-failure) map of Redcliffs. The same was done to map the evidence of deformation on the cliff face (i.e. discontinuities) exposed on the cliff face to develop a post-failure map of Redcliffs' cliff (face).		The (annotated) photograph maps of the cliff top and cliff face were developed as a result of the aerial photograph analysis and logging of the cliff face.

Developing a slope (cross-section) model

Methodology	Purpose	Equipment	Processing Software	Procedure	Additional Literature	Comments
(Total Station) Laser Scanning	To generate (post-June failure) cross sections of the cliff face	Total Station Pencil and Paper Tape Measure	Terramodel 10.41 Microsoft Publisher	Similar to photogrammetry, the cliff face was broken down into seven segments. The total station was set up at key surveying positions designated for each section to survey the cliff face(s) at a face-on view. The data was then transferred onto *TERRAMODEL 10.41* and converted into cross-section models that portrayed (sections of) the slope before and after each major collapse. Each cross section model was edited to fit a scale of 1:50 and combined with the cross sections generated from the LIDAR data to create difference models.		The cross sections scanned at each segment of the cliff faces combines to form a representation of that particular subdivision / section of the cliff face.
Aerial LiDAR Analysis	To generate cross sections of the cliff face prior to the 13 June 2011 quake (i.e. pre- and post- February 2011 trigger earthquake)		ArcMap10 Microsoft Publisher	The pre- and post-Feb LIDAR data were uploaded onto ArcpMap10 and converted into a raster. Lines were drawn on the raster image, along the line of sight the total station would have used to survey the particular section of the cliff to generate cross sections that matched the surveyed sections. The cross section images are then exported onto Microsoft Publisher and edited to match the 1:50 scale of the post-June cross sections developed in the field.	(Collins & Stock, 2012)	The 2003 and post-February 2011 LIDAR data was provided by John Thyne, Geography Department from the University of Canterbury. The lithology is interpolated on every cross section to finalise the cross section models.

Behavioural investigation of cliff top fissures

Methodology	Purpose	Equipment	Processing Software	Procedure	Additional Literature	Comments
Monitoring cliff top fissures	To determine if creeping of cliff top fissures were occurring (i.e. increasing in size), and if so, whether it was influenced by the weather, gravity, or seismicity.	Pencil and Paper Nails Spray Can Tape Measurer Marker Pen	Microsoft Excel	Main fissures found by the cliff edge (by Mark Yetton) were selected to be monitored over an extended period of time. A reference point was marked (either) by drawing reference markings on either side of a crack using a marker pen, or a pair of nails hammered at each end of the fissure to measure from. Monitoring comprised of fortnightly visits to each site to measure the width of each fissure, while also noting the weather and seismic activity over the 2 weeks. The recorded measurements were then tabulated and graphed on Microsoft Excel, making note (of key dates) on the graph of any major event that happened as well (i.e. seismicity or weather).		The selection and monitoring of surface fractures were done with the help of Mark Yetton from Geotech ltd. Measurements of the fractures were taken every fortnightly up to the week of the 13 June 2011 aftershock

Characterisation of cliff top fissures

Methodology	Purpose	Equipment	Processing Software	Procedure	Additional Literature	Comments
Ground Penetrating Radar (GPR)	To determine the depth at which fissures formed at the top of the cliff penetrate into the cliff	50 Hz and 100 Hz Antennas Trigger Unit, Cables, and Laptop Tape Measure, and Stepping Apparatus	pulseEKKO 100 processing Software Reflexw	The appropriate antennas were connected to the triggering unit and attached to the stepping apparatus. A tape measure was used to accurately 'step' at 50 cm increments whilst conducting the survey and provide a visual path on the ground oriented similarly to the yellow line. The data was then uploaded onto Reflexw where it was processed accordingly.	(Grandjean and Goury, 1996); (Rashed et al, 2003); (Daniels, 2004)	The preliminary results from the test run indicated a lack in depth of penetration from the equipment. This method was abandoned due the unpromising preliminary results and the lack of access to the fissures of interest after the June earthquake.
Resistance Tomography	A secondary attempt to investigate the depth of penetration of surface fractures	Electrodes, Cables, and Tigre System Laptop	Tigre System Control Software Res2D	Using the trace line outlined in Figure 6, x64 electrodes were planted into the ground following the 'two cables with Tigre 128' sequence (Tigre User Manual). The necessary parameters were then inputted into the Tigre System and laptop before executing the survey and leaving the program to run for an extended period of time. The data collected was then uploaded from the Tigre System Control Software to Res2D and processed, applying the necessary filters before being interpreted	(Hack, 2000)	Similar to the GPR, the application of this method on top of Redcliffs only went as far as the testing phase.

Appendix II

Processed (Terrestrial Photogrammetry) Stereonets

Photogrammetry Face 1

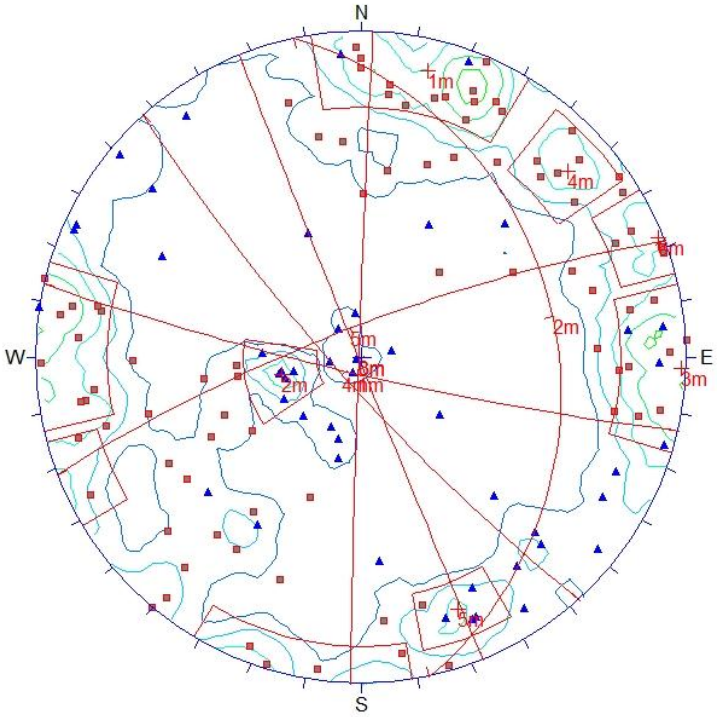

CLASSIFICATION

Plane [87]

Trace [48]

Equal Angle
Lower Hemisphere
135 Poles
135 Entries

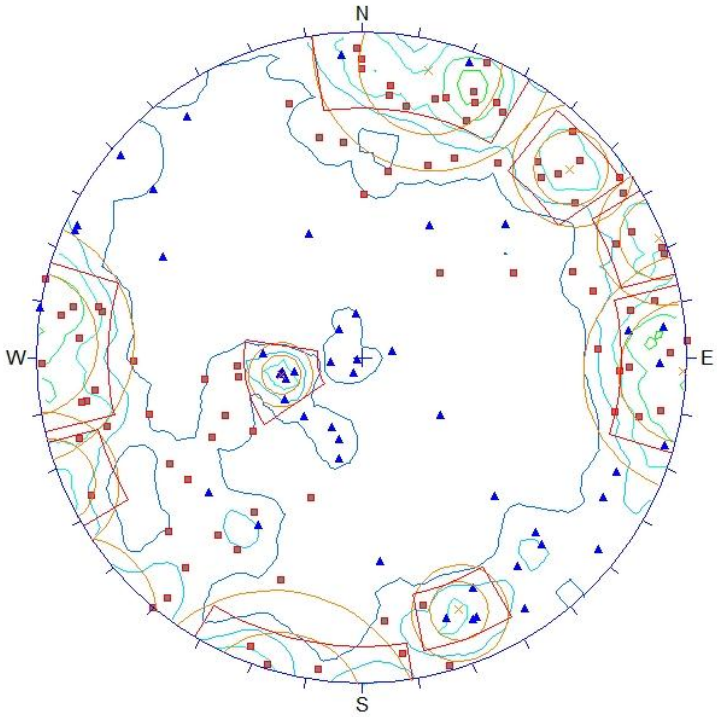

CLASSIFICATION

Plane [87]

Trace [48]

Equal Angle
Lower Hemisphere
135 Poles
135 Entries

Photogrammetry Face 2

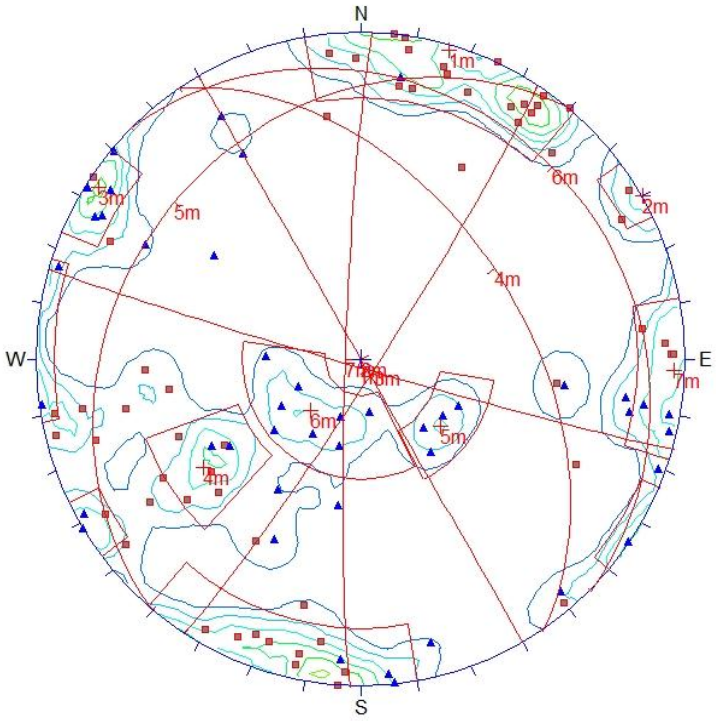

CLASSIFICATION

Plane [59]

Trace [44]

Equal Area
Lower Hemisphere
103 Poles
103 Entries

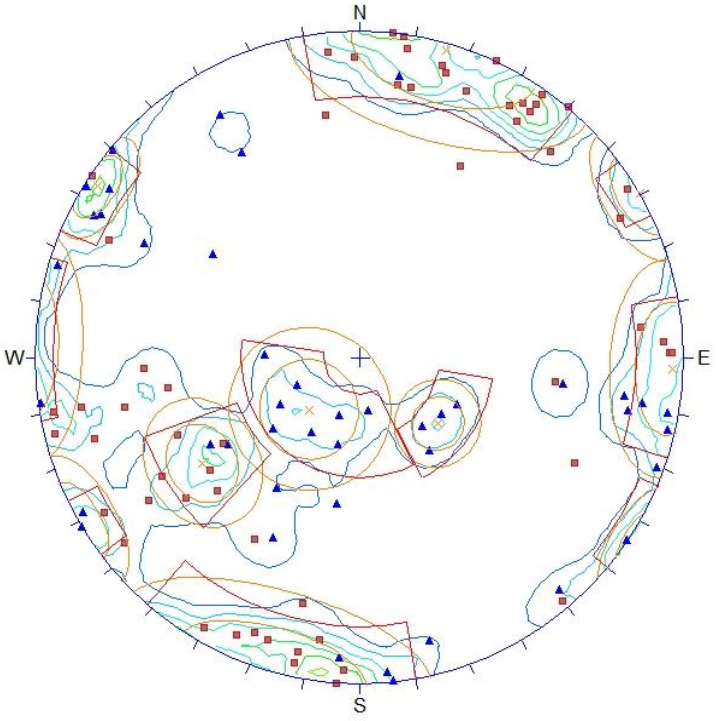

CLASSIFICATION

Plane [59]

Trace [44]

Equal Area
Lower Hemisphere
103 Poles
103 Entries

Photogrammetry Face 3

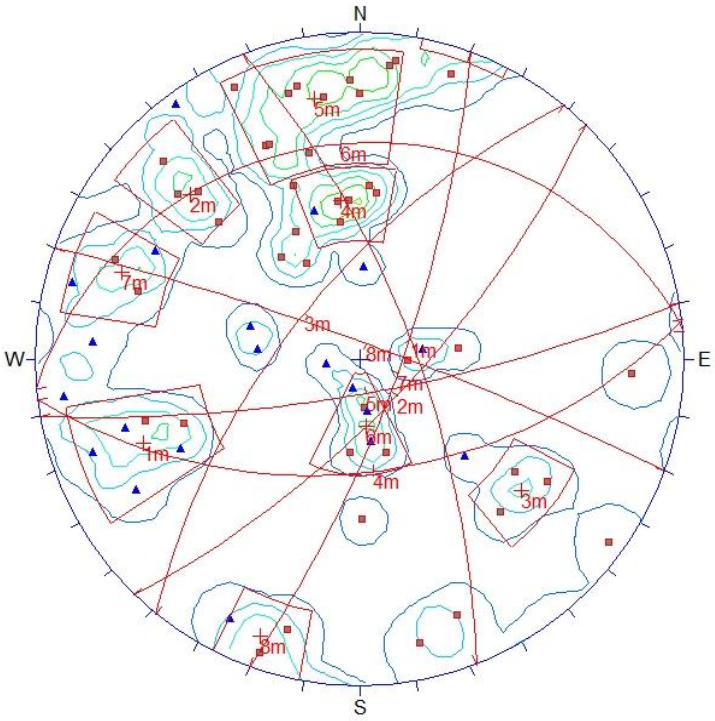

CLASSIFICATION

Plane [44]

Trace [20]

Equal Angle
Lower Hemisphere
64 Poles
64 Entries

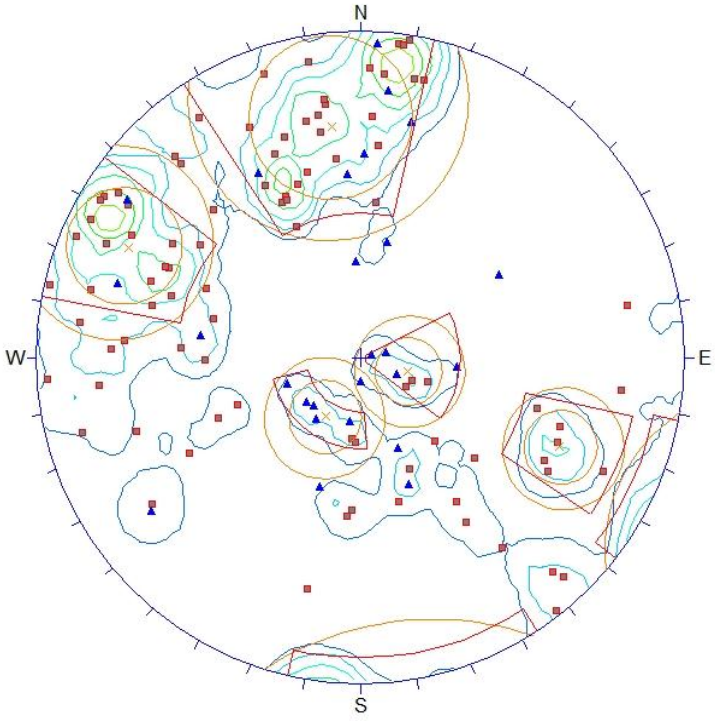

CLASSIFICATION

Plane [90]

Trace [26]

Equal Angle
Lower Hemisphere
116 Poles
116 Entries

Photogrammetry Face 4

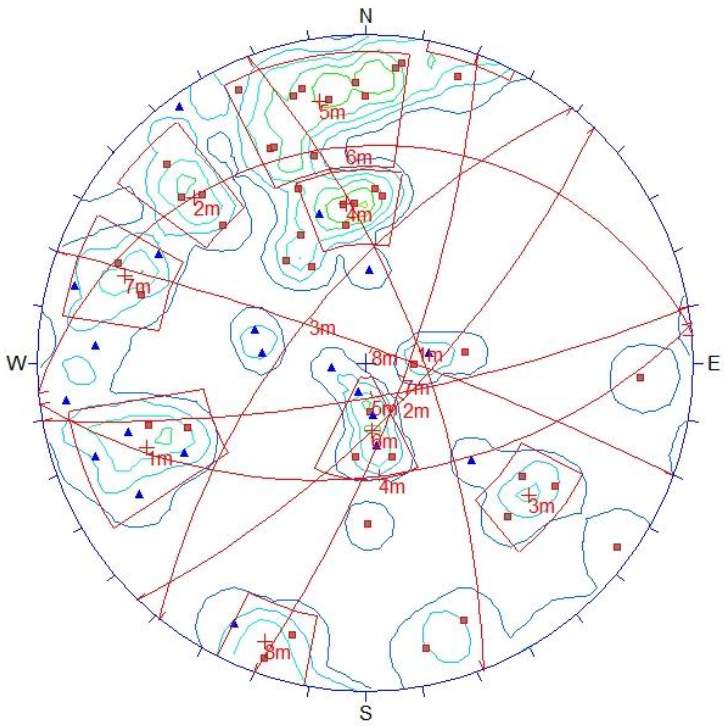

CLASSIFICATION

Plane [44]

Trace [20]

Equal Angle
Lower Hemisphere
64 Poles
64 Entries

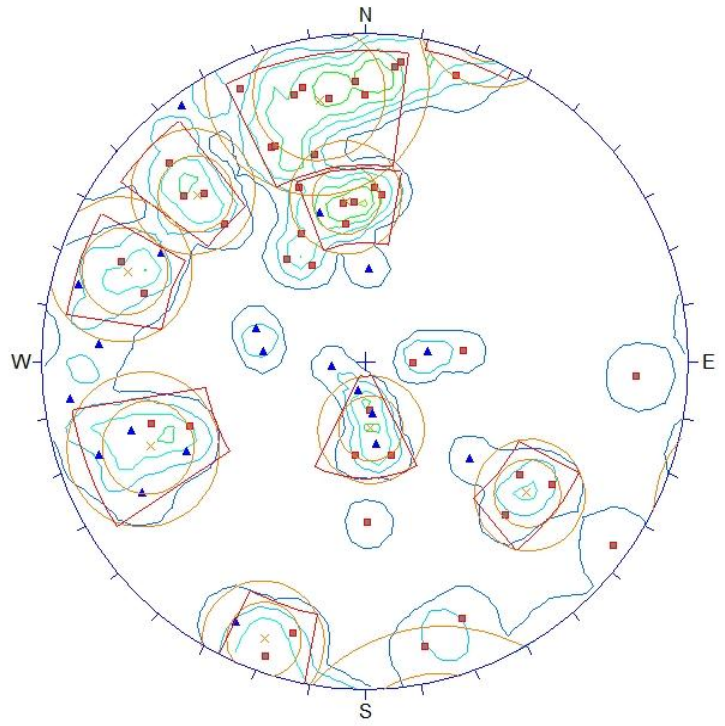

CLASSIFICATION

Plane [44]

Trace [20]

Equal Angle
Lower Hemisphere
64 Poles
64 Entries

Photogrammetry Face 5

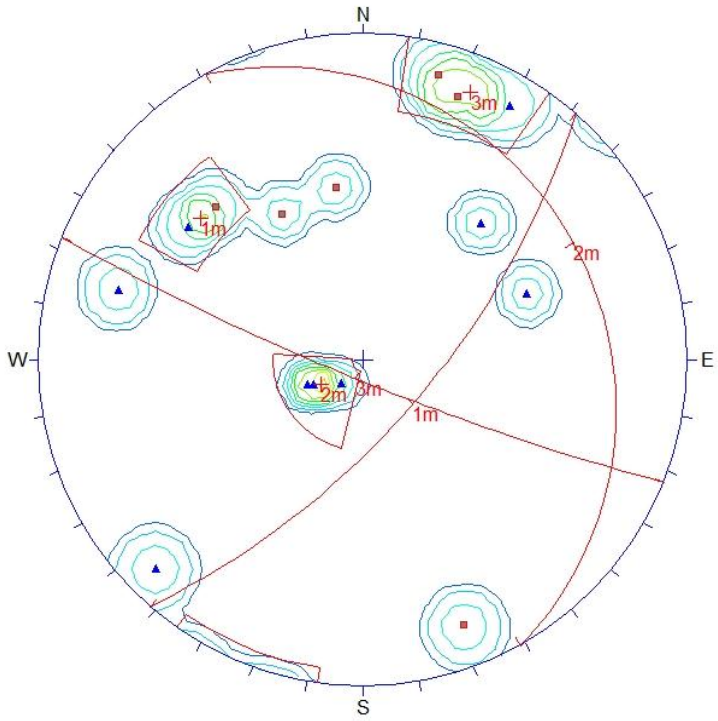

CLASSIFICATION

Plane [6]

Trace [9]

Equal Angle
Lower Hemisphere
15 Poles
15 Entries

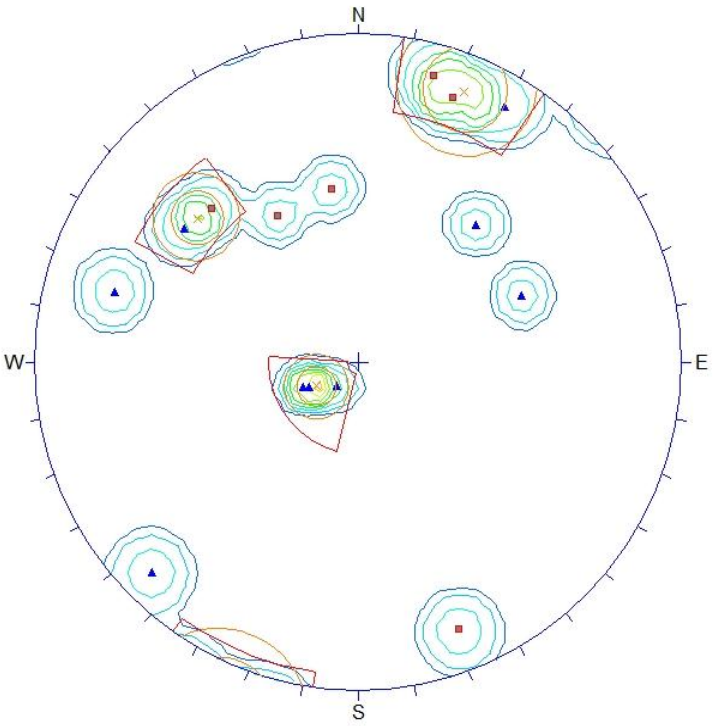

CLASSIFICATION

Plane [6]

Trace [9]

Equal Angle
Lower Hemisphere
15 Poles
15 Entries

Appendix III

Cliff edge photographs,
22 February – 13 June 201

Site Comparisons (before and after the aftershock 13/6/2011)

Reuben Lo

Site 1

A – B = 620 mm (13/6/2011)

$A^1 – B^1$ = 705 mm (17/6/2011)

Site Comparisons (before and after the aftershock 13/6/2011)

Reuben Lo

Site 2

A – B = 712 mm (13/6/2011)

$A^1 – B^1$ = 729 mm (17/6/2011)

Site Comparisons (before and after the aftershock 13/6/2011)

Reuben Lo

Site 3

A – B = 7480 mm (13/6/2011)

$A^1 – B^1$ = 7483 mm (17/6/2011)

Site Comparisons (before and after the aftershock 13/6/2011)

Reuben Lo

Pencil Length: 140mm

Site 4

No accurate measurements can be made due to the lack of a reference. However, it can be seen that a clear vertical and horizontal displacement occurred on the retaining wall after the 13/6/2011 quake.

A – B = 647 mm (17/6/2011)

Note, the measurement taken included a vertical component, as it was done on an angle.

Site Comparisons (before and after the aftershock 13/6/2011)

Reuben Lo

Site 5

15/4 (point of arrowhead) – 17/4 = 5 mm (17/4/2011)

15/4 (point of arrowhead) – 14/6 = 19mm (14/6/2011)

Site Comparisons (before and after the aftershock 13/6/2011)

Reuben Lo

Image Not Available

Site 6

A revisit after 13/6/2011 was not possible as all possible entrances were blocked off by falling debris and was decided too risky to attempt an access.

Site Comparisons (before and after the aftershock 13/6/2011)

Reuben Lo

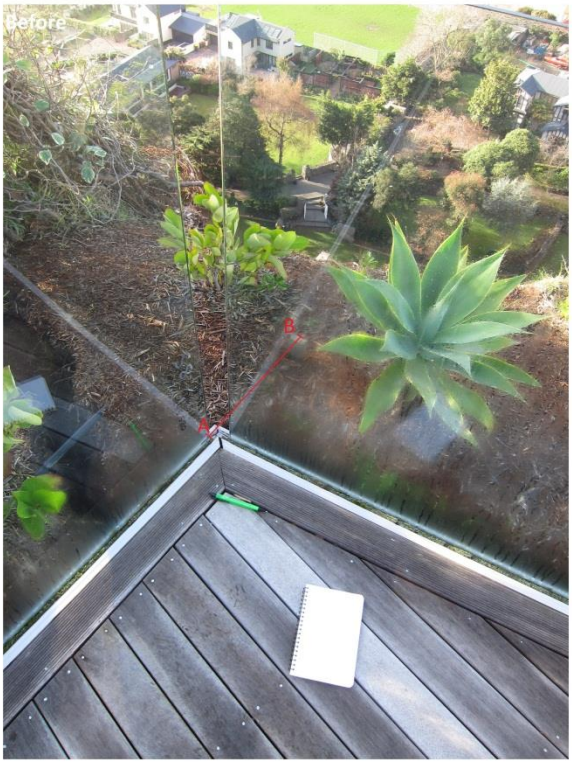

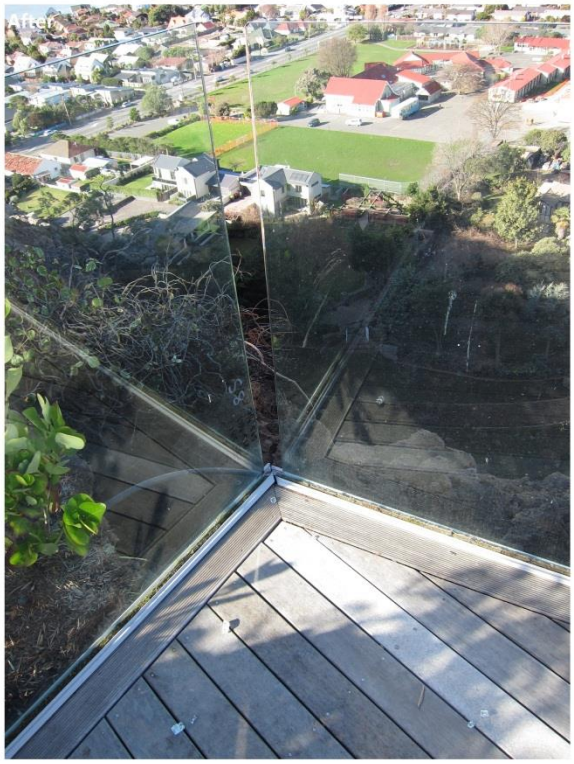

Site 7

Since the quake on 13/6/2011, it is evident that part of the site has collapsed and no further measurements could be made.

A – B = 580 mm (13/6/2011)

Site Comparisons (before and after the aftershock 13/6/2011) Reuben Lo

Site 8

Another site which collapsed after the 13/6/2011 quake which made it impossible to take any more measurements.

A – B = 3883 mm (13/6/2011)

Site Comparisons (before and after the aftershock 13/6/2011)

Reuben Lo

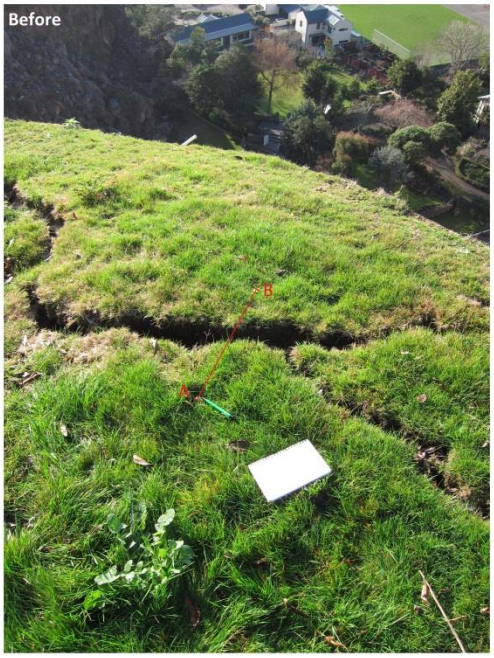

Site 10

Another site unable to continue measuring as part of the site has collapsed.

A - B = 520 mm (13/6/2011)

Site Comparisons (before and after the aftershock 13/6/2011)

Reuben Lo

Site 11

A - B = 621 mm (13/6/2011)

A' - B' = 690 mm (17/6/2011)
Note, it is evident that the 'after' measurement includes a verticle component (i.e. on an angle) compared to the 'before' picture (which is near horizontal).

Appendix IV

Annotated cross sections

Face 1.1

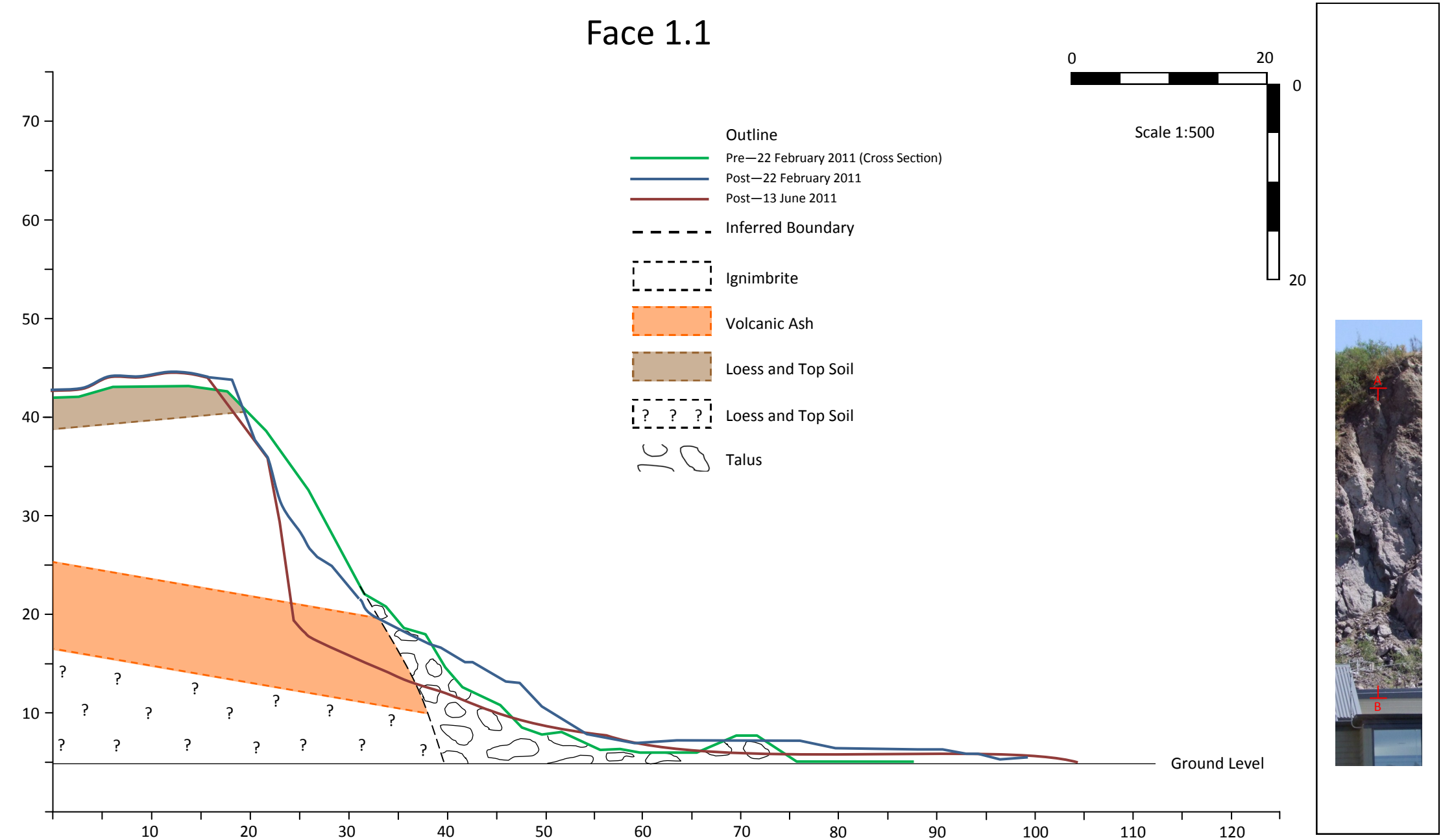
0
20
0
20
Scale 1:500
Outline
Pre—22 February 2011 (Cross Section)
Post—22 February 2011
Post—13 June 2011
Inferred Boundary
Ignimbrite
Volcanic Ash
Loess and Top Soil
Loess and Top Soil
Talus
Ground Level
70
60
50
40
30
20
10
10
20
30
40
50
60
70
80
90
100
110
120
A
B

Face 1.2

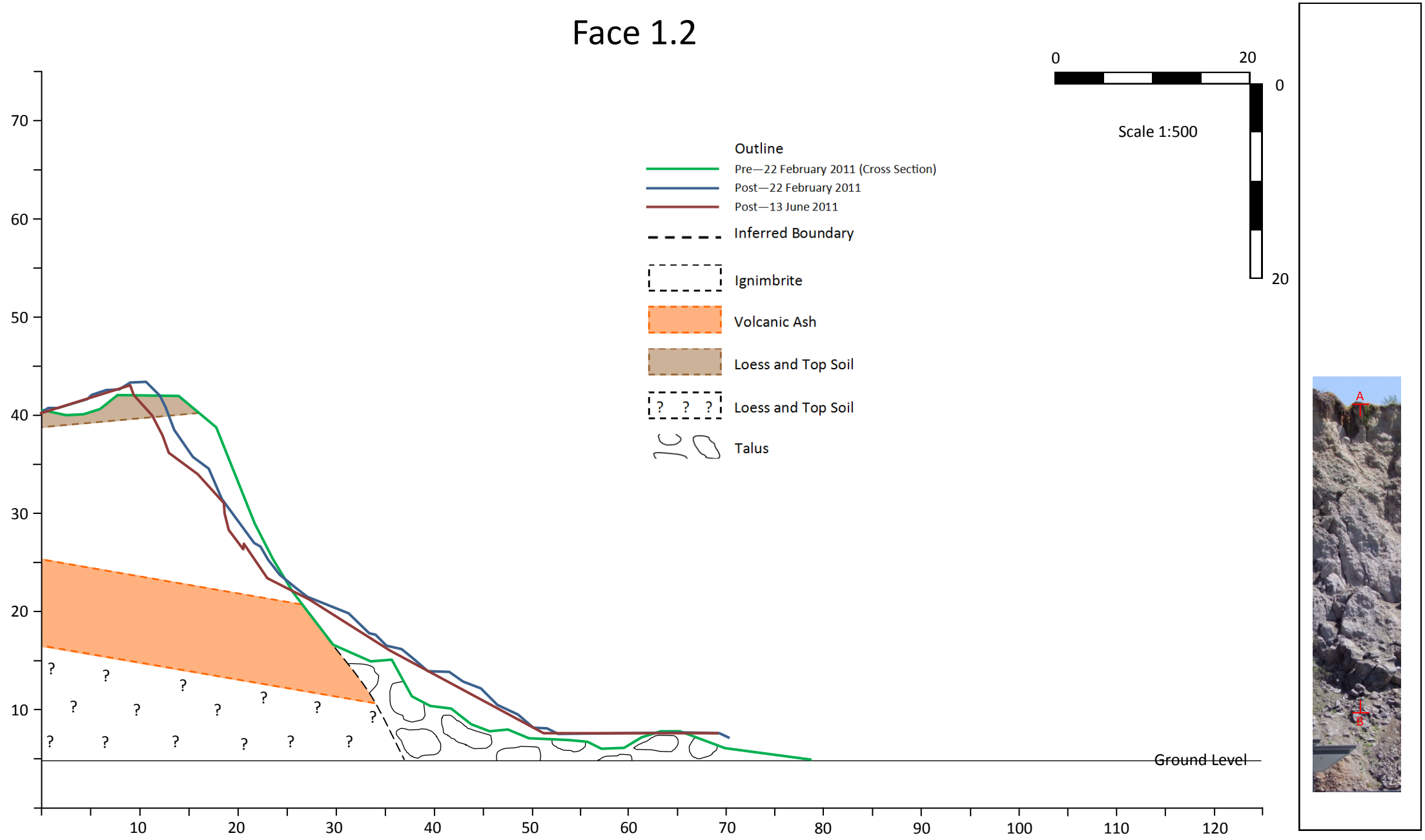
0
20
0
20
Scale 1:500
Outline
Pre—22 February 2011 (Cross Section)
Post—22 February 2011
Post—13 June 2011
Inferred Boundary
Ignimbrite
Volcanic Ash
Loess and Top Soil
Loess and Top Soil
Talus
Ground Level
70
60
50
40
30
20
10
10
20
30
40
50
60
70
80
90
100
110
120
A
B

Face 1.3

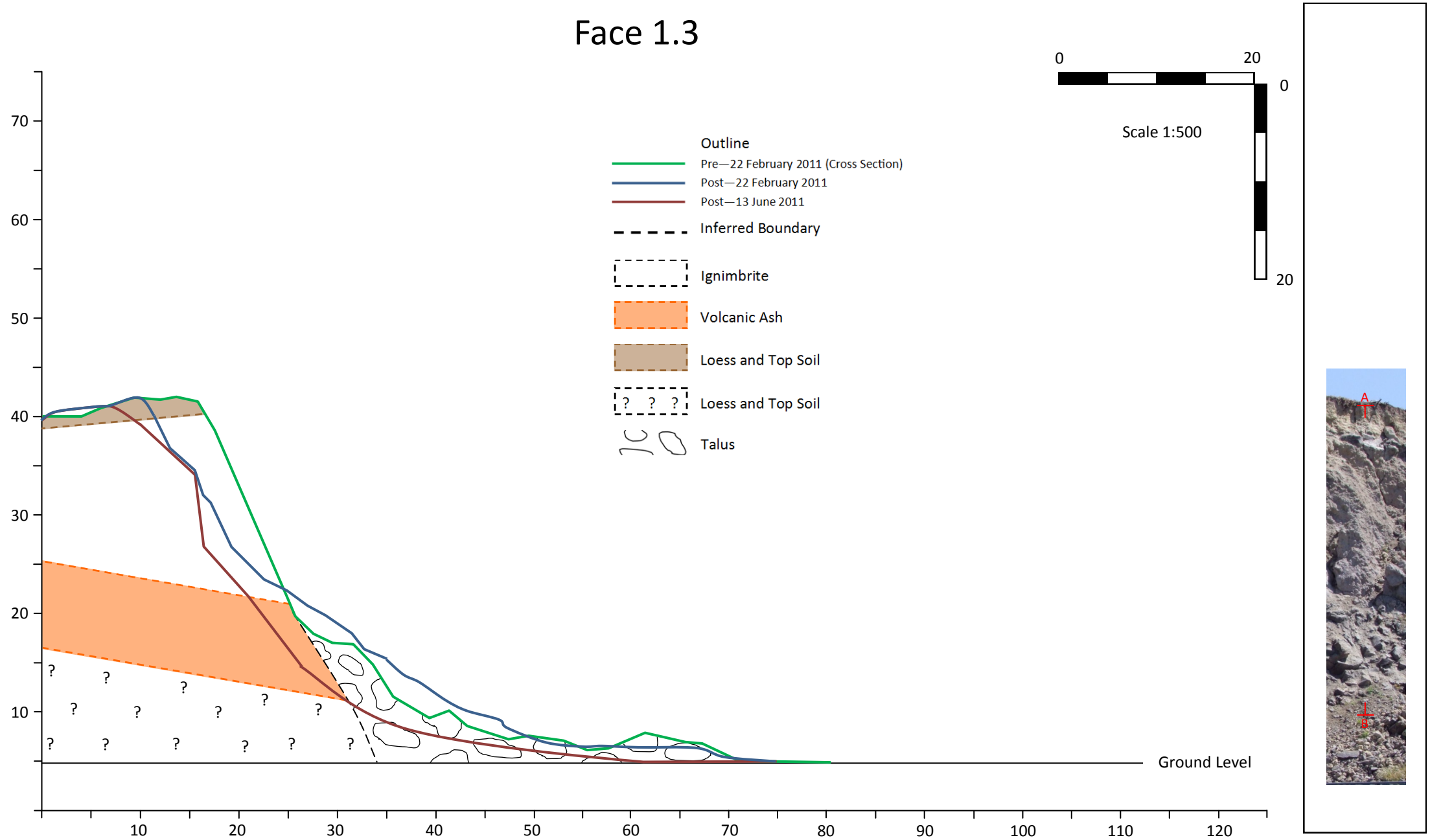
0
20
0
20
Scale 1:500
Outline
Pre—22 February 2011 (Cross Section)
Post—22 February 2011
Post—13 June 2011
Inferred Boundary
Ignimbrite
Volcanic Ash
Loess and Top Soil
? ? ?
Loess and Top Soil
Talus
Ground Level
70
60
50
40
30
20
10
10
20
30
40
50
60
70
80
90
100
110
120
A
B

Face 2.2

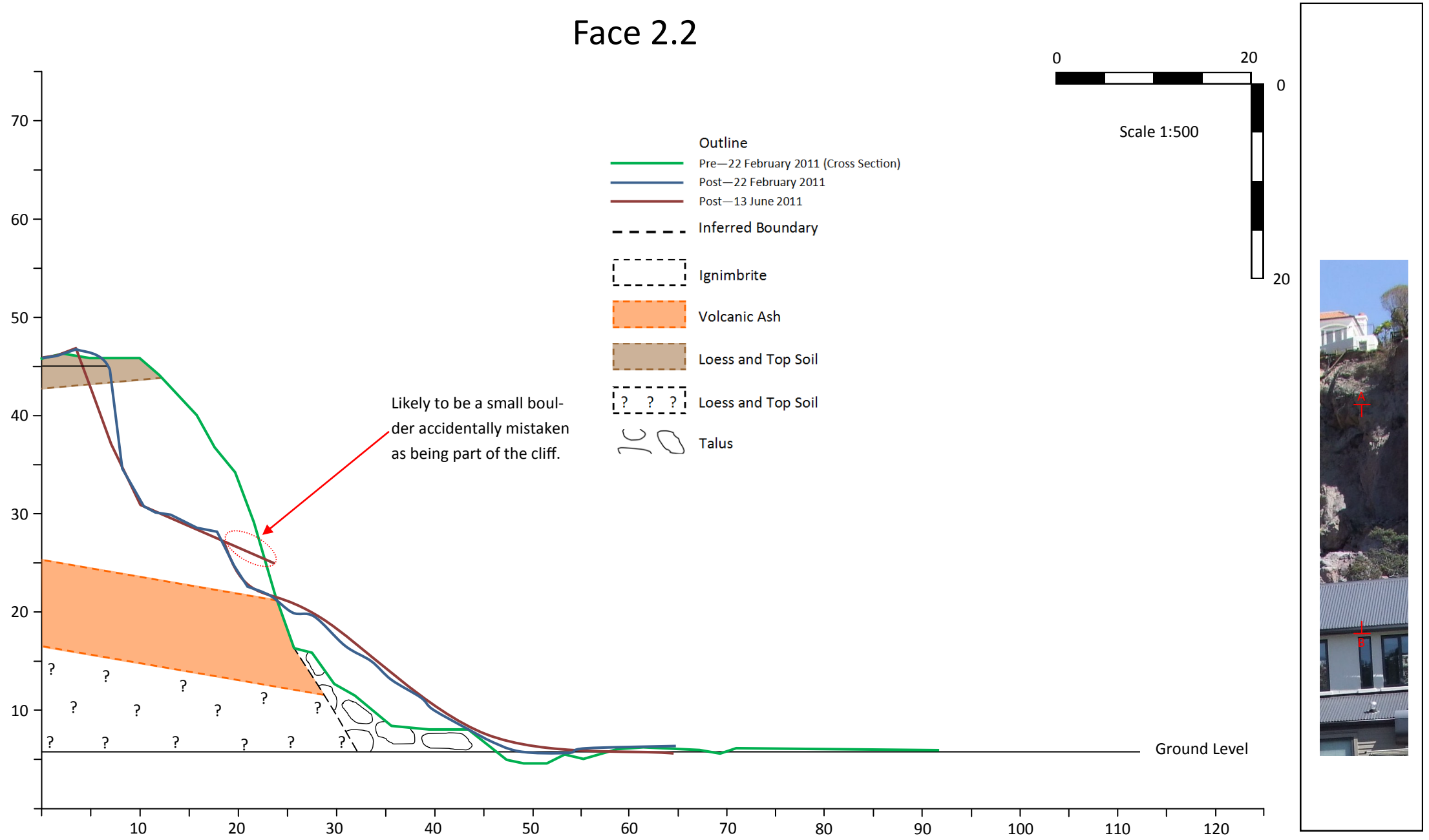
0
20
0
20
Scale 1:500
Outline
Pre—22 February 2011 (Cross Section)
Post—22 February 2011
Post—13 June 2011
Inferred Boundary
Ignimbrite
Volcanic Ash
Loess and Top Soil
Loess and Top Soil
Talus
Likely to be a small boul-
der accidentally mistaken
as being part of the cliff.
Ground Level
70
60
50
40
30
20
10
10
20
30
40
50
60
70
80
90
100
110
120

Face 2.2

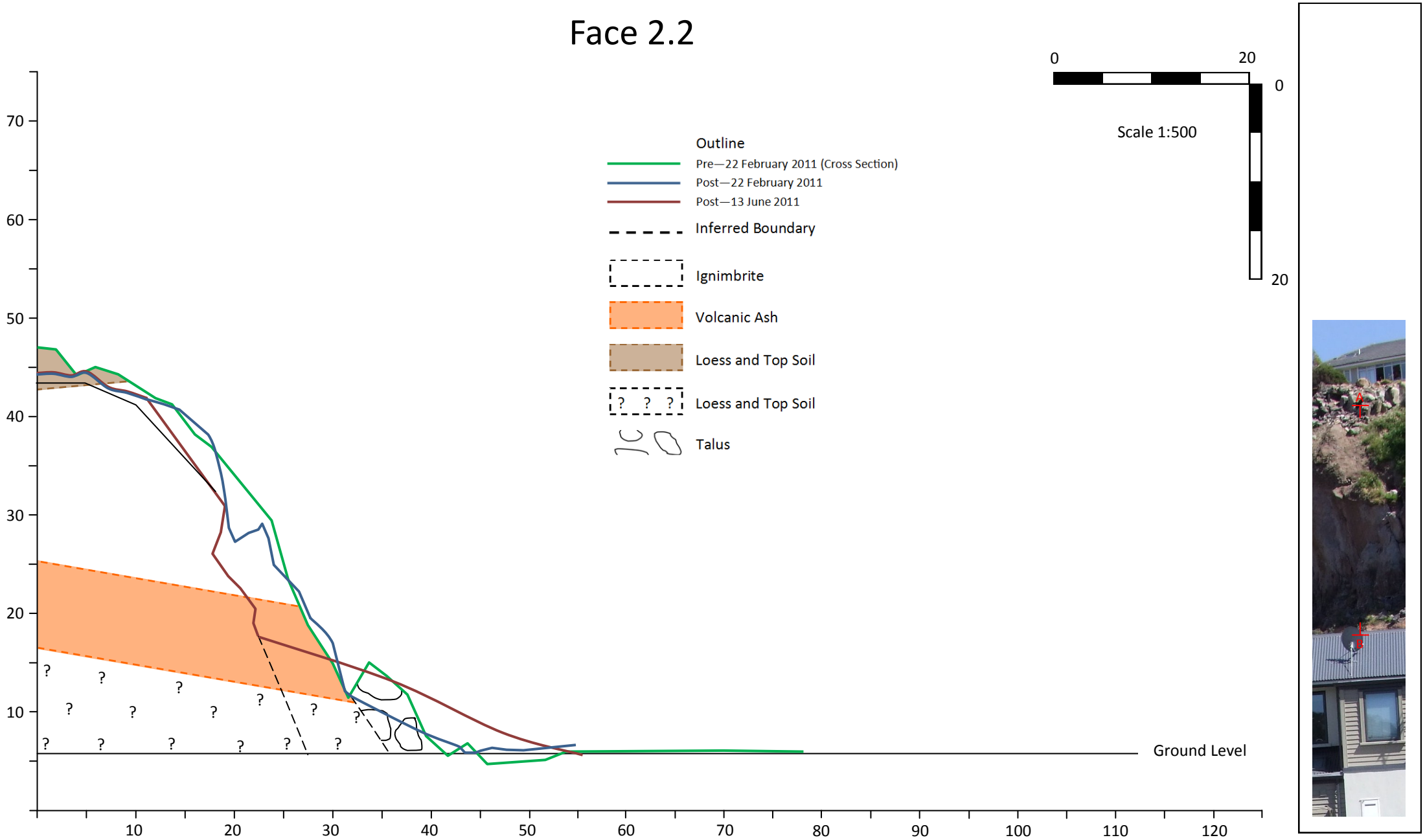
0
20
0
20
Scale 1:500
Outline
Pre—22 February 2011 (Cross Section)
Post—22 February 2011
Post—13 June 2011
Inferred Boundary
Ignimbrite
Volcanic Ash
Loess and Top Soil
? ? ?
Loess and Top Soil
Talus
Ground Level
70
60
50
40
30
20
10
10
20
30
40
50
60
70
80
90
100
110
120

Face 3.1

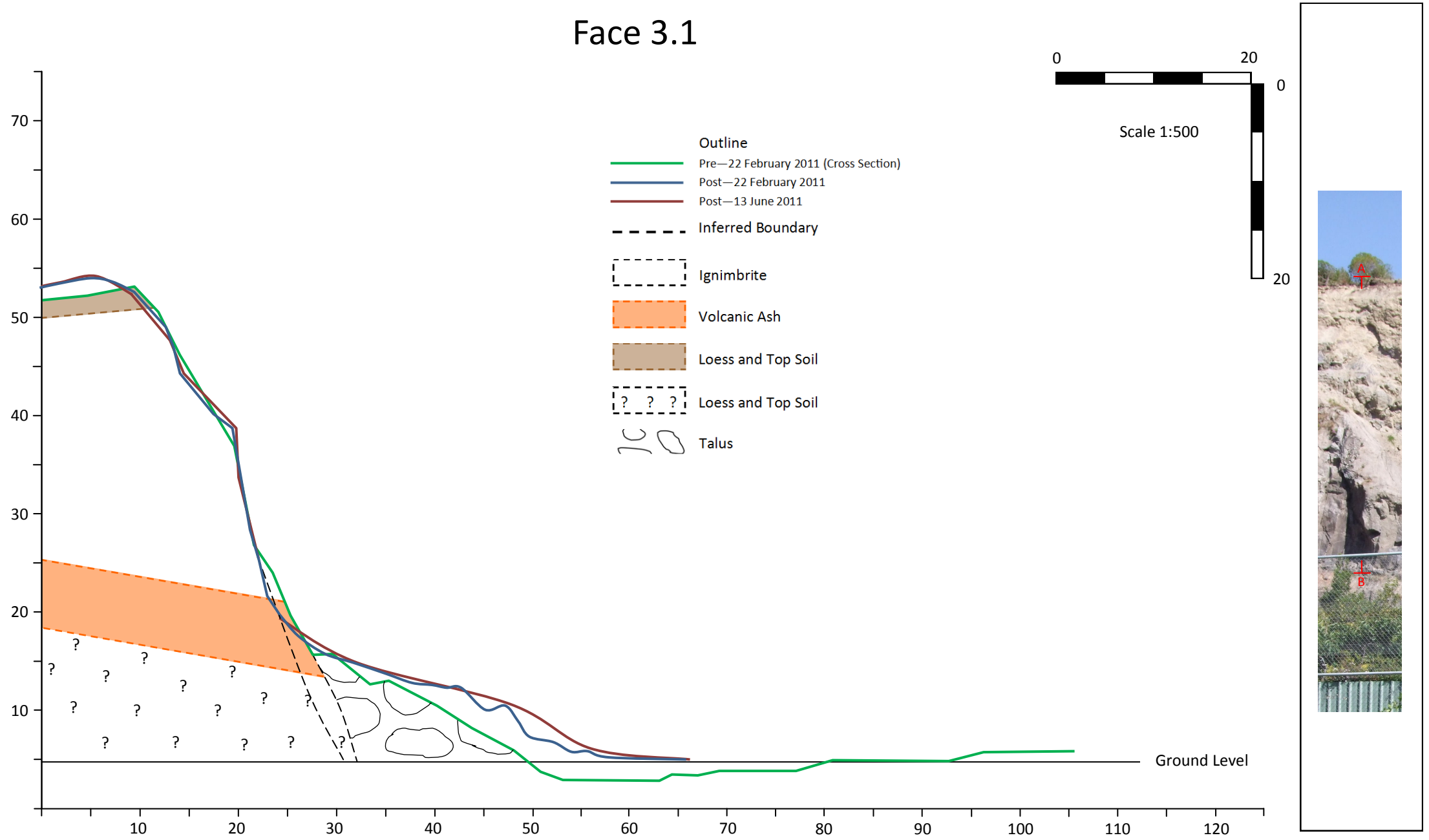
0
20
0
20
Scale 1:500
Outline
Pre—22 February 2011 (Cross Section)
Post—22 February 2011
Post—13 June 2011
Inferred Boundary
Ignimbrite
Volcanic Ash
Loess and Top Soil
Loess and Top Soil
Talus
Ground Level
70
60
50
40
30
20
10
10
20
30
40
50
60
70
80
90
100
110
120
A
B

Face 3.2

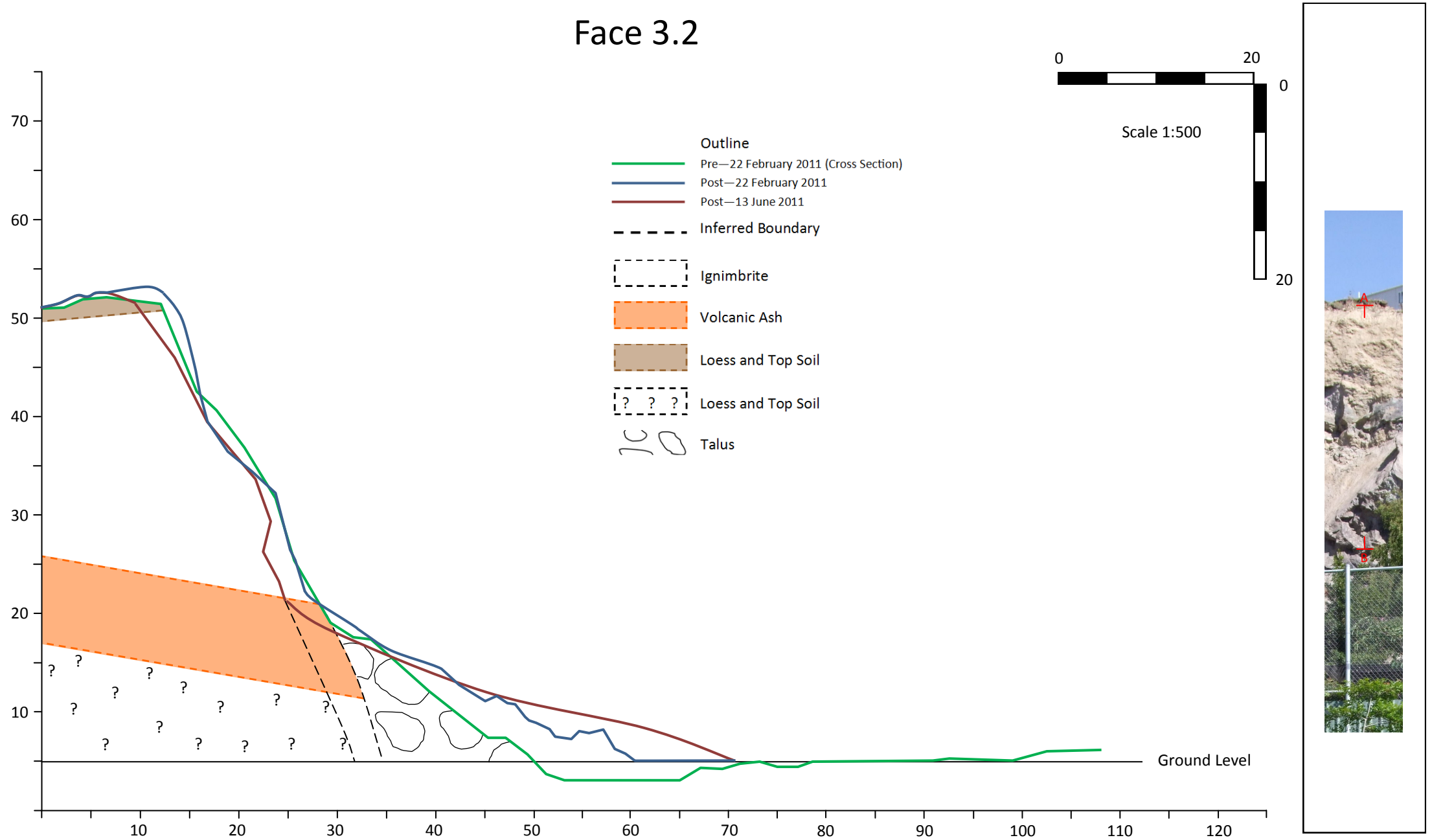
0
20
0
20
Scale 1:500
Outline
Pre—22 February 2011 (Cross Section)
Post—22 February 2011
Post—13 June 2011
Inferred Boundary
Ignimbrite
Volcanic Ash
Loess and Top Soil
Loess and Top Soil
Talus
Ground Level
70
60
50
40
30
20
10
10
20
30
40
50
60
70
80
90
100
110
120

Face 3.3

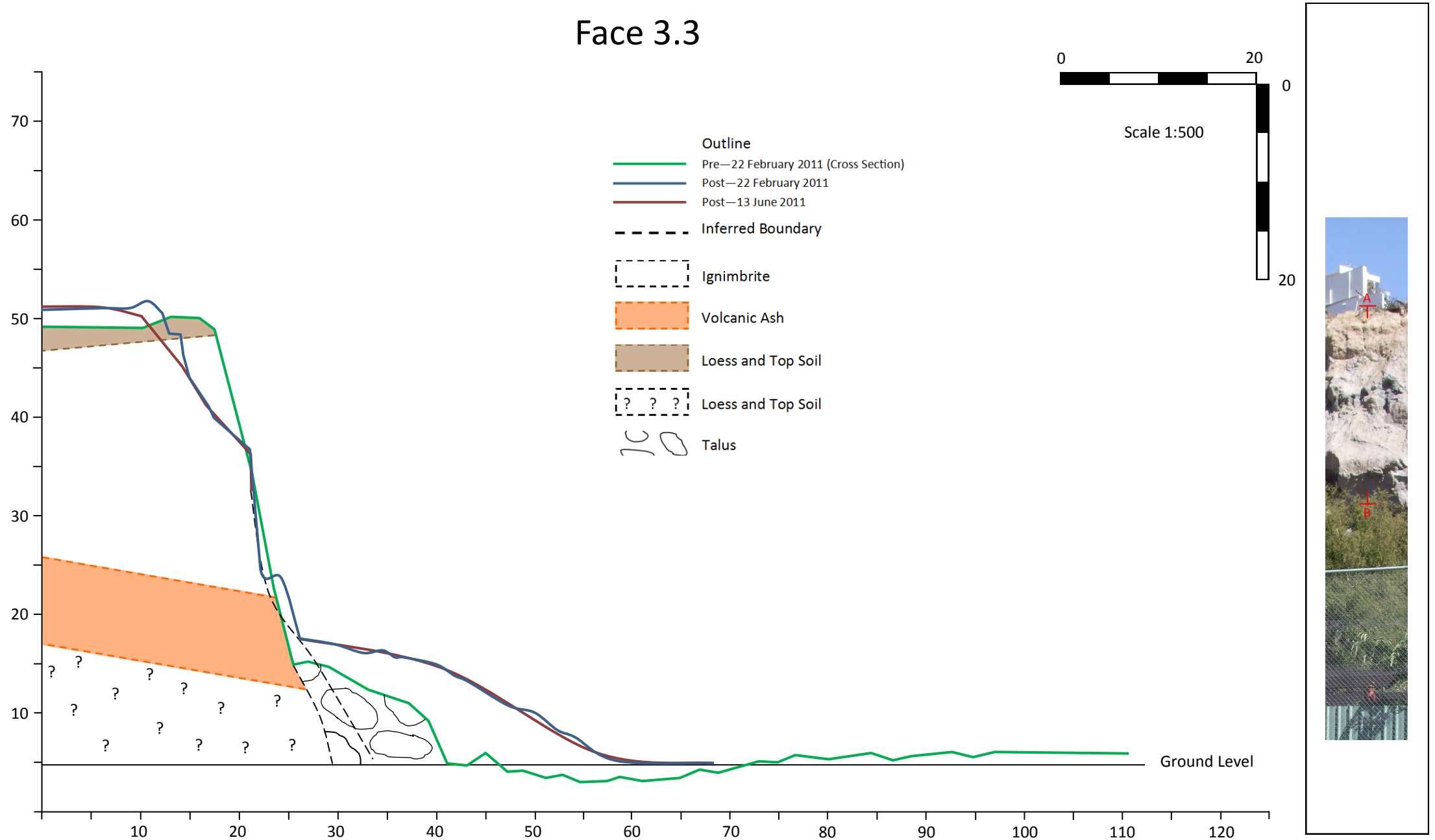
0
20
0
20
Scale 1:500
Outline
Pre—22 February 2011 (Cross Section)
Post—22 February 2011
Post—13 June 2011
Inferred Boundary
Ignimbrite
Volcanic Ash
Loess and Top Soil
Loess and Top Soil
Talus
Ground Level
70
60
50
40
30
20
10
10
20
30
40
50
60
70
80
90
100
110
120
A
B

Face 3.4

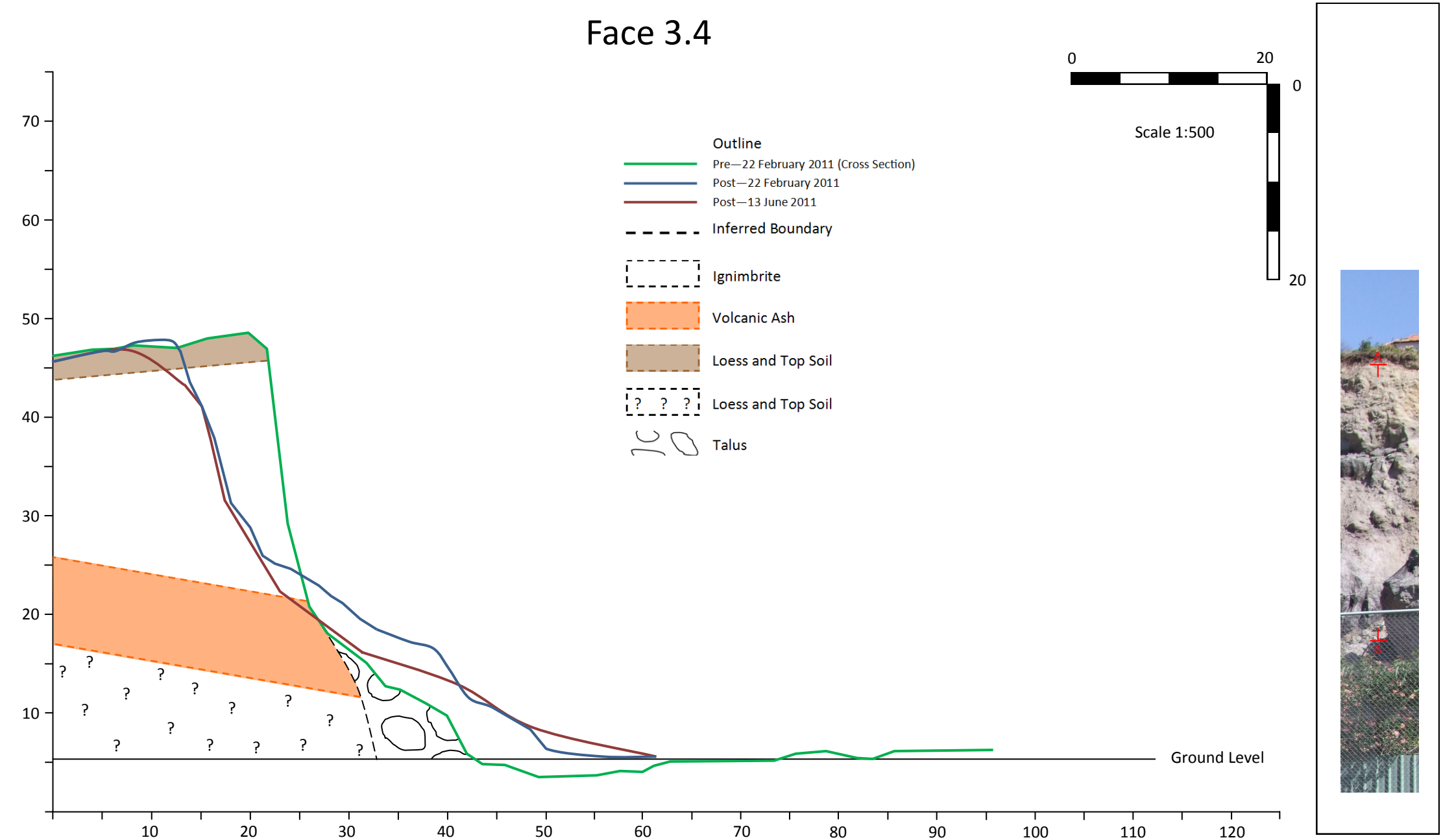
0
20
0
20
Scale 1:500
Outline
Pre—22 February 2011 (Cross Section)
Post—22 February 2011
Post—13 June 2011
Inferred Boundary
Ignimbrite
Volcanic Ash
Loess and Top Soil
Loess and Top Soil
Talus
Ground Level
70
60
50
40
30
20
10
10
20
30
40
50
60
70
80
90
100
110
120

Face 4.1

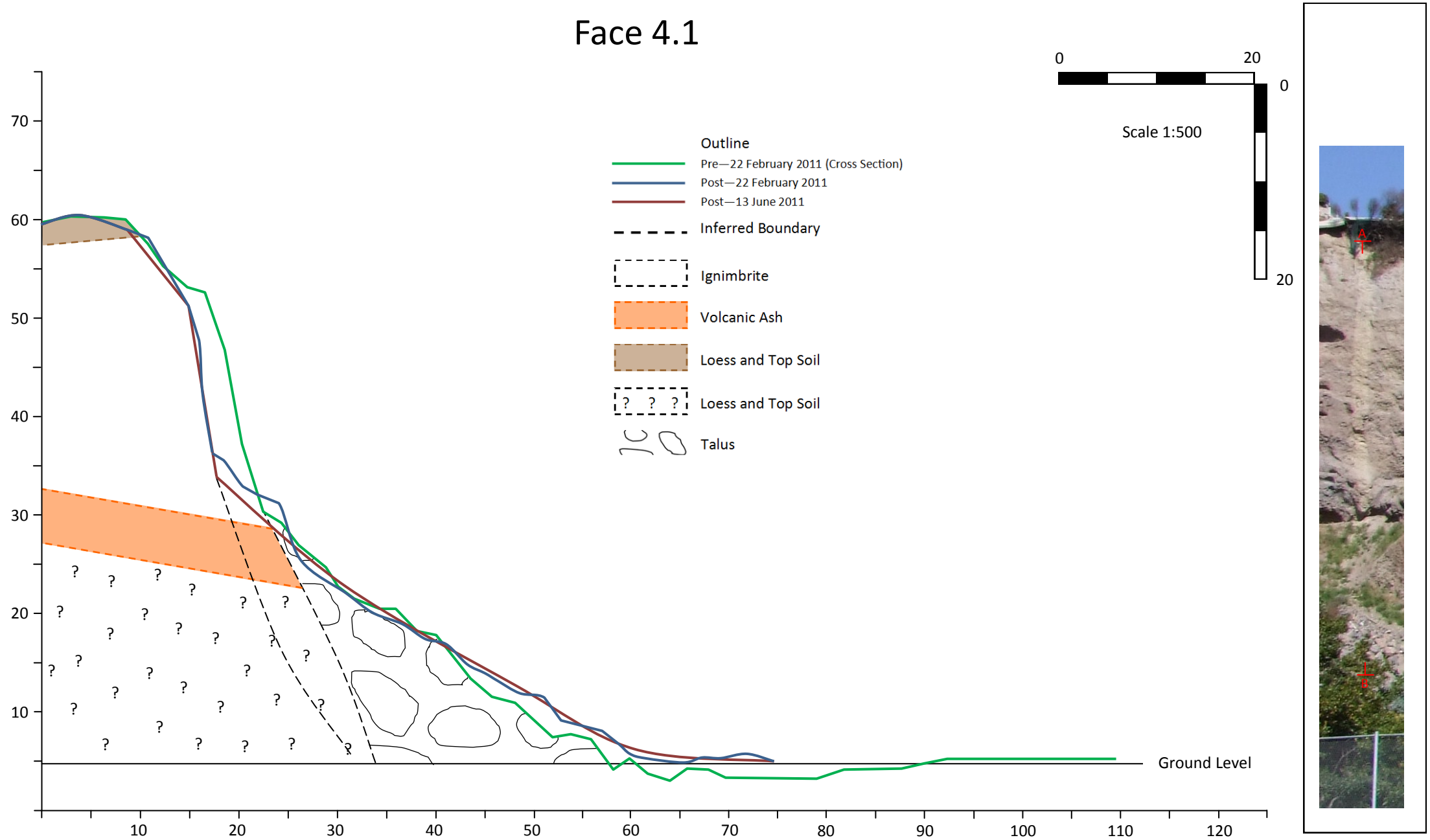
0
20
0
20
Scale 1:500
Outline
Pre—22 February 2011 (Cross Section)
Post—22 February 2011
Post—13 June 2011
Inferred Boundary
Ignimbrite
Volcanic Ash
Loess and Top Soil
Loess and Top Soil
Talus
Ground Level
70
60
50
40
30
20
10
10
20
30
40
50
60
70
80
90
100
110
120

Face 4.2

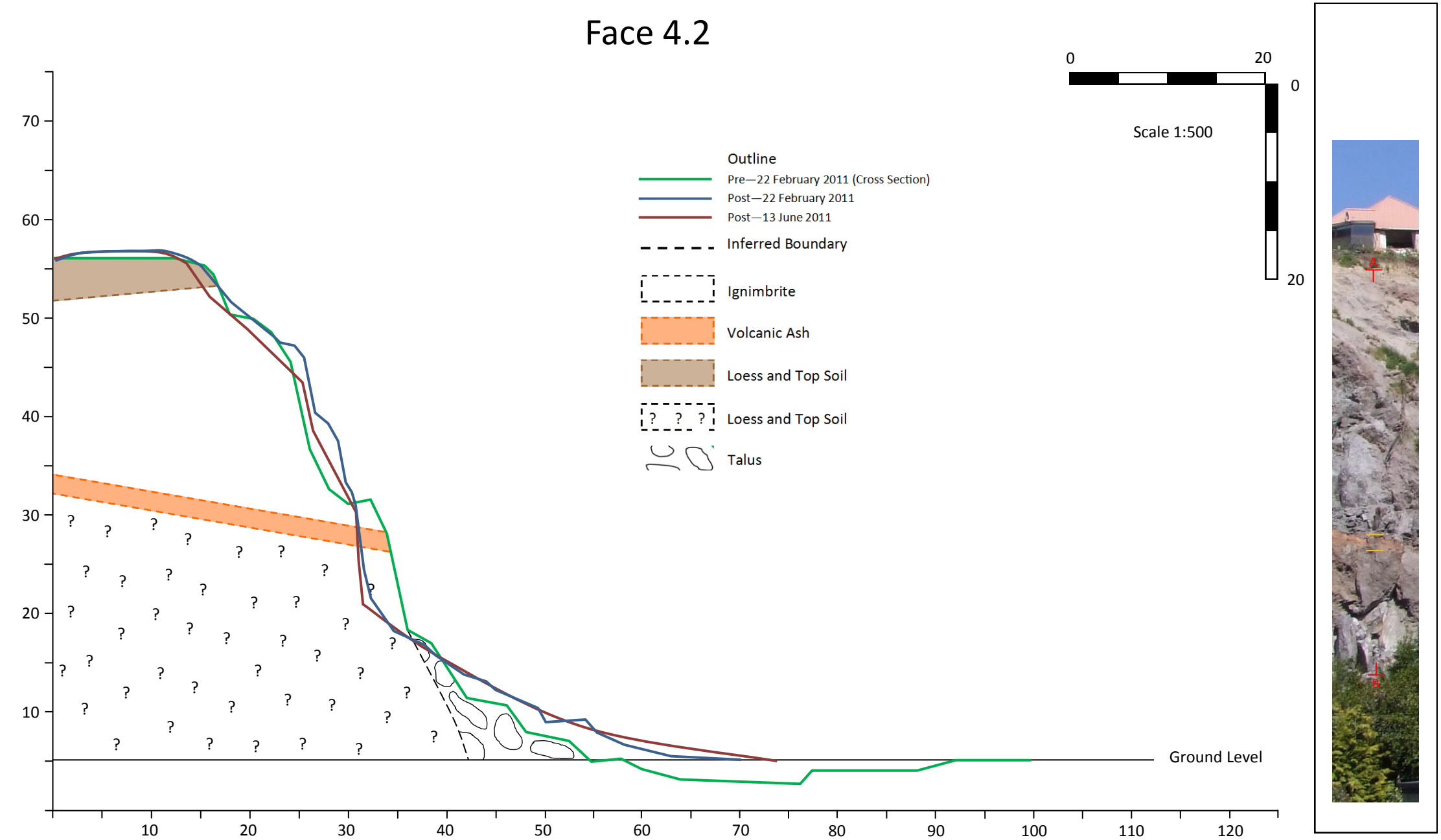
0
20
0
20
Scale 1:500
Outline
Pre—22 February 2011 (Cross Section)
Post—22 February 2011
Post—13 June 2011
Inferred Boundary
Ignimbrite
Volcanic Ash
Loess and Top Soil
Loess and Top Soil
Talus
Ground Level
70
60
50
40
30
20
10
10
20
30
40
50
60
70
80
90
100
110
120

Face 4.3

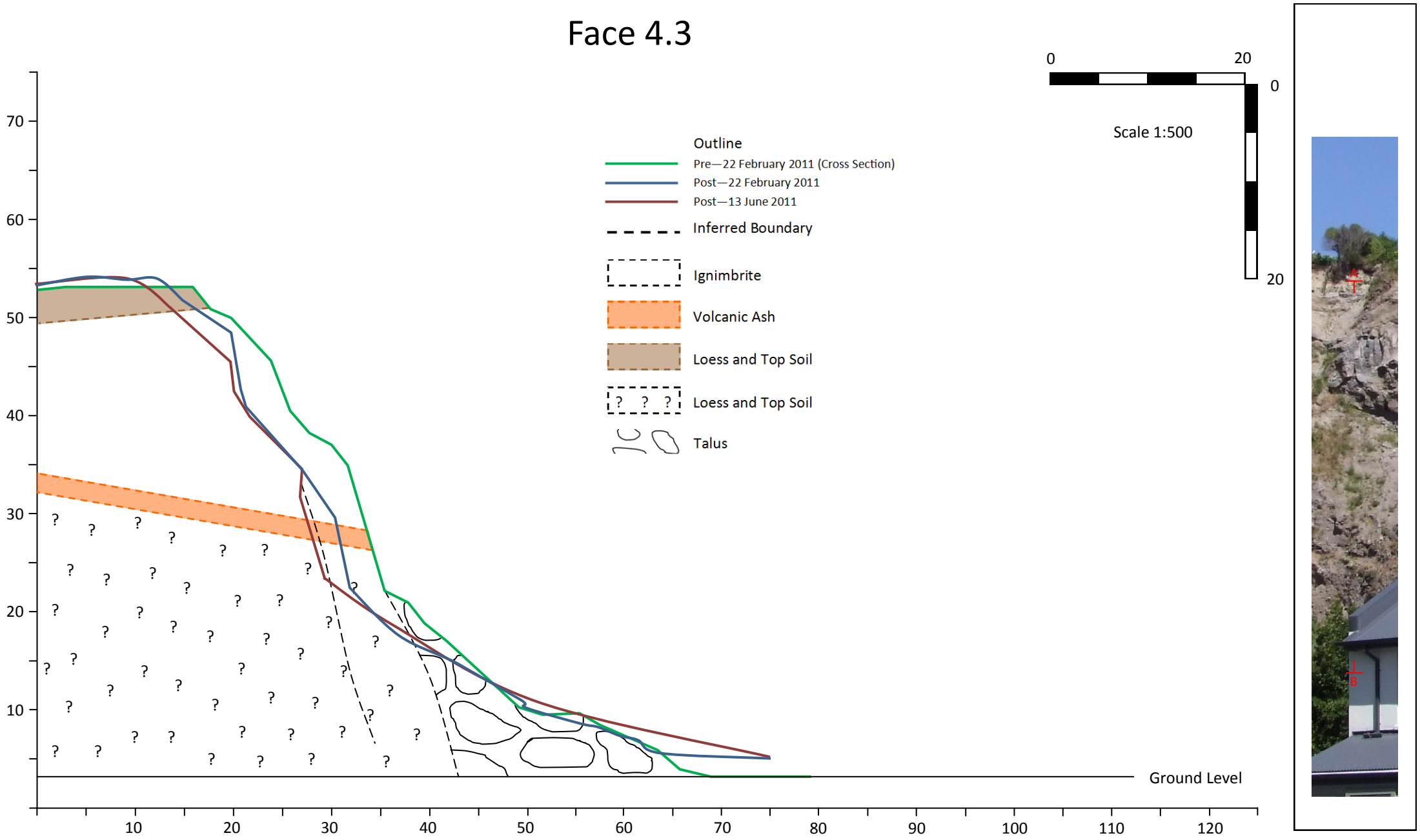
0
20
0
20
Scale 1:500
Outline
Pre—22 February 2011 (Cross Section)
Post—22 February 2011
Post—13 June 2011
Inferred Boundary
Ignimbrite
Volcanic Ash
Loess and Top Soil
Loess and Top Soil
Talus
Ground Level
70
60
50
40
30
20
10
10
20
30
40
50
60
70
80
90
100
110
120

Face 5.1

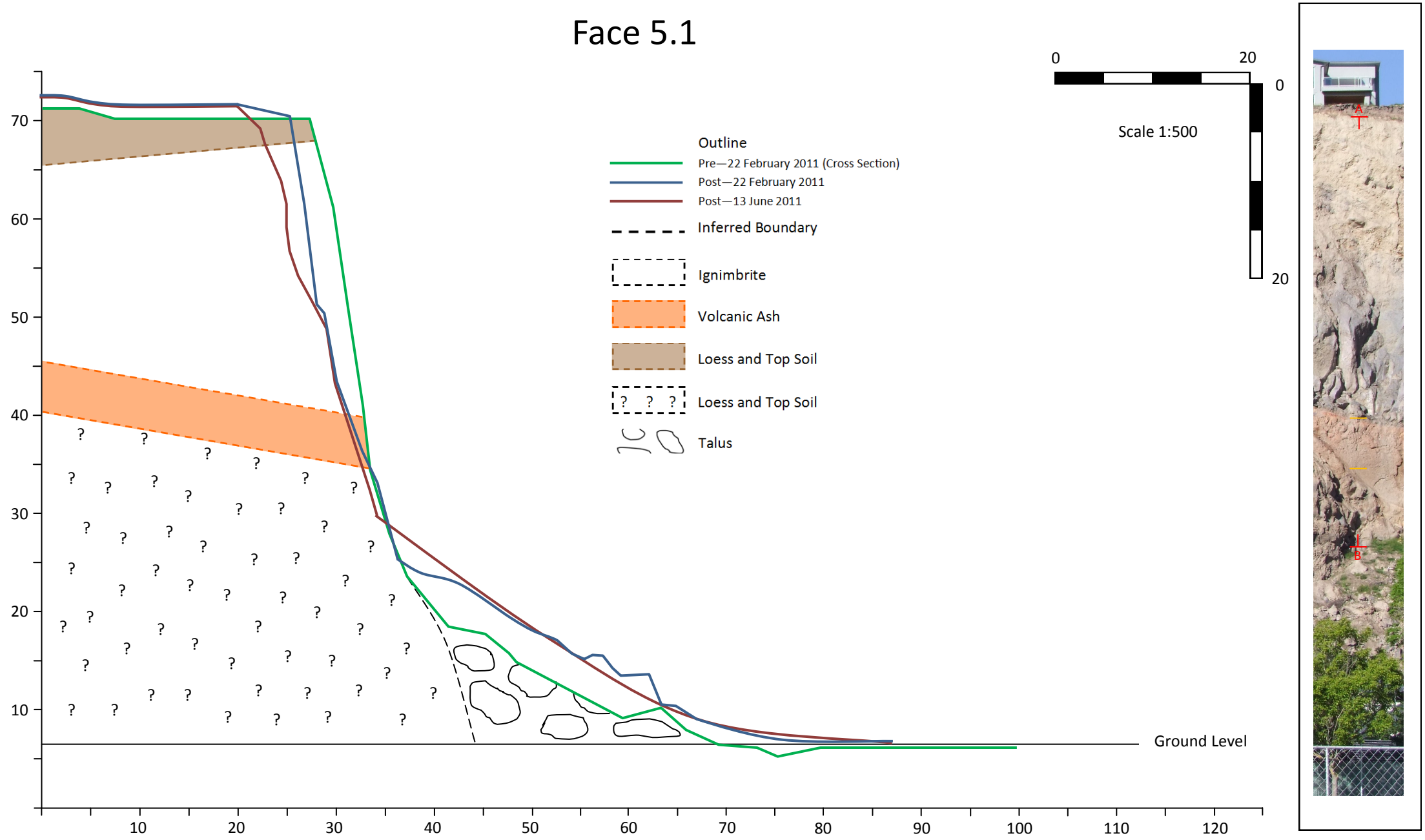
0
20
0
20
Scale 1:500
Outline
Pre—22 February 2011 (Cross Section)
Post—22 February 2011
Post—13 June 2011
Inferred Boundary
Ignimbrite
Volcanic Ash
Loess and Top Soil
Loess and Top Soil
Talus
Ground Level
70
60
50
40
30
20
10
10
20
30
40
50
60
70
80
90
100
110
120
A
B

Face 5.2

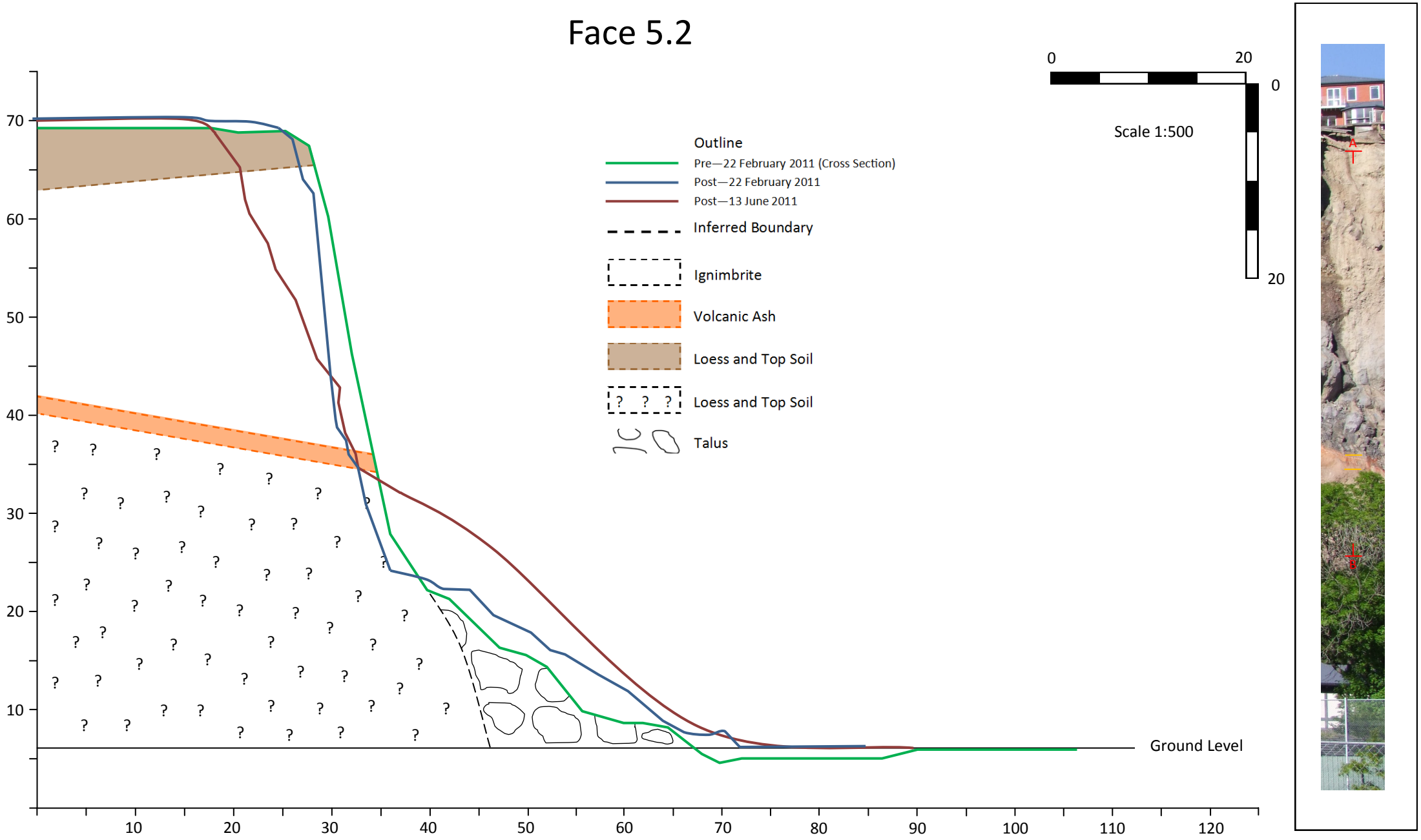
0
20
0
20
Scale 1:500
Outline
Pre—22 February 2011 (Cross Section)
Post—22 February 2011
Post—13 June 2011
Inferred Boundary
Ignimbrite
Volcanic Ash
Loess and Top Soil
? ? ?
Loess and Top Soil
Talus
Ground Level
70
60
50
40
30
20
10
10
20
30
40
50
60
70
80
90
100
110
120

Face 5.3

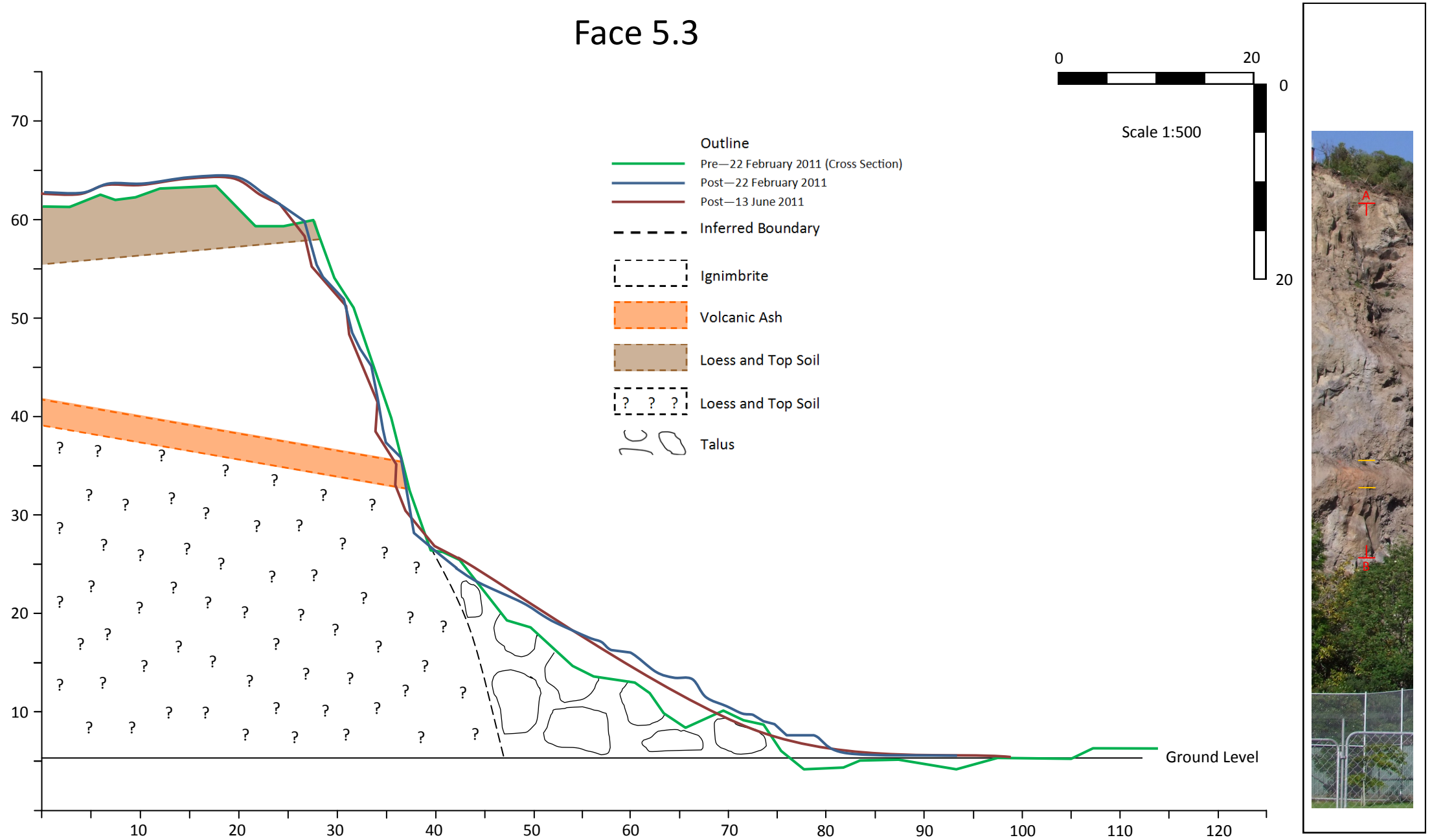
0
20
0
20
Scale 1:500
Outline
Pre—22 February 2011 (Cross Section)
Post—22 February 2011
Post—13 June 2011
Inferred Boundary
Ignimbrite
Volcanic Ash
Loess and Top Soil
? ? ?
Loess and Top Soil
Talus
Ground Level
70
60
50
40
30
20
10
10
20
30
40
50
60
70
80
90
100
110
120
A
B

Face 5.4

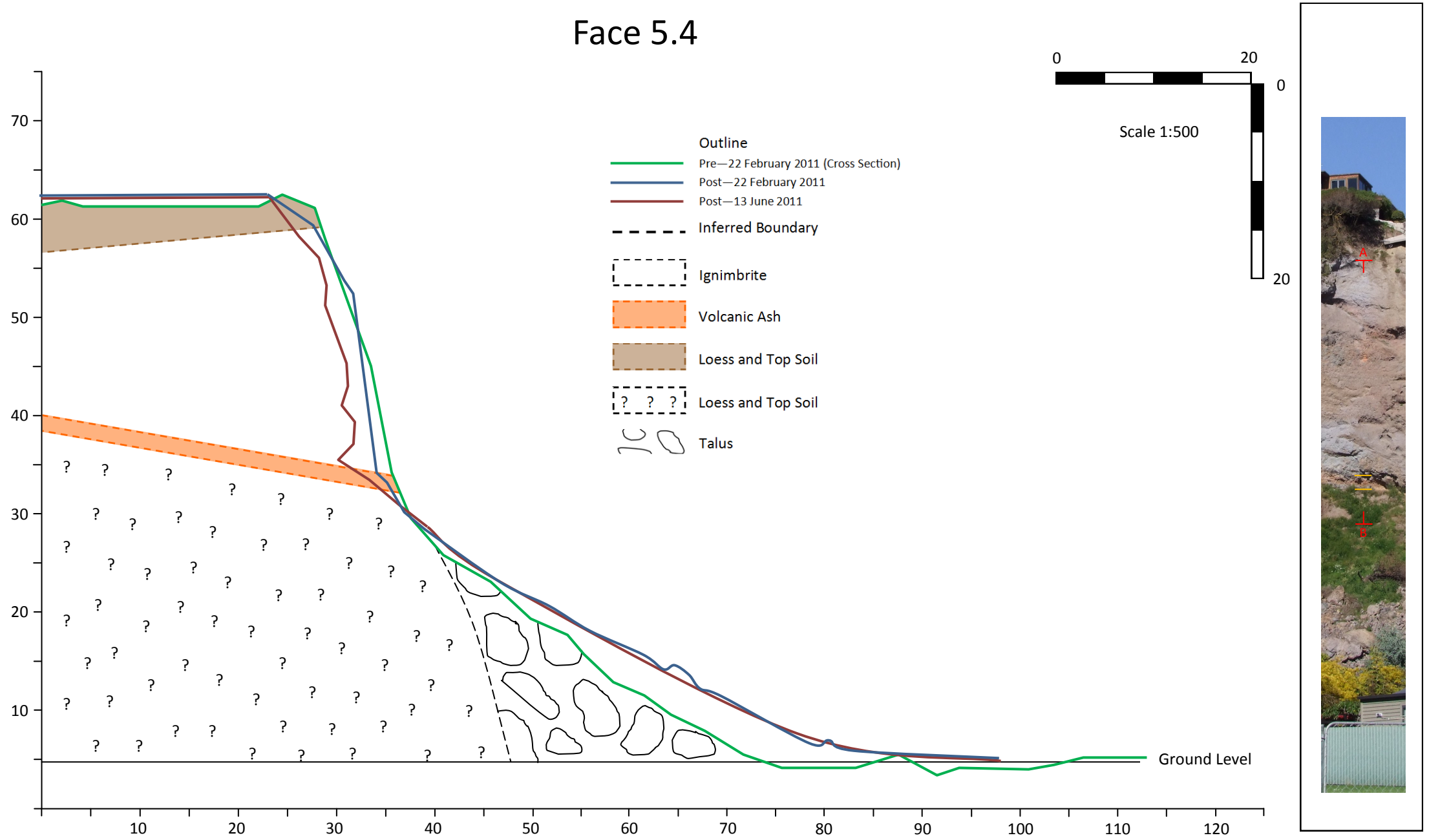
0
20
0
20
Scale 1:500
Outline
Pre—22 February 2011 (Cross Section)
Post—22 February 2011
Post—13 June 2011
Inferred Boundary
Ignimbrite
Volcanic Ash
Loess and Top Soil
? ? ?
Loess and Top Soil
Talus
Ground Level
70
60
50
40
30
20
10
10
20
30
40
50
60
70
80
90
100
110
120

Face 6.1

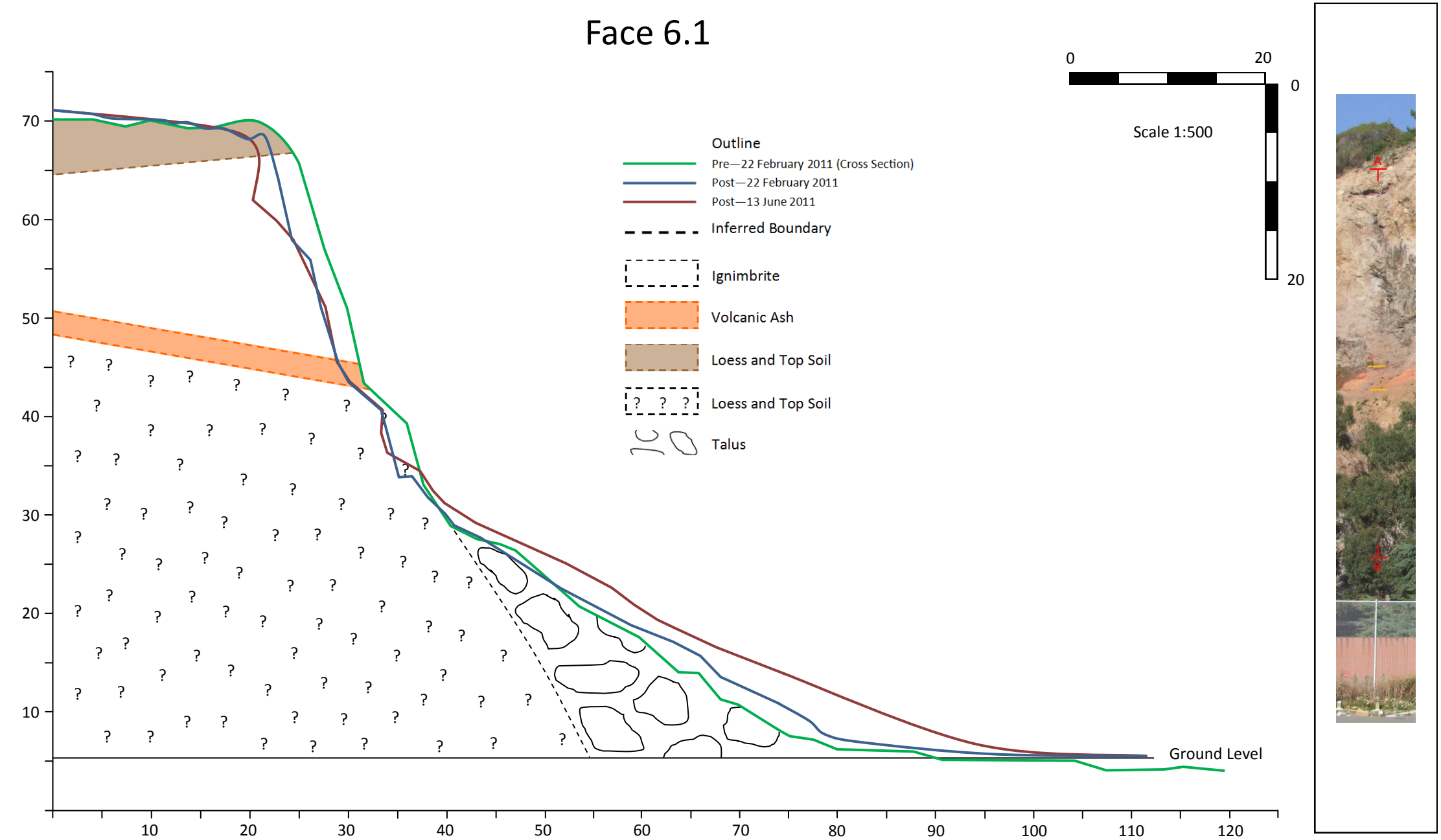
0
20
0
20
Scale 1:500
Outline
Pre—22 February 2011 (Cross Section)
Post—22 February 2011
Post—13 June 2011
Inferred Boundary
Ignimbrite
Volcanic Ash
Loess and Top Soil
Loess and Top Soil
Talus
Ground Level
70
60
50
40
30
20
10
10
20
30
40
50
60
70
80
90
100
110
120

Face 6.2

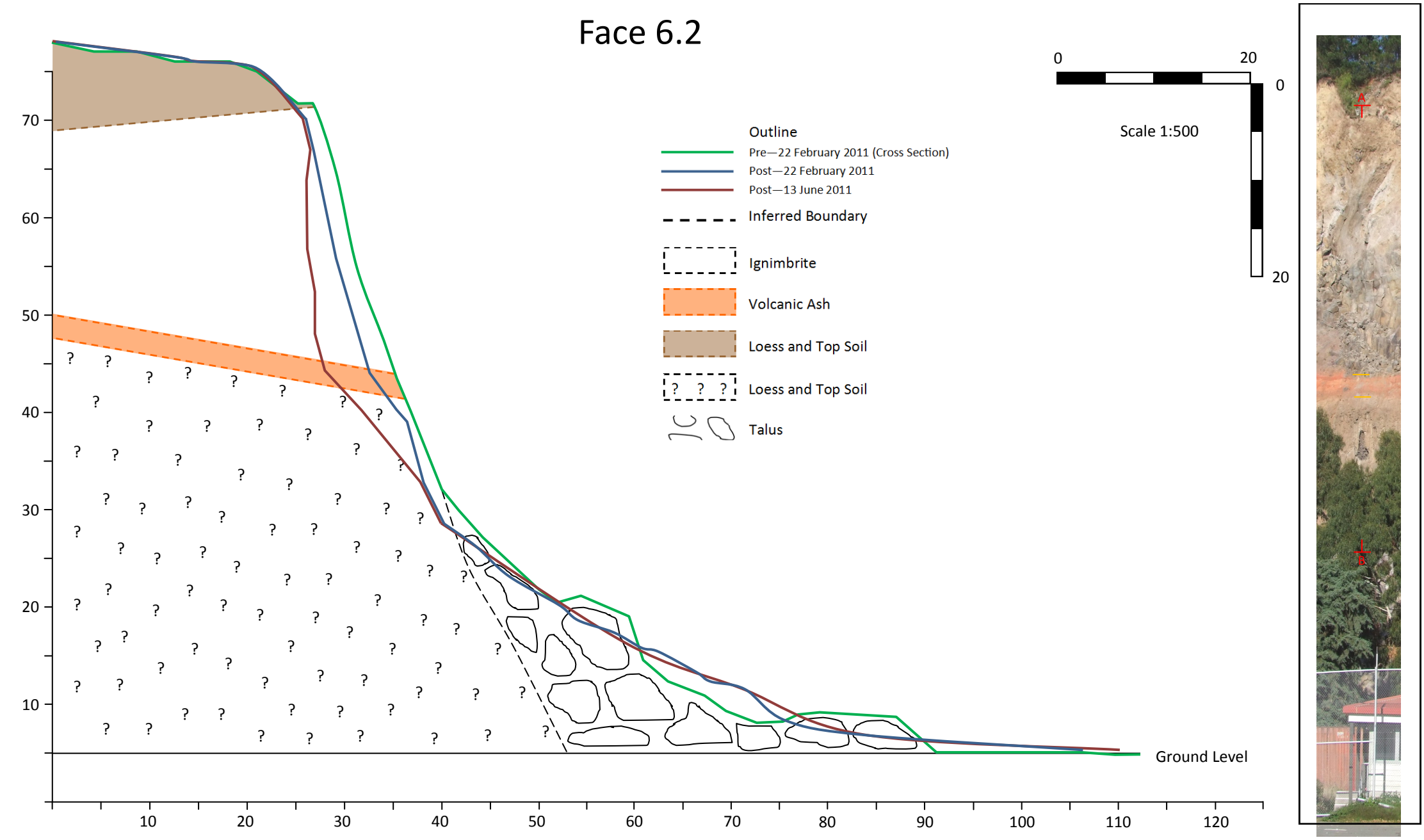
0
20
0
20
Scale 1:500
Outline
Pre—22 February 2011 (Cross Section)
Post—22 February 2011
Post—13 June 2011
Inferred Boundary
Ignimbrite
Volcanic Ash
Loess and Top Soil
Loess and Top Soil
Talus
Ground Level
70
60
50
40
30
20
10
10
20
30
40
50
60
70
80
90
100
110
120

Face 6.3

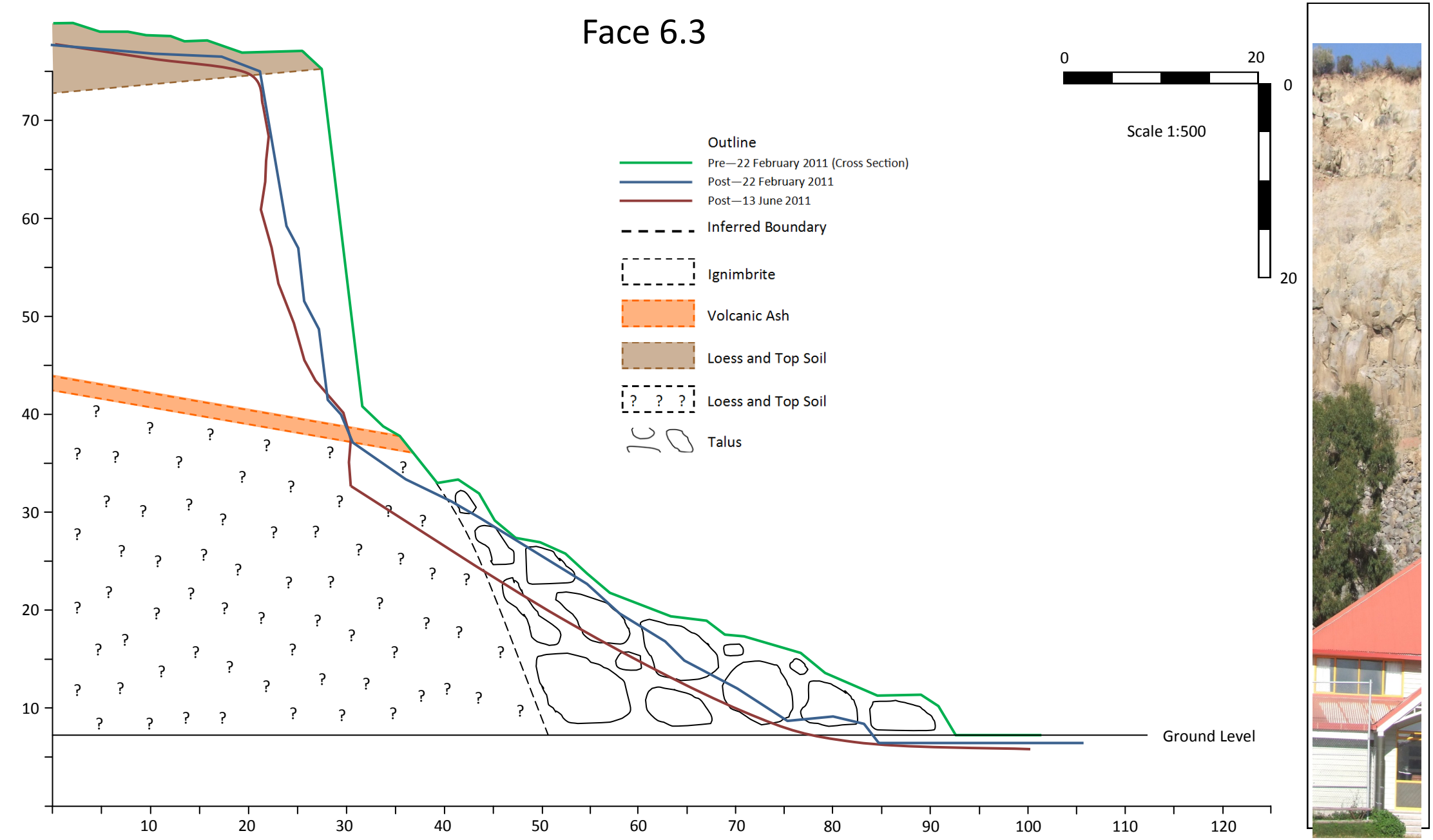
Outline
Pre—22 February 2011 (Cross Section)
Post—22 February 2011
Post—13 June 2011
Inferred Boundary
Ignimbrite
Volcanic Ash
Loess and Top Soil
Loess and Top Soil
Talus
0
20
0
20
Scale 1:500
Ground Level
10
20
30
40
50
60
70
80
90
100
110
120

Face 6.4

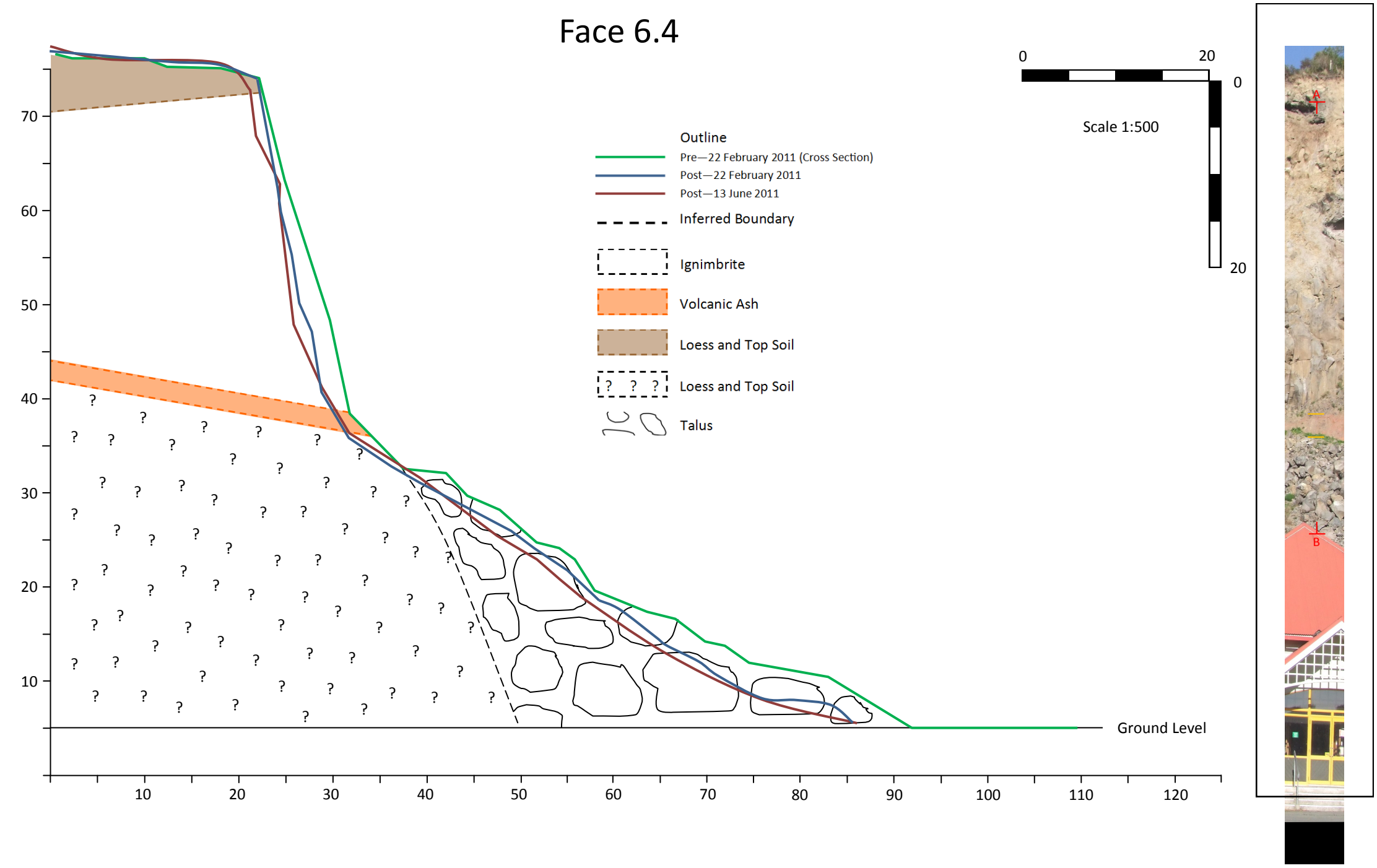
0
20
0
20
Scale 1:500
Outline
Pre—22 February 2011 (Cross Section)
Post—22 February 2011
Post—13 June 2011
Inferred Boundary
Ignimbrite
Volcanic Ash
Loess and Top Soil
Loess and Top Soil
Talus
Ground Level
10
20
30
40
50
60
70
80
90
100
110
120
10
20
30
40
50
60
70
A
B

Face 6.5

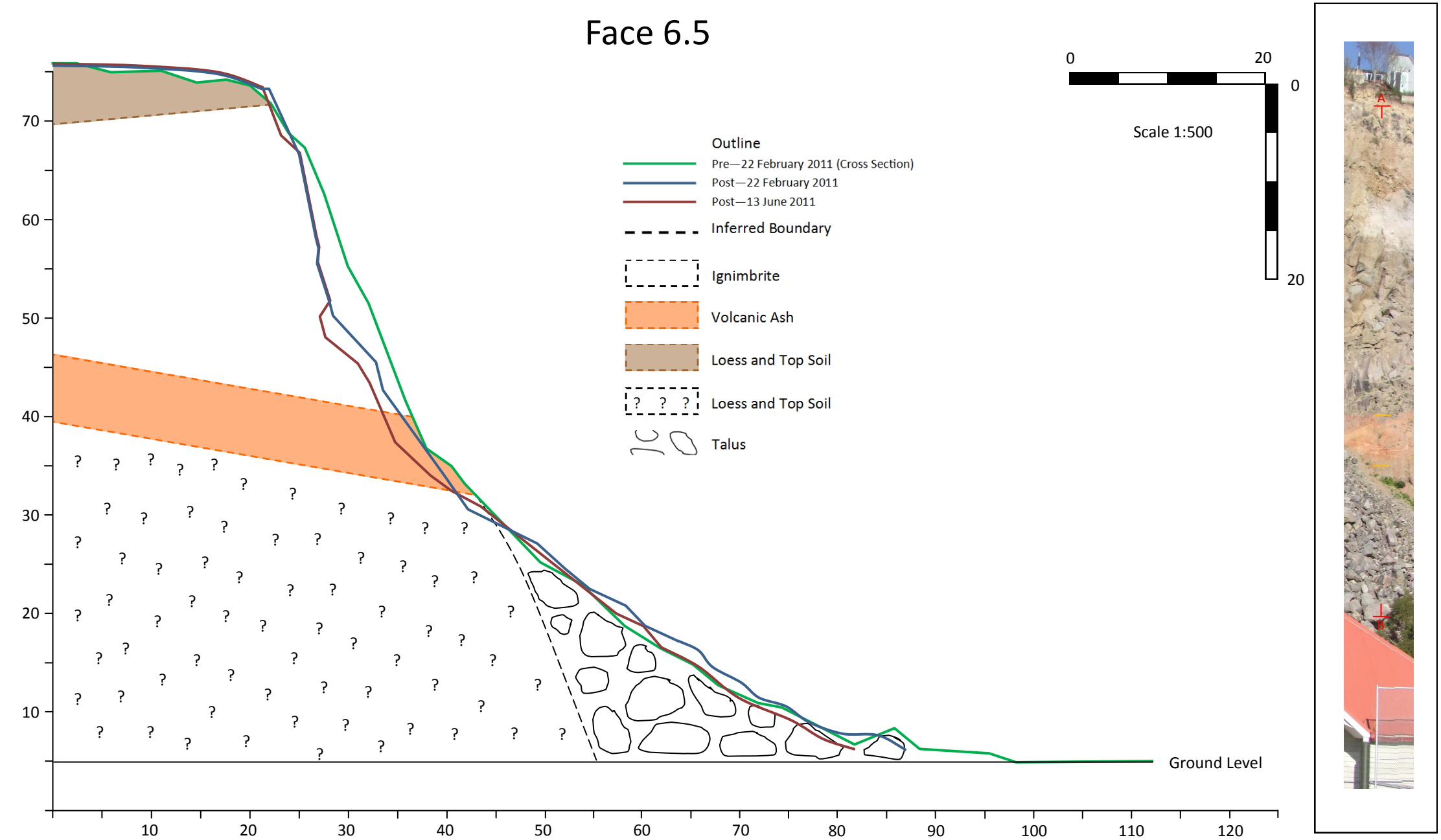
0
20
0
20
Scale 1:500
Outline
Pre—22 February 2011 (Cross Section)
Post—22 February 2011
Post—13 June 2011
Inferred Boundary
Ignimbrite
Volcanic Ash
Loess and Top Soil
? ? ?
Loess and Top Soil
Talus
Ground Level
10
20
30
40
50
60
70
80
90
100
110
120

Face 6.6

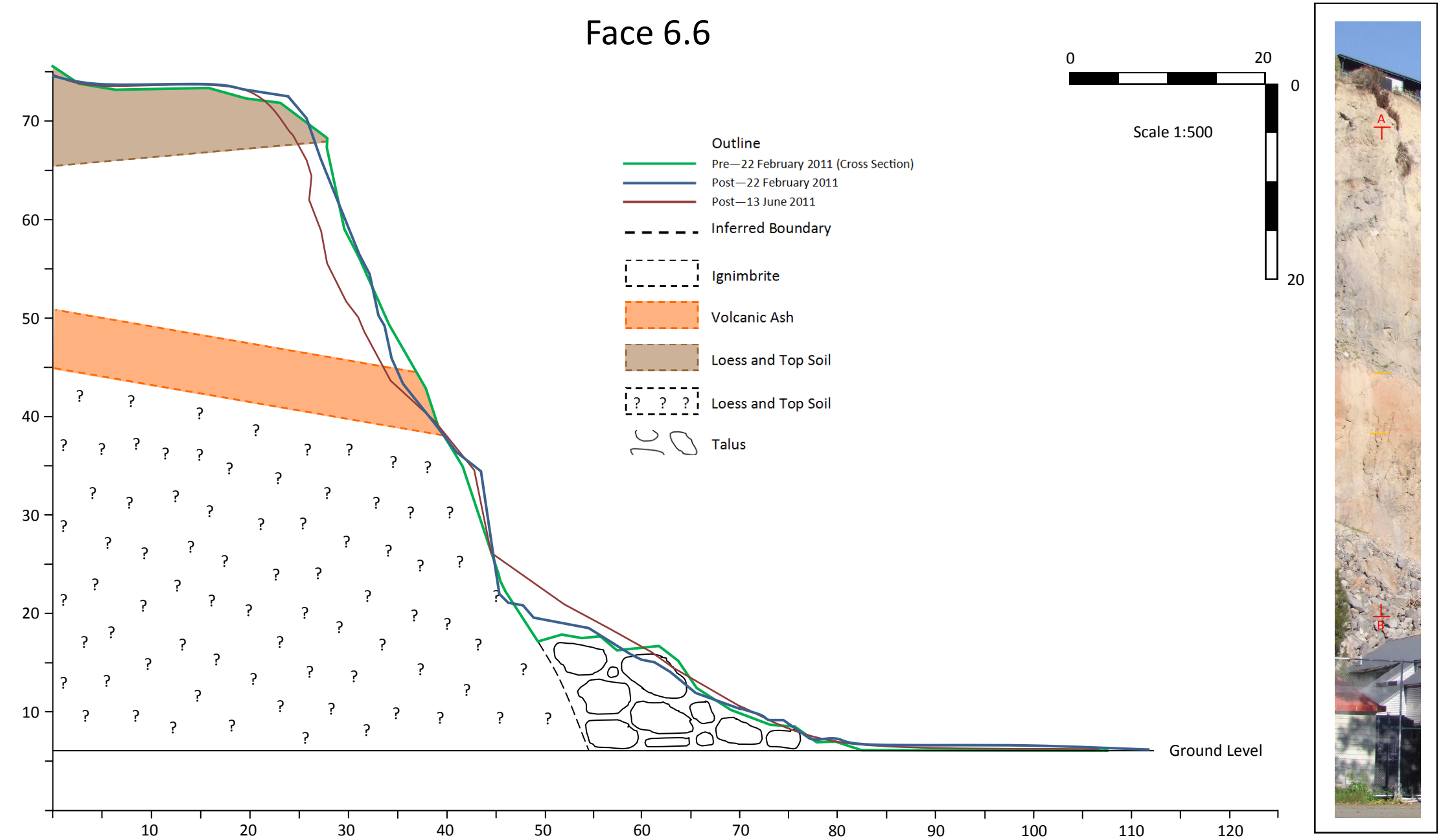
0
20
0
20
Scale 1:500
Outline
Pre—22 February 2011 (Cross Section)
Post—22 February 2011
Post—13 June 2011
Inferred Boundary
Ignimbrite
Volcanic Ash
Loess and Top Soil
Loess and Top Soil
Talus
Ground Level
70
60
50
40
30
20
10
10
20
30
40
50
60
70
80
90
100
110
120
A
B

Face 7.1

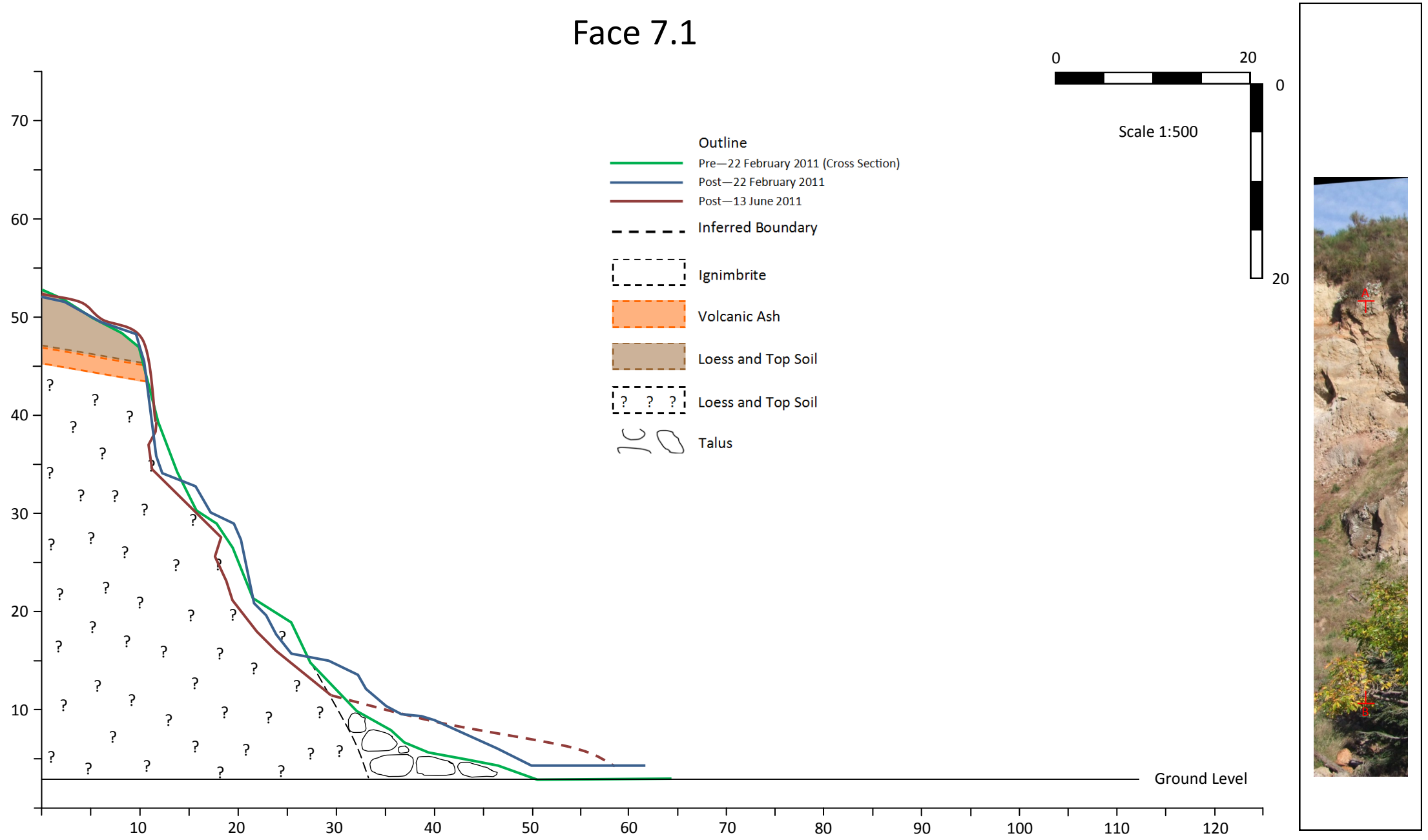
0
20
0
20
Scale 1:500
Outline
Pre—22 February 2011 (Cross Section)
Post—22 February 2011
Post—13 June 2011
Inferred Boundary
Ignimbrite
Volcanic Ash
Loess and Top Soil
Loess and Top Soil
Talus
Ground Level
70
60
50
40
30
20
10
10
20
30
40
50
60
70
80
90
100
110
120
A
B

Face 7.2

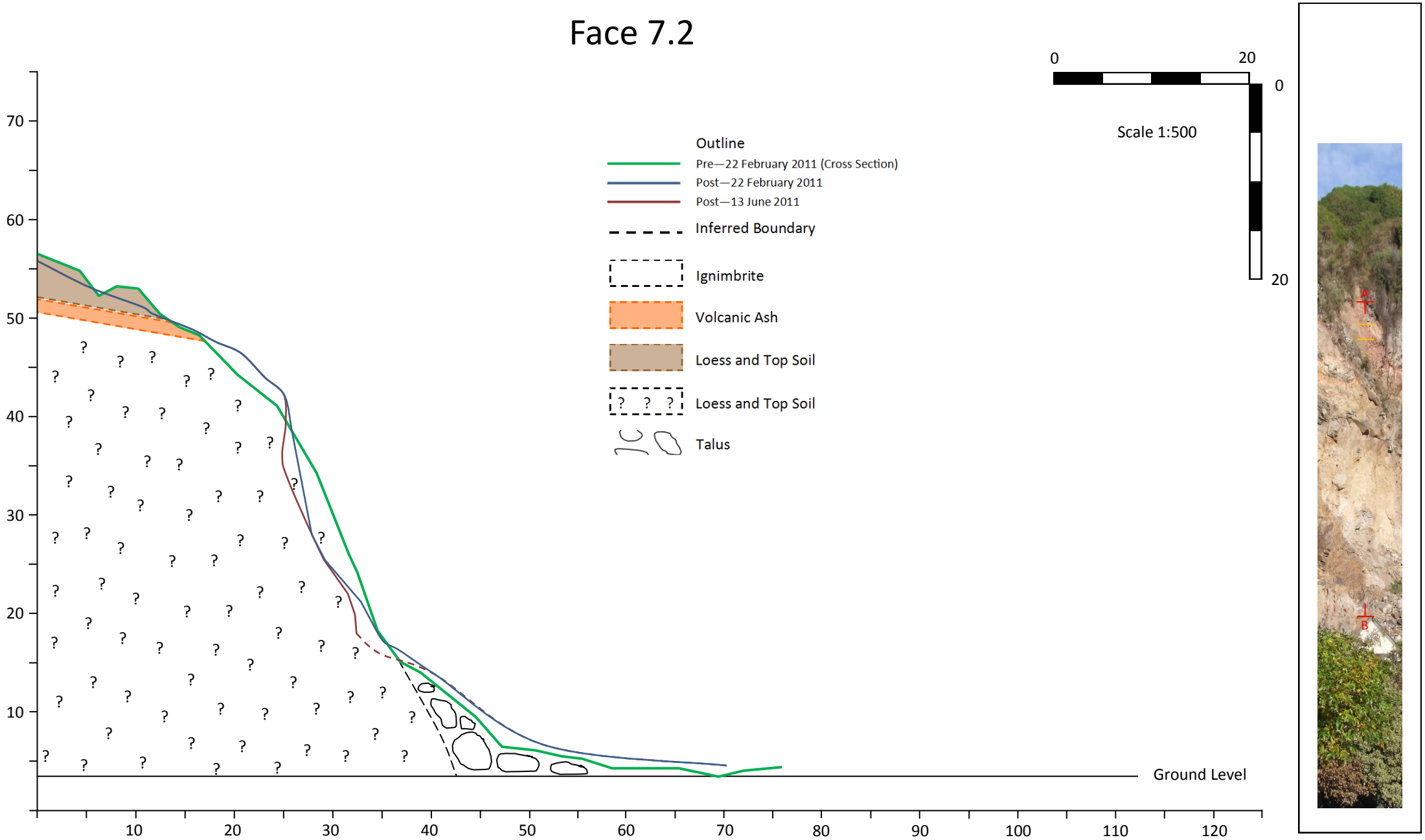
0
20
0
20
Scale 1:500
Outline
Pre—22 February 2011 (Cross Section)
Post—22 February 2011
Post—13 June 2011
Inferred Boundary
Ignimbrite
Volcanic Ash
Loess and Top Soil
Loess and Top Soil
Talus
Ground Level
70
60
50
40
30
20
10
10
20
30
40
50
60
70
80
90
100
110
120
A
B

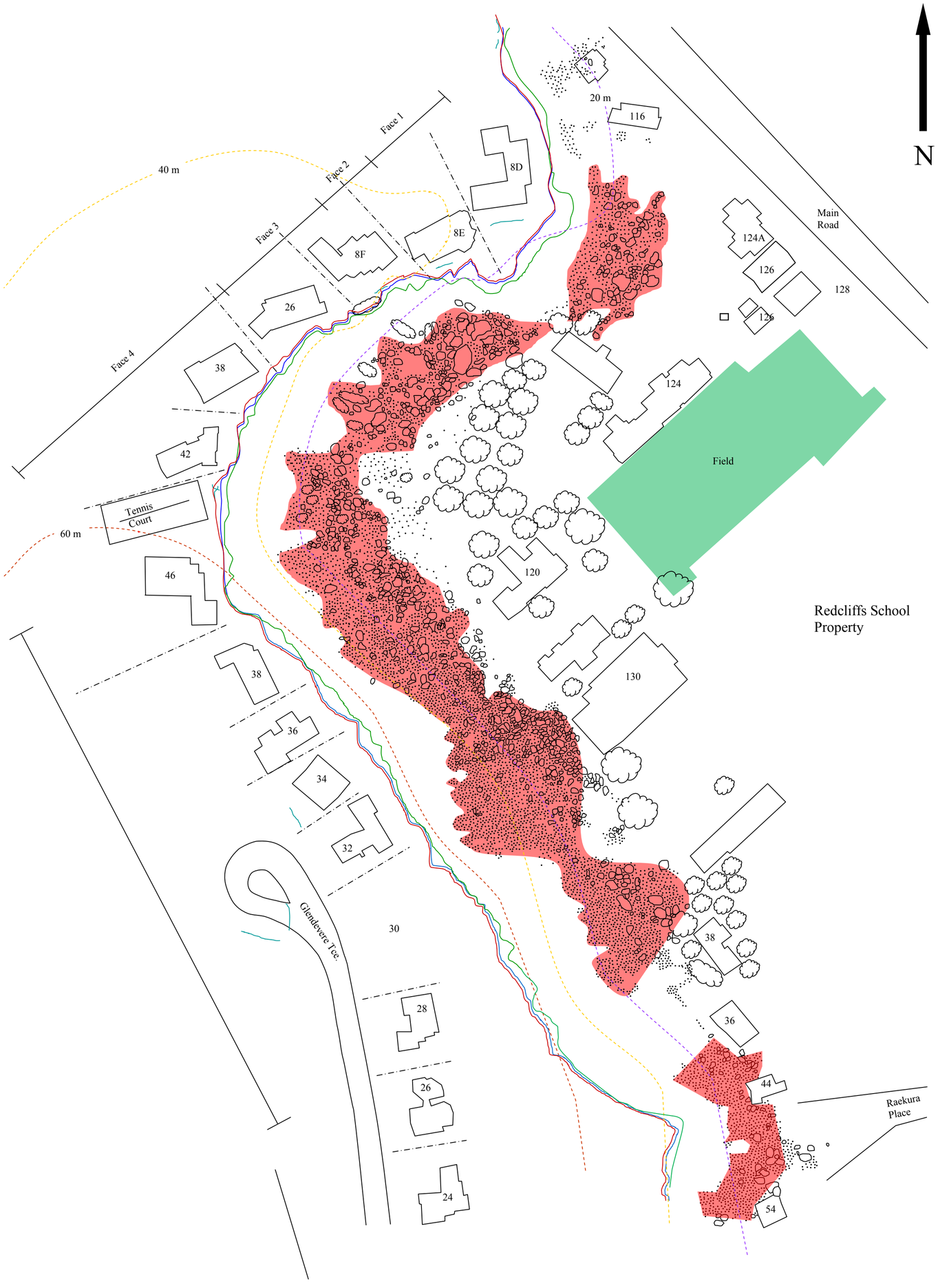

Legend

- Road (Road Name)
- Property Boundary
- Buildings (Property Number)
- Outlines of the cliff edge
  - Pre– 22 February 2011
  - Post– 22 February 2011
  - Post– 13 June 2011*
- Fissure
- Talus
- Contour lines (60 m, 40 m, 20 m)
- Trees
- Talus Debris (circular shapes indicate a large boulder size rock, whereas dots represent smaller size rocks)

Detailed Engineering Geology Site Map

8D Balmoral Lane to 24 Glendevere Terrace

Redcliffs—Christchurch

0 50 100

Scale 1:1000
(1 cm : 10 m)

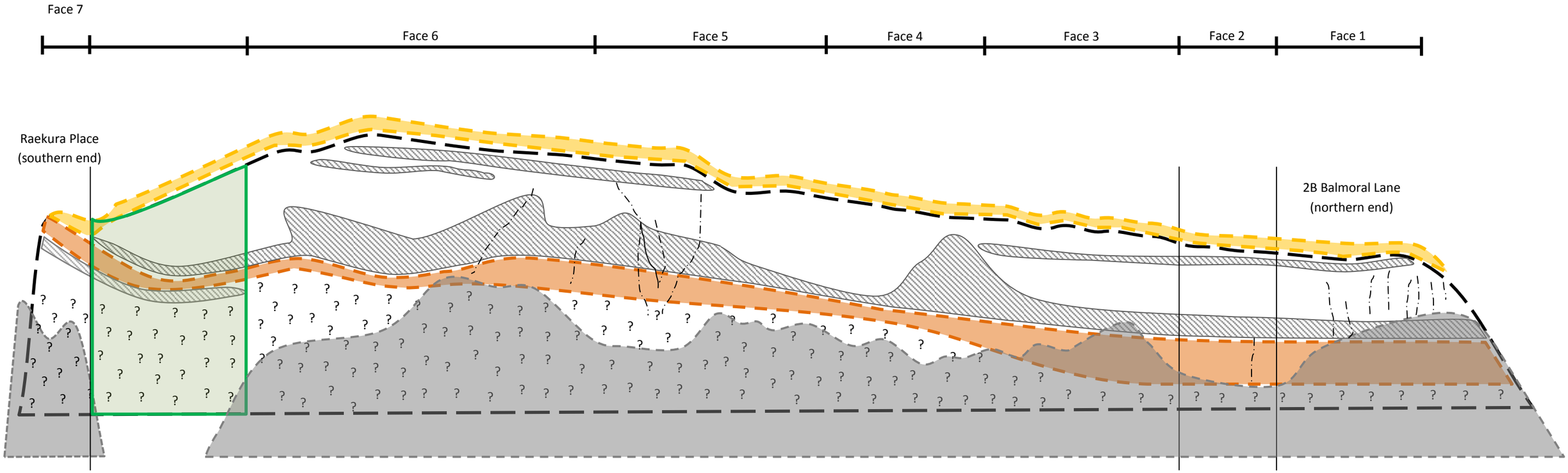

Key

Loess and Top Soil - thickness varies between 3 - 5 m

(Interlayered)

Ignimbrite - thickness varies between 15 - 60 m

Ignimbrite - thickness varies between 15 - 60 m

Ash - thickness varies between 4 - 20 m

Unknown Igneous Rock - thickness varies between 15 - 60

Post-failure rock mass defects observed on the cliff face

Geology Map of Redcliffs

(Map 2)

Scale 1: 100

This map is a general representation of the volcanic deposits and structural condition of the cliff face. Mapping was carried out following the 13 June 13 2011. Therefore the geology map represents the newly exposed cliff face after the 13th June earthquakes, but before the 23rd December 2011 earthquakes.